

South Dakota State University

Open PRAIRIE: Open Public Research Access Institutional Repository and Information Exchange

Electronic Theses and Dissertations

2016

A FRET Investigation into Molecular Mechanisms of Cardiac Troponin Activation in Reconstituted Thin Filaments

Maria Eleni Moutsoglou
South Dakota State University

Follow this and additional works at: <https://openprairie.sdstate.edu/etd>



Part of the [Biochemistry Commons](#)

Recommended Citation

Moutsoglou, Maria Eleni, "A FRET Investigation into Molecular Mechanisms of Cardiac Troponin Activation in Reconstituted Thin Filaments" (2016). *Electronic Theses and Dissertations*. 682.
<https://openprairie.sdstate.edu/etd/682>

This Dissertation - Open Access is brought to you for free and open access by Open PRAIRIE: Open Public Research Access Institutional Repository and Information Exchange. It has been accepted for inclusion in Electronic Theses and Dissertations by an authorized administrator of Open PRAIRIE: Open Public Research Access Institutional Repository and Information Exchange. For more information, please contact michael.biondo@sdstate.edu.

A FRET INVESTIGATION INTO MOLECULAR MECHANISMS OF
CARDIAC TROPONIN ACTIVATION IN RECONSTITUTED THIN FILAMENTS

BY

MARIA ELENI MOUTSOGLOU

A dissertation submitted in partial fulfillment of the requirements for the

Doctor of Philosophy

Major in Biochemistry

South Dakota State University

2016

A FRET INVESTIGATION INTO MOLECULAR MECHANISMS OF
CARDIAC TROPONIN ACTIVATION IN RECONSTITUTED THIN FILAMENTS

This dissertation is approved as a creditable and independent investigation by a candidate for the Doctor of Philosophy in Biochemistry degree and is acceptable for meeting the dissertation requirements for this degree. Acceptance of this does not imply that the conclusions reached by the candidate are necessarily the conclusions of the major department.

David P. Cartrette, Ph.D.
Academic Advisor

Date

David P. Cartrette, Ph.D.
Head, Department of Chemistry and Biochemistry

Date

Dean, Graduate School

Date

*This dissertation is dedicated to Ray's Corner:
good people, strong drinks.*

ACKNOWLEDGEMENTS

This research was supported by the National Institutes of Health (NIH) grant RO1 HL097106 and the Center for Biological Control and Analysis by Applied Photonics (BCAAP).

My sincerest thanks to Dr. GiHo H. Kim for providing support in obtaining the time-resolved FRET distances and FCS traces, and for his friendship and kind mentoring over the years. Thank you to Dr. Pieter de Tombe and Mohit Kumar at Loyola for their services in providing the functional assessment of mutated troponin constructs.

Thank you to my committee, Dr. David Cartrette, Dr. Adam Hoppe, Dr. James Rice, and Dr. Nicole Klein, for their time and efforts in helping me obtain my degree.

Thank you to my PI, Dr. John Robinson, for his guidance in my work, implementing a no spending limit policy for my precious fluorophores, and letting me set up speakers in the lab without complaint (loud music is the best enzyme for scientific results). Thanks to Troy Lackey, for taking me with patience under his wing when I was a fledgling scientist back in 2010, and teaching me how to make and run the most pristine SDS-PAGE gels. Thank you to Dr. Steve Wu, who helped me develop skills in molecular biology, and for taking a few of the JMR lab members to Flogging Molly in NYC. Thanks to Dr. Shalini Low-Nam, for both her friendship and mentorship. Thank you to Dr. Cartrette, for hitting a home run for me in the bottom of the ninth. Thank you to lovely Stephanie Jensen in the office, who always went out of her way to help me out. And of course, thanks to my adventurous and intelligent protégées who joined me in the lab over the years, for your willingness to make me endless amounts of buffers, use lasers

to startle Gooley Gus (RIP), and accompany me on visits to Chicken Sam in many frantic attempts to purify myosin. May all our troponins continue to tingle!

I may have quit halfway through this intellectual adventure if not for my family and friends, and their ability to minimize the stress that comes with obtaining a graduate degree. My thanks and love go to Tyrel Deutscher, who has given me valuable peace of mind over the years. Thank you to my dad (Alex) and mom (Joyce), and clever and beautiful sisters (Daphne, Nefeli, and Eleni), who maintained their support even during my trying times of financial destitution, physical exhaustion, and mental duress.

CONTENTS

ABBREVIATIONS	ix
LIST OF FIGURES	xi
LIST OF TABLES	xiv
ABSTRACT	xvi
THE CALCIUM-DEPENDENT STRUCTURE AND DYNAMICS OF THE C- TERMINAL REGION OF CARDIAC TROPONIN I	1
1 INTRODUCTION	3
1.1 An overview of cardiac muscle activation	3
1.2 Troponin: the command center for muscle activation	10
1.2.1 Troponin C: the Ca ²⁺ -binding subunit of the thin filament	13
1.2.2 Troponin T: the tropomyosin-binding anchor of the thin filament	13
1.2.3 Troponin I: the inhibitory subunit of the thin filament	14
1.2.4 Sample stability and resolution limits: barriers to resolving native protein structure and dynamics	17
1.2.5 Crystal structures and proposed atomistic models of Tn	19
1.3 Mutations in C-TnI associated with heart failure	22
1.4 A multi-site FRET assay in a most native environment	23
2 METHODS	25
2.1 Native protein purification	25
2.1.1 Acetone powder from bovine left ventricle tissue	25
2.1.2 Purification of tropomyosin from acetone powder	25
2.1.3 Purification of actin from acetone powder	26
2.2 Mutagenesis and DNA amplification and purification	27
2.3 Bacterial expression and recombinant protein purification	28
2.3.1 Preparation of troponin C	28
2.3.2 Preparation of troponin I	30
2.3.3 Preparation of troponin T	31
2.4 Development of FRET assay	31
2.4.1 Calculation of the Forster critical distance	31
2.4.2 Dye labeling of proteins	33
2.5 Troponin and regulated actin reconstitution	34
2.6 Steady-state fluorescence spectroscopy	35
2.7 Epifluorescence imaging of regulated actin filaments	36
2.8 Time-resolved fluorescence spectroscopy	37
2.8.1 Time-correlated single photon counting (TCSPC)	37
2.8.2 Fluorescence correlation spectroscopy	38
2.8.3 Statistical analysis	39
2.9 Functional characterization of mutated Tn	39
2.9.1 Tn exchange into skinned cardiomyocytes	39
2.9.2 Muscle mechanics experiments	40
2.9.3 Statistical analysis	41
3 RESULTS & DISCUSSION	42
3.1 Designing a FRET assay on troponin	42
3.1.1 Donor and acceptor fluorophore selection	45

3.1.2 Theoretical FRET efficiencies and $C\alpha$ distances	48
3.1.3 Preparing the FRET assay in regulated actin	49
3.2 Quality assessment of singly- and doubly-labeled regulated actin	55
3.3 Epifluorescence imaging reveals stability of filaments under various conditions	55
3.3.1 Tn binding to Tm-actin is dependent on ionic strength	55
3.3.2 Incubation time affects Tn binding to Tm and actin	57
3.3.4 The quantity of Tm affects filament stability	59
3.3.5 Proteins did not undergo proteolysis after reconstitution and incubation	60
3.3.6 Ca^{2+} does not affect the physical characterization of regulated actin filaments	60
3.4 FCS as a filament screening tool	63
3.5 TCSPC measurements of regulated actin filaments.....	67
3.6 Calculating FRET efficiency and inter-dye distance	70
3.7 Inter-dye distances reveal the dynamics of the C-TnI	75
3.7.1 Dynamics of the C-TnI with respect to the N-lobe of TnC.....	75
3.7.2 Dynamics of the C-TnI with respect to the inter-lobe linker of TnC.....	80
3.7.3 Dynamics of the C-TnI with respect to the C-lobe of TnC.....	81
3.7.4 The majority of Ca^{2+} -dependent dynamics are within TnI residues 182-211	83
3.8 Functional characterization of a FRET pair in the switch region and N-lobe of TnC 88	
3.9 Actin ultimately determines Tn structure and dynamics during activation	91
3.9.1 The role of TnI in the steric blocking mechanism of thin filament activation.....	92
3.9.2 Minimal switch region dynamics: implications on the “drag and release” mechanism.....	93
3.9.3 The order in the disorder: the fly-casting mechanism of C-TnI.....	95
3.10 Mutations in the C-TnI emphasize its functional importance.....	96
MECHANISMS OF ACTION OF INOTROPIC AGENTS, MYOSIN BINDING, AND PKA-MEDIATED PHOSPHORYLATION OF TnI TO MODULATE CARDIAC THIN FILAMENT ACTIVATION AND CALCIUM SENSITIVITY	98
4 INTRODUCTION	100
5 METHODS	105
5.1 Purification of myosin from chicken pectoralis major muscle.....	105
5.2 Myosin digest into subfragment-1.....	106
5.3 Phosphorylation of TnI in regulated actin	106
5.4 Steady state fluorescence spectroscopy	108
5.4.1 Calcium titrations	108
5.4.2 Concentration of free calcium	109
5.4.3 Myosin S1 titrations	110
5.4.4 Determining EC_{50} of EGCG.....	110
5.5 Cosedimentation assays.....	111
5.5.1 Chemomechanical binding assay	111
5.5.2 S1 binding to regulated actin with PKA treatment and small molecules.....	112
5.6 Statistical analysis.....	112
6 RESULTS	113
6.1 Two-colored FRET in regulated actin filaments	113
6.2 Characterizing the binding of myosin subfragment-1	115
6.3 PKA-mediated phosphorylation of TnI Ser-23/24.....	118
6.4 Physical characterization of regulated actin	119
6.5 Determining the concentration of free Ca^{2+}	124
6.6 Screening for Ca^{2+}-induced activation	125
6.6.1 Bepridil and S1 both increased Tn activation and Ca^{2+} sensitivity.....	126

6.6.2 EGCG and TnI phosphorylation reduced Ca ²⁺ sensitivity	129
6.6.3 Ca ²⁺ sensitivity is correlated to the Ca ²⁺ -depleted FRET efficiency	129
6.7 Screening for myosin-induced activation	129
6.7.1 S1-induced activation of Tn occurs independently of Ca ²⁺	130
6.7.2 Bepridil eliminates S1-induced activation of Tn	130
6.7.3 EGCG and PKA treatment reduce myosin sensitivity	130
6.8 Control measurements for PKA treatment.....	133
6.9 S1 binds to rAc with small molecules and PKA treatment.....	135
6.10 A high throughput single point drug screen	135
7 DISCUSSION	138
7.1 Cooperative activation by Ca ²⁺ is dependent on the presence of rigor-S1	139
7.2 Cys84Ser substitution in TnC prevents levosimendan binding	141
7.3 Bepridil and rigor-S1 promote a stabilized open conformation of the N-lobe to increase Ca ²⁺ sensitivity	142
7.4 The effect of TnI Ser-23/24 phosphorylation on Tn activation	143
7.5 EGCG may destabilize Ca ²⁺ -dependent allosteric changes in Tn	146
7.6 Ca ²⁺ sensitivity reflects the level of Tn activation under resting conditions	148
7.7 A drug screening tool—and beyond	149
APPENDIX	151
WORKS CITED	165
CURRICULUM VITAE.....	179

ABBREVIATIONS

AEDANS	5-(acetamidoethyl)-aminonaphthelene-1-sulfonic acid
AF	Alexa Fluor®
ATP	adenosine triphosphate
Act	actin
amp	ampicillin
BME	2(β)-mercaptoethanol
C-Tn(I/C/T)	carboxy-terminus of Tn(I/C/T)
CCD	charge-coupled device
CM	carboxymethyl or cardiomyopathy
CR	central region of TnT
cryo-EM	cryo-electron microscopy
cTn(I/C/T)	cardiac Tn(I/C/T)
D	donor only
DA	donor-acceptor
DC1	principle dichroic mirror
DCM	dilated cardiomyopathy
DDPM	N-(4-dimethylamino-3,5-dinitrophenyl)maleimide
DEAE	diethylaminoethyl
DMSO	dimethyl sulfoxide
DNA	deoxyribose nucleic acid
DTT	dithiothreitol
EDTA	ethylenediaminetetraacetic acid
EGCG	epigallocatechin gallate or epigallocatechin-3-gallate
EGTA	ethylene glycol tetraacetic acid
F-actin	filamentous actin
FCS	fluorescence correlation spectroscopy
FRET	Förster resonance energy transfer
fsTn(I/C/T)	fast skeletal Tn(I/C/T)
G-actin	globular actin
GnHCl	guanidine hydrochloride
HCM	hypertrophic cardiomyopathy
HTS	high throughput screening
IDR	intrinsically disordered region
IR	inhibitory region of TnI
kan	kanamycin
LB	labeling buffer
L-B	lysogeny broth
MHC	myosin heavy chain
MOPS	3-(N-morpholino)propanesulfonic acid
mcTn(I/C/T)	mouse cardiac Tn(I/C/T)
MTS	Manning-Tardiff-Schwartz atomistic model of cTn
myc-TnT	N-terminal tag (sequence: N-EQKLISEEDL-C) on TnT
N-Tn(I/C/T)	amino-terminus of Tn(I/C/T)
NMR	nuclear magnetic resonance

PDBID	Protein Data Bank identification
PKA	protein kinase A
PKC	protein kinase C
PKD	protein kinase D
RCM	restricted cardiomyopathy
rAc	regulated actin
rcTn(I/C/T)	rat cardiac Tn(I/C/T)
S1	myosin subfragment-1
SABS	second actin binding site of TnI
SDS-PAGE	sodium dodecyl sulfate polyacrylamide gel electrophoresis
SR	sarcoplasmic reticulum
ss	steady state or slow skeletal
sTn(I/C/T)	skeletal Tn(I/C/T)
TCSPC	time-correlated single photon counting
Tm	tropomyosin
Tn	troponin
TnC	troponin C
TnI	troponin I
TnT	troponin T
TnT(T1)	amino-terminal end of TnT
TnT(T2)	carboxy-terminal end of TnT
tr	time-resolved
WB	working buffer

Amino Acids (three letter code, one letter code)

Small

Glycine	Gly, G
Alanine	Ala, A

Nucleophilic

Serine	Ser, S
Threonine	Thr, T
Cysteine	Cys, C

Hydrophobic

Valine	Val, V
Leucine	Leu, L
Isoleucine	Ile, I
Methionine	Met, M
Proline	Pro, P

Aromatic

Phenylalanine	Phe, F
Tyrosine	Tyr, Y
Tryptophan	Trp, W

Acidic

Aspartic acid	Asp, D
Glutamic acid	Glu, E

Amide

Asparagine	Asn, N
Glutamine	Gln, Q

Basic

Histidine	His, H
Lysine	Lys, K
Arginine	Arg, R

LIST OF FIGURES

Sections 1-3

Figure 1. Organization of the sarcomere showing the interdigitation of the thin and thick filaments.

Figure 2. A simplified schematic of Ca^{2+} - and myosin-dependent activation of the thin filament.

Figure 3. Structure of the Ca^{2+} -saturated cTn core.

Figure 4. Mouse cTnI and rat cTnC sequence alignment with human.

Figure 5. Multi-site FRET assay on troponin.

Figure 6. Emission spectra of FRET dye pairs, inter-C α distances, and theoretical FRET efficiencies for troponin.

Figure 7. Purification of rcTnC.

Figure 8. Purification of mcTnI.

Figure 9. Purification of rcTnT.

Figure 10. Purified troponin subunits.

Figure 11. Tropomyosin and F-actin purified from bovine left ventricle muscle.

Figure 12. Ionic strength affects Tn binding to Tm and actin.

Figure 13. Physical characterization of labeled regulated actin filaments.

Figure 14. Assessment of sample purity of reconstituted rAc.

Figure 15. Calcium does not affect the physical morphology of regulated actin.

Figure 16. Fluorescence correlation spectroscopy estimates the molecular weight of a freely-diffusing particle.

Figure 17. Dependence of the diffusion coefficients on molecular mass.

Figure 18. Lifetime measurements of donor-only and donor/acceptor rAc filaments.

Figure 19. Correcting the FRET efficiency with the acceptor labeling efficiency removes the influence of a donor-only population in Tn-DA-decorated filaments.

Figure 20. FRET efficiencies in Tn within thin filaments with and without Ca^{2+} .

Figure 21. Inter-dye distances in Tn reconstituted in thin filaments with and without Ca^{2+} .

Figure 22. Relative FRET efficiency and inter-dye distance changes upon Ca^{2+} binding to Tn within the thin filament.

Figure 23. Dynamics of the C-terminal region of TnI (residues 151 to 211) in reconstituted thin filaments.

Figure 24. Schematic model of the structure and displacement of the switch region and C-terminal end with respect to TnC under Ca^{2+} -saturated and Ca^{2+} -depleted conditions.

Sections 4-7

Figure 25. Functional characterization of wild type and mutated Tn.

Figure 26. A steady-state FRET assay for measuring Tn activation.

Figure 27. Purification of myosin from chicken pectoralis muscle.

Figure 28. Chymotryptic digest of myosin into subfragment-1.

Figure 29. Quantification of PKA-dependent TnI phosphorylation.

Figure 30. Functional characterization of mutated Tn.

Figure 31. Assessment of sample purity of thin filaments and myosin subfragment-1.

Figure 32. Chemical structures of small molecules.

Figure 33. Filament morphology of rAc-DA with small molecules, myosin S1, and PKA treatment.

Figure 34. Calibration of the concentration of free Ca^{2+} .

Figure 35. Effect of small molecules, PKA treatment, and S1 binding on the Ca^{2+} -dependent activation of regulated actin.

Figure 36. The effect of small molecules and Ca^{2+} on the activation of thin filaments by myosin.

Figure 37. Control measurements of PKA treatment of rAc titrated with Ca^{2+} .

Figure 38. Control measurements of treatment of reporter filaments with PKA titrated with S1.

Figure 39. SDS-PAGE shows myosin binding with small molecules and PKA treatment.

Figure 40. High throughput screening (HTS) strategy.

LIST OF TABLES

Table 1. Recombinant troponin proteins expressed in *Escherichia coli* and purified.

Table 2. Sarcomeric proteins (gene), their molecular weights, and molar extinction coefficients (ϵ) at 280 nm.

Table 3. Maleimide fluorophores used, where ϵ is the molar extinction coefficient at 280 nm, CF is the correction factor at 280 nm, Q is the quantum yield, λ_{abs} and λ_{em} are the absorption and emission maximum wavelengths, respectively.

In Appendix

Table A1. Fitting results of rAc-TCSPC measurements of donor-only regulated actin filaments.

Table A2. Fitting results of rAc-TCSPC measurements of donor/acceptor regulated actin filaments with ATTO655 on TnC residue 35.

Table A3. Fitting results of rAc-TCSPC measurements of donor/acceptor regulated actin filaments with ATTO655 on TnC residue 89.

Table A4. Fitting results of rAc-TCSPC measurements of donor/acceptor regulated actin filaments with ATTO655 on TnC residue 127.

Table A5. Correcting FRET efficiency with the acceptor labeling ratio.

Table A6. Non-corrected and f_a -corrected mean FRET efficiencies and inter-dye distances.

Table A7. FRET efficiency and inter-dye distance at acceptor position TnC35C.

Table A8. FRET efficiency and inter-dye distances at acceptor residue TnC89C.

Table A9. FRET efficiency and inter-dye distances at acceptor residue TnC127C.

Table A10. Calcium-induced changes in FRET efficiency and inter-dye distance in Tn within thin filaments.

Table A11. FRET efficiency and inter-dye distances from steady-state FRET and theoretically-derived from the MTS molecular model.

Table A12. Fitting results for Ca^{2+} titrations of PKA-treated thin filaments, and thin filaments with PKA treatment, small molecules, and S1.

Table A13. Fitting results for S1 titrations of reporter filaments.

Table A14. Fitting results for Ca^{2+} titrations of phosphorylated reporter filaments, and filaments mock-treated with PKA or ATP.

Table A15. Fitting results for S1 titrations of phosphorylated reporter filaments, and filaments mock-treated with PKA or ATP.

ABSTRACT

A FRET INVESTIGATION INTO MOLECULAR MECHANISMS OF
CARDIAC TROPONIN ACTIVATION IN RECONSTITUTED THIN FILAMENTS

MARIA ELENI MOUTSOGLOU

2016

Cardiomyopathies (CM) are the leading cause of death in America, and can develop from mutations in sarcomeric proteins, leading to altered protein structure and function. Current therapies target upstream signaling pathways to treat the symptoms of heart failure, but are associated with increased mortality by affecting downstream signaling pathways and other muscle types. Rational drug design can develop therapies to treat CM at the protein level. However, a detailed knowledge of how sarcomeric proteins regulate muscle contraction is required. Muscle contraction occurs through a cyclic interaction between actin thin and myosin thick filaments, regulated by intracellular Ca^{2+} concentration. Troponin (Tn), the Ca^{2+} -binding protein in muscle, allosterically regulates actin and myosin interactions (crossbridge formation) by facilitating the release of two troponin I (TnI) actin binding sites at high Ca^{2+} , the inhibitory region (IR) and the second actin binding site (SABS). The mechanism to remove TnI crossbridge inhibition is not well understood. A multi-site Förster resonance energy transfer (FRET) assay in cardiac Tn in reconstituted thin filaments was used to investigate the Ca^{2+} -dependent structure and dynamics of the SABS, and show current theories behind Tn activation are biased using structures developed in isolated Tn. The SABS underwent large Ca^{2+} -dependent conformational changes, suggesting this region plays an important structural role in

muscle regulation. The mechanisms behind thin filament Ca^{2+} sensitivity were also assessed to facilitate rational drug design. Titrations monitoring FRET efficiency (Tn activation) by Ca^{2+} and myosin showed the drug bepridil works in a similar mechanism to rigor myosin binding, which in native muscle increases Ca^{2+} sensitivity. The Ca^{2+} -desensitizing drug EGCG, however, does not work in a similar mechanism to protein kinase A (PKA)-mediated phosphorylation of cardiac TnI, which in native cardiac muscle disrupts residues in TnC responsible for binding Ca^{2+} at Site II. A single point drug screen was developed for Tn in reconstituted thin filaments using a novel correlation between the Ca^{2+} -depleted FRET efficiency and Ca^{2+} sensitivity. This study shows the utility of performing Tn structural studies in an environment that mimics native muscle.

THE CALCIUM-DEPENDENT STRUCTURE AND DYNAMICS OF THE C-
TERMINAL REGION OF CARDIAC TROPONIN I

ABSTRACT SECTIONS 1-3

Heart failure is the leading cause of death in the United States. To facilitate drug design, the molecular mechanisms behind muscle regulation must be resolved. Cardiac muscle contraction occurs through the Ca^{2+} -dependent cyclic interaction between thin and thick filaments, regulated by the heterotrimeric protein complex troponin (Tn). At low Ca^{2+} , the C-terminus of cardiac troponin I (C-cTnI) has two regions bound to actin to inhibit myosin binding (crossbridge formation): the inhibitory region (IR) and the second actin binding site (SABS). At high Ca^{2+} , the Herzberg model of Tn activation suggests the switch region binds an exposed hydrophobic pocket of N-TnC, dragging the IR off actin to remove crossbridge inhibition. While structural studies have attempted to describe the mechanism of Tn activation, the Ca^{2+} -dependent nature of C-cTnI remains elusive due to the complex inter- and intramolecular interactions between the proteins of the thin filament. This study attempts to resolve the structure and dynamics of C-cTnI within the reconstituted thin filament using a multi-site Förster resonance energy transfer (FRET) assay. Epifluorescence imaging and fluorescence correlation spectroscopy were used to monitor filament quality prior and during measurements. Ensemble time-resolved FRET was used to derive the inter-dye distances with and without Ca^{2+} . Regions of cTnC displayed independent Ca^{2+} dynamics, most evident in the inter-lobe linker. The switch region had minimal Ca^{2+} -dependent dynamics (≈ 0.5 nm decrease in inter-dye distance with Ca^{2+}), and maintained a ≈ 5 nm distance from the regulatory core of Tn, ≈ 3 nm

farther than predicted by the Ca^{2+} -saturated crystal structure of cTn. Steady-state FRET measurements performed on isolated cTn with donors on cTnI(151-189) and an acceptor on cTnC89 showed good agreement with atomistic model-derived distances, suggesting actin and tropomyosin (Tm) alter the overall architecture of cTn. Functional studies in isolated rat ventricular fibers monitored force as a function of Ca^{2+} , and showed mutagenesis in the cTnI switch region and N-lobe of cTnC did not alter the native function of cTn. cTnI177 appears to act as a pivot point separating the static switch region and the highly dynamic C-terminal end of cTnI. Residues after cTnI177 underwent the greatest Ca^{2+} -dependent changes (distances decreased by ≈ 1.5 nm), leading to the designation of this region as the SABS. The binding of the SABS on actin may account for the apparent displacement of the switch region from the cTn core. This suggests the Hertzberg model may incorrectly assign the role of the switch region; instead, some other mechanism may account for the removal of the IR and SABS from actin.

1 INTRODUCTION

This dissertation is based on a study of the Ca^{2+} -dependent interactions between two thin filament regulatory proteins: troponins I and C. Mutations in the C-terminal region of cardiac troponin I are known to cause cardiomyopathies through an interruption in protein structure and function. However, the structure of this region of cardiac TnI is not well defined due to its highly mobile nature and complex interactions with both actin and troponin C. This author hypothesizes the C-terminal region of cardiac TnI plays a dynamic role in muscle regulation. In this study, a Förster resonance energy transfer (FRET) assay was developed to investigate the Ca^{2+} -dependent structure and dynamics of the C-terminal region of troponin I in reconstituted thin filaments. The presence of tropomyosin and actin may influence the structure of cardiac troponin, and the mechanisms of troponin activation currently presented in literature may be biased from structural studies performed on troponin in isolation. An overview of basic muscle contraction is given below to understand how proteins in the heart work together to regulate myocardial activation.

1.1 An overview of cardiac muscle activation

In 2009, the Center for Disease Control (CDC) stated heart disease was the leading cause of death in the United States.¹ Cardiomyopathies result from functional changes or a weakening in heart muscle, often as a result of mutations in sarcomeric proteins. While current therapies attempt to slow the progression of heart disease by addressing symptoms, direct therapies targeting sarcomeric proteins (called sarcomeric modulators) would be more effective in reducing mortality by eliminating some of the negative side effects of current therapies.² In order to facilitate the development of

informed drug design, the underlying mechanisms governing cardiac muscle regulation must be resolved.

Cardiac muscle is striated muscle composed of fibrous myocytes (heart muscle cells). Myocytes contain myofibrils comprised of bundles of sarcomeres. Sarcomeres are the repeating contractile unit of muscle cells containing a network of proteins with two types of filaments: thin and thick. Following a change in action potential (depolarization) in myocytes, the sarcoplasmic reticulum (SR) releases Ca^{2+} into the myofibrils. Intracellular Ca^{2+} regulates muscle contraction at the level of the thin filament by interacting with the troponin (Tn) complex.³ When cytosolic $[\text{Ca}^{2+}]$ reaches $\approx 10 \mu\text{M}$, conformational changes in the thin filament cause thin and thick filaments to slide past each other (contraction), mediated by crossbridge interactions between actin protomers and myosin catalytic heads.⁴⁻⁵ This is known as the sliding filament model, coined by Huxley and Hansen in 1954.⁴ Ryanodine receptors in the SR facilitate Ca^{2+} release and its subsequent uptake via the sarco/endoplasmic reticulum Ca^{2+} -ATPase (SERCA), leading to muscle relaxation.⁶ A schematic view of the relaxed and contracted sarcomere is shown in Figure 1.

Thin filaments are repeating structural units, where each functional unit is composed of seven actin monomers, one tropomyosin (Tm) dimer, and one Tn complex. Tn is composed of troponin T (TnT, Tm-binding), troponin C (TnC, Ca^{2+} -binding), and troponin I (TnI, ATPase inhibition). Globular α -actin (G-actin) monomers polymerize to form F-actin in a double helix with an axial rise of $\approx 27.6 \text{ \AA}$.⁷

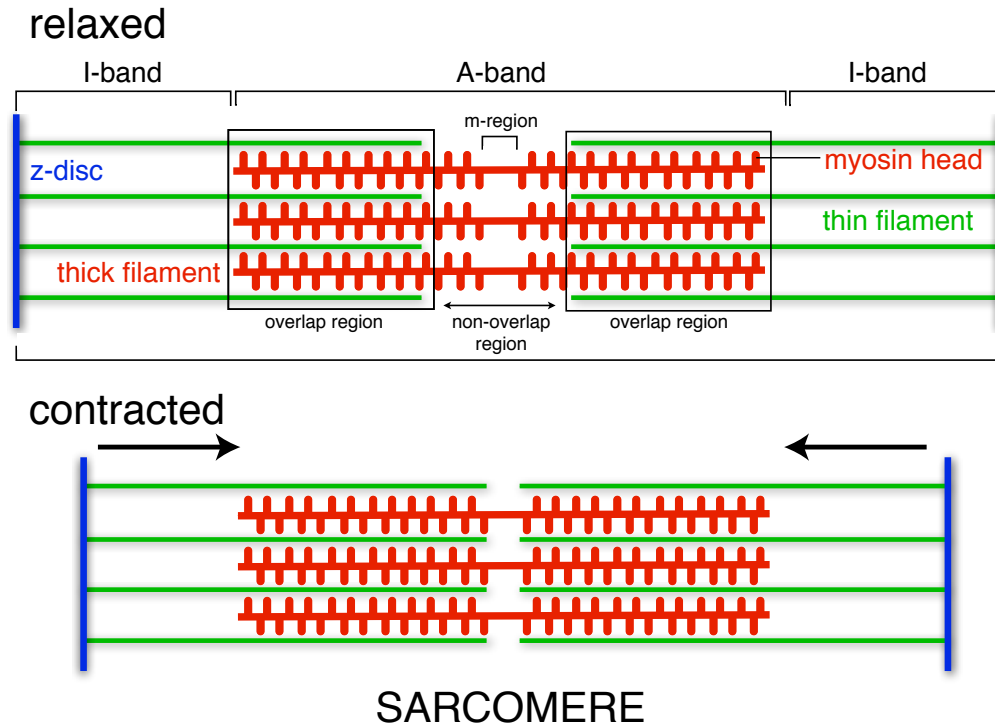


Figure 1. Organization of the sarcomere showing the interdigitation of the thin and thick filaments. ATP hydrolysis by myosin motors causes filaments to slide past each other, shortening sarcomere length. Intracellular $[Ca^{2+}]$ controls myosin heads, cyclically attaching and detaching from actin during relaxation and contraction. Labeled are thin filaments (green) composed of troponin, tropomyosin, and actin; thick filaments (red) composed primarily of myosin; Z-discs, composed of α -actinin, define a sarcomere unit and crosslink the thin filaments; overlap regions, where myosin overlaps actin thin filaments; the non-overlap region, absent thin filaments; the I-bands, absent myosin; the A-band, the length encompassing one thick filament; and m-region, portion of the thick filament without myosin heads.

The actin structure is divided into four subdomains: subdomains 3 and 4 in the inner domain of one actin monomer interact with subdomains 3 and 4 of an adjacent monomer; subdomains 1 and 2 in the outer domain face outward, where subdomain 1 provides the binding site for myosin heads.⁸ Actin filaments are anchored to the Z-discs (Figure 1), which regulate the length of the thin filament.⁹ Tm is a rod-like coiled-coil dimer that acts as a molecular ruler. Tm runs along F-actin, providing binding sites for the N-terminal tail of TnT at every seventh actin protomer, ensuring an equal distribution of Tn every ≈ 40 nm.¹⁰⁻¹¹ Tm binds in the grooves of F-actin between subdomains 1 and 3 (close to the myosin binding site),¹² with a tail-to-tail overlapping region between Tm molecules.¹³

Thick filaments are composed of myosin-II, which is divided into two regions. The N-terminal end is composed of two motor or catalytic domains (globular heads). Each motor domain associates with two light chains (regulatory and essential) and a heavy chain. The C-terminal end is composed of an α -helical tail that forms a coiled-coil with the heavy chain.¹⁴ The motor domain is termed subfragment-1 (S1), and protrudes outward from the rigid filamentous region of bundled myosin tails (Figure 2). S1 is an ATPase catalyzing the hydrolysis of adenosine triphosphate (ATP) into adenosine diphosphate (ADP) and inorganic phosphate (P_i). S1 binding to actin facilitates the release of ADP and P_i .¹⁵

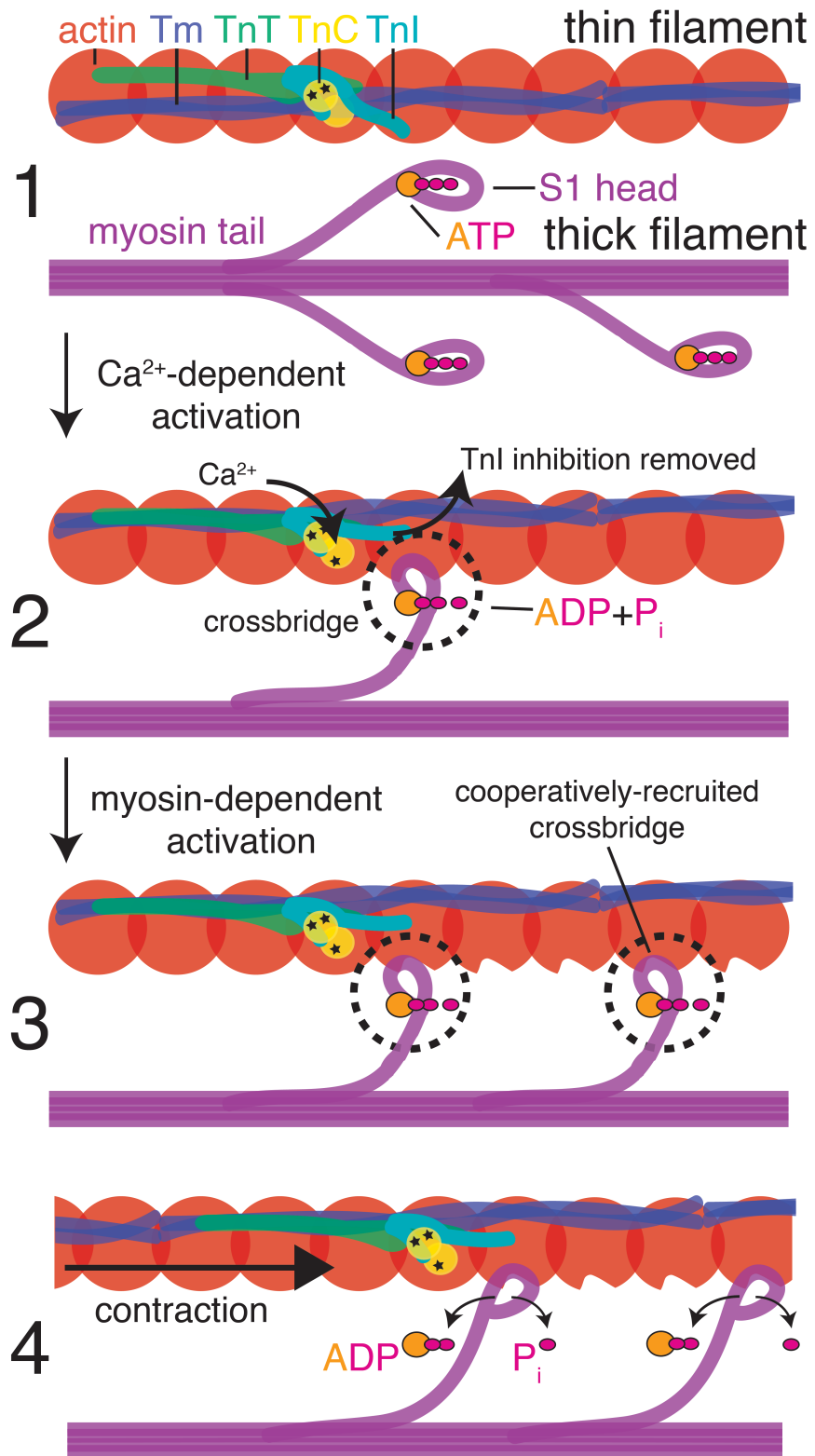


Figure 2

Figure 2. A simplified schematic of Ca^{2+} - and myosin-dependent activation of the thin filament. One regulatory unit is composed of seven actin protomers (red circles), one α -helical Tm dimer (blue), and one Tn complex composed of TnT (green), TnI (cyan), and TnC (yellow). For simplicity, actin is depicted as a single, straight filament; in native muscle, F-actin is a double helix composed of two strands of actin. When muscle is relaxed (state **1**) at low Ca^{2+} , TnC has a $\text{Mg}^{2+}/\text{Ca}^{2+}$ ions (black stars) bound to Sites III and IV. The TnI inhibitory region (IR) and second actin binding site (SABS) are bound to actin, forcing Tm in a position to prevent myosin binding. The thick filament is composed of myosin, where myosin tails are intertwined, and the catalytic heads (S1) protrude outward. At state **1**, myosin has ATP bound, and is not interacting with actin. When intracellular Ca^{2+} increases at state **2**, Ca^{2+} binds to Site II in TnC causing Ca^{2+} -dependent activation of the thin filament. Conformational changes propagate through Tn, causing the release of the IR and SABS from actin, allowing Tm to move away from myosin S1 binding sites. Actin activates the S1 ATPase, where crossbridge formation leads to hydrolysis of ATP into ADP and inorganic phosphate (P_i), with P_i is still associated with the S1 head. Energy from ATP hydrolysis forces S1 into a higher energy conformation. S1 binding to actin is cooperative, allowing for downstream crossbridge formation (state **3**). When ADP and P_i are released from S1 (state **4**), S1 changes conformation to a lower energy state, dragging the thin filament to contract (powerstroke). S1 then binds ATP and releases actin, and Ca^{2+} is released from TnC; the thin and thick filaments thus to return to state **1**.

The schematic in Figure 2 describes the Ca^{2+} -and myosin dependent activation of the thin filament leading to contraction. At low Ca^{2+} (Figure 2, state **1**), Tn is in an inactive conformation, with the inhibitory region (IR) and second actin binding site (SABS) of TnI bound to actin, forcing Tm in a position that blocks myosin binding sites on actin to prevent crossbridge formation.¹⁶ At high Ca^{2+} (Figure 2, state **2**), Ca^{2+} binds to Site II of TnC, causing conformational changes in Tn that promote IR and SABS release from actin.¹⁷⁻¹⁸

Tm is free to move away from the myosin binding sites, allowing crossbridge formation. S1 hydrolyzes ATP, forcing the catalytic head into a higher energy conformation, with both P_i and ADP still associated with S1.¹⁹⁻²⁰ Myosin then binds actin in this higher energy state. More myosin heads are cooperatively recruited to bind to actin (Figure 2, state **3**). Figure 2, state **4** shows the actin-activated release of ADP and P_i from S1,²¹ causing S1 to change to a lower energy conformation, dragging the thin filament along in the powerstroke (contraction).²² When ATP binds to S1, myosin releases actin, leading to relaxation. This cycling of ATP by myosin and actin is known as the crossbridge cycle.

The detailed mechanism of activation of the thin filament to promote myosin binding is still under investigation. One proposed mechanism is the steric blocking model: in the absence of Ca^{2+} , Tm blocks myosin-binding positions on actin due to the inhibitory properties of TnI (as described previously). When Ca^{2+} binds to TnC, conformational changes in Tn cause TnI to remove its inhibitory properties, allowing Tm to move away from the myosin binding site, promoting myosin binding and ATPase activity. Another proposed mechanism is the cooperative/allosteric model, which

emphasizes the importance of actin conformational changes during activation to promote myosin binding.²³⁻²⁵ Further studies are needed to verify these mechanisms.

In the next section, more detail is given to the structure and function of the Tn complex as understood and presented in contemporary scientific literature. This is useful in understanding why this study utilized the entire thin filament to investigate TnI in an attempt to mimic the native muscle environment. Some of the mechanisms of Tn activation and TnI structure outlined in the Introduction will be revisited in the Results and Discussion section to compare and contrast to the conclusions reached by this study.

1.2 Troponin: the command center for muscle activation

In the sarcomere, contracted and relaxed states exist in a dynamic equilibrium, where Ca^{2+} transients and other modifications shift the balance. Muscle contraction occurs when a certain fraction of Tn is in the active state. The components of cardiac Tn dynamically interact to modulate muscle activation using allosteric and cooperative mechanisms to translate the signal across the myofilament. Tn activation itself can be modulated by covalent and non-covalent modifications, including Ca^{2+} binding, crossbridge formation, post-translational modifications, mutations, and intracellular acidification. Changes in these modifications contribute to the contractile dysfunction associated with heart failure.²⁶

Tn uses allostery to control activation: conformational changes in Tn are propagated along the thin filament to promote crossbridge formation. Tn is able to fulfill this role due to its two distinct subdomains: the N-terminal region of TnT, which grips the Tn complex onto the Tm-actin filament; and the regulatory core of C-TnT, TnI and TnC. These domains are mainly composed of α -helices connected by flexible linkers.²⁷

Figure 3 shows the Manning-Tardiff-Schwartz (MTS) molecular model, with certain regions of TnT, TnI, and TnC discussed in more detail in the following sections. The MTS model utilized the 52kDa cardiac crystal structure of Tn, and was used as a reference in the Results and Discussion section. In the following text, “on” and “open” may be used interchangeably to describe the active state of Tn, and “off” and “closed” may be used to describe the inactive state of Tn.

Understanding how Tn translates on or off signals to actin during activation is imperative to a complete understanding muscle regulation. Of particular importance are the unique structure-function relationships between actin and TnI (the inhibitory protein), and TnI and TnC (the Ca^{2+} binding protein). This assay was designed to monitor the structural transition of C-TnI with respect to three specific sites on TnC, allowing for a triangulation of the relative position C-TnI during activation, and broaden the understanding of the Ca^{2+} -induced dynamics between TnI and TnC. Though nuclear magnetic resonance (NMR) spectroscopy and X-ray crystallography have given insights into the Ca^{2+} -saturated and Ca^{2+} -depleted structural nature of Tn, this assay was designed to directly probe the Ca^{2+} -dependent dynamics of C-TnI in relation to TnC reconstituted into thin filaments in solution. Using thin filaments as a simple biochemical model²⁸ for muscle activation yields insight into the behavior of Tn in the presence of Tm and actin.

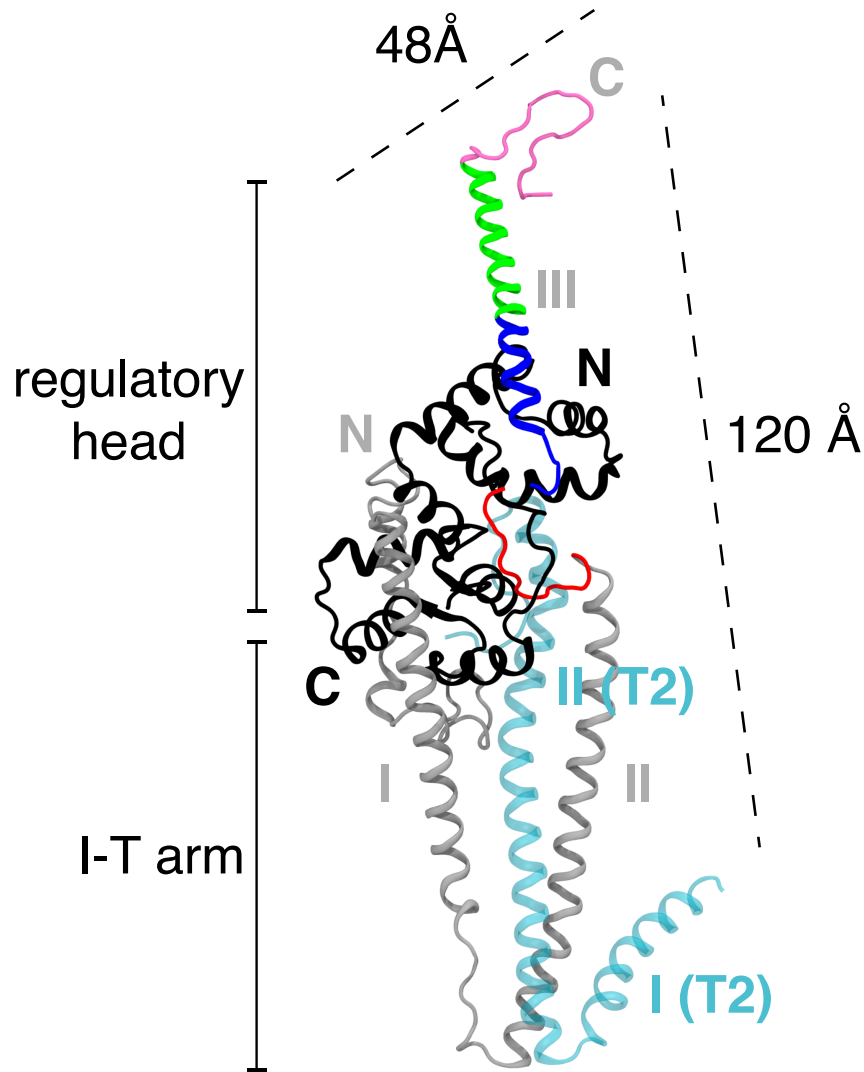


Figure 3. Structure of the Ca²⁺-saturated cTn core. Ribbon representation of the MTS molecular model of Ca²⁺-bound cTn, where TnI (grey), TnT (T2) (cyan), and TnC (black) are shown. Helices I and II of the T2 region of TnT and helices I-III of TnI are labeled. For the C-terminal region of TnI, the inhibitory region (residues 138-149, red), the switch region (residues 151-167, blue), the mobile domain (residues 168 to 189, green), and the C-terminal end (residues 190 to 211, pink). The switch region is bound to the hydrophobic pocket of the N-lobe of TnC.

1.2.1 Troponin C: the Ca²⁺-binding subunit of the thin filament

Troponin C is an ≈18 kDa, 161-residue protein known as the Ca²⁺-sensitive switch of the myofibril. Cardiac TnC is composed of two globular lobes connected by a flexible linker.²⁹ The N- and C-lobes (N: amino terminus; C: carboxy terminus) each contain two EF-hand structural motifs (helix-loop-helix) that bind divalent cations at sites numbered I-IV (N-ward to C-ward). Sites III and IV in the C-lobe constitutively bind Mg²⁺ or Ca²⁺. Sites I and II in skeletal TnC (sTnC) bind Ca²⁺ at physiological levels,³⁰ but only Site II in cTnC binds Ca²⁺.³¹ Site I is unable to bind Ca²⁺ due to mutations in two acidic residues responsible for coordinating Ca²⁺ (D29L, D31A), and an insertion of a valine at residue 28.³² The chelation residues coordinating Ca²⁺ at Site II are D65, D67, E76, S69, and T71.³³ When Ca²⁺ binds to Site II, the N-lobe of cTnC partially opens, as opposed to a full opening in sTnC when two Ca²⁺ bind.³⁴⁻³⁵ This opening occurs through a structural rearrangement of the B and C helices, revealing a hydrophobic cleft where the switch region of TnI is thought to bind to stabilize the open conformation of the N-lobe of TnC.³⁵⁻³⁶ The C-lobe of TnC requires no other protein interactions to stabilize its open conformation.²⁹ Residues 44-66 of helix I of TnI bind to the C-lobe.^{27, 37} Due to the lobes' individual roles within TnC, the C-lobe has been termed the structural domain, and the N-lobe the regulatory domain.

1.2.2 Troponin T: the tropomyosin-binding anchor of the thin filament

Troponin T is a ≈36 kDa protein responsible for anchoring the Tn complex onto the thin filament through interactions with Tm. The N-terminus of TnT modulates ATPase activity, and the C-terminus interacts with Tm in a Ca²⁺-sensitive manner.³⁸⁻³⁹ TnT is a flexible, elongated protein with two distinct regions: T1, the Tm-binding region

(residues 1-181, human numbering); and T2, which interacts with the core of Tn (residues 181-288, human numbering).⁴⁰ Notably, T1 was removed to promote sample stability in the Takeda crystal structure, as this region increases aggregation of isolated Tn.²⁷ T1 has an isoform-specific N-terminal extension (residues 1-76) that is negatively charged due to its composition of mostly of aspartate and glutamate residues.⁴¹

Tobacman first suggested the N-terminal extension participates in Ca^{2+} -dependent regulation, where a deletion of the first 38 residues in bovine cTnT resulted in a decrease in ATPase activity.⁴² Chandra et al. suggested the ATPase activity inhibition conferred by the N-terminal deletion is due to changes in interactions at the Tm-Tm overlap region.⁴³

Residues 98-136 (human numbering) in the central region (CR) in T1 interact with the C-terminal region of Tm to affix Tn onto the actin filament,⁴⁴ and the N-terminal extension modulates this interaction.⁴⁵ Residues 183-200 form a flexible linker connecting T1 and T2 together. Helix II (residues 226 to 279) in T2 forms the I-T arm with helix II of TnI.²⁷ The C-terminal region of TnT in the I-T arm interacts with the C-lobe of TnC²⁷ and Tm.⁴⁶⁻⁴⁷ Interactions between the T2 region and TnI, TnC, and Tm occur in a Ca^{2+} -dependent manner,³⁹ and T2 has been shown to play a role in both Ca^{2+} -dependent regulation and in length-dependent activation.⁴⁵ The behavior of TnT during muscle regulation is modulated by protein kinase C (PKC)-mediated phosphorylation sites at Thr 194, 203, and 284, and at Ser 198, which can result in an increase or decrease in thin filament sensitivity, depending on the site phosphorylated.⁴⁸

1.2.3 Troponin I: the inhibitory subunit of the thin filament

Troponin I is a ≈ 24 kDa protein known as the inhibitory subunit of Tn. At intracellular $[\text{Ca}^{2+}] = 10^{-6}$ M, TnI inhibits crossbridge formation by preventing myosin

binding to actin (ATPase activity).⁴⁹ Absent other Tn subunits, TnI is still capable of inhibiting ATPase activity in the myofilament.⁵⁰ However, regulation of this inhibition requires the Ca^{2+} sensitivity of TnC.⁵¹⁻⁵² TnI and TnC interact in an antiparallel manner, where the N-terminus (residues 35-72) of TnI interacts with the C-terminus of TnC.

Post-translational modifications on TnI in the form of phosphorylation primarily down-modulate cardiac contractility. Cardiac TnI has an isoform-specific ≈ 32 -residue N-terminal extension with two protein kinase A (PKA)-dependent phosphorylation sites at serines at 23 and 24 (human numbering).⁵³ Ser-23/24 can also be phosphorylated by protein kinase D (PKD), causing reduced Ca^{2+} sensitivity of TnC.⁵⁴ Yasuda et al. used mice expressing non-phosphorylatable cTnI to show PKA-mediated phosphorylation at Ser-23/24 contributes significantly to cardiac relaxation.⁵⁵ When not phosphorylated, the extension stabilizes the N-terminus of TnC.⁵⁶ Phosphorylation increases Ca^{2+} release by destabilizing Ca^{2+} binding through changes in the interactions between the N-TnI with N-TnC.⁵⁷⁻⁵⁸ TnI also contains PKC-mediated phosphorylation sites at Ser-43/45, and on Thr144 in the inhibitory region (IR).⁵⁹ Phosphomimetic mutations at Ser-43/45 showed reduced thin filament sensitivity to Ca^{2+} .⁶⁰ Under Ca^{2+} -depleted conditions, Thr144 was shown to be involved in strong crossbridge-dependent activation of ATPase activity,⁶¹ suggesting Thr144 modulates crossbridge formation.

C- and N-TnI domains play structural and regulatory roles, respectively. Helix II (residues 91-136) of TnI forms a coiled-coil with helix II of TnT to form the I-T arm. The I-T arm and helix I of TnI (residues 44-80) enclose the C-lobe of TnC.²⁷ The regulatory region of TnI comprises residues 138-211. Included is the inhibitory region (residues 138-149), which interacts with actin under Ca^{2+} -depleted conditions^{17, 62} to inhibit myosin

ATPase activity (muscle contraction).⁵⁰ The structure of the IR for cTnI has not been resolved using X-ray crystallography, though FRET studies in cTn have predicted the IR switches from a β -turn coil into a quasi α -helix with Ca^{2+} .⁶³

Upon Ca^{2+} binding, the switch region (residues 151-167) binds to the partially-exposed hydrophobic pocket of the N-lobe of TnC, stabilizing the fully open state of the N-lobe. According to a model first developed by Herzberg, the binding of the switch region drags the IR off actin, removing its inhibitory effects from actin-tropomyosin.⁶⁴⁻⁶⁵ Residues 168-211 are required for full ATPase inhibition through Ca^{2+} -dependent interactions with actin (termed the second actin binding site, SABS).⁶⁶⁻⁶⁷ This region is composed of the mobile domain (residues 168-189) and C-terminal end (residues 190-211), and has been the subject of numerous studies. However, the complete structure, dynamics, and functional details of this region remain unresolved. The fly-casting mechanism has been proposed to describe the role of TnI(168-211): under Ca^{2+} saturating conditions, these residues are an intrinsically disordered region (IDR), and able to sample multiple potential binding sites on actin that catalyze a return to the off state upon Ca^{2+} release.⁶⁸ Deletion experiments, where the last 17 residues of sTnI were removed, showed the affinity of TnI for the thin filament decreases in the absence of this C-terminal region, suggesting interactions with actin and TnC are in a Ca^{2+} -dependent equilibrium.⁶⁹

The next sections include a brief overview of some of the proposed structures of different isoforms of C-TnI, and the mechanism in which C-TnI binds to either actin or TnC as understood in literature. This is helpful in discovering some of the drawbacks of the current methodology, and why structural biology investigations benefit when

performed in a more native environment. Also noted are the unresolved portions of cardiac and skeletal TnI structures. Of particular importance is the unresolved C-terminal region, the subject of this study.

1.2.4 Sample stability and resolution limits: barriers to resolving native protein structure and dynamics

A number of studies on skeletal and cardiac Tn have attempted to reveal the structure and dynamics of C-TnI, and identify specific interactions with TnC and actin. Unfortunately, due to sample stability issues or the resolution limits of the selected method, many studies were performed on free Tn, individual Tn subunits, or on Tn with amino acid deletions. This gives rise to the question of whether the Ca^{2+} -depleted structure/dynamics of the C-TnI can be fully understood in the absence of actin. X-ray crystallography is a useful method that provides high resolution 3D protein structure at atomic resolution. Progress in resolving the crystal structure of the entire cTn complex and Ca^{2+} -depleted cTn has been impeded by practical issues, such as sample aggregation or growing high quality crystals. To grow crystals, proteins are exposed to a non-native environment, where pH, ionic strength, temperature, and detergents used differ dramatically to the native muscle environment.⁷⁰ Solution conditions could promote proteins to settle into non-native structures. Additionally, more mobile regions of proteins cause disorder in the crystal lattice, altering X-ray diffraction and preventing resolution.⁷¹ NMR spectroscopy can resolve protein structure and dynamics in solution. However, NMR can only be used for proteins or peptides <40 kDa.⁷² Tn itself is a 75 kDa complex, and only an incomplete complex can be studied using NMR. To overcome the barriers in X-ray crystallography and NMR spectroscopy, this study utilized FRET spectroscopy to

resolve TnI-C structure and dynamics in solution. There is essentially no size limitation with FRET, therefore allowing the incorporation of FRET-labeled Tn into reconstituted thin filaments. Additionally, FRET can resolve large-scale conformational changes (≈ 10 Å) in large assemblies.⁷³ More detail into developing a FRET assay to study structural biology is given in the Results and Discussion section.

Equating skeletal Tn structure and function to cardiac Tn can also be problematic. While the amino acid sequences between cardiac, fast skeletal, and slow skeletal C-terminal regions of TnI are highly conserved,⁷⁴ there are some substantial structural differences in TnT, TnC, and TnI isoforms. cTnT has an 18 residue N-terminal extension that may affect the cooperative activation of the thin filament.⁷⁵ Comparing the results of deletion experiments in rabbit sTnT⁷⁶ and bovine cTnT⁴² shows the N-terminal extension in cTnT alters Ca^{2+} -dependent ATPase activity. In addition, sequence heterogeneity between fast skeletal (fs)TnT and cTnT suggests variations in structure impose a tissue-specific function for TnT.⁷⁷ As mentioned previously, cTnC does not bind Ca^{2+} at Site I, which effects the kinetics of the Ca^{2+} -sensitive inhibitory properties of TnI (switching of TnI off actin to TnC).⁷⁸ Ca^{2+} binding to cTnC induces only a partial opening of the N-lobe, compared to a full opening in sTnC. sTnI has no N-terminal extension, which includes PKA-mediated phosphorylation sites at Ser-23/24 in TnI, important for modulating the Ca^{2+} sensitivity of the TnC.⁷⁹

Structural studies performed in isolated or fragmented Tn or in individual Tn subunits can still give insight into the mechanism of activation. Of concern to molecular and atomistic modeling, however, is the inherent bias introduced by incorporating

structures developed from isolated Tn. Proposed models for both skeletal and cardiac C-TnI structure and function will be reviewed as presented in the literature.

1.2.5 Crystal structures and proposed atomistic models of Tn

The Takeda crystal structure of the Ca^{2+} -saturated cTn core

Takeda et al. solved Ca^{2+} -bound human cTn structures using X-ray crystallography in 2003 (human numbering will be used in this section).²⁷ In total, four structures were resolved: two 46 kDa structures (A and B, PDBID 1J1D), and two 52 kDa structures (A and B, PDBID 1J1E). The N-terminal extension of TnI and T1 region of TnT were removed to promote sample stability. TnI Helix III comprises residues 150-159 of the switch region, which is bound to the hydrophobic cleft of the Ca^{2+} -bound N-lobe of TnC. Helix III is followed by a flexible linker, where a glycine at residue 160 kinks helix IV (residues 164-189) to protrude rigidly outward from the core domain. Glycine is a small amino acid that destabilizes α -helices. Insufficient electron density prevented resolving the IR (138-147) and C-terminal end (192-211) most likely due to their mobile nature. At high Ca^{2+} , the IR is in an extended conformation to allow the switch region to interact with the N-lobe of TnC, suggesting under Ca^{2+} -depleted conditions, the IR changes both its position and potentially its conformation in order to bind to actin.

The Vinogradova fsTn crystal structures with and without Ca^{2+} bound

In 2005, Vinogradova et al. solved the Ca^{2+} -saturated and Ca^{2+} -depleted crystal structures of chicken fast skeletal (fs) Tn at 3.0 and 7.0 Å resolutions, respectively.⁸⁰ The disordered C-terminal region (last 40 residues) juts perpendicularly away from the Tn

core. In the absence of Ca^{2+} , the IR forms an α -helix and binds to actin. When Ca^{2+} binds to TnC, the IR helix extends to a loop, allowing the switch region to reach the hydrophobic cleft of the TnC N-lobe, corresponding to an ≈ 8 Å movement. The linker between the C- and N-lobes forms an α -helix. Vinogradova and colleagues suggest the disordered inter-lobe linker for TnC seen in the Takeda structure may be due to the absence of stabilizing interactions from the cardiac-specific N-terminal extension.

The Murakami atomistic model of sTn

In 2005, Murakami et al. used NMR to analyze a ≈ 52 kDa ternary sTn complex, showing the mobile domain (human cTnI160-210) of sTnI as a β -sheet flanked by two short α -helices.⁸¹ The mobile domain tumbled independently of the Tn core around a pivot point between TnI Gly160 and Lys164 (human cardiac numbering), suggesting a capacity for this domain to interact with actin under Ca^{2+} -depleted conditions. Under Ca^{2+} -saturated conditions, the C-terminal end was less mobile due to contact of the switch region with N-TnC. This is in agreement with anisotropy measurements in reconstituted thin filaments by Zhou et al., who showed the flexibility of C-TnI decreases when Ca^{2+} binds.⁸² Using the ratio of chemical shift differences at high and low Ca^{2+} , Murakami et al. showed there was greater mobility in residues sTnI170-180 (mcTnI199-211), with less mobility in sTnI140-169.

The Pirani/Vinogradova atomistic model of the Ca^{2+} -saturated and Ca^{2+} -depleted thin filament

In 2006, Pirani and Vinogradova et al. reconstructed the Ca^{2+} bound and unbound atomistic models of the thin filament using Tm, actin, and the Vinogradova fsTn crystal structures.⁸⁰ The model was aligned to electron microscopy (EM) images of isolated

skeletal thin filaments.⁸³ The EM/atomistic reconstruction of the thin filament showed an “extra appendage” that extended outward from Tn under Ca^{2+} -depleted conditions; this was attributed to C-TnI. This region branched outward from the I-T arm to form a bridge between two actin monomers. How this extension was connected to the rest of TnI was not resolved. The authors claim the N-lobe of TnC is positioned relatively remotely from the actin surface both with and without Ca^{2+} . This suggests if the switch region is tethered away from N-TnC by the IR bound to actin, the switch region would have to travel an appreciable distance (more than 1 nm) to bind to the N-TnC at high Ca^{2+} .

The Manning-Tardiff-Schwartz (MTS) atomistic model of the thin filament

In 2012, Manning, Tardiff, and Schwartz presented molecular models of the thin filament at high and low Ca^{2+} .⁸⁴ The 52 kDa cTn crystal structure,²⁷ Pirani atomistic model of the thin filament,⁸³ and fsTn⁸⁰ were used to predict Tn and Tm/actin intramolecular interactions. Tn relaxation was a result of reduced interactions between the N-lobe of TnC and switch peptide of TnI, resulting in favored interactions between the IR and SABS regions with actin. This supports the fly-casting mechanism and Herzberg model of Tn activation. Under low Ca^{2+} , the mobile domain had a “rigid” conformation favoring actin binding that forced Tm in a position to block myosin binding sites on actin, which supports the steric blocking model. Additionally, as a result of TnC N-lobe conformational changes, the I-T arm rotated, translating a deactivating structural change to Tm through TnT. The greatest Ca^{2+} -dependent dynamics were seen in the I-T arm, the cTnT T1-T2 linker, and mobile domain of TnI. This study’s FRET-derived distances at high Ca^{2+} were compared to MTS model distances in the Results and

Discussion section, as the MTS model includes the crystal structure cTn core with molecularly-derived residues for the C-terminal end (mcTnI189-211).

1.3 Mutations in C-TnI associated with heart failure

Molecules that modulate the Ca^{2+} sensitivity of the thin filament are a therapeutic option to improve contractile function. Resolving the mechanism of thin filament activation could lead to rational structure-based drug design. Sarcomeric protein mutations are responsible for cardiomyopathies by interrupting the regulatory functions governed by those proteins.² Cardiomyopathies (CM) develop when myocytes “sense” changes in contractility due to amino acid mutations that disrupt protein structure; the myocytes alter signaling cascades to initiate compensatory mechanisms, resulting in a CM phenotype.⁸⁵ Familial hypertrophic cardiomyopathy (HCM),⁸⁶ restrictive cardiomyopathy (RCM),⁸⁷⁻⁸⁸ and familial dilated cardiomyopathy (DCM)⁸⁹ are the three most common forms of heart failure associated with mutations in genes encoding for sarcomeric proteins. Here, mutations in *TNNI3*, the gene encoding cTnI, will be discussed briefly to highlight the importance of cTnI’s IR and SABS (C-terminal end) for normal cardiac function. RCM is distinguished by impaired ventricular filling and reduced end diastolic volume due left ventricular wall stiffness, with preserved myocardial wall thickness and systolic function.⁹⁰ Mutations in hcTnI that cause RCM are primarily focused in the IR (Leu144Gln, Arg145Trp) and C-terminal end (Ala171Thr, Lys178Glu, Asp190Gly, Arg192His, Arg204His).^{88,91} These mutations increase the Ca^{2+} sensitivity of force development, decrease ATPase activity, and decrease ATPase inhibition.⁹²⁻⁹³ HCM is characterized by contractile dysfunction, a thickened left ventricle (hypertrophy), and arrhythmia.⁸⁶ HCM is primarily a genetically inherited disease, as

opposed to RCM and DCM, which are both acquired and genetically inherited.⁹⁴ Four of the 29 total TNNI3 mutations causing HCM are found in the IR, with the majority (22) found at the C-terminal end.⁹⁵⁻⁹⁷ These mutations have shown contrasting effects on Ca^{2+} sensitivity and Ca^{2+} -activated force of myofibrils.⁹⁸ DCM causes a thinning of the left ventricle (dilated) and poor systolic function.⁹⁹ DCM mutations have been discovered in the N-terminus of cTnI: a mutation near the Ser-23/24 phosphorylation site (Arg21Cys) decreases phosphorylation rates *in vitro*, while a Ala2Val caused decreased TnT/TnI interactions.⁸⁹ As of yet, no mutations in the C-terminal region of TnI have been discovered that cause of DCM.

The high density of HCM- and RCM-causing mutations in C-TnI demonstrate the essential role of the two actin binding sites in this region to maintain normal cardiac muscle function. A greater understanding of the Ca^{2+} -dependent structure and dynamics of this region, particularly of the second actin binding site of TnI, would yield insight into why these site mutations yield such dramatic phenotype changes to reduce mortality.

1.4 A multi-site FRET assay in a most native environment

A multi-site FRET assay was developed to resolve the Ca^{2+} -dependent structure and dynamics of the C-terminal region of cTnI in reconstituted regulated actin. The inter-dye distances derived at high and low Ca^{2+} clarify the role of cTnI in modulating muscle activation. Other studies lack the exhaustive assessment of filaments involving a combination of biochemical and spectroscopy methods that ensure a high degree of confidence in sample quality. Solution conditions mimicking the native environment of the sarcomere yield a more accurate assessment of Tn structure, as opposed to structures derived from isolated Tn.²⁸ This is the first assay designed to use FRET to map the

position of C-cTnI with respect to the N-lobe, inter-lobe linker, and C-lobe of cTnC, and to confirm the hypothesis that the SABS of cTnI plays a vital structural and functional role in regulating muscle activation. Here, the switch region (helix III) of cTnI was shown to have minimal Ca^{2+} -dependent dynamics, and most likely is a rigid helix comprising residues 151-177 that maintains a distance of ~ 5 nm away from the cTn core. This is surprising considering the Herzberg model predicts switch binding to N-TnC upon Ca^{2+} binding. Helix III is connected by a short loop to a more mobile helix (called helix IV). The SABS consists of residues 189-211, and is the most dynamic region of C-cTnI. cTnC undergoes region-dependent Ca^{2+} -induced movement. This study has shown at low Ca^{2+} , the SABS is bound to actin; when Ca^{2+} binds to cTnC at Site II, the SABS is displaced from actin, where the regulatory region of cTn would translate this activating signal to TnT(T1), Tm, and finally actin to promote cooperative activation of the thin filament. The binding of the switch region to cTnC may require further thin filament modifications, such as myosin binding or phosphorylation. The surprisingly long distances resolved between the switch region and the N-lobe of cTnC compared to previous studies may be due to the displacement of the C-terminal region away from the core of cTn by the SABS binding to actin.

2 METHODS

2.1 Native protein purification

2.1.1 Acetone powder from bovine left ventricle tissue

Acetone powder was prepared from fresh bovine hearts at 4°C as described.¹⁰⁰ Connective tissue, blood vessels, and blood were removed, and the left ventricle was ground in a pre-chilled meat grinder. The minced meat was soaked in 0.1 M KCl and 0.15 M potassium phosphate (pH 6.5) for 10 min, then filtered through pre-soaked cheesecloth. The mince was stirred in 0.05 M NaHCO₃ (sodium bicarbonate) for 10 min and filtered, then stirred in 1 mM EDTA (pH 7.0) for 10 min, filtered, and stirred again in the same buffer for 5 min. Mince was filtered, then stirred in deionized and distilled H₂O (ddH₂O) for 5 min, and filtered. Mince was stirred in 1 L of acetone for 10 min at 25°C, filtered, and repeated four times. The mince was then dehydrated overnight in the hood, and stored at -20°C for up to a year. Purity was assessed using sodium dodecyl sulfate-polyacrylamide gel electrophoresis (SDS-PAGE, 12% bis/acrylamide, monomer to cross-linker ratio 29:1) with Precision Plus Protein Kaleidoscope Protein Standards (Bio-Rad, Hercules, CA).

2.1.2 Purification of tropomyosin from acetone powder

Tm was purified from acetone powder as described.¹⁰¹ Briefly, about 100 g of acetone powder was extracted with a high salt solution (1.0 M KCl, 0.5 mM dithiothreitol [DTT]) at pH 7.0, filtered through cheesecloth, and the residue extracted again with the high salt solution. After adjusting the pH to 4.6 for 30 min, the solution was centrifuged for 20 min at 6,000 xg, and the pellet was dissolved in the high salt

buffer with pH 7.0. The insoluble material was removed using centrifugation at 6,000 xg for 10 min. This procedure was repeated twice, with the final pellet dissolved in ddH₂O supplemented with 0.5 mM DTT. Ammonium sulfate (0-53%, mass calculated with <http://www.encorbio.com/protocols/AM-SO4.htm>) was added slowly to the solution, with pH maintained at 7.0 at 4°C with stirring for 30 min. The precipitate was removed with centrifugation for 30 min at 11,000 xg, and the supernatant was brought to 65% saturation with ammonium sulfate, with pH maintained at 7.0. The precipitate was pelleted with centrifugation, dissolved in 0.5 mM DTT, and dialyzed against 2 mM 2-mercaptoethanol (BME). Tm consisting of a native mixture (9:1) of α : β isoforms was aliquoted, lyophilized, and stored at -80°C for up to 1 year. Purity was assessed using SDS-PAGE. Gels were stained using GelCode™ Blue Safe Protein Stain (Fisher Scientific Company, LLC, Hampton, NH).

2.1.3 Purification of actin from acetone powder

Actin was purified from acetone powder as described.¹⁰⁰ Briefly, 5 to 10 g of acetone powder was dissolved in Buffer A (2 mM Tris-HCl [Trizma® hydrochloride, Tris(hydroxymethyl)aminomethane hydrochloride] (pH 8.0), 0.5 mM BME, 0.2 mM CaCl₂, 0.005% sodium azide, and 0.2 mM Na₂ATP) (20 mL/g acetone powder) and stirred for 30 min. Extract was filtered through sterilized cheesecloth. The filtrate was then centrifuged at 20,000 xg for 1 hour at 4°C. The supernatant was polymerized by adding drop-wise (the same volume as the supernatant volume) a solution of 50 mM KCl, 2 mM MgCl₂, and 1 mM ATP to the filtrate at 4°C while stirring, with continued stirring for two hours. Solid KCl was added to the solution to reach a concentration of 0.8 M and stirred for 30 min. The solution was centrifuged at 150,000 xg for 1.5 hours, and the

pellet was resuspended in Buffer A supplemented with 0.8 M KCl, 2 mM MgCl₂, and 1 mM ATP. The sample was centrifuged at 150,000 xg for 1.5 hours, and the pellet was resuspended in Buffer A at 1.5 mL/g acetone powder. The pellet was homogenized with a Dounce homogenizer, and dialyzed against Buffer A for 16 hours, with three additional buffer exchanges for a total of 48 hours. Globular actin (G-actin) was clarified with centrifugation at 150,000 xg for 1.5 hours. The supernatant containing G-actin was then polymerized with 50 mM KCl, 2 mM MgCl₂, and 1 mM ATP added drop-wise with stirring, and stirred for 2 hours at 4°C. Filamentous (F-actin) was stored at 4°C in Buffer A for up to four months. Purity was confirmed using SDS-PAGE.

2.2 Mutagenesis and DNA amplification and purification

Wild type (WT) rat cardiac troponin T (TnT) and WT rat cardiac troponin C (TnC) plasmids were obtained from the Herbert C. Cheung lab (University of Alabama). WT mouse cardiac troponin I (TnI) and myc-tagged mouse cardiac TnT plasmids were gifts from the R. John Solaro lab (University of Illinois at Chicago). Primers were ordered from Integrated DNA Technologies (Coralville, IA), diluted to 1 µg/mL with ddH₂O, and stored in -20°C. Cysteine-less (Cys-less), Cys-lite (removal of one native Cys), and single Cys mutations in TnC and TnI (Table 1) were made using QuikChange Lightning Site-Directed Mutagenesis kits (Agilent Technologies, Santa Clara, CA) by following the protocol provided. PCR products were transformed into XL10-Gold Ultracompetent Cells (Agilent Technologies, Santa Clara, CA) following the protocol provided. 100 µL of cells were inoculated onto lysogeny broth (L-B, Fisher BioReagents, Hampton, NH) agar plates supplemented with the appropriate antibiotic (100 µg/mL), and incubated overnight at 37°C. Minipreps were prepared in triplicate with 2 mL of L-B

supplemented with the appropriate antibiotic (100 $\mu\text{g}/\text{mL}$). Single colonies were inoculated into the medium, and grown overnight with shaking at 37°C. Plasmids were purified using Wizard Plus SV Minipreps DNA Purification System kits (Promega Corporation, Madison, WI) following the protocols provided. Purified plasmids were sequenced using single pass DNA sequencing by ACGT, Inc. (Wheeling, IL). Upon sequence confirmation, plasmids were stored at -20°C.

Table 1. Recombinant troponin proteins expressed in *Escherichia coli* and purified.

Protein	Mutation/Modification	Species	Vector	Antibiotic Resistance	Cloning Sites
troponin T	N-terminal His-tag	mouse cardiac	pSBETa	kan ^r	NdeI-BamHI
	none	rat cardiac	pET-3d	amp ^r	NcoI-BamHI
troponin C	none	rat cardiac	pET-3d	amp ^r	NcoI-BamHI
	C84S C35S, C84S, S89C C35S, C84S, T127C				
troponin I	none	mouse cardiac	pET-3d	amp ^r	NcoI-BamHI
	C81I, C98S, S151C				
	C81I, C98S, L160C				
	C81I, C98S, S167C				
	C81I, C98S, L174C				
	C81I, C98S, V177C				
	C81I, C98S, I182C				
	C81I, C98S, V189C				
	C81I, C98S, I196C				
	C81I, C98S, S200C				
	C81I, C98S, G204C				
	C81I, C98S, K208C				
	C81I, C98S, G211C				

2.3 Bacterial expression and recombinant protein purification

2.3.1 Preparation of troponin C

WT rat cardiac TnC, Cys-lite TnC (C84S), and Cys-less TnC (C35S, C84S) were sub-cloned into the pET-3d vector with ampicillin (amp) resistance for expression. The plasmids were thawed on ice, and 0.5 μL of plasmid were added to 50 μL of BL21 (DE3)

competent *Escherichia coli* cells (New England Biolabs, Ipswich, MA). Cells were transformed using heat shock (42°C, 42 sec), and incubated with 250 µL S.O.C. medium (Super Optimal broth with Catabolite repression, 2% tryptone, 0.5% yeast extract, 10 mM NaCl, 2.5 mM KCl, 10 mM MgCl₂, 10 mM MgSO₄, 20 mM glucose) shaking for 1 hour at 37°C. 100 µL of cells were inoculated onto L-B agar plates supplemented with 100 µg/mL ampicillin and incubated at 37°C overnight. Pre-cultures were prepared by selecting a single colony, and inoculating 3 mL of L-B broth supplemented with 100 µg/mL ampicillin. The pre-culture was incubated at 37°C under shaking for 6 hours. Bacteria were overexpressed in large growths, where 500 µL of cells from the pre-culture were inoculated into 500 mL of Terrific Broth (TB, Fisher BioReagents) (typically total 2 L growths) supplemented with 100 µg/mL ampicillin under shaking for 18 hours at 37°C.

Troponin C was purified from cells as described with some modifications.¹⁰²⁻¹⁰⁴ Briefly, cells were harvested with centrifugation at 8,000 rpm for 9 min with a JA-10 rotor, and used immediately or stored at -80°C for up to a month. Cells were re-suspended in less than 100 mL of 2.5 mM EDTA, 0.5 mM PMSF, 50 mM Tris-HCl (pH 8.0), and 15 mM BME with a stir bar at 4°C for 30 min. Cells were lysed on ice with ultrasonification in a Misonix ultrasonix liquid processor (power, 50; 10 sec on, 20 sec off) for 25 min of “on” time. Cellular debris was removed from the lysate with two rounds of centrifugation. First, the lysate was centrifuged at 18,000 rpm for 25 min using a JA-20 rotor. The supernatant was then centrifuged at 35,000 rpm for 45 min in a Beckman XL-90 ultracentrifuge using a Ti-45 rotor. Ammonium sulfate (0-60%, mass calculated with <http://www.encorbio.com/protocols/AM-SO4.htm>) was added slowly with stirring to the supernatant at 4°C over the course of an hour, then centrifuged for 30

min at 10,000 rpm with a JA-14 rotor. Ammonium sulfate was added to the supernatant (60-80%) and centrifuged for 30 min at 10,000 rpm with a JA-14 rotor. The pellet was re-suspended in and dialyzed against 1 L Buffer A-TnC (50 mM Tris-HCl (pH 7.5), 50 mM NaCl, 5 mM CaCl₂, 1 mM MgCl₂, and 1 mM DTT) overnight.

TnC was purified from the lysate using hydrophobic interaction chromatography. The lysate was loaded onto a column with a matrix of Phenyl Sepharose 6 Fast Flow (High Sub) (GE Healthcare Life Sciences) equilibrated with Buffer A-TnC using a fast protein liquid chromatograph (FPLC, ÄKTAprime, GE Healthcare Life Sciences) and a UV lamp to monitor absorption at 280 nm. Non-specific proteins with weak hydrophobic interactions were removed with 50 mM Tris-HCl (pH 7.5), 1 M NaCl, 0.1 mM CaCl₂, and 1 mM DTT. TnC was eluted from the column with 50 mM Tris-HCl (pH 7.5), 1 mM EDTA, and 1 mM DTT. SDS-PAGE was used to analyze peaks from absorbance at 280 nm. Fractions containing purified protein were combined, lyophilized, and stored at -80°C for up to three years.

2.3.2 Preparation of troponin I

WT mouse cardiac TnI and cysteine-modified TnI (see Table 1) were purified similarly to TnC, with some modifications. The pelleted cells were re-suspended in CM buffer supplemented with 0.5 mM PMSF. The ammonium sulfate precipitations were 0-27% and 27-60%, and the pellet from the second cut was re-suspended in and dialyzed against 1 L of CM buffer overnight. TnI was purified from the lysate using weak cation exchange chromatography. The lysate was loaded onto a column with a matrix of CM (carboxymethyl) Sepharose Fast Flow (GE Healthcare Life Sciences) equilibrated with

CM buffer. TnI was eluted with a gradient elution of 0 to 100% mixtures of CM buffer and CM buffer supplemented with 300 mM NaCl.

2.3.3 Preparation of troponin T

WT rat cardiac TnT and mouse cardiac TnT with an N-terminal polyhistidine myc-tag (amino acid sequence, N-EQKLISEEDL-C) were purified similarly to TnC, with some modifications. Cells were grown for 36 hours at 37°C with shaking. The pelleted cells were re-suspended in CM buffer (6 M urea, 30 mM citric acid (pH 6.0), 1mM EDTA, and 1 mM DTT) supplemented with 0.5 mM PMSF. The ammonium sulfate precipitations were 0-35% and 40-60%, and the pellet from the second cut was re-suspended in and dialyzed against 1 L of DEAE buffer (6 M urea, 50 mM Tris-HCl (pH 8.0), 1 mM EDTA, 1 mM DTT) overnight. TnT was purified from the lysate using weak anion exchange chromatography. The lysate was loaded onto a column with a matrix of DEAE (diethylaminoethyl) Sepharose Fast Flow (GE Healthcare Life Sciences) equilibrated with DEAE buffer. TnT was eluted with gradient elution from 0 to 100% mixtures of DEAE buffer and DEAE buffer supplemented with 500 mM KCl.

2.4 Development of FRET assay

2.4.1 Calculation of the Förster critical distance

The Förster distance (R_0) is the distance at which 50% of the donor molecules decay by energy transfer, and 50% decay by radiative and non-radiative processes.¹⁰⁵ For each FRET pair (AF546, FRET donor-ATTO655, FRET acceptor; ATTO550, FRET donor-ATTO655, FRET acceptor), R_0 was determined using excitation and emission spectra provided by Life Technologies and ATTO-Tec GmbH using¹⁰⁵

$$R_0^6 = \frac{9000(\ln 10)\kappa^2 Q_D}{128\pi^2 N n^4} \int_0^\infty F_D(\lambda) \varepsilon_A(\lambda) \lambda^4 d\lambda, \quad (1)$$

where κ^2 is the relative orientation in space of the donor and acceptor transition dipoles, assumed 2/3; N is Avogadro's number = $6.023 \times 10^{23} \text{ mol}^{-1}$; n is the refractive index, assumed to equal 1.4 for biological particles in an aqueous solution; Q_D is the quantum yield of the donor in the absence of an acceptor, obtained from product literature; $F_D(\lambda)$ is the corrected fluorescence intensity of the donor from wavelength range λ to $\lambda + \Delta \lambda$, with the total intensity normalized to 1; $\varepsilon_A(\lambda)$ is the acceptor molar extinction coefficient at its maximum absorption wavelength λ_{abs} (see Figure 6B-C). $\int_0^\infty F_D(\lambda) \varepsilon_A(\lambda) \lambda^4 d\lambda$ is the spectral overlap integral in units of $\text{M}^{-1} \text{ cm}^{-1} (\text{nm})$ between the donor emission and the acceptor absorption normalized to one.¹⁰⁵ A MatLab script (MatLab and Statistics Toolbox Release 2015a, The MathWorks, Inc., Natick, MA) was used to calculate R_0 , and the code can be found in the Appendix.

Table 2. Sarcomeric proteins (gene), their molecular weights, and molar extinction coefficients ε at 280 nm.

Protein	Species	Molecular Weight (kDa)	ε ($\text{M}^{-1} \text{ cm}^{-1}$)
Troponin C (TNNC1)	rat cardiac	18.4	4,480
Troponin I (TNNI3)	mouse cardiac	24.3	11,460
Troponin T (TNNT2)	rat cardiac	35.7	15,470
Troponin	reconstituted cardiac	78.4	31,410
α -Tropomyosin (TPM1)	bovine cardiac	32.7	21,760
β -Tropomyosin (TPM2)	bovine cardiac	32.8	
Actin (ACTC1)	bovine cardiac	42.0	43,960
Myosin subfragment-1	chicken skeletal	110	90,850
Myosin (MYSS)	chicken skeletal	500	0.56*

*units are mL/mg cm^{-1}

2.4.2 Dye labeling of proteins

Cys residues of proteins were selectively labeled with maleimide-containing fluorescent dye molecules. Lyophilized fluorophores were briefly centrifuged, and stock solutions were prepared at 10 mM in dimethyl sulfoxide (DMSO for UV-spectroscopy $\geq 99\%$, Sigma-Aldrich, St. Louis, MO) and stored at -20°C for up to six months. Cys residues were reduced by dialysis against labeling buffer (LB: 50 mM MOPS (pH 7.2), 3 M urea, 100 mM KCl, 1 mM EDTA) containing 5 mM DTT. DTT was removed with three dialysis steps against LB. Reduced proteins (100 μM) were reacted with a 5-fold excess of dye molecule for 12 hr at 4°C under nitrogen with stirring. Labeling was terminated with 5 mM DTT. The labeling was repeated for a total of three reactions to increase the labeling efficiency (f_A , molar concentration of dye relative to total concentration of protein). Unreacted dye molecules were removed by size exclusion FPLC (Sephacryl S-100 HR, ÄKTAprime Plus, GE Life Sciences) in LB. Single-cysteine modified proteins will be abbreviated as TnXYC, where X is either the troponin protein I or C, and Y is the modified Cys residue. TnC35C, TnC89C, and TnC127C were labeled with ATTO655. TnIX₁C, where X₁ is either 151, 160, 167, 174, 177, 182, and 189 were labeled with Alexa Fluor® 546. TnIX₂C, where X₂ is either 196, 200, 204, 208, and 211 were labeled with ATTO550. Protein and dye concentrations were determined by absorption spectroscopy using the extinction coefficients ($\text{M}^{-1} \text{cm}^{-1}$) in Tables 2 and 3.

The concentration of dye-labeled proteins was determined by absorption spectroscopy using

$$[\textit{protein}] = (A_{280} - CF_{280}A_{max})/\varepsilon, \quad (2)$$

where A_{max} is absorption maximum of the dye and CF_{280} is the correction factor for dye absorption at 280 nm. The labeling efficiency f_A is the concentration of dye divided by the concentration of the protein.

Table 3. Maleimide fluorophores, where ϵ is the molar extinction coefficient at 280 nm, CF is the correction factor at 280 nm, Q is the quantum yield, λ_{abs} and λ_{em} are the absorption and emission maximum wavelengths, respectively.

Fluorophore	Molecular Weight (g/mol)	ϵ ($M^{-1} \text{ cm}^{-1}$)	CF_{280}	Q	λ_{abs} (nm)	λ_{em} (nm)
Alexa Fluor® 546 (AF546) (donor) ¹	1034	104,000	0.08	0.79	532	554
ATTO 550 (donor) ²	816	120,000	0.12	0.80	554	576
ATTO 655 (acceptor) ²	812	125,000	0.08	0.30	663	684

¹Life Technologies, Cincinnati, OH
²ATTO-Tec GmbH, Siegen, Germany

2.5 Troponin and regulated actin reconstitution

Tn was reconstituted as described⁴⁹ with some modifications. TnC, TnI, and TnT were combined in the following molar ratios: for WT, unlabeled, and donor-labeled Tn, 1:1.2:1.4, respectively; for donor-acceptor-labeled Tn, 1.2:1:1.4, respectively. Individual Tn components were dialyzed against DEAE buffer for 3 hours at 4°C, and combined in glass vials and incubated at room temperature with gentle shaking for 2 hours. Tn was then stepwise dialyzed for 2 hours at 4°C against 50% DEAE and 50% high salt buffer (HSB: 1 M KCl, 20 mM MOPS (pH 7.0), 1.25 mM MgCl₂, 1.25 mM CaCl₂, 5 mM DTT), HSB, WB supplemented with 625 mM KCl, 425 mM KCl, 225 mM KCl, and 75 mM KCl. Tn was aliquoted and stored at -80°C for up to one year. After thawing prior to measurements, uncomplexed TnI and TnT were removed using centrifugation at 10,000 xg for 1 min. Donor-only Tn (Tn-D) was prepared from TnIX₁C labeled with AF546 or

ATTO550. Donor/acceptor Tn (Tn-DA) was prepared from TnIX₂C labeled with AF546 or ATTO550 and TnCXC labeled with ATTO655. An asterisk (*) represents dye-conjugated proteins, e.g., TnI151C*AF546.

Regulated actin filaments (rAc) were prepared by incubating Tn, Tm, and F-actin (7 μ m in protomer) at a molar ratio of 1:5:7 in WB at 4°C on ice. The order of protein addition was F-actin, Tm, then Tn. rAc were incubated at 4°C for at least a week prior to use, and stored for up to three months.

2.6 Steady-state fluorescence spectroscopy

Steady-state (ss) ensemble FRET spectroscopy was performed on paired D-only and DA samples of Tn containing donors labeled with AF546 on TnI residue 151, 160, 167, 174, 177, 182, and 189, or containing a donor and an acceptor labeled with ATTO655 on TnC residue 89. Paired samples were donor concentration-matched using absorption spectroscopy, where ϵ and λ_{abs} used are shown in Table 3. Tn was diluted to 500 nM (in donor concentration) in WB supplemented with 75 mM KCl into a 50 μ L Quartz Fluorometer Cell (Starna Cells, Inc., Atascadero, CA), and incubated at room temperature (RT, 22°C) for 10 min. Emission spectra were collected at RT on a Fluorolog-3 spectrofluorometer (Horiba), with 530 nm excitation, and emission monitored from 540 to 630 nm (monochromator slit width 4 nm, 1 sec integration time). Energy transfer E was calculated using

$$E = \frac{1}{f_A} \left(1 - \frac{I_{DA}}{I_D} \right), \quad (3)$$

where f_A is the acceptor labeling efficiency, I_{DA} is the intensity at 570 nm for the donor in the presence of an acceptor, and I_D is the intensity at 570 nm for the donor in the absence

of an acceptor. Inter-dye distance (R) between the donor and acceptor dyes was calculated using the Förster relation

$$R = R_0 \left(\frac{1 - E}{E} \right)^{1/6}, \quad (4)$$

where R_0 is the Förster distance of the donor/acceptor dye pair. The R_0 for FRET pair AF546-ATTO655 was 5.5 nm.

2.7 Epifluorescence imaging of regulated actin filaments

All regulated actin filaments were imaged post-reconstitution. rAc, or rAc stained with phalloidin*AF488 (Life Technologies, Cincinnati, OH) at a 1:35 actin:phalloidin were diluted to 10 nM in WB and deposited on glass coverslips (25 mm, ThermoFisher Scientific, Pittsburgh, PA). Fluorescence images were collected on an inverted microscope (IX71, Olympus USA, Center Valley, PA) with a TE cooled interline CCD camera (Clara, Andor) with a 100x (N.A. 1.4) oil immersion objective (UPlanSApo, Olympus). A xenon lamp (X-Cite 120PC, Lumen Dynamics) was used for excitation. For AF488, the filters 475/35: 495: 550/88 (Semrock) (excitation: dichroic: emission) were used. For AF546 and ATTO550, the filters 545/25: 565: 605/70 (Chroma) were used. For ATTO655, the filters 620/60: 660: 700/75 (Chroma) were used. Images were pseudo-colored and merged using ImageJ 1.47v (National Institutes of Health, Bethesda, MD). Length was calibrated by imaging a dual axis linear scale (Edmund Optics, Barrington, NJ).

2.8 Time-resolved fluorescence spectroscopy

2.8.1 Time-correlated single photon counting (TCSPC)

TCSPC measurements were performed at room temperature ($20 \pm 2^\circ\text{C}$) using 500 nM (in Tn) donor-only rAc (rAc-D) and donor/acceptor rAc (rAc-DA) in WB, or WB supplemented with 3 mM CaCl_2 using a MicroTime 200 confocal fluorescence lifetime microscope (PicoQuant GmbH, Berlin, Germany) based on an inverted microscope (IX71, Olympus USA, Center Valley, PA). Samples were placed on glass coverslips (25 mm width, ThermoFisher Scientific, Pittsburgh, PA) or in glass-bottomed microwell plates (96-well SensiPlate Plus, 175 μm height, glass bottom, E&K Scientific, Santa Clara, CA), and incubated at room temperature for 30 min prior to measurements. Excitation light from a 532 nm pulsed diode laser (LDH-P-FA-530-B, PicoQuant) was passed, respectively, through a quarter wave plate, a single mode fiber optic, a laser cleanup filter (534/635-25, Semrock, Lake Forest, IL), a principle dichroic mirror (DC1) (ZT532/638rpc, Chroma, Bellows Falls, VT), and a 100x (N.A. 1.3) oil immersion objective (UPlanFLN, Olympus). Emitted light was passed through the objective and DC1, then through a 550 nm long pass filter (HQ550lp, Chroma), 50 μm pinhole, a secondary dichroic (ZT532/638PC, Chroma), a bandpass filter (HQ580/70, Chroma), and recorded on an avalanche photodiode (MPD PDM series $\phi=100 \mu\text{m}$, Micro Photon Devices, Italy), respectively. Data were collected until the maximum count per channel exceeded 10,000 (typically 10 min). Background intensity averaged 80 counts/sec.

The photon counting histograms of TCSPC data were convolved with the instrument response function (IRF), and fit to a two-exponential decay model $I(t) = a_1 e^{-t/\tau_1} + a_2 e^{-t/\tau_2}$, where $I(t)$ is the intensity of the donor as a function of time t , and a_i

is the fraction of fluorophores with lifetime τ_i (SymphoTime Version 5.2, PicoQuant).

Amplitude-weighted mean lifetimes $\langle\tau\rangle = \sum_i a_i \tau_i / \sum_i a_i$ of the donor in the presence of the acceptor dye $\langle\tau_{DA}\rangle$ and the donor in the absence of the acceptor dye $\langle\tau_D\rangle$ were used to obtain the FRET efficiency E

$$E = \frac{1}{f_A} \left(1 - \frac{\langle\tau_{DA}\rangle}{\langle\tau_D\rangle} \right), \quad (5)$$

where f_A is the labeling efficiency of the acceptor. The distance R between the donor and acceptor dyes is given by the Förster relation in Eq. 4. The R_0 for FRET pair AF546-ATTO655 was 5.5 nm, and for 6.4 nm for FRET pair ATTO550-ATTO655.

2.8.2 Fluorescence correlation spectroscopy

FCS measurements and analysis were performed by Dr. Gi-Ho Kim on rAc, TnC, and dyes in WB, or on Tn in WB supplemented with 75 mM KCl. Freely-diffusing TnC and Tn at 500 pM, and rAc filaments at 500 nM (in Tn) were examined using the time resolved confocal microscope described above, with a 0.4 fL effective confocal volume positioned 50 μm above the top surface of the glass coverslip. The effective confocal volume was determined by fitting the autocorrelation function of free AF546 dye (1 nM in ddH₂O) with fixed correlation time (0.029 msec).¹⁰⁶ Excitation from the pulsed 532 nm laser was attenuated to 50 μW . Photon arrival times were collected for approximately 10 min. Data were analyzed by calculating the autocorrelation function¹⁰⁷

$$G(t) = \frac{\langle F(t) \delta F(t + \Delta t) \rangle}{\langle F(t) \rangle^2}, \quad (6)$$

where $\delta F = F(t) - \langle F \rangle$ is the fluctuation in fluorescence from the temporal average

$\langle F(t) \rangle = \frac{1}{T} \int_0^T F(t) dt$ (SymphoTime Version 5.2, PicoQuant). To recover the

translational correlation times, the data were fit to a pure diffusion model with one or two species

$$G(\tau) = \sum_{i=1}^n \rho_i \left(1 + \frac{\tau}{\tau_i}\right)^{-1} \left(1 + \frac{\tau}{\tau_i \kappa^2}\right)^{-1/2}, \quad (7)$$

where $\sum_i^n \rho_i = 1/\langle N \rangle$, $\langle N \rangle$ is the average number of molecules in the confocal volume;

$\kappa = z_0/\omega_0$, where $z_0 = 1.4 \mu\text{m}$ and $\omega_0 = 0.22 \mu\text{m}$ are the radial and axial radii,

respectively, of the Gaussian beam profile at $1/e^2$ of its maximum intensity; and τ_i is the lateral diffusion time of the i^{th} diffusing species.

2.8.3 Statistical analysis

The standard error of the mean (SEM) was calculated for $n = 3$ FRET efficiencies for each donor residue determined from rAc filaments reconstituted on different days.

2.9 Functional characterization of mutated Tn

2.9.1 Tn exchange into skinned cardiomyocytes

All animal protocols were approved by the Animal Care and Use Committee at Loyola University School of Medicine, and conducted according to the NIH Guidelines for Care and Use of Animals in Research (NIH Publication No. 85-23, revised 1996). Cardiac myocytes were isolated from left ventricles of rats, detergent skinned, and subjected to Tn exchange as previously described.¹⁰⁸ Briefly, myocytes were isolated from rat left ventricular tissue, snap frozen, and stored at -80°C . Frozen tissue was homogenized and filtered through a $70 \mu\text{m}$ cell strainer, then pelleted by centrifugation at $120 \times g$ for 1 min at 4°C . Cells were skinned by resuspending the cell pellet in relaxing solution (97.92 mM KOH, 6.24 mM ATP, 10 mM EGTA, 10 mM Na_2CrP , 47.57 mM

potassium propionate, 100 mM BES, and 6.54 mM MgCl₂) supplemented with 1% Triton X-100, and incubated on a rocking table (room temperature, 15 min). Triton was removed through two rounds of washing: myocytes were pelleted by centrifugation (300 xg, 5 min, 4 °C), then suspended in 1 mL of ice cold relaxing solution. To replace endogenous Tn with recombinant Tn constructs, skinned myocytes in relaxing solution were co-incubated (4°C, overnight) with exogenous Tn (2 mg/ml). Unbound Tn was removed with two rounds of washing through the pellet/suspension sequence just described. Myocytes were placed on ice and used within 8 hrs.

To determine the efficiency of Tn exchange, a portion of the myocyte preparation was analyzed by Western blot as previously described.¹⁰⁹ Briefly, total protein homogenates were resolved by 12% SDS-PAGE and blotted onto a nitrocellulose membrane. Blots were probed with a mouse monoclonal antibody against cardiac TnT (Clone JLT-12, Sigma), which detects both native and exogenous myc-tagged TnT. A secondary anti-mouse HRP-conjugated antibody (Promega W402B) allowed the relative TnT content (native vs. exogenous) to be quantified by chemi-luminescence (ECL, BioRad).

2.9.2 Muscle mechanics experiments

Myocytes with clear striation patterns were selected and attached to a force transducer (Aurora Scientific Inc. 403A transducer, Aurora, ON, Canada) and a high-speed piezo translator (Thor Labs, Newton, NJ). Cells were perfused with a closely placed pipette through a constant perfusion control system (VC-8M Eight Channel Mini-Valve Perfusion System, Warner Instruments, Hamden, CT). Cells were perfused with solutions of varying calcium concentrations (pCa 10.0–pCa 4.5). In each perfusate,

developed force was measured at two sarcomere lengths (1.9 μm and 2.3 μm). Cells were perfused with maximally activating Ca^{2+} solution at the beginning and the end to calculate time-dependent run down. Any cell showing more than 20% run down in maximal force was discarded. All data were acquired by custom-made LabView software and analyzed using Origin Pro 8.0. Individual force-pCa curves were fit to a modified Hill equation $(P/P_o)=[\text{Ca}^{2+}]^{n_H}/(\text{Ca}_{50}^{n_H} + [\text{Ca}^{2+}]^{n_H})$, where n_H is the Hill coefficient. All force data were normalized by the cross sectional area of the cell. Cell cross-sectional elliptical area was calculated using a calibrated on-screen monitor as described previously.¹⁰⁸

2.9.3 Statistical analysis

Non-linear regression and statistical analysis were performed using GraphPad Prism ver. 6.0 (La Jolla, CA). The mean \pm SEM of the parameters recovered from the fitting are reported. The recovered parameters from different samples were compared using two-way ANOVA. Statistical significance was defined as $P < 0.05$.

3 RESULTS & DISCUSSION

3.1 Designing a FRET assay on troponin

The sequence of rat cTnC is identical to hcTnC, except for residue 119, which is an isoleucine in human and methionine in rat. Figure 4A shows the sequence alignment for rc and hcTnC. The 52 kDa Takeda crystal structure resolved the hcTnC structure to a 3.3 Å resolution, except for two residues in the central linker.²⁷ Figure 4C shows the secondary structure of cTnC, with FRET acceptor residues highlighted: 35 is in the N-lobe, 89 is in inter-lobe linker, and 127 is in the C-lobe. None of the residues selected are involved in Ca²⁺ or Mg²⁺ binding.

mcTnI is a 211 residue protein, and Figure 4B shows the sequence alignment between mc and hcTnI (210 residues). Figure 4C shows the secondary structure of cTnI with donor residues highlighted in green. hc and mcTnI residues differences in C-TnI are marked in yellow. Two of the three residue variances in the C-TnI were mutated to Cys for modification with fluorescent probes (mouse I182C and G211C). All donor residues and acceptor residues were visualized using the MTS molecular model of Ca²⁺-bound Tn (Figure 5).⁸⁴ Donor positions span the C-terminal region of cTnI, beginning at TnI151 in the switch region, and acceptor positions are located on the N-lobe, the inter-lobe linker, and the C-lobe of cTnC.

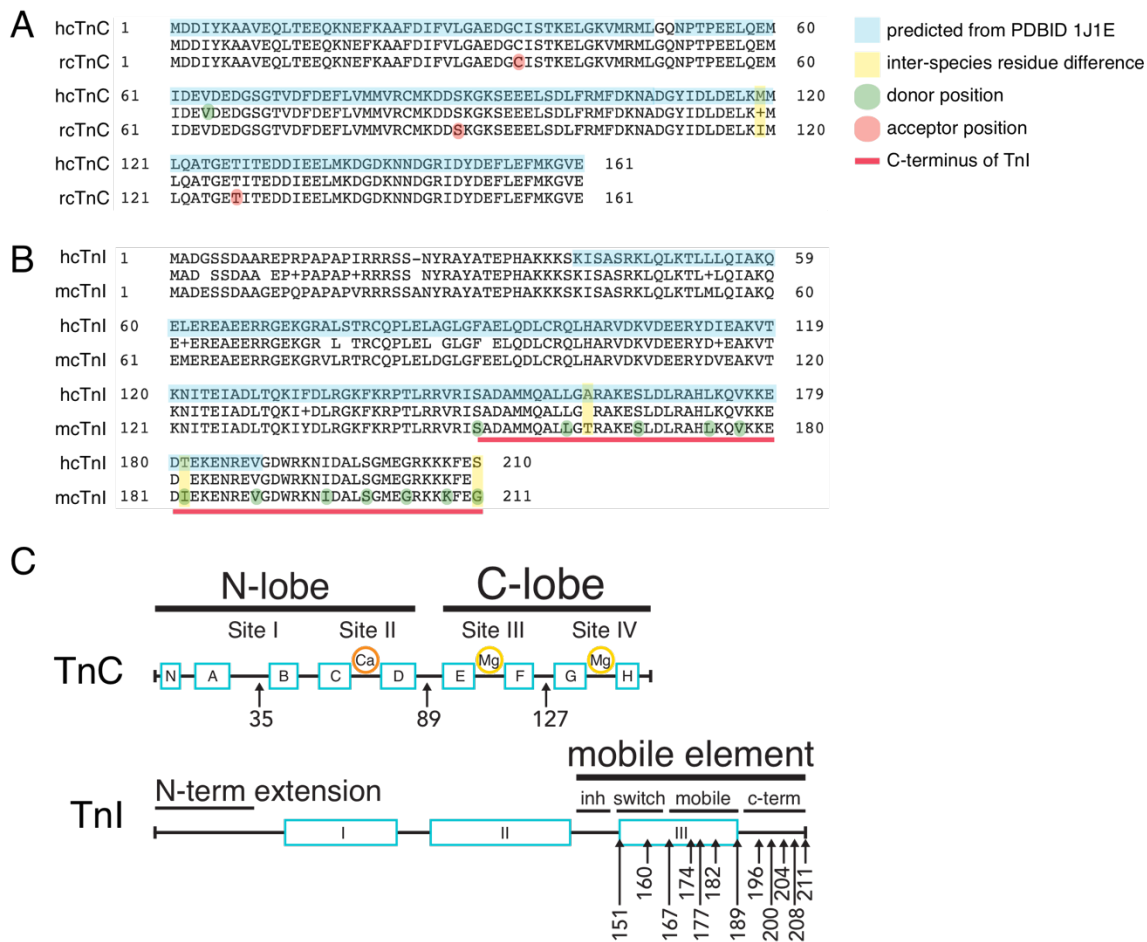


Figure 4

Figure 4. Mouse cTnI and rat cTnC sequence alignment with human. Highlighted in blue are residues resolved in the Ca^{2+} -saturated 52 kDa core of human cardiac Tn (PDBID 1J1E).²⁷ **(A)** A sequence alignment was performed using the Basic Local Alignment Search Tool (BLAST) for hc TnC (gene name TNNC1, UniProt identifier P63316) and rcTnC (UniProt identifier Q4PP99). hcTnC, aligned, and rcTnC residues are shown in the top, middle, and bottom lines, respectively. Residue variances are shown in yellow. The residues selected for acceptor labeling are highlighted in red: C35, S89, and T127. **(B)** BLAST alignment of the amino acid sequences of hcTnI (gene name TNNI3, UniProt identifier P19429) and mcTnI (UniProt identifier P48787). The C-terminal region (residues 151-211 in mouse numbering) is identified by the magenta line, with amino acid residue differences between hc and mc in C-TnI highlighted in yellow. Residues selected for donor labeling are highlighted in green: S151, L160, S167, L174, V177, I182, V189, I196, S200, G204, K208, and G211. **(C)** Schematic showing the domain organization of cardiac TnC and TnI. Helices are depicted as blue rectangles. Sites III and IV of TnC bind Mg^{2+} constitutively. Site II of TnC binds regulatory Ca^{2+} .

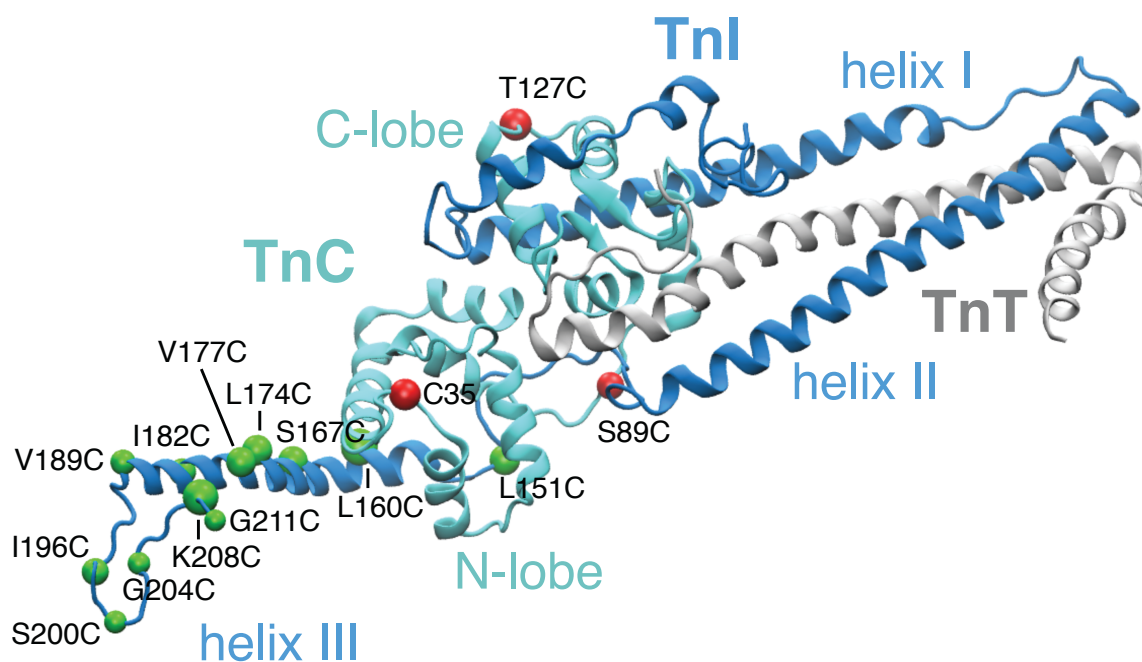


Figure 5. Multi-site FRET assay on troponin. Ribbon representation of MTS model resolved from the 52 kDa core of Ca^{2+} -saturated Tn. Single Cys mutants with covalently-bound donor dyes span the switch (151, 160, 167), mobile (174, 177, 182, 189), and C-terminal (196, 200, 204, 208, 211) domains of TnI (green spheres). Acceptors dyes are covalently bound to single Cys mutants (red spheres) on TnC between the A and B helices (35) in the N-lobe, the linker between the N- and C-lobes (89), and between helices F and G (127) in the C-lobe.

3.1.1 Donor and acceptor fluorophore selection

The qualifications for designing a FRET pair were: fluorophores must (i) be excited and emit at visible wavelengths (400-700 nm), (ii) have low molecular mass ≈ 1 kDa, (iii) have a long carbon linker (C_x , $x \leq 5$), (iv) have an extinction coefficient $> 100\text{K}$ (bright), (v) and be thiol-reactive.

Labeling with low molecular weight fluorophores reduces potential tertiary structure perturbations. A long carbon linker, the carbon group spacer between the fluorescent moiety and the reactive moiety, increases the ease of the reactive moiety reaching the specific residue for labeling, leading to a higher degree of labeling. All fluorophores used had a five-carbon linker, where $C_5 = \approx 7.7 \text{ \AA}$ for AF546, ATTO550, ATTO655. This introduced a threshold to the derived inter-dye distances, where distances have an inherent error range of $\pm 1.54 \text{ nm}$. Time-resolved FRET measurements were repeated in triplicate to gauge the error range. The linker also allows for free rotation of the dyes to reduce steric hindrance,¹¹¹ which could cause variations in the assumed orientation factor ($\kappa^2 = 2/3$) that would influence the rate of energy transfer E . Additionally, the quantum yield can be reduced when the dye linker is too short.¹¹² A high extinction coefficient ϵ , which is the capacity for the fluorophore to absorb a photon of light, is important for both donor and acceptor excitation (either directly-excited for the former or from sensitized emission for the latter). Molecular brightness, or the fluorescence output per fluorophore, is proportional to the product of ϵ and the quantum yield (Q), which is the number of photons emitted per photon absorbed.¹⁰⁵ Cysteine was chosen as the reactive residue due its low native prevalence (two in both TnC¹¹³ and TnI¹¹⁴). Thiol-reactive fluorophores covalently bind to cysteine residues with high efficiency and specificity within a certain pH range.¹¹⁵ Maintaining a pH below 8 in the labeling reaction buffer ensured amine groups remained protonated, and did not undergo nucleophilic attack by maleimide moieties.

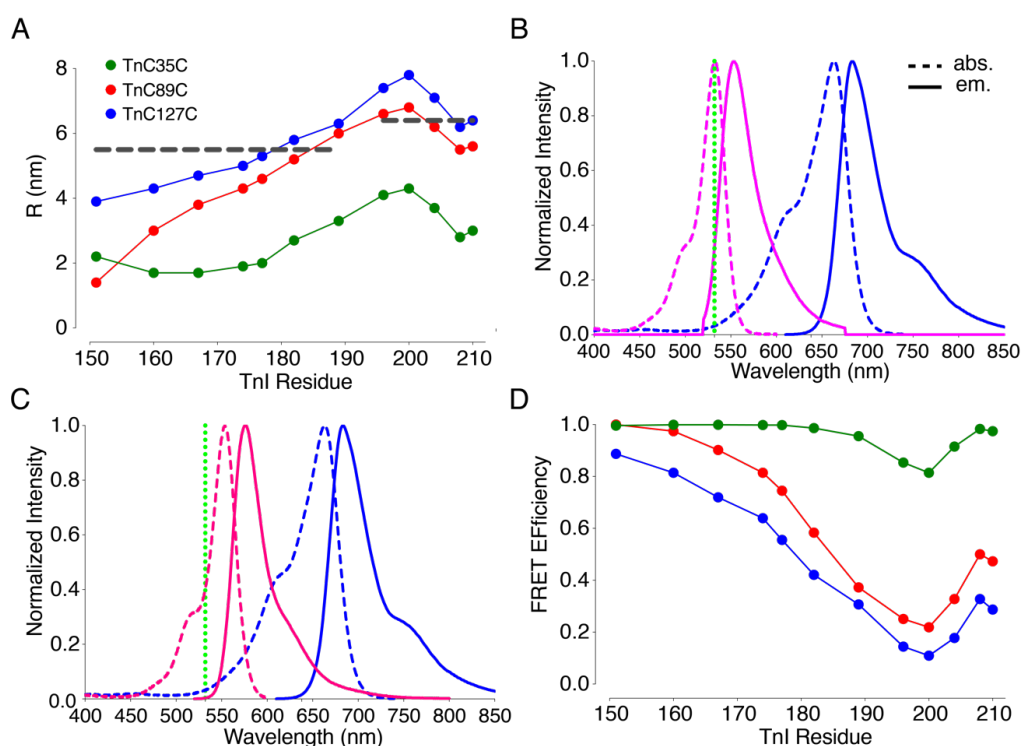


Figure 6. Emission spectra of FRET dye pairs, inter-C α distances, and theoretical FRET efficiencies for troponin. (A) C α (R_{mod}) bond lengths between donor residues on TnI and acceptor residue 35C on TnC (green), 89C (red), and 127C (blue) determined using the MTS model⁸⁴ and VMD.¹¹⁶ Dashed grey lines at 5.5 and 6.4 nm indicate the R_0 for AF546/ATTO655 and ATTO550/ATTO655, respectively. (B) Normalized absorption and emission spectra for AF546 (magenta) and ATTO655 (blue) used to determine the spectral overlap needed to calculate R_0 . Dashed lines indicate absorption; solid lines indicate emission. The confocal time-resolved microscope used in this study has an excitation wavelength at 532 nm (green dashed line). (C) Normalized absorption and emission spectra for ATTO550 (pink, donor) and ATTO655 (blue, acceptor). 532 nm excitation (green dashed line). (D) Theoretical FRET efficiencies E calculated from C α bond lengths in (A). A consistent coloring scheme is used in panels A and D.

3.1.2 Theoretical FRET efficiencies and C α distances

The carbon- α (C α) distances between TnI donor residues (151, 160, 167, 174, 177, 182, 189, 196, 200, 204, 208, 211) and TnC acceptor residues (35, 89, 127) were estimated using the MTS molecular model in VMD version 1.9.2.¹¹⁶ Figure 6A shows the C α distances (R_{mod}), which range from ≈ 2 nm to ≈ 8 nm. The Förster critical distance (R_0) between the donor and acceptor fluorophores was an important consideration in the design of this FRET assay. The R_0 is the distance at which resonant energy transfer is 50% efficient,¹⁰⁵ and should be close to the theoretical C α distances to ensure both small and large conformational changes can be resolved. The FRET efficiency strongly depends on inter-dye distance when close to the R_0 .¹⁰⁵ The broad range of distances in this assay required a selection of two FRET pairs, one with $R_0 = 5.5$ nm (donor-acceptor, AF546-ATTO655), and the other with $R_0 = 6.4$ nm (ATTO550-ATTO655). TnI residues 151-189 were labeled with AF546, and residues 196-211 were labeled with ATTO550. TnC residues were labeled with ATTO655.

Figures 6B-C show the excitation and emission spectra for the FRET pairs (donor-acceptor) AF546-ATTO655 and ATTO550-ATTO655 provided by Life Technologies (Alexa Fluor® dyes) and ATTO-Tec, GmbH (ATTO dyes). To measure energy transfer, the donor must be promoted to its excited state. The confocal setup was equipped with a picosecond pulsed laser at 532 nm to excite the donor (λ_{exc}). The peak absorption (excitation) wavelengths λ_{abs} for AF546 and ATTO550 are 532 and 554 nm, respectively; therefore, the fluorophores are adequately excited at λ_{exc} . The probability of directly exciting ATTO655 is low at λ_{exc} ($< 3\%$), compared to AF546 ($\approx 100\%$) and ATTO550 ($\approx 40\%$). Figure 6D shows the theoretical FRET efficiencies for each acceptor,

calculated using Eq. 4 from R_{mod} and the R_0 for each donor/acceptor FRET pair.

Particularly for acceptor position TnC35, some of the theoretical E appear too close to 1.0 to provide accurate estimations of inter-dye distances. If the conformation of Tn within thin filaments is similar the MTS model (and by association, the Takeda structure), the experimentally-derived E should closely follow Figure 2D.

3.1.3 Preparing the FRET assay in regulated actin

Single Cys mutants were introduced on a Cys-less TnI with native Cys 81 and 98 mutated to isoleucine and serine, respectively, and a Cys-less TnC plasmid with native Cys 35 and 84 mutated to serines. The complete list of single Cys TnI and TnC plasmids, in addition to the WT plasmids for TnI, TnC, and TnT, are shown in Table 1. Plasmids were sequenced prior to purification to confirm mutagenesis. Henceforth, proteins will be identified by their single Cys residue (e.g., TnI151C or TnI151). Plasmids were transformed into *E. coli*, and purified using fast protein liquid chromatography (FPLC). Figures 7-9 show representative results for recombinant TnC, TnI, and TnT purification. SDS-PAGE 12% (29:1) was used to analyze the purity of the Tn subunits. Panel C in Figures 7-9 shows the fractions containing purified Tn subunits. When a lane is overloaded, contaminant protein bands may appear. Figure 10, shows a representative SDS-PAGE gel loaded with 5 μM of Tn subunits, where contaminant proteins were too diluted to resolve. Since measurements will be performed using nanomolar concentrations of Tn, the likelihood of contaminant proteins in the sample solution is small. The staining intensity difference between equimolar-loaded subunits is due to the differences in molecular mass; higher molecular mass proteins provide more binding sites for Coomassie dye, and consequently stain more intensely.

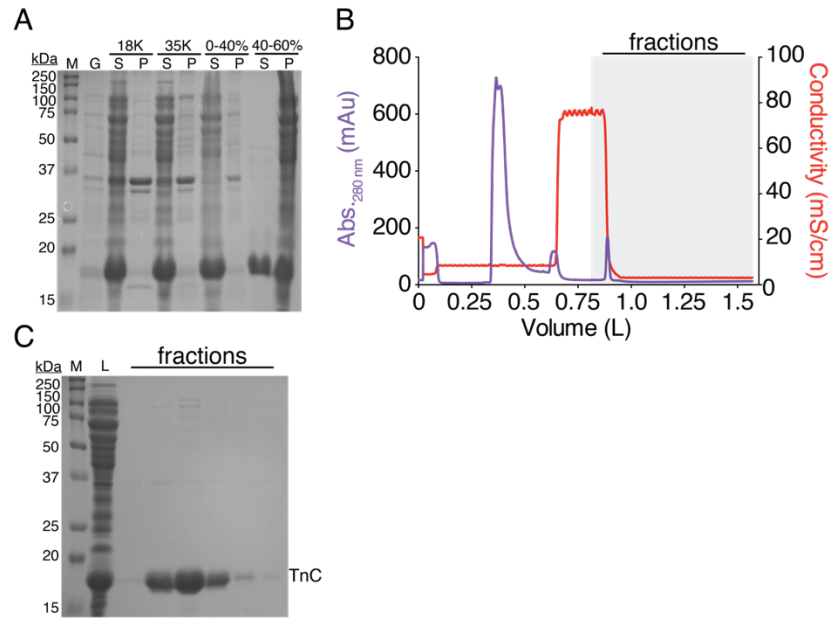


Figure 7. Purification of rcTnC. Representation of results from purification of recombinant rcTnC127C. **(A)** SDS-PAGE (12%, 29:1) of the cell lysis of BL21(DE3) competent *E. coli* cells and subsequent clarification using centrifugation and $(\text{NH}_4)_2\text{SO}_4$ precipitation. Molecular weight markers (M), *E. coli* grow (G), supernatant (S) and pellet (P) from 18 K rpm, 35 K rpm, 0-40% $(\text{NH}_4)_2\text{SO}_4$ precipitation 14 K rpm, and 40-60% $(\text{NH}_4)_2\text{SO}_4$ precipitation 14 K rpm sedimentation. **(B)** Resolution of TnC on Phenyl Sepharose. Absorbance at 280 nm (purple), conductivity (red), and fraction collection (grey box) are shown. The pellet containing TnC from the second $(\text{NH}_4)_2\text{SO}_4$ precipitation in (A) was loaded in the presence of 5 mM CaCl_2 . Weak hydrophobic products from the lysate were removed in the presence of 0.1 mM CaCl_2 and 1 M NaCl. TnC was eluted with a Ca^{2+} -free buffer. **(C)** Detection of purified TnC from the elution peak (around 0.9 L) from the absorbance at 280 nm. Molecular weight marker (M), sample loaded (L), and samples from the eluted fractions with purified TnC are shown.

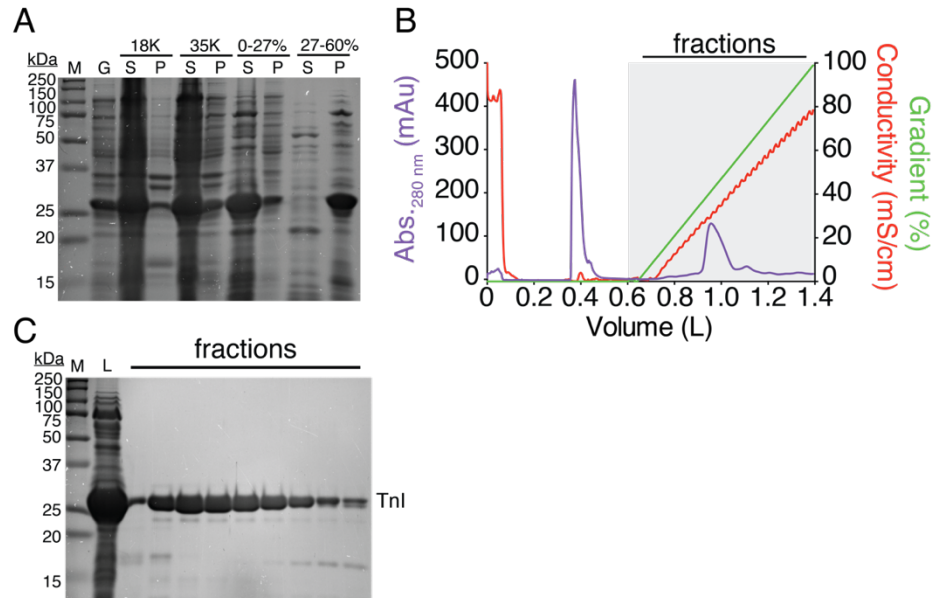


Figure 8. Purification of mcTnI. Representation of results from purification of recombinant mcTnI167C. **(A)** SDS-PAGE (12%, 29:1) of the cell lysis of BL21(DE3) competent *E. coli* cells and subsequent clarification using centrifugation and $(\text{NH}_4)_2\text{SO}_4$ precipitation. Molecular weight markers (M), *E. coli* grow (G), supernatant (S) and pellet (P) from 18 K rpm, 35 K rpm, 0-27% $(\text{NH}_4)_2\text{SO}_4$ precipitation 14 K rpm, and 27-60% $(\text{NH}_4)_2\text{SO}_4$ precipitation 14 K rpm sedimentation. **(B)** Resolution of TnT on DEAE Sepharose. Absorbance at 280 nm (purple), conductivity (red) and 500 mM KCl gradient (green), and fraction collection (gray box) are shown. The pellet containing TnI from the second $(\text{NH}_4)_2\text{SO}_4$ precipitation in (A) was loaded in a buffer containing no salt. **(C)** Detection of purified TnI around the 30% gradient mixture from the absorbance at 280 nm. Molecular weight marker (M), sample loaded (L), and samples from the eluted fractions with purified TnI are shown.

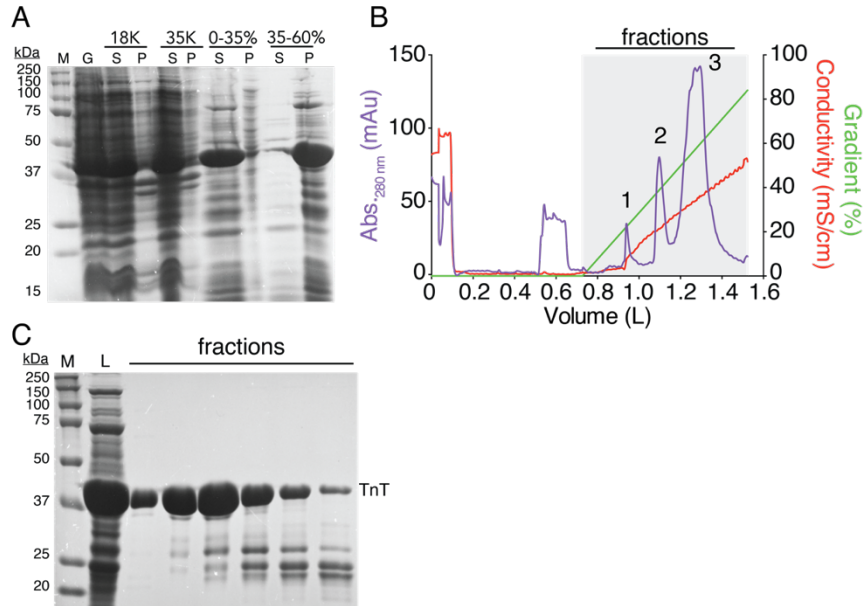


Figure 9. Purification of rcTnT. Representation of results from purification of WT rcTnT. **(A)** SDS-PAGE (12%, 29:1) of the cell lysis of BL21(DE3) competent *E. coli* cells and subsequent clarification using centrifugation and $(\text{NH}_4)_2\text{SO}_4$ precipitation. Molecular weight markers (M), *E. coli* grow (G), supernatant (S) and pellet (P) from 18 K rpm, 35 K rpm, 0-35% $(\text{NH}_4)_2\text{SO}_4$ precipitation 14 K rpm, and 35-60% $(\text{NH}_4)_2\text{SO}_4$ precipitation 14 K rpm sedimentation. **(B)** Resolution of TnT on DEAE Sepharose. Absorbance at 280 nm (purple), conductivity (red) and 500 mM KCl gradient (green), fraction collection (gray box) are shown. The pellet containing TnT from the second $(\text{NH}_4)_2\text{SO}_4$ precipitation in (A) was loaded in a buffer containing no salt. **(C)** Detection of purified TnT from elution peak 1 (around 0.9 L, 30% gradient) from the absorbance at 280 nm. Molecular weight marker (M), sample loaded (L), and samples from the eluted fractions with purified TnT are shown.

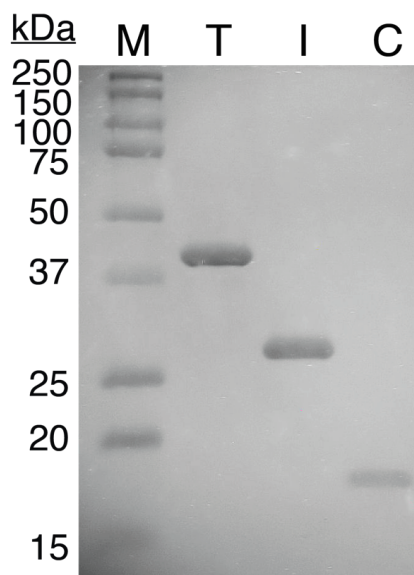


Figure 10. Purified troponin subunits. SDS-PAGE (12%, 29:1) showing purified TnT (T), TnI (I), and TnC (C) loaded at 5 μ M. Also shown are molecular weight markers (M).

Cys residues were site-specifically labeled with maleimide-containing fluorophores in a denaturing high urea buffer (6 M) to reveal Cys residues buried in globular protein form. The labeling reaction was at pH 7.2 to reduce non-specific amine labeling, and unbound dye was removed using size-exclusion chromatography. The degree of labeling (labeling ratio, f_A) was determined using Eq. 2. Typically, the labeling ratios for TnI*AF546 exceeded 95%; unfortunately, labeling ratios were at or below 80% for proteins labeled with ATTO dyes, although the labeling reaction was repeated three times. Labeling ratios were determined immediately prior to Tn reconstitution to ensure the highest degree of accuracy. Labeled proteins will henceforth be written as TnX###C*fluorophore, where X is the Tn subunit, ### is the Cys residue, and *fluorophore denotes covalent modification (e.g., TnC151C*AF546).

TnI, TnC, and TnT were combined to form reconstituted Tn through serial dilutions against high molar urea, to high salt, to low salt (150 mM KCl) for storage. Tn was stored for no longer than 6 months at -80°C , as these samples visibly precipitated (precipitate settled to bottom of tube), and were discarded. Tn reconstituted with a donor labeled on TnI, WT TnC, and WT TnT will henceforth be written as Tn-D, and Tn reconstituted with a donor on TnI, an acceptor on TnC, and WT TnT will henceforth be written as Tn-DA. Cardiac Tm and actin were purified from acetone powder from bovine left ventricle tissue. Figure 11 resolves the two Tm isoforms, α and β . Around 15-20% of skeletal Tm is in the β -isoform in adult larger mammals (such as bovine and human), whereas cardiac Tm is primarily composed of the α isoform.¹¹⁷ Tm and actin were resolved at 37 and 48 kDa, respectively, using SDS-PAGE.

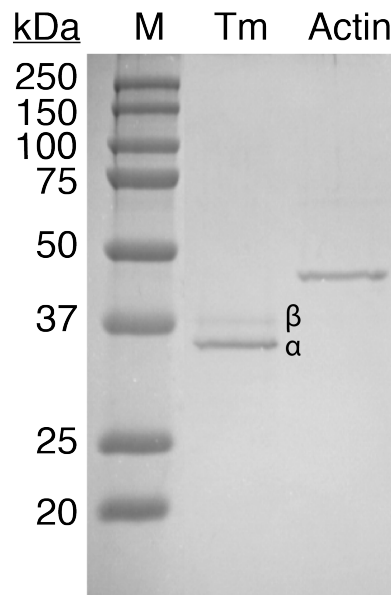


Figure 11. Tropomyosin and F-actin purified from bovine left ventricle muscle.

Molecular weight markers (M), tropomyosin (Tm) consisting of α and β isoforms, and F-actin (Actin) are shown.

3.2 Quality assessment of singly- and doubly-labeled regulated actin

The sarcomere in striated muscle is composed of a highly ordered structural array of muscle proteins arranged in filaments. To maintain the physiological function of thin filaments *in vitro*, preserving filament structure after reconstitution is imperative to maintaining a native-like environment. In muscle, there is generally one Tn bound for every one Tm dimer that lies across 7 actin monomers.³ Regulated actin filaments (rAc) were reconstituted at a ratio of 1:5:7 (Tn:Tm:Actin) with an ionic strength of 75 mM KCl. Filaments reconstituted with Tn-D, Tm, and actin will henceforth be written as rAc-D, and with Tn-DA, Tm, and actin will be written as rAc-DA. Epifluorescence imaging was used as the primary control to monitor thin filament morphology, as there were various conditions (buffer composition, incubation time, concentration of thin filament proteins) that influenced the integrity of rAc. All measurements on rAc were performed in working buffer (WB: 75 mM KCl, 50 mM MOPS pH 7.0, 5 mM MgCl₂, 2 mM EGTA, 5 mM BME), unless otherwise stated.

3.3 Epifluorescence imaging reveals stability of filaments under various conditions

3.3.1 Tn binding to Tm-actin is dependent on ionic strength

rAc-DA was reconstituted with TnI182C*AF546, TnC89C*ATTO655, and with actin labeled with phalloidin-AF488 in WB with 75, 150, 225, or 300 mM total KCl, and incubated for 1 hour at 4°C. Filaments were deposited at 10 nM (in Tn) on glass coverslips, and imaged using epifluorescence microscopy. Figure 12 shows the directly-excited emission from TnI182C*AF546, TnC89C*ATTO655, and actin*phalloidin-

AF488. As ionic strength increases from 75 mM, the amount of Tn in solution increases, evident by an increase in background points of fluorescence. The amount of Tn bound to actin and Tm decreases, evident by the decrease in white signal from the merged images. White indicates a co-localization of green, red, and blue signals. The approximate length of actin, and the emission intensity from phalloidin-AF488, remains relatively constant across all ionic strengths. Therefore, an ionic strength of 75 mM promotes Tn binding to Tm and actin. However, Tn was still not congruently bound across actin, evident by large gaps in co-localized signal across the actin filaments.

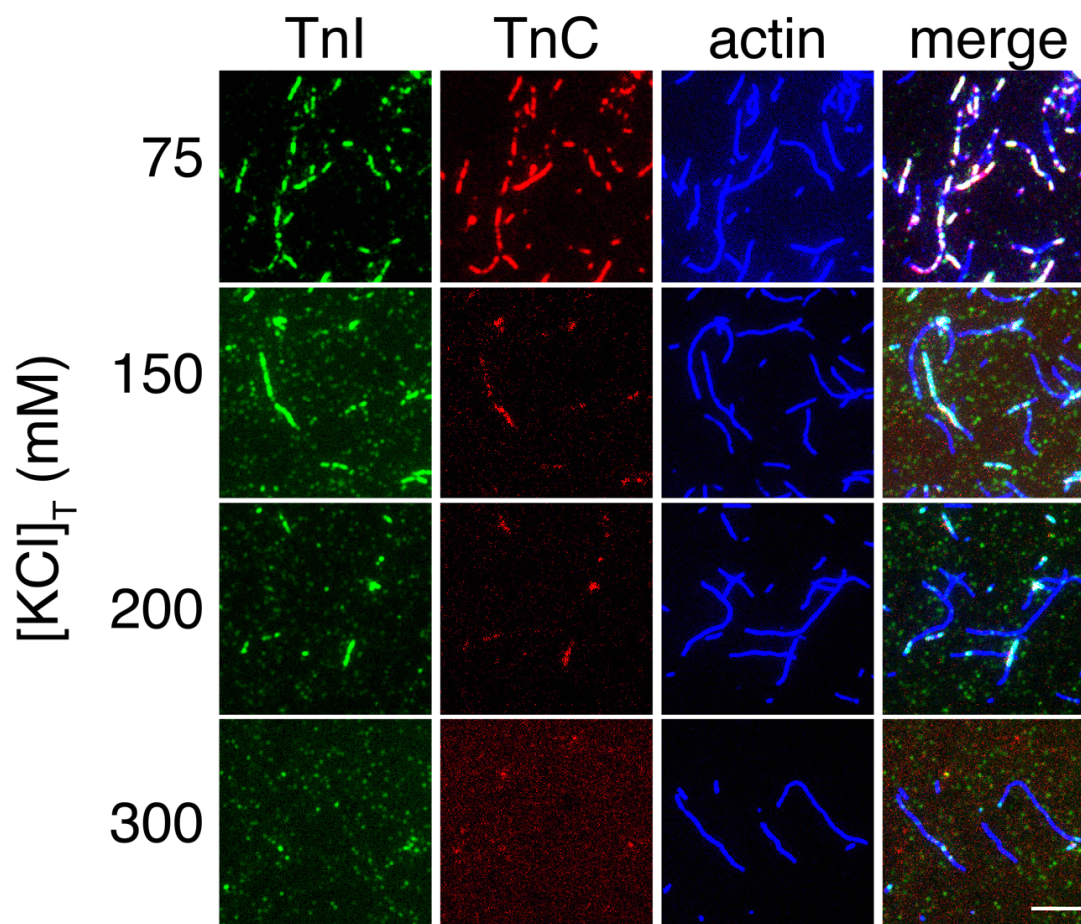


Figure 12

Figure 12. Tn binding to actin and Tm depends on ionic strength. rAc with Tn-DA (TnI182C*AF546, TnC89C*ATTO655) was reconstituted with Tm and actin stained with phalloidin-AF488 at a ratio of 1:1:7 (Tn:Tm:Actin) at a total ionic strength of 75, 150, 200, and 300 mM KCl, and incubated for 1 hour at 4°C. Filaments were diluted to 10 nM, and deposited on glass coverslips. Emission from AF546 (excitation, 545/25; emission 605/70), ATTO655 (excitation 620/60; emission 700/75), AF488 (excitation, 475/35; emission 550/88), and merged images are shown. With higher ionic strength (>75 mM KCl), Tn is dissociated from Tm and actin, evident by the appearance of points of fluorescence in the AF546 and ATTO655 images, and the disappearance of colocalized Tn on actin (decrease in white from merge images). The scale bar is 5 μ m.

3.3.2 Incubation time affects Tn binding to Tm and actin

rAc-D reconstituted with TnI211C*ATTO550, Tm, and actin stained with phalloidin-AF488 (1:1:7) was imaged after incubation at 4°C for 1 day, 1 week, and 3 months. Figure 13A shows the emission from labeled TnI and actin, and the merged images. A 1 day incubation yielded short filaments with sparse Tn binding, and isolated Tn was visible in the background. Filaments showed congruently bound Tn and elongated filaments (5-10 μ m) after 1 week, with little to no Tn in the background. A 3-month incubation yielded even longer filaments (>10 μ m), though the amount of Tn bound appears relatively unchanged from the 1 week incubation. The presence of congruently bound Tn-DA, suggested by the co-localized emission from TnI (green) and TnC (red), indicates Tn incorporated onto Tm and actin as an intact assembly.

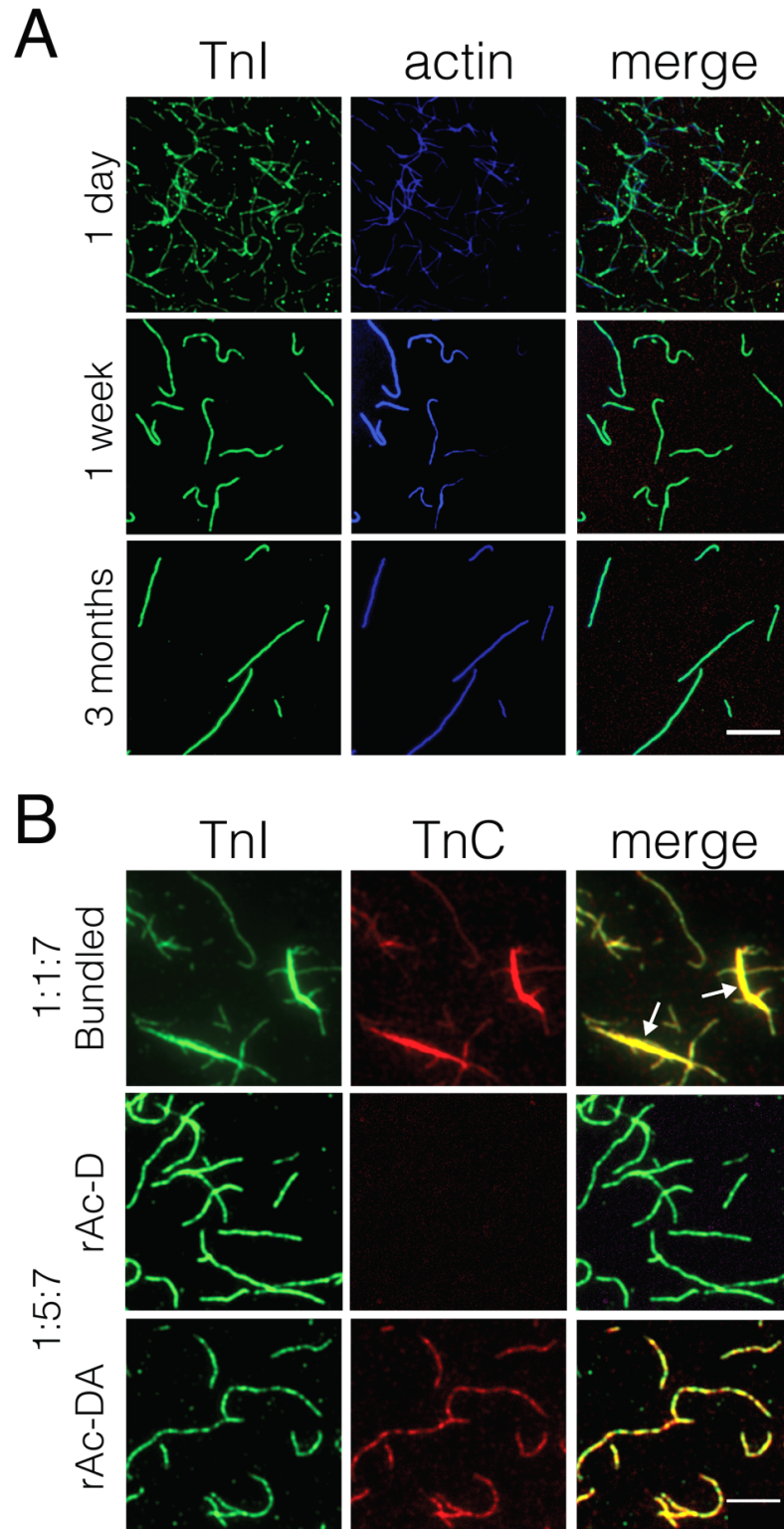


Figure 13

Figure 13. Physical characterization of labeled regulated actin filaments. (A)

Incubation time affects filament remodeling. Epifluorescence images of rAc-D with Tn-D (TnI211*ATTO550, TnC, TnT) and actin stained with phalloidin*AF488 was diluted to 10 nM in WB 1 day, 1 week, and 3 months after reconstitution at 4°C. Emission from ATTO550 (excitation, 545/25; emission 605/70), AF488 (excitation, 475/35; emission 550/88), and merged images show filament remodeling with time. Filaments appear longer, less dense, and more continuously decorated with Tn after 1 week. The scale bar is 5 μ m. **(B)** The quantity of Tm affects filament stability. Epifluorescence images of rAc-DA with Tn-DA (TnI189C*AF546, TnC127C*ATTO655, TnT) showing aggregated (bundled) filaments reconstituted with a 1:1:7 mixture of Tn:Tm:actin. Single (non-bundled) filaments made with a 1:5:7 mixture of Tn:Tm:actin with rAc-D with Tn-D (TnI189C*AF546) and rAc-DA are shown. Emission from AF546 (excitation 545/25; emission 605/70), directly-excited ATTO655 (excitation 620/60; emission 700/75), and the merged images are shown. The scale bar is 5 μ m.

3.3.4 The quantity of Tm affects filament stability

Filaments reconstituted with Tn:Tm:Act at a ratio of 1:1:7 had a 25% chance of bundling. Bundling was evident in epifluorescence imaging by the appearance of thicker filaments, with the tails showing multiple “single” filament threads. Figure 13B shows an example of bundled rAc-DA reconstituted from Tn-DA (TnI182C*AF546, TnC127C*ATTO655). Increasing the Tm concentration in solution during reconstitution dropped the bundling rate to <10%. Figure 13B shows the emission from rAc-D reconstituted with Tn-D (TnI182C*AF546) and rAc-DA reconstituted with Tn-DA

(TnI182C*AF546) at a ratio of 1:5:7 Tn:Tm:Act. Filaments appear non-bundled and single. All rAc reconstitutions were therefore performed with a Tn:Tm:Act ratio of 1:5:7, unless otherwise stated, and incubated for at least 1 week prior to measurements.

3.3.5 Proteins did not undergo proteolysis after reconstitution and incubation

Sample purity and protein integrity of reconstituted filaments were assessed using SDS-PAGE. Figure 14 shows rAc reconstituted with WT Tn at a ratio of 1:1:7, and the pre-spin mixture and sedimented pellet of rAc reconstituted at a ratio of 1:5:7. The proteins showed minimal to no degradation after both Tn and rAc reconstitution. TnC had a faint band due to its low molecular mass. When rAc is sedimented, the pellet should show actin at a ≈ 7 times higher intensity than Tn subunits. Therefore, the intensity of Tm in the pellet should be similar to the Tn subunits, and similar to Tm in rAc reconstituted with a ratio of 1:1:7. The similarities in the Tm band intensities for the reserved (W) and pellet (P) of 1:1:7 and 1:5:7 rAc, respectively, showed the amount of Tm bound to actin remains unchanged regardless of the amount of Tm present in solution.

3.3.6 Ca^{2+} does not affect the physical characterization of regulated actin filaments

This assay was designed to monitor Ca^{2+} -dependent conformational changes in Tn. To determine if changes were coming from Tn structural changes or filament instability with Ca^{2+} , filaments were imaged with and without Ca^{2+} . rAc-DA reconstituted with Tn-DA (TnI182C*AF546, TnC127C*ATTO655) was diluted to 500 nM, and imaged at 10 nM (no Ca^{2+} , apo). rAc-DA was then supplemented with 3 mM CaCl_2 and imaged at 10 nM after 10 min, 2 hours, and 5 hours to determine if Ca^{2+} affected filament

morphology. Figure 15 shows Ca^{2+} had no effect on filament morphology, evident by similar emission profiles, suggesting Ca^{2+} -induced changes in dynamics or structure are not due to filament dissociation.

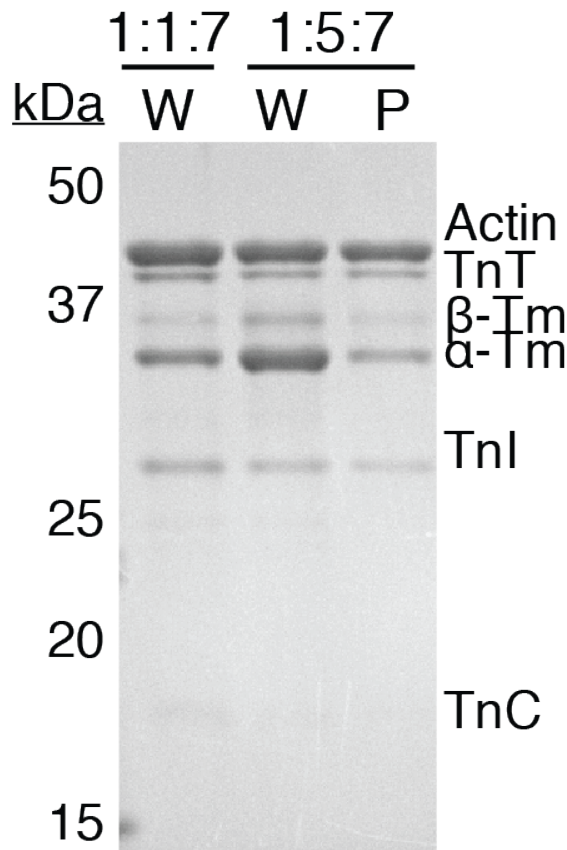


Figure 14. Assessment of sample purity of reconstituted rAc. SDS-PAGE (12%, 29:1) of rAc reconstituted with WT Tn, Tm, and actin at a ratio of 1:1:7 or 1:5:7. TnI, TnC, TnT, Tm with α and β isoforms, and actin are resolved. A pre-spin mixture (W) of 1:1:7 rAc (5 μM in actin protomer), and the W and pellet (P) of sedimented 1:5:7 rAc (5 μM in actin protomer) are shown. Molecular weight markers are not shown.

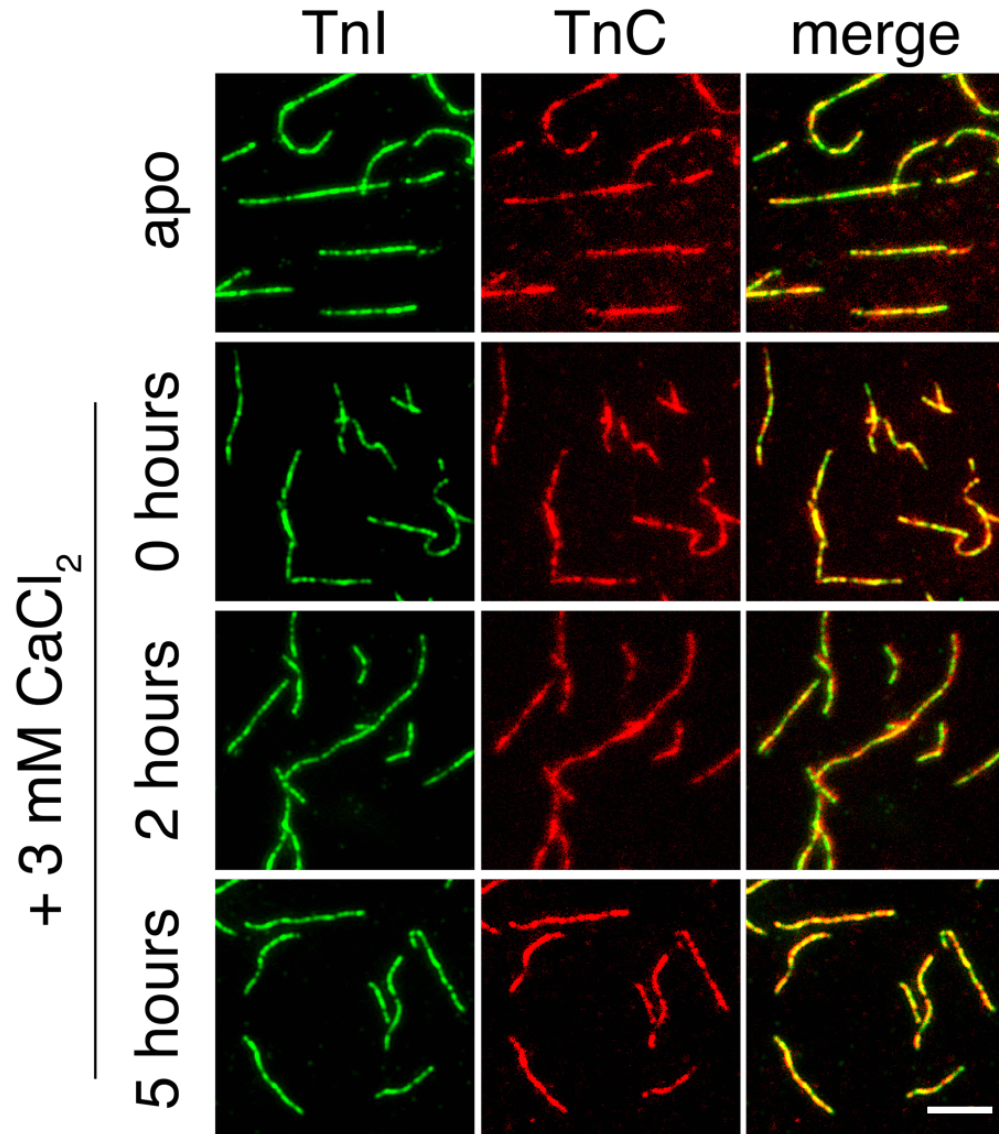


Figure 15. Calcium does not affect the physical morphology of regulated actin. rAc-DA filaments reconstituted with Tn-DA (TnI182C*AF546, TnC127C*ATTO655) were diluted to 500 nM, then imaged at 10 nM (no Ca²⁺, apo). rAc-DA was then supplemented with 3 mM CaCl₂ and imaged after 0, 2, and 5 hours. Emission from AF546 (excitation 545/25; emission 605/70), directly-excited ATTO655 (excitation 620/60; emission 700/75), and the merged images are shown. The scale bar is 5 μ m.

3.4 FCS as a filament screening tool

Fluorescence correlation spectroscopy (FCS) can be used to estimate the mobility of molecules in solution.¹¹⁸ The primary parameter in FCS is not the emission from the fluorophore, but the fluctuations in the emission intensity at thermodynamic equilibrium over time. These fluctuations can be quantified by temporally autocorrelating the recorded intensity signal,¹⁰⁵ and the fluctuations depend on the rate of diffusion of a fluorophore through the confocal volume. Assuming the fluorescent properties of AF546 and ATTO550 do not change with time, and assuming a constant excitation power and a three-dimensional Gaussian intensity profile,¹¹⁹ the translational correlation time τ_C and diffusion coefficient D can be determined for a sample.

FCS was used during data collection to assess filament diffusion. To determine if the sample contained Tn bound to Tm-actin or unbound Tn, the fluorescence emission from isolated AF546, TnC127C*AF546, Tn-D (TnC127C*AF546), and rAc-D (TnC127C*AF546), called rAc^{C*}, were analyzed using FCS. As the FRET assay was designed with donors on TnI, a representative data set of rAc-D (TnI211C*ATTO550), called rAc^{I*}, was also included in the normalized autocorrelations shown in Figure 16. rAc were fit to a model of two diffusing species (Eq. 7), and all other traces were fit to a model of a single diffusing species. AF546, TnC, and Tn had translational correlation times of 0.03, 0.10, and 0.16 msec, respectively. The translational correlation times (fractional amplitude) for rAc^{C*} were 2.48 (0.44) and 18.23 (0.56) msec, and for rAc^{I*} were 4.16 (0.46) and 81.61 (0.54) msec.

The faster time components for rAc samples are most likely due to shorter fragments of rAc filaments, and not free Tn or TnI, as the correlation times for these

shorter components are more than an order of magnitude longer than correlation times for free Tn and TnI. Aggregates of TnI and Tn may account for this shorter correlation time component; however, the low prevalence of aggregates evident in epifluorescence imaging would not support that claim. The second or slow components for rAc samples is attributed to longer filaments, which are visible in epifluorescence images, and range between 5-15 μm in length.

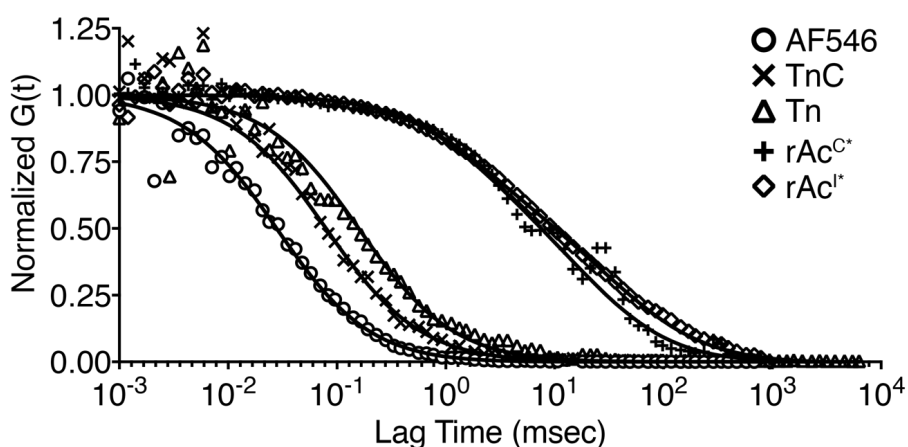


Figure 16. Fluorescence correlation spectroscopy estimates the molecular weight of a freely-diffusing particle. Correlation times correlate to sample molecular weights. The normalized autocorrelation function of free AF546 dye (500 pM, \circ), labeled TnC (TnC127*AF546, 500 pM, \times), Tn reconstituted with TnC127C*AF546 (100 nM, \triangle), rAc reconstituted with TnC127C*AF546 (rAc^{C*}, 100 nM, $+$), and rAc reconstituted with TnI211C*ATTO550 (rAc^{I*}, 100 nM, \diamond) are shown. Solid lines represent fits of AF546, TnC, and Tn samples to a model of a single diffusing species with translational correlation times of 0.03, 0.10, and 0.16 msec, respectively, or rAc fit to a model of two diffusing species to determine correlation times (fractional amplitudes), where rAc^{C*} has 2.48 (0.44) and 18.23 (0.56) msec, and rAc^{I*} has 4.16 (0.46) and 81.61 (0.54) msec.

Molecular diffusion D and friction F are related by $F = -f v$, where f is the translational frictional coefficient and v is velocity. Friction and molecular size are related by Stokes' equation, where $f = 6\pi\eta a$ for a smooth sphere with a minimal hydrodynamic radius a for a molecule of a certain molecular weight, and η is the viscosity of the solution. Einstein's relation

$$D = \frac{k_B T}{f} = \frac{k_B T}{6\pi\eta a}, \quad (8)$$

shows the diffusion coefficient is inversely proportional to size, where k_B is Boltzmann's constant, and T is temperature. The radius a can be calculated from the molecular mass M of the molecule using

$$a = \sqrt[3]{\frac{3M/N_A}{4\pi\rho}}, \quad (9)$$

where N_A is Avogadro's number = $6.023 \times 10^{23} \text{ mol}^{-1}$, and ρ is the mean density of the molecule, assumed to be $\approx 1 \text{ g/mL}$ for globular proteins. The diffusion coefficient is therefore proportional to $M^{-1/3}$, giving a proportionality constant of ≈ -0.33 . Translational correlation times are related to diffusion coefficients by

$$\tau_c = \frac{\omega_0^2}{D}, \quad (10)$$

where $\omega_0 = 0.22 \text{ }\mu\text{m}$ is the axial radius of the confocal detection volume.¹²⁰ The dependence of the diffusion coefficient on the molecular mass of the labeled sample is shown in Figure 17 for molecules of known molecular mass, which are 1.0, 18.4, and 78.3 kDa for AF546, TnC, and Tn, respectively. The experimental data were fit using linear regression (log scale). The slope yielded a proportionality constant of -0.40, which

differs by 18% from the theoretical value. This difference may come from a misestimation of the confocal volume.

FCS gives molecular mass properties of a sample by monitoring the translational correlation times. rAc was analyzed using FCS from TCSPC measurements, which allowed for rejection of samples showing large populations of non-incorporated Tn, free TnC, or an excess of free dye. Using epifluorescence imaging and FCS provided means of examining only reconstituted rAc filaments that met certain quality standards: i) labeled Tn should be congruently bound to the filaments, ii) there should be no aggregates of Tn and TnI, iii) filaments should not be bundled, iv) there should not be a large population of unbound Tn or TnI (donor) in solution. These standards were in place to assure reconstituted filaments replicate native filament conditions by reducing artifacts introduced in the complex sample preparation.

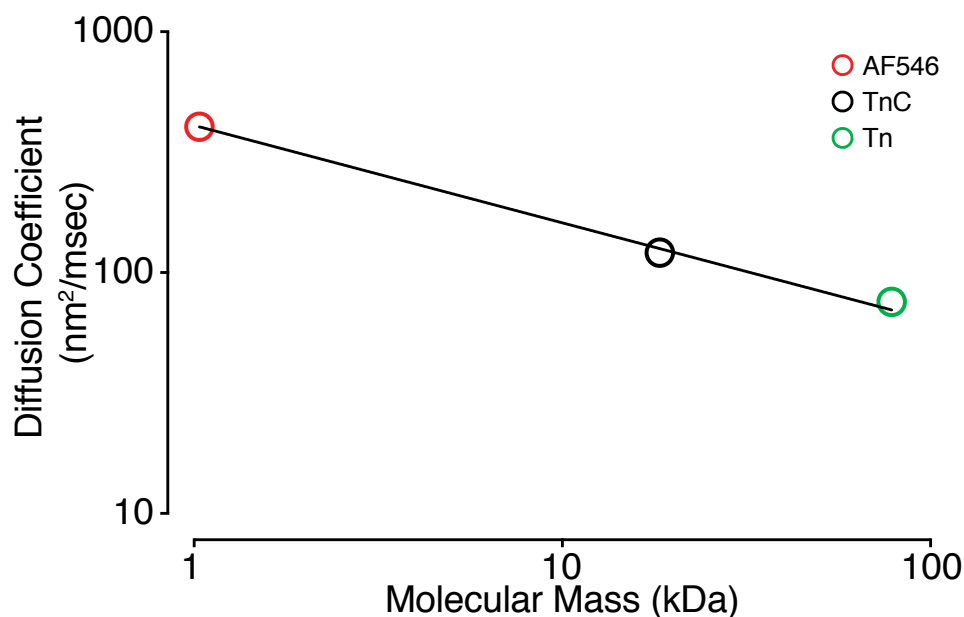


Figure 17

Figure 17. Dependence of the diffusion coefficients on molecular mass. Free AF546 dye (red), TnC127C*AF546 (black), and Tn-D (TnC127C*AF546) (green) were analyzed using FCS, and the autocorrelation was fit to a model of a single diffusing species. The translational correlation times were converted to diffusion coefficients and plotted against known molecular masses. The data were fit using linear regression (log scale) (black line), which yielded a slope and Y-intercept of -0.40 and -0.39, respectively. $R^2=0.98$.

3.5 TCSPC measurements of regulated actin filaments

Ensemble lifetime measurements were performed using time correlated single photon counting (TCSPC). Following excitation by a pulse of light, the donor fluorophore absorbs the photon, and the lifetime is the average amount of time the fluorophore remains in this excited state.¹⁰⁵ The sample is excited thousands of times, and the lifetimes are compiled into a histogram of intensity with respect to time. One benefit of using time-resolved methods to perform FRET measurements is the lifetime of a sample is not dependent on the concentration of fluorophores in the confocal volume, thereby removing the need for donor concentration-matching in paired D and DA samples. Lifetime is calculated from a multiexponential fit to the TCSPC histogram, and the peak intensity value does not affect the lifetime. Lifetimes are also independent of static quenching. Static quenching is the formation of a non-fluorescent complex between the donor and acceptor, creating a population of “invisible” donors that upon excitation do not release a photon during relaxation.^{105, 121} In steady-state FRET measurements,

where the emission intensity of the donor is used to calculate transfer efficiency, these “dark” complexes can yield falsely higher transfer efficiencies.

The donor lifetime was collected in filaments absent an acceptor (rAc-D, reconstituted with Tn-D with TnI151C*AF546, TnI160C*AF546, TnI167C*AF546, TnI174C*AF546, TnI177C*AF546, TnI182C*AF546, TnI189C*AF546, TnI196C*ATTO550, TnI200C*ATTO550, TnI204C*ATTO550, TnI208C*ATTO550, or TnI211C*ATTO550, for a total of 12 donor positions), and in the presence of an acceptor (rAc-DA, reconstituted with Tn-DA with either TnC35C*ATTO655, TnC89C*ATTO655, or TnC127C*ATTO655 as the acceptor, for a total of 36 unique FRET pairs). rAc filaments were diluted to 500 nM in WB (apo), or WB supplemented with saturating Ca^{2+} (+Ca, 3 mM). The laser power and collection time were adjusted to reach a peak of >10,000 counts to ensure reasonable photon counting statistics,¹²² which typically took ≈ 10 min. An average background of 80 counts/sec for the avalanche photodiode (APD) detector indicated a good signal to noise ratio. Fluorescence decays were convolved with the instrument response function (IRF, at FWHM = 85 ps), and amplitude-weighted lifetimes were recovered from a nonlinear least-squares multi-exponential fitting. χ^2 values show goodness of fit, with a value = 1 indicating a perfect fit. To confirm reproducibility, measurements were repeated at least three times on separately reconstituted filaments. Figure 18 shows a typical set of fluorescence decays for ATTO550 in rAc-D (Tn-D, TnI208C*ATTO550) and rAc-DA (Tn-DA, TnI208C*ATTO550, TnC127C*ATTO655) under apo and +Ca conditions.

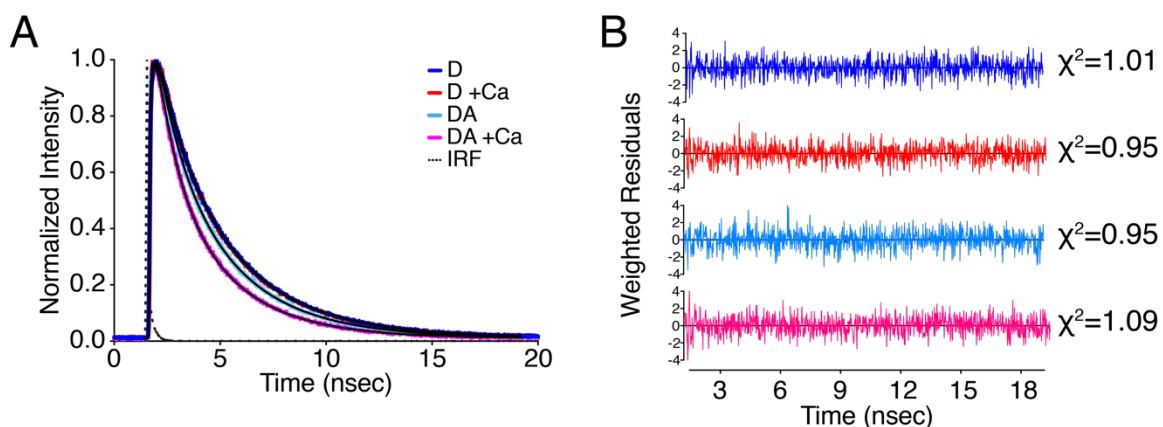


Figure 18. Lifetime measurements of donor-only and donor/acceptor rAc filaments.

Representative lifetime decay data from TCSPC analysis showing the normalized emission intensity decay from the donor in rAc-D reconstituted with Tn-D (TnI208C*ATTO550) and rAc-DA reconstituted with Tn-DA (TnI208C*ATTO550, TnC127C*ATTO655) diluted to 500 nM in WB or WB supplemented with 3 mM CaCl₂ (+Ca). **(A)** ATTO550 lifetime decays for rAc-D (blue), rAc-D +Ca (red), rAc-DA (cyan), and rAc-DA +Ca (magenta). Black lines represent fits to a multi-exponential decay model to the data convolved with the instrument response function (IRF, dotted line). Amplitude-weighted mean lifetimes $\langle\tau_D\rangle$ are 3.30, 3.28, 3.01, 2.64 nsec, respectively. **(B)** Weighted residuals from fits in (A) with χ^2 values shown. A consistent coloring scheme is used in (A-B).

A representative table of lifetime (fractional amplitude), amplitude-weighted mean lifetime, χ^2 , and E for rAc-D, and for rAc-DA with an acceptor attached to TnC residue 35, 89, or 127 can be found in Tables A1-4. Donor-only lifetime decays were fit to three-exponential fit for samples labeled with AF546, and two-exponential fits for samples labeled with ATTO550. The inverse lifetime is the sum of rates that depopulate

the excited state, and therefore a fluorophore in solution (ideally a donor-only filament) should show single exponential decay lifetimes, indicating no competing paths for excited state depopulation.¹⁰⁵ The heterogeneous character of the donor-only lifetime decays, particularly those with a three-exponential fitting, may be due to self-quenching from interactions between the dye and protein residues (dynamic quenching). Because the decay is heterogeneous, the amplitude-weighted mean lifetime was used for calculating E to remove any assumptions as to the nature of the individual decay rates.¹²³ rAc—DA lifetime decays were always fit to a three exponential function. For most fits, τ_1 was less than 1 ns, and accounted for less than 20% of the total lifetime, and is attributed to scattering from the glass coverslip or the solution.

3.6 Calculating FRET efficiency and inter-dye distance

The donor dye was not sensitive to Ca^{2+} , evident from the comparison of donor lifetimes in rAc-D filaments under apo and +Ca conditions. Table A1 shows the lifetimes of donor-only filaments from one reconstitution set. The average Ca^{2+} -induced lifetime change ($\langle \tau_D \rangle_{+Ca} - \langle \tau_D \rangle_{apo}$) \pm SEM is 0.02 ± 0.01 ns ($n = 12$). Although the change is not significant, apo and +Ca E were calculated from $\langle \tau_D \rangle$ and $\langle \tau_{DA} \rangle$ collected in the absence or presence of 3 mM CaCl_2 , respectively, to maintain similar environmental conditions around the donor dye.

The amplitude-weighted mean lifetime of the donor in the absence $\langle \tau_D \rangle$ and presence of an acceptor $\langle \tau_{DA} \rangle$ was used to calculate transfer efficiency E using Eq. 5. The inter-dye distance R between D and A dyes was calculated using the Förster relation (Eq. 4). Due to the dependence on distance of resonant energy transfer, an increase in transfer

efficiency corresponds to a decrease in the inter-dye distance. To account for absent acceptor fluorophores in rAc-DA filaments (i.e., a donor-only population), E were corrected using the acceptor labeling efficiency f_A . The FRET efficiency E is typically calculated using

$$E = (\langle\tau_D\rangle - \langle\tau_{DA}\rangle)/\langle\tau_D\rangle. \quad (11)$$

The amplitude-weighted mean lifetime of the donor in rAc-DA filaments is

$$\langle\tau_{DA}\rangle = f_A\langle\tau_{DA}'\rangle + (1 - f_A)\langle\tau_D\rangle, \quad (12)$$

where $\langle\tau_{DA}'\rangle$ is the lifetime of the donor in the presence of an acceptor, and $\langle\tau_D\rangle$ is the lifetime of the donor in the absence of an acceptor determined from TCSPC measurements of rAc-D filaments. $(1 - f_A)\langle\tau_D\rangle$ and $f_A\langle\tau_{DA}'\rangle$ are the contributions to donor lifetime from populations of Tn-D and Tn-DA within rAc-DA filaments, respectively. To correct E for the presence of this donor-only population, $\langle\tau_{DA}\rangle$ is substituted with $\langle\tau_{DA}'\rangle = \frac{\langle\tau_{DA}\rangle}{f_A} - \frac{\langle\tau_D\rangle}{f_A} + \langle\tau_D\rangle$ from Eq. 12 to yield Eq. 5.

The presence of a donor-only population in rAc-DA samples inflates $\langle\tau_{DA}\rangle$, resulting in lower transfer efficiencies and longer inter-dye distances. To emphasize confidence in utilizing f_A as a correction factor for calculating E from lifetime decays, a representative example of uncorrected E and R and f_A -corrected E and R obtained from three separately reconstituted rAc-D (Tn-D, TnI211C*ATTO550) and rAc-DA (Tn-DA, TnI211C*ATTO550, TnC127C*ATTO655) are shown in Table A5. The data were chosen due to the large variation in f_a , where f_a ranges from 0.33 to 0.85. Table A6 shows the average E and $R \pm$ SEM. Figure 19 shows the changes in E and R when using f_A correction, where values for E increase and R decrease. This suggests f_A can be used to correct for a population of donors absent an acceptor in rAc-DA samples. Even with

diverse sample conditions in separately reconstituted filaments, the mean E and R show a smaller variance compared to the uncorrected data. The Ca^{2+} -depleted and Ca^{2+} -saturated FRET efficiencies for the three acceptor positions were plotted for each donor residue (Figure 20). Tables A7, A8, and A9 show the E and R with and without Ca^{2+} for all donors with respect to acceptor TnC35C, TnC89C, and TnC127C, respectively.

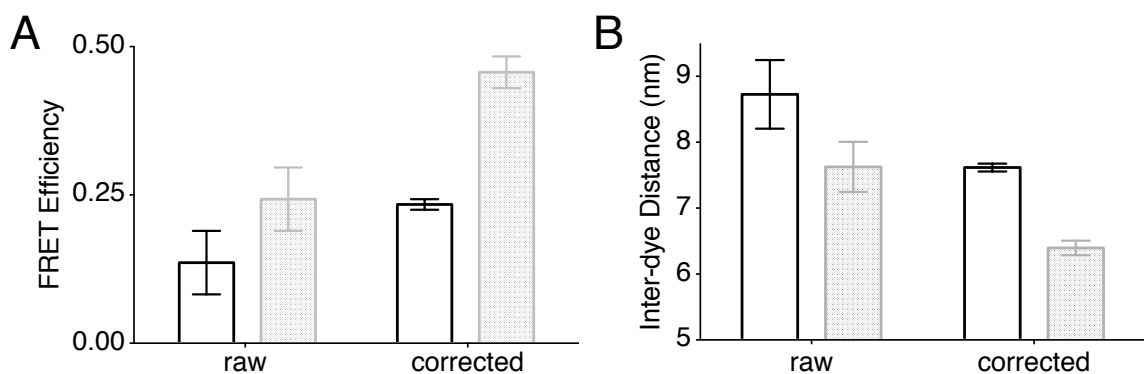


Figure 19. Correcting the FRET efficiency with the acceptor labeling efficiency removes the influence of a donor-only population in Tn-DA-decorated filaments.

Representative data for separately reconstituted rAc-D (Tn-D, TnI211C*ATTO550) and rAc-DA (Tn-DA, TnI211C*ATTO550, TnC127C*ATTO655) filaments. **(A)** The non-corrected (raw) and f_a -corrected mean FRET efficiency E for rAc (apo, black), and rAc supplemented with 3 mM CaCl_2 (+Ca, grey). Error bars represent SEM ($n = 3$). **(B)** The mean inter-dye distance R calculated from E (raw) and E_c (corrected) for rAc, and rAc supplemented with 3 mM CaCl_2 . Error bars represent SEM ($n = 3$). A consistent coloring scheme is used in panels A-B.

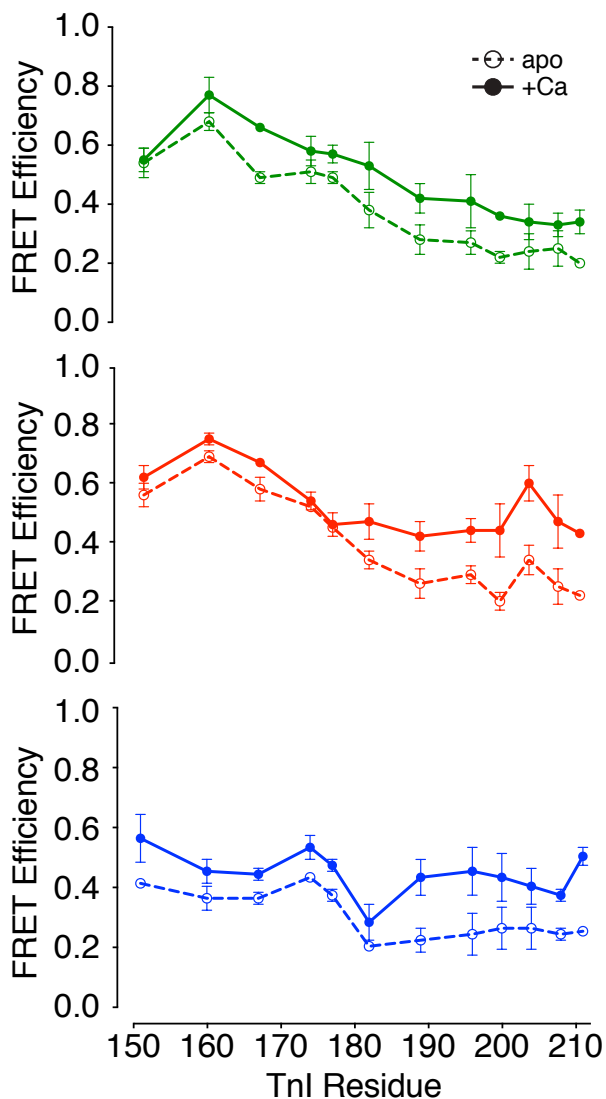


Figure 20. FRET efficiencies in Tn within thin filaments with and without Ca^{2+} . rAc filaments were diluted to 500 nM in WB (apo, open circles and dotted line) or WB supplemented with 3 mM CaCl_2 (+Ca, solid circles and solid line). Transfer efficiencies were calculated from the amplitude-weighted mean lifetime of the donor, and the donor in the presence of the acceptor on TnC35C (green), TnC89C (red), or TnC127C (blue). Increases in E with Ca^{2+} indicate the donor on TnI moving closer to TnC. Average $E \pm \text{SEM}$ ($n = 3$) is shown.

Studies utilizing FRET as a structural biology method should take heed of the influence on E (and R) by the orientation of the fluorophores. This influence depends on the constrained nature of the covalently attached dyes, and the influence on the emission and absorption dipole moments of the donor and acceptor fluorophores, respectively.¹²⁴ In calculating FRET efficiency, the orientation factor κ^2 was assumed to be $2/3$, as both the donor and acceptor have C_5 linkers that should allow for free rotation of the dyes to sample random orientations.¹¹¹ If there is not free rotation, an error of up to 35% could be introduced to R calculations.¹⁰⁵ To completely remove any doubt about the distances obtained, fluorescence anisotropy measurements, which determine whether or not covalently attached fluorophores are freely rotating in solution, would need to be performed on both the donors and acceptors in the future to determine whether the fluorophores are constrained.¹⁰⁵ Anisotropy values would give a tailored R_0 for each FRET pair (instead of using a universal R_0 based on isolated fluorophore emission spectra), which would theoretically produce more accurate calculation of R . These experiments are time-consuming and sample intensive, and thus would be more appropriate for a future study. Conveniently, Xing et al. published anisotropy results for an AEDANS (5-(iodoacetamidoethyl)amino-naphthalene-1-sulfonic acid) fluorophore covalently bound to mcTnI residues 151C, 160C, 167C, 188C, and 210C in thin filaments, and reported no change in fluorophore mobility across all TnI residues.¹²⁵ This provides a small level of insight into the protein environment of some of the donor residue positions.

3.7 Inter-dye distances reveal the dynamics of the C-TnI

3.7.1 Dynamics of the C-TnI with respect to the N-lobe of TnC

The Ca^{2+} -depleted and Ca^{2+} -saturated R for rAc with acceptor TnC35 are plotted for each donor residue (Figure 21A). The Ca^{2+} -induced change in inter-dye distance ($\Delta R = R_{+ca} - R_{Ca}$) is shown in Figure 22B, with the corresponding change in E for reference in Figure 22A. A comparison between recovered +Ca R and R_{mod} is shown in Figure 22D. Average ΔE and ΔR values \pm SEM ($n = 3$) are shown in Table A10. Negative ΔR values indicate the donor and acceptor fluorophores move closer together in space due to Tn conformational changes.

The switch region (residues 151-167) maintained a distance of ≈ 5.3 nm from the N-lobe of TnC, ≈ 3 nm farther than predicted by the MTS model. TnI167 had an appreciable $\Delta R = -0.60$ nm, though other residues in the switch region had minimal ΔR . TnI167 may be in a portion of the switch region moving closer to the N-lobe; however, the switch region and N-TnC are too far apart to be interacting. ΔR were greater in the C-terminal end (residues 182-211) than in the switch region, suggesting a more dynamic nature probably corresponding to the second actin binding site (SABS) lifting off actin when Ca^{2+} binds to N-TnC. Because apo and +Ca R values increased sharply after TnI177, the N-TnC may be positioned in the middle of the switch region, with TnI177-211 extending laterally away from N-TnC.

The minimal Ca^{2+} -induced movements in the switch region are slightly surprising, though not a novel discovery. Cordina et al. used paramagnetic relaxation enhancement NMR in a recombinant binary complex of rcTnC/TnI to show movement in the switch region (residues 151 and 159) and IR (residue 143) was small, suggesting the switch

region remains close to the N-lobe of TnC to increase the probability the switch region will bind to the incompletely open N-lobe.¹²⁶ They averaged the Ca^{2+} -induced distance changes for TnI residues 151 and 159 with respect to the N-lobe, and observed $\Delta R_{\text{av}} = -0.95$ nm. The FRET-derived ΔR_{av} for TnI151, 160, and 167 is -0.33 nm. Differences may be due to the influence on TnC and TnI structure from TnT, Tm, and actin that force the switch region away from N-TnC; a binary TnC/TnI complex may retain a more compact structure.

Ca^{2+} -induced distance changes with respect to the N-TnC were smaller than those in the inter-lobe linker (acceptor TnC89C) and C-lobe (acceptor TnC127C). This suggests the change in distance was due to TnC movement, not TnI movement. One of the novel benefits of this study was maintaining the same donors on TnI and altering the acceptor positions on TnC, allowing for insights into both TnC and TnI dynamics, as all Ca^{2+} -induced ΔR would be the same if TnC was immobile. NMR has shown N-TnC has independent dynamics,¹²⁷ though the results presented here show N-TnC has only minimal dynamics compared to the rest of TnC. The partial opening of this N-lobe when Ca^{2+} binds does not cause dramatic movement of the lobe in space. However, spatial movement may not be resolved using FRET if TnC35C moves orbitally with respect to a donor on TnI—movement space would not translate to a change in distance. These inquiries could be clarified in the future by applying the resolved distance constraints from all acceptors towards molecular modeling.

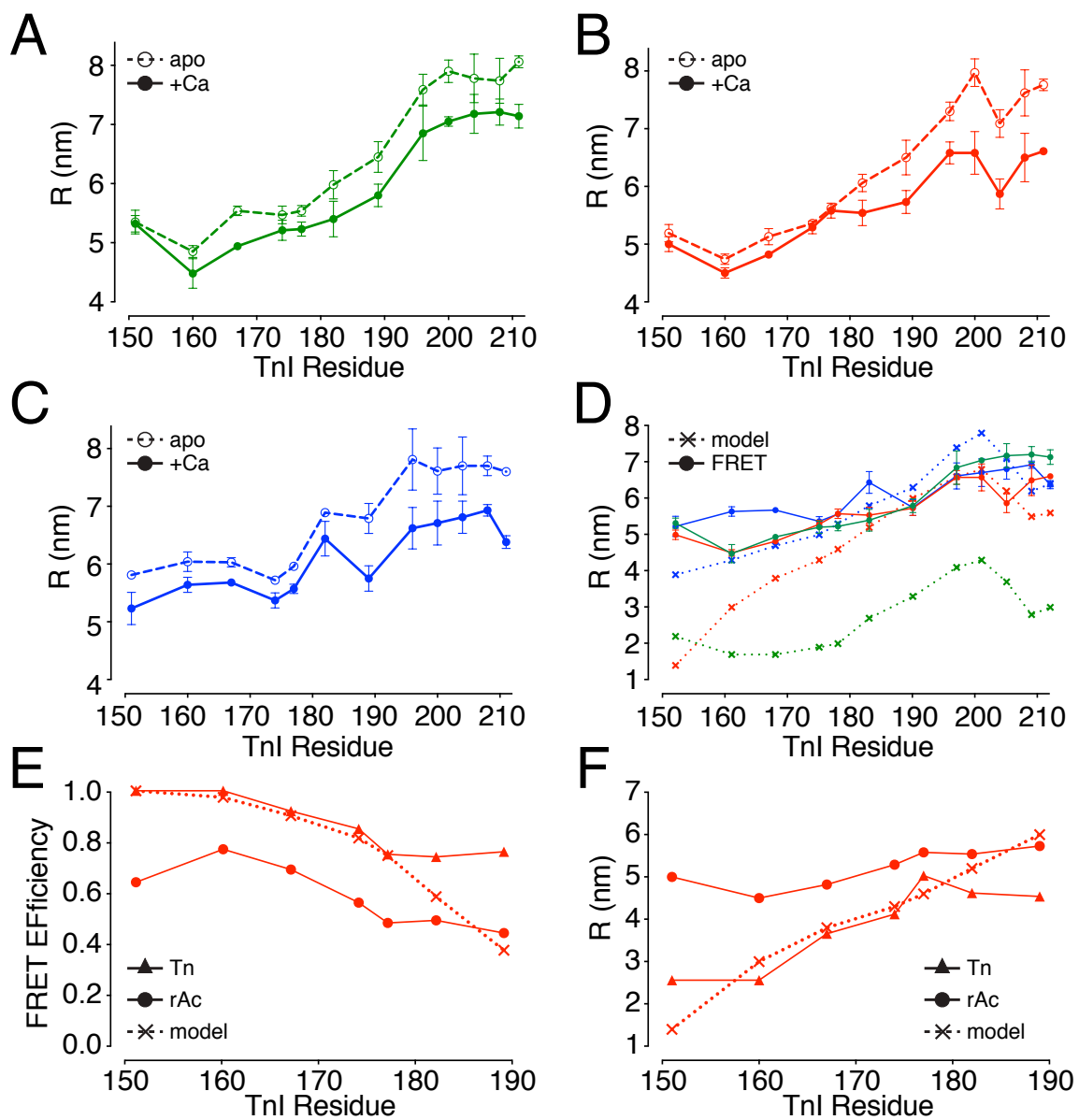


Figure 21

Figure 21. Inter-dye distances in Tn reconstituted in thin filaments with and without Ca^{2+} . The inter-dye distance (R) was calculated from E in the absence (apo, open circles and dotted lines) and presence of 3 mM CaCl_2 (+Ca, closed circles and solid lines). **(A)** R with acceptor TnC35C (green) vs. TnI donor. **(B)** R with TnC89C (red). **(C)** R with TnC127C (blue). **(D)** +Ca FRET-derived R (●, solid lines) and MTS model-derived⁸⁴ R_{mod} (✕, dotted lines) for acceptor position 35C, 89C, and 127C. **(E)** +Ca E derived from steady-state ensemble FRET of isolated Tn (500 nM in Tn) in WB +3 mM CaCl_2 (▲, solid line) from $n = 1$ reconstitution, +Ca E from trFRET of rAc (●, solid line) from Figure 19B, and theoretical E derived from the MTS model (✕, dotted line) from Figure 6D. **(F)** R calculated from E in (E), where R_{mod} is from Figure 6A, and rAc R is in (D). Color scheme and symbols are preserved from (A-F).

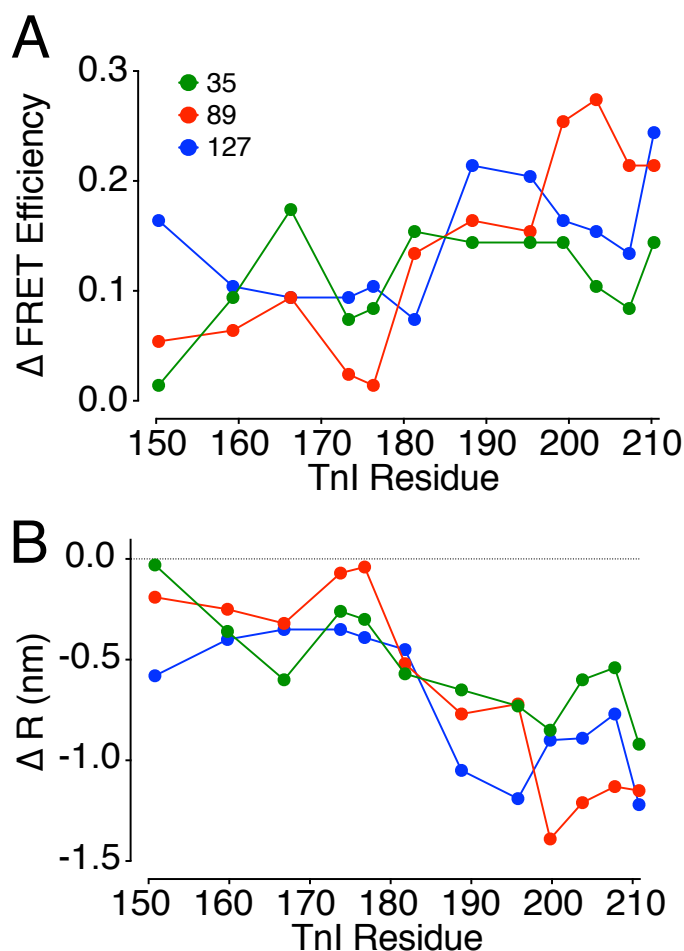


Figure 22. Relative FRET efficiency and inter-dye distance changes upon Ca^{2+} binding to Tn within the thin filament. (A) The change in E was obtained by subtracting the mean +Ca E from the mean apo E . The positive values indicate a closer proximity of the donors on TnI and acceptors on TnC. Changes in E for acceptor position 35, 89, and 127 are in red, green, and blue, respectively. **(B)** Inter-dye distances (R) were obtained by subtracting the +Ca mean distances from apo distances. The negative values indicate a closer proximity of the C-TnI to TnC35C (green), TnC89C (red), or TnC127C (blue).

3.7.2 Dynamics of the C-TnI with respect to the inter-lobe linker of TnC

The +Ca and apo R with acceptor TnC89 are plotted for each donor residue (Figure 21B). The Ca^{2+} -induced ΔR is shown in Figure 22B, with the corresponding change in E for reference in Figure 22A. In switch region, +Ca R were longer compared to R_{mod} ; however, the MTS model seemed to predict with some accuracy the +Ca R for TnI(182-211), seen in a superposition of the red solid (R) and dotted (R_{mod}) lines in Figure 21D. The switch region maintained a distance ≈ 5 nm from the inter-lobe linker, with a sharp increase after TnI177 in both R (distance) and ΔR (dynamics). Without Ca^{2+} , the C-terminal end extended away from the inter-lobe linker beyond TnI177. Interestingly, at high Ca^{2+} , R dropped to ≈ 6 nm at the C-terminal end, as opposed to ≈ 7 nm for TnC35C, indicating both the inter-lobe linker of TnC and the C-terminal end of TnI may dynamically move towards each other. This is consistent with NMR studies in sTnC¹²⁷ and human cTnC,^{29, 35} and in the MTS modeling.⁸⁴

The longer inter-dye distances between the switch region and the core of Tn compared to R_{mod} are dramatically pronounced with respect to TnC89C. Robinson et al. performed time-resolved measurements on cTn alone, cTn-Tm, and cTn in rAc using the FRET pair TnI151C*AEDANS-TnC89C*DDPM, and showed a Ca^{2+} -induced $\Delta R = -0.4$ nm for Tn in rAc.⁴⁹ This is two times larger than the $\Delta R = -0.19$ nm from this study. Robinson et al. also showed the recovered Ca^{2+} -depleted distances increased by 0.4 nm from Tn and Tn-Tm to rAc, suggesting structural changes in Tn are influenced by actin. Robinson et al. reported a +Ca R in rAc of 2.42 nm, not dramatically different from $R_{\text{mod}} = 1.40$ nm in isolated Tn. There is an important point to consider when comparing Robinson et al.'s results to those presented in this study: the ionic strength of their sample

buffer was 150 mM KCl, compared to 75 mM KCl in this study. When imaging rAc with an ionic strength of 150 mM, a large population of unbound Tn was present in solution (Figure 12). Free Tn could falsely decrease distances derived from Tn in rAc.

To determine if distances recovered in isolated Tn using this study's FRET constructs would correspond more closely to both Robinson's and the R_{mod} distances, steady state FRET was performed in Tn with donor residues TnI(151-189) (donor AF546) with acceptor TnC89C. Figure 22E and 22D show the comparison of FRET-derived E and R , respectively, from Tn alone and Tn within rAc, and the E and R_{mod} predicted by the MTS model. Values are shown in Table A11. R for isolated Tn clearly correlate to R_{mod} , where the switch region and TnI(174-189) are in close proximity to the Tn core. However, for R derived from Tn within rAc, there is a clear structural influence on TnI and TnC from the presence of Tm and actin. Importantly, this shows a more native environment is necessary to define the structure-function role of Tn. Utilizing epifluorescence imaging and FCS can give confidence in filament integrity, where samples with unbound Tn in solution are discarded prior to measurement.

3.7.3 Dynamics of the C-TnI with respect to the C-lobe of TnC

Apo and +Ca R with acceptor TnC127 are plotted for each donor residue (Figure 21C). ΔR is shown in Figure 22B, with the corresponding change in E for reference in Figure 22A. Apo R in the switch region maintained a distance of ≈ 6 nm, compared to ≈ 5 nm with acceptors on TnC35 and 89. Of particular interest are the ΔR at TnI151 and 160 ($\Delta R_{\text{av}} = -0.8$ nm), which differ from the almost non-existent ΔR at those TnI residues with acceptors on TnC35 and 89. Because NMR relaxation studies have shown the C-lobe has intra-lobe dynamics,¹²⁷ this author concludes the entire C-lobe must alter its

position in space when Ca^{2+} binds, moving closer to the C-terminal region of TnI. This is in agreement with reports of a Ca^{2+} -dependent rotation of the I-T arm around the actin filament, shown in MTS modeling.⁸⁴ With Ca^{2+} , R only increased ≈ 0.8 nm from the switch region to residue 211, indicating the C-lobe and TnI182-211 both alter their conformation/position such that the C-lobe becomes “enclosed” in space by the C-terminal region of TnI. TnI177 still appears to still behave as a pivot point for greater Ca^{2+} -induced dynamics in the C-terminal end, with ΔR values increasing from ≈ -0.5 to ≈ -1.2 nm N- to C-ward, respectively (Figure 22B).

Cordina et al. monitored the Ca^{2+} -induced distance changes in the IR (TnI151 and 159) with respect to the C-lobe in a binary complex of TnC/TnI, where $\Delta R_{\text{av}} = 0.97$ nm, indicating the switch region moved farther away from the C-lobe with Ca^{2+} .¹²⁶ Averaging this study's ΔR from TnI 151, 160, and 167 showed $\Delta R_{\text{av}} = -0.44$ nm, suggesting in the presence of Tm and actin, the switch region and the C-lobe move closer together. Therefore, both TnC and TnI may undergo spatial rearrangement when in reconstituted thin filaments that are not observed in a binary TnC/TnI complex.

In this section, the dynamics and distances with respect to each region of TnC were described. It appears that the MTS model predicted the position of the C-lobe with some accuracy at high Ca^{2+} , but appears to have incorrectly predicted the position of the N-lobe with respect to C-TnI. In the next section, the structure and general dynamics of cTnI with respect will be discussed in greater detail, with comparisons to literature reports of C-TnI dynamics.

3.7.4 The majority of Ca²⁺-dependent dynamics are within TnI residues 182-211

A pictorial summary of Figure 22B is shown as a primary sequence color map in Figure 23A, with a secondary structure model in Figure 23B. A cursory glance across all acceptor positions shows large Ca²⁺-dependent dynamics are focused at the C-terminal end (from residues 182-211). The largest changes were seen in TnI196 and 200, located in the second actin binding region of TnI. These results are consistent with those by Jayasundar et al., who proposed a molecular model with constraints from FRET-derived distances in free cTn. The second actin binding site, which they predicted was in the mobile domain (TnI182-189), underwent greater conformational changes than the inhibitory region.¹²⁸ Structural studies such as those by Jayasundar may have been focusing on the wrong “mobile” domain, however, as the results in this study predict the greatest dynamics are in TnI196-211.

Observing the trend in R in C-TnI with respect to the three acceptor positions can give some insight into the secondary structure of the C-TnI. The MTS model predicted an extended α -helix comprising TnI158-189 (predicted from the Takeda crystal structure 1J1E), and a denatured C-terminal end (residues 190-211). A FRET study by Dong et al. showed the switch region in mcTnI150-165 maintains an α -helix both with and without Ca²⁺.¹²⁹ The results of study suggest the switch region may be part of a helix-loop-helix motif, where the switch region is helix III (residues 151-177), with a loop connecting helix IV (residues 180-189). The loop allows for the relatively rigid switch region to connect to the dynamic helix IV. There may be similarities in the structure and dynamics of the two actin binding sites in TnI. The SABS comprises residues TnI189-211, and is slightly C-ward from where Murakami predicted the SABS in sTnI.⁸¹ Dong et al. used

intra-molecular FRET on TnI to show when Ca^{2+} binds, the IR experiences a $\approx 9 \text{ \AA}$ increase in length, and the conformation changes from a β -turn coil to a quasi α -helix with Ca^{2+} .⁶³ The SABS may undergo a similar conformational change, where the C-terminal end becomes more extended when not bound to actin, evident from the Ca^{2+} -dependent disappearance in an apparent “kink” at residue TnI196. RKKK is a critical amino acid sequence for actin binding found in the IR,¹³⁰ and this sequence is also found in the SABS at TnI(205-208). Peak inter-dye distance and Ca^{2+} -dependent dynamics were observed around TnI196, where glycines at TnI190, 201, and 204 could be responsible for imparting mobility. In summary, the switch region (helix III) is an α -helix with minor Ca^{2+} -dependent dynamics; a pivot point at residue TnI177 leads into a dynamic α -helix (helix IV) and the dynamic SABS (189-211). This is illustrated in Figure 23B.

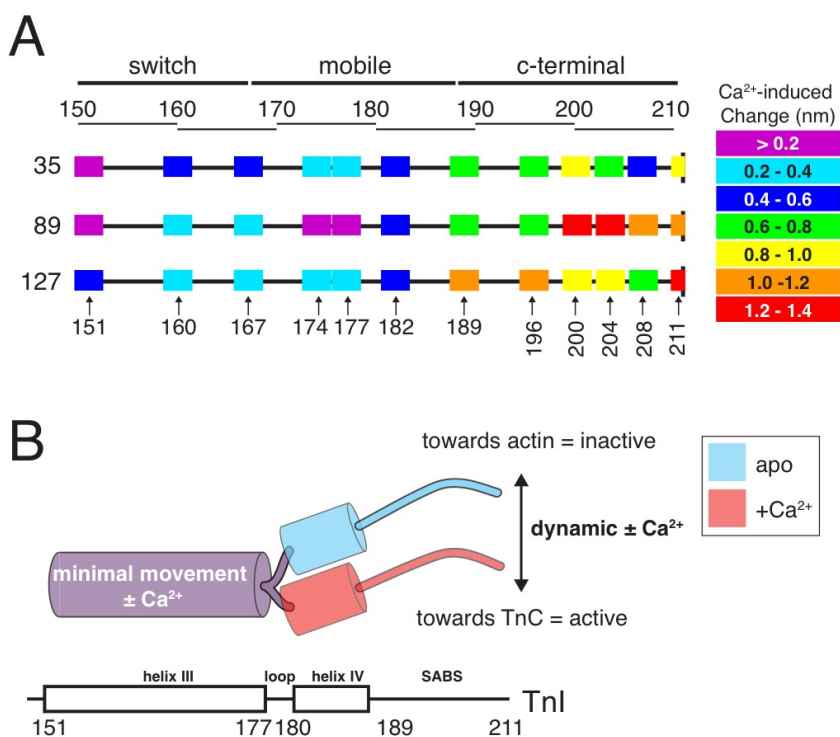


Figure 23

Figure 23. Dynamics of the C-terminal region of TnI (residues 151 to 211) in reconstituted thin filaments. (A) Primary sequence map of the Ca^{2+} -induced dynamics of C-TnI compared to the N-lobe, flexible linker, and C-lobe of TnC. The color-coded results of the Ca^{2+} -induced distance changes (ΔR) from Table A11. The number of residues represented by each box is three, with the residue attached to the donor in the middle (e.g., for donor position 151, the box represents residues 150, 151, and 152). **(B)** The model depicts a helix-loop-helix motif, where helix III (151-177) and helix IV (180-189) are shown. Helix III remains relatively static in the absence of Ca^{2+} (apo) and with Ca^{2+} bound, with a pivot point near residue 177 leading into helix IV. Residues 182 to 211 comprise the second actin binding site (SABS). The SABS has the greatest Ca^{2+} -dependent dynamics.

A simplified approach to the results presented in the previous sections is shown in Figure 24 as a highly schematic model of the Ca^{2+} -dependent activation of Tn within the thin filament. For simplicity, only one actin strand is shown in a “straightened” formulation without helical twisting; in native muscle, two actin chains form a double helical strand, each with its own Tm dimer and evenly-spaced Tn complex. TnC is positioned perpendicularly relative to the actin filament,¹³¹⁻¹³² above the interface between two adjacent actin protomers. The C-terminal region of TnI bridges two actin monomers, with the inhibitory region bound on one monomer, and the SABS bound on the other.⁸¹ In the absence of Ca^{2+} , the IR and the SABS are bound to actin, displacing the switch region away from the N-lobe. When Ca^{2+} binds to Site II, the inhibitory region and SABS move off actin; the switch region, however, undergoes minor Ca^{2+} -induced

movements towards the N-lobe and does not bind to the partially-exposed hydrophobic pocket. The SABS undergoes major Ca^{2+} -induced movements towards TnC. TnC itself has independent dynamics, with the greatest dynamics evident in the inter-lobe linker.

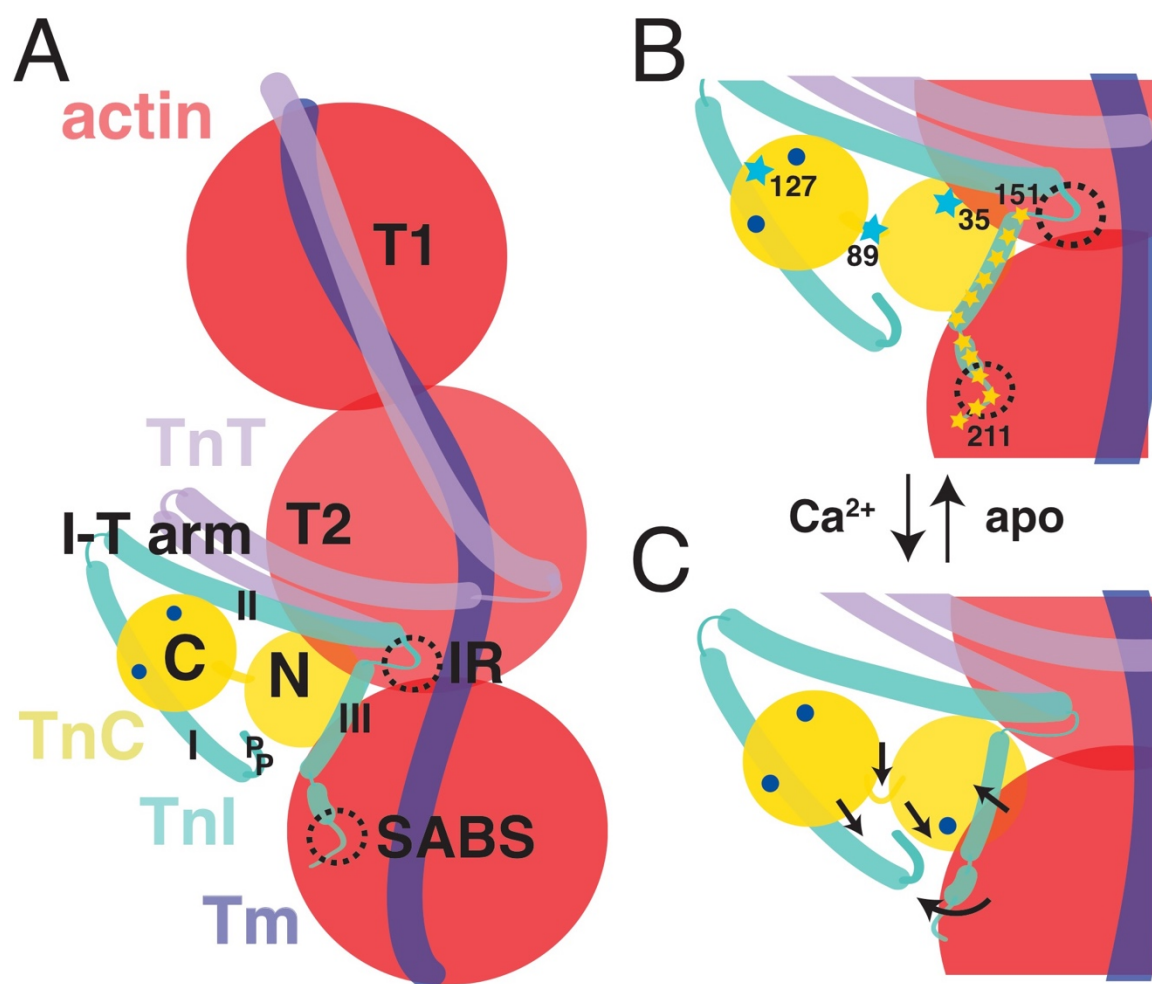


Figure 24

Figure 24. Schematic model of the structure and displacement of the switch region and SABS with respect to TnC under Ca^{2+} -saturated and Ca^{2+} -depleted conditions.

(A) The thin filament under low Ca^{2+} , with actin (red), Tm (blue), TnT (purple), TnI (cyan), and TnC (yellow) shown. For TnI, the N-terminal phosphorylation sites at Ser-23/24 (P), helix I, the I-T arm (helix II), helix III (switch region), and the actin binding sites (black dotted circles) consisting of the IR and second acting binding site (SABS) are shown. For TnC, the N-lobe and Sites III and IV occupied by $\text{Mg}^{2+}/\text{Ca}^{2+}$ (blue circles) on the C-lobe are shown. For TnT, the T1 and T2 regions are shown. (B) Close-up from (A) showing TnI, TnC, TnT, and the actin surface under low Ca^{2+} . Yellow stars represent the 12 donor positions spanning from TnI(151-211). TnI(151-177) form helix III, known as the switch region; TnI(180-189) form helix IV; and TnI(189-211) form the SABS. The three acceptor positions are shown on TnC35 (N-lobe), 89 (flexible linker), and 127 (C-lobe). TnC lies across actin, where the N-lobe is positioned out of the page, and the C-lobe into the page. Helix I of TnI and the I-T arm are in the plane of the page. (C) Same as (B), but under +Ca conditions, where Ca^{2+} is bound to Site II on the N-lobe of TnC (blue circle). Black arrows depict Ca^{2+} -induced movement. The IR has moved off actin. Movement in the switch region is minimal. The N- and C-lobes move towards actin, where the inter-lobe linker is the most dynamic region of TnC. TnI177 acts as the pivot point, bridging the non-dynamic switch region and dynamic SABS, which lifts off actin, moving ~1-1.4 nm towards TnC. TnC35, 89, and 127 are positioned such that they are ~equidistant from residue 151 of TnI.

The physiological importance of C-TnI is supported by myocardial stunning, a phenomenon where cTnI(193-211) is selectively degraded,¹³³ resulting in contractile dysfunction.¹³⁴ Functional studies have predicted the importance of these residues in inhibiting thin filament activation. Tachampa et al. exchanged recombinant cTn containing mcTnI(1-193) and hcTnI(1-192) into skinned rat cardiac trabeculae, and showed a resulting $\approx 50\%$ decrease in maximal force and cooperative activation. Actin-activated ATPase activity also dropped by $\approx 50\%$.¹³⁵ Importantly, they showed a $\approx 50\%$ increase in Ca^{2+} sensitivity, but only when cTn was reconstituted into thin filaments. This author hypothesizes the SABS is responsible for the reduction in Ca^{2+} sensitivity when Tn is reconstituted into thin filaments¹³⁶ due to the displacement of the switch region away from the N-lobe of TnC.

3.8 Functional characterization of a FRET pair in the switch region and N-lobe of TnC

Tn containing TnI151C and TnC35C was selected to determine whether potential functional or structural effects from mutagenesis could account for the unexpectedly large distance between switch region and the N-lobe of TnC. Mutant Tn containing mcTnI (C81I, C98S, S151C), rcTnC (C84S), N-terminal myc-mcTnT and WT Tn containing mcTnI, rcTnC, and N-terminal myc-mcTnT were exchanged into isolated rat myofibrils. The efficiency of exchange of WT Tn ($53.73 \pm 3.94\%$) and mutant Tn ($43.64 \pm 6.23\%$) were estimated from Western blots of the exchanged cells (Figure 25A-B). Figure 25C shows measurements of force at different Ca^{2+} concentrations. During measurements, the sarcomere length (SL) was maintained at either $1.9 \mu\text{m}$ or $2.3 \mu\text{m}$. Two sarcomere lengths were used to determine if mutagenesis had any effect on the Ca^{2+}

sensitivity of force development, as sarcomere length determines the Ca^{2+} response of the sarcomere.¹³⁷

At 1.9 μm and 2.3 μm SL, peak force (Figure 25D) and Ca^{2+} sensitivity (pCa_{50}) (Figure 25E) were not statistically different between fibers exchanged with WT and mutant Tn ($P > 0.05$). The mutagenesis required for this FRET pair negligibly affected the Ca^{2+} -dependent regulatory activity of the mutant Tn compared to WT Tn, suggesting no significant structure or functional perturbations of the switch region by the mutagenesis required for this FRET pair. In the future, these experiments should be repeated with FRET-labeled Tn in order to determine if dye modification affects the native function of Tn. Ideally, these measurements would be performed on all paired D/DA Tn.

The previous sections have attempted to explain and give credence to the surprising observation of C-TnI structure and dynamics in reconstituted thin filaments. In the next section, the importance of actin and Tm on Tn structure will be discussed, along with a comparison between results derived from this FRET assay and current mechanisms of Tn activation proposed in literature.

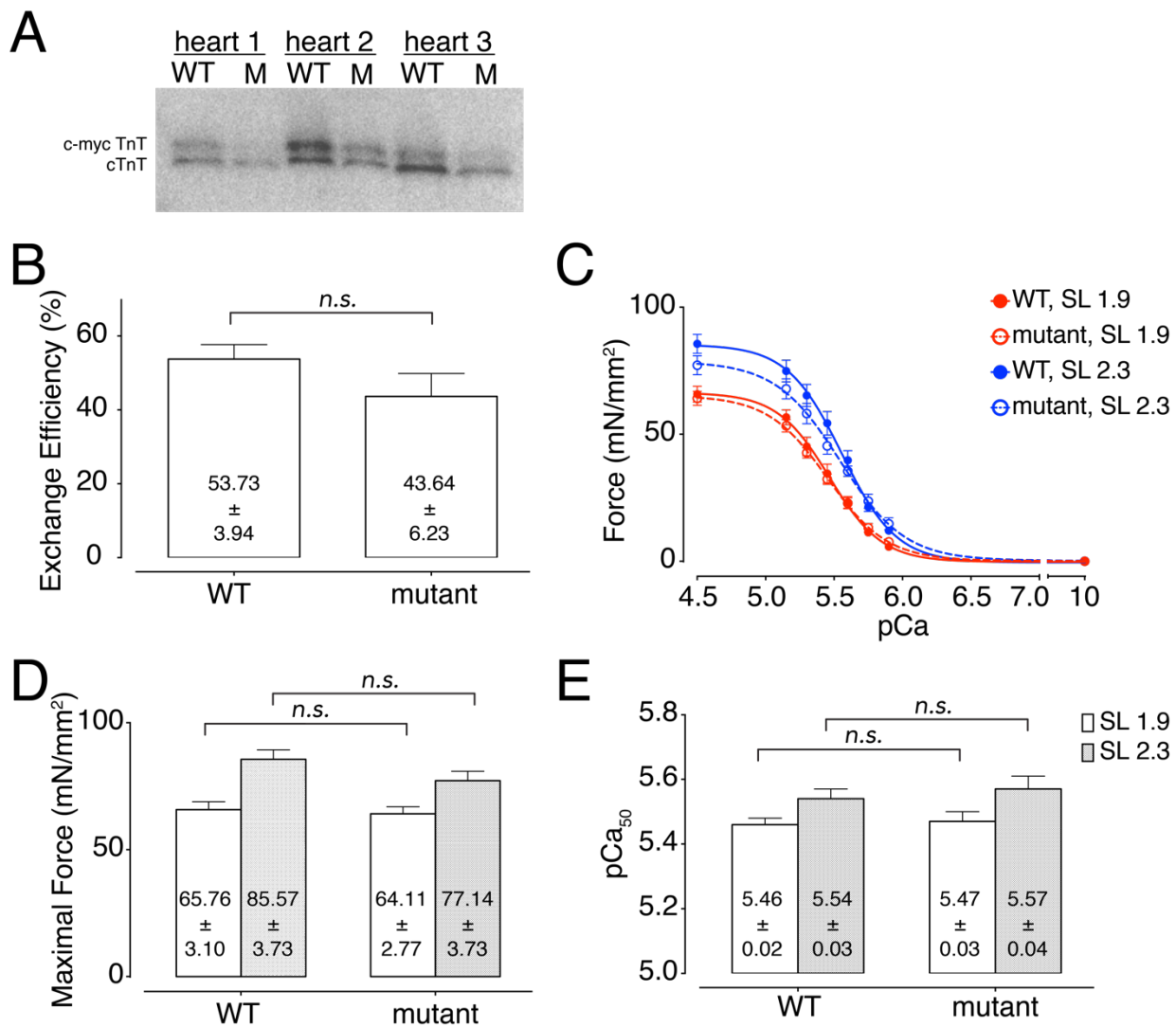


Figure 25

Figure 25. Functional characterization of wild type and mutated Tn. WT Tn consisting of myc-mcTnT, mcTnI, rcTnC and mutant Tn consisting of myc-mcTnT, mcTnI151C, rcTnC35C were exchanged into skinned cardiomyocytes isolated from rat ventricles. **(A)** Western blot analysis of reserved fibers. Exchanged myc-TnT was compared to native TnT to determine the Tn exchange efficiency. (WT: $n = 3$ hearts; mutant: $n = 3$ hearts) **(B)** Shown is the mean exchange efficiency from samples in (A) \pm SEM. Differences were not significant ($P > 0.05$, two-way ANOVA). **(C)** Pooled data (mean \pm SEM, WT: $n = 9$ fibers; mutant: $n = 9$ fibers) from force-pCa measurements of fibers at short (red, 1.9 μm) and long (blue, 2.3 μm) sarcomere lengths (SL). Lines for mutant (dotted line) and WT (solid) exchanges are drawn using the mean Ca^{2+} -sensitivity pCa_{50} and maximum force F_{max} recovered from individual fits of fibers. **(D)** Average maximum force \pm SEM from (C) for SL at 1.9 μm (white) and SL 2.3 μm (grey). **(E)** Average $\text{pCa}_{50} \pm$ SEM from (C). A consistent coloring scheme is used in (D-E).

3.9 Actin ultimately determines Tn structure and dynamics during activation

The muscle field emphasizes the importance of the switch region as the molecular toggle for cardiac muscle regulation, responsible for dragging the IR and SABS off actin to remove myosin binding inhibition. This may be a biased view, however, as the switch region/N-lobe interactions are based on isolated or fragmented Tn structures solved using NMR or X-ray crystallography. In reconstituted thin filaments, the switch region was around 5 nm from the N-lobe (both apo and +Ca), too far to promote an interaction. Other modulatory modifications to the thin filament (like crossbridge formation) may be

required to push the switch region into the hydrophobic pocket of N-TnC in native muscle, whereas for Tn in the absence of actin, the fully active conformation is energetically preferred. Hence, why some of the previously-mentioned studies in Tn reported limited Ca^{2+} -induced movements of the switch region due to its close proximity to the N-lobe, as Tn was already in an active-like conformation, even at low Ca^{2+} .^{126, 128} Temporarily averting full binding of the switch region may be a stopgap mechanism to prevent hyperactivation from Ca^{2+} binding, where full thin filament activation requires additional steps. Therefore, the Herzberg model of TnC activation may still hold true,⁶⁴ though Ca^{2+} alone may not promote switch region binding to N-TnC. Conversely, the inability of the N-lobe to fully open due to the inactivity of Site I may indicate the switch region evolved out of vogue in cardiac muscle as the major Tn structural change; instead, SABS and IR lift off actin in an isoform-specific mechanism.

3.9.1 The role of TnI in the steric blocking mechanism of thin filament activation

The steric blocking mechanism for muscle activation dictates that the IR inhibits Tm movement under low Ca^{2+} , where Tm blocks myosin binding sites and prevents ATPase activity. Under high Ca^{2+} conditions, TnC competes with actin, causing liftoff of the IR to allow Tm movement away from myosin binding sites.^{51, 138-139} A three-state model of activation branching from the steric blocking model has been proposed by McKillop and Geeves,²³ and this mechanism is consistently discussed in terms of Tm position correlated to the activation level. However, some studies have shown Tm undergoes minor Ca^{2+} -¹⁴⁰⁻¹⁴¹ and myosin-induced¹⁴¹ movement on actin. A mechanism proposed by Patchell et al. stated IR-dependent actin conformational changes are

responsible for promoting myosin binding, and not the position of Tm on actin.²⁴ Using electron microscopy (EM) on filaments reconstituted with actin, Tm, and the C-terminal half of hcTnI (residues 132-210), Galinska-Rakoczy et al. showed this fragment of TnI lies across two adjacent actin protomers.¹¹ Murakami et al. developed their atomistic model based those results,⁸¹ where sTnI-IR binds to the N-terminal region of actin,¹⁴² and SABS binds to the DNase-I loop (interface between actin protomers) near the N-terminal region of actin and a region in the C-terminal region of actin.⁸¹ The DNase loop may facilitate interactions between actin protomers in the thin filament that promote myosin crossbridge formation.¹⁴³⁻¹⁴⁴

The three-state model in terms of Tn would dictate: 1) in the absence of Ca^{2+} , Tn is in an inactive state, with complete ATPase inhibition due to IR/SABS bound to actin (blocked); 2) when Ca^{2+} binds, Tn is in a semi-inactive state, where TnI may have removed some of its inhibitory properties from actin, but the switch region is not bound to N-TnC, and myosin may weakly bind (closed); 3) myosin binds to actin in the presence of Ca^{2+} , causing the fully-activated state, pushing the switch region into the hydrophobic pocket of N-TnC, and inducing cooperative activation of the thin filament. The second half of this of dissertation goes into greater detail of Tn activation by myosin binding.

3.9.2 Minimal switch region dynamics: implications on the “drag and release” mechanism

Since most of the Ca^{2+} -dependent dynamics appear to be focused in the C-terminal end of TnI instead of the switch region, the “drag and release” mechanism¹⁴⁵ may not be relevant to TnI when in the cardiac thin filament, as this study has shown the

switch region does not bind to the hydrophobic pocket of N-TnC when Ca^{2+} is bound to Site II. The dramatic difference in distance from the switch region to the inter-lobe linker between isolated Tn to Tn in rAc should be compelling evidence to prompt a discussion towards a modified theory of thin filament activation. Functional *in situ* studies have attempted to support the “drag and release” mechanism, but may still be biased in their analysis of results. A study monitoring simultaneous FRET and force in skinned cardiac fibers showed strong crossbridge formation stabilized the N-lobe opening, evident from an increase in the ensemble-averaged FRET in the presence of myosin and Ca^{2+} .¹⁴⁶ In a 2014 follow-up study, time-resolved FRET was used to monitor the effect of sarcomere length on N-lobe opening, where N-lobe opening was sensitive to Ca^{2+} binding, crossbridge state, and sarcomere length.¹⁴⁷ Unfortunately, the FRET assay in both studies only monitored intra-N-lobe conformational changes; the authors were essentially blind in monitoring switch region binding to the N-lobe. Removing the assumption that Ca^{2+} causes switch region binding to N-TnC, the results from both of studies can instead be explained using conclusions presented in this dissertation: the N-lobe may experience minor opening with Ca^{2+} , but crossbridge formation is ultimately responsible for pushing the switch region into the hydrophobic pocket. As crossbridge formation is a function of sarcomere length, N-lobe opening would correlate to sarcomere length. In order to truly determine the role of the switch region, simultaneous force and time-resolved fluorescence should be performed on one of the FRET constructs developed in this study, where the donor is in the switch region and the acceptor in the N-lobe of TnC. The *in vitro* behavior of the switch region with Ca^{2+} or myosin binding could thus be compared to *in situ* behavior.

Other FRET studies in rAc lend credence that myosin binding promotes N-TnC and switch region interactions. Xing et al. used trFRET to show the Ca^{2+} -saturated R between donor residues in the switch region of mcTnI(151, 160, 167) and Cys374 in actin in reconstituted thin filaments increased by as much as 0.7 nm upon S1 binding, indicating S1 causes the switch region to move farther from actin,¹²⁵ and potentially into the hydrophobic pocket in the N-lobe of TnC. Wang et al. developed a multi-site steady-state FRET assay in rAc with five donor positions ranging from TnI(108-211) (mouse cardiac numbering) on hcTnI and an acceptor on Cys374 in actin.¹⁴⁸ Like Xing et al., Wang and coauthors saw an increase in inter-dye distance with S1 binding at TnI residue 152C.

3.9.3 The order in the disorder: the fly-casting mechanism of C-TnI

The fly-casting mechanism states a highly disordered SABS participates in long-range sampling of the thin filament to catalyze TnI binding to actin upon Ca^{2+} dissociation.⁶⁸ This mechanism is based on the assumption that the SABS is an intrinsically disordered region, and does not undergo conformational switching similar to the IR. Julien et al. attempted to discover nascent structure in the IDR using NMR on an sTnC/TnI chimera comprised of the N-lobe of sTnC and sTnI(126-211).¹⁴⁹ They reported no secondary structure, contrary to the skeletal Murakami and cardiac MTS models already discussed. Again, these minimalistic structural studies raise concerns regarding their physiological relevance to native cardiac protein structure and function *in vivo*. The fly-casting mechanism may still apply in part; perhaps the potential absence of secondary structure in the SABS after TnI189 still allow this region to participate in sampling the actin surface for potential binding sites.

3.10 Mutations in the C-TnI emphasize its functional importance

As outlined in the introduction, RCM- and HCM-causing mutations in TNNI3 are found at a high density in the C-terminal region.⁹⁷ Most of the mutations are missense, meaning one amino acid has been substituted for another. The structure and dynamics of this region found using this multi-site FRET assay could potentially give insight into the mechanisms behind the disease-causing mutations. Notably, mutations in hcTnI around the pivot point (K178E in human, K179E in mice) and a residue in the SABS (R192H in human, R193H in mice) have been implicated in patients with RCM.⁸⁸ Both cause a dramatic increase in Ca^{2+} sensitivity and decrease in ATPase inhibition.⁹²⁻⁹³ This suggests both residues play essential roles in regulating muscle contraction. Yumoto et al. utilized circular dichroism and NMR to show K178E in an hcTnI129-210 peptide imparted a small structural change in residues hcTnIK177-T181.⁹³ Structural perturbations around the pivot point could result in a loss of mobility in the C-terminal region, affecting the ability of the SABS to bind actin. The arginine to histidine substitution at 193 results in a loss of TnI inhibitory function, potentially due to the loss of a positive charge potentially important for maintaining actin associations.¹⁵⁰ Davis et al. showed exchange of mcTnI(R193H) into mouse myocytes promoted shortened sarcomere lengths in a Ca^{2+} -independent manner, possibly due to a heightened contracted state as a result of increases in myosin-actin interactions even at low intracellular Ca^{2+} .¹⁵⁰ Deletion mutations at hcTnI177 and 178 result in HCM again emphasize the importance of the pivot point for conferring mobility to the second actin binding site.¹⁵¹ Of the 29 HCM mutations in TNNI3, 12 are found after hcTnI195.⁹⁷ This supports the conclusion that the SABS of TnI plays an essential role in regulating muscle contraction. Alterations of this binding

site could either hinder SABS binding to actin, or enhance SABS release; either way, changes in the binding of this region result in dramatic changes in the muscle phenotype and function leading to the development of cardiomyopathies.

MECHANISMS OF ACTION OF INOTROPIC AGENTS, MYOSIN BINDING, AND
PKA-MEDIATED PHOSPHORYLATION OF TnI TO MODULATE CARDIAC THIN
FILAMENT ACTIVATION AND CALCIUM SENSITIVITY

ABSTRACT SECTIONS 4-7

To pump blood, the heart fills and empties through periods of relaxation and contraction regulated by Ca^{2+} binding to cTnC and myosin binding to actin. Activation is further tuned by protein kinase A (PKA)-mediated phosphorylation of Ser-23/24 in cTnI. Small molecules that target the thin filament to affect cardiac output by altering activation by Ca^{2+} and myosin are called cardiotonic agents, used to improve cardiac function in heart failure patients. This study hypothesized these agents may mimic mechanisms of myosin binding and TnI phosphorylation to modulate Tn activation. Steady-state FRET was used to monitor structural changes in Tn in reconstituted thin filaments, a physiologically relevant model of cardiac activation. Ca^{2+} and rigor-S1 titrations were performed as a two dimensional screening method to assess the effects on cooperativity and sensitivity from bepridil and levosimendan, Ca^{2+} sensitizers that target the N-lobe of TnC, and EGCG, a green tea compound with potential for Ca^{2+} desensitizing effects that targets the C-lobe of TnC. Filaments were treated with PKA to determine if compounds acted in a similar mechanism to TnI Ser-23/24 phosphorylation. For Ca^{2+} titrations, bepridil and S1 increased the level of active Tn, induced negative cooperativity, and increased Ca^{2+} sensitivity. Notably, bepridil eliminated S1-induced activation of Tn, suggesting bepridil and S1 activate the thin filament with a similar mechanism, where both work by stabilizing the open conformation of the N-lobe of TnC.

While both EGCG and PKA treatment reduced Ca^{2+} and myosin sensitivity, EGCG decreased the level of active Tn under Ca^{2+} -depleted conditions, while Ser-23/24 phosphorylation did not alter the level of active Tn. This suggests independent mechanisms for conferring Ca^{2+} desensitivity to the thin filament. A correlation was discovered between the Ca^{2+} -depleted FRET efficiency and C_{a50} . This study shows proof of concept of a high throughput screen (HTS) to discover and develop small molecule compounds that target sarcomere proteins to modulate cardiac output in the treatment of heart failure.

4 INTRODUCTION

Muscle contraction is mediated by the Ca^{2+} -triggered cyclic interaction of myosin motors with regulated actin filaments, where ATP hydrolysis by myosin enables thick and thin filaments to slide past one other, causing shortening.¹⁵² Thin filaments are composed of troponin (Tn), tropomyosin (Tm), and actin. Cardiac Tn is a heterotrimer composed of troponin I (TnI), which inhibits actin-activated ATPase through interactions with actin; troponin T (TnT), which binds to Tm and TnI to tether Tn to the thin filament; and troponin C (TnC), which binds Ca^{2+} . Cardiac TnC is composed of two EF hand globular domains (lobes) connected by a flexible linker.²⁷ The C-lobe (structural domain) has two high-affinity divalent cation binding sites always occupied by Ca^{2+} or Mg^{2+} , stabilizing the open conformation of the structural domain.²⁷ The N-lobe (regulatory domain) has one low-affinity binding site (Site II). When Ca^{2+} floods the sarcomere during diastole (relaxation), Ca^{2+} binds to TnC at Site II, causing conformational changes in Tn-Tm that modulate myosin binding to actin (crossbridge formation), leading to systole (contraction).⁶⁴⁻⁶⁵

Historically, the mechanism of activation has been thought to occur through a structural rearrangement in the B/C helices in the N-lobe of TnC, which exposes a hydrophobic pocket where the switch region of TnI binds, stabilizing the open conformation of the regulatory domain.³⁶ The inhibitory region (IR) and the second actin binding site (SABS) of TnI come off actin as a result of Ca^{2+} -dependent conformational changes in Tn, allowing for a Tn-Tm-actin conformation that promotes crossbridge formation and muscle contraction. While Ca^{2+} binding is a critical step in initiating contraction by stabilizing the active state of Tn, Ca^{2+} alone does not account for the

activation-dependence of the contractile properties of the myocardium. Strong (rigor) crossbridge formation also plays a prominent role in activation itself: the strong force-generating crossbridge positively and cooperatively activates the thin filament,¹⁵³ affecting the activation of Tn and its affinity for Ca^{2+} .^{49, 154}

In addition to the regulatory effects by Ca^{2+} and myosin on myofilament activation, post-translational modifications of sarcomeric proteins also modulate activation by changing the response of the myofilament to Ca^{2+} . Kinase-mediated serine and threonine phosphorylation of cTnI can alter myofilament properties in response to stress or exercise.¹⁵⁵ cTnI contains a ≈ 33 residue, isoform-specific N-terminal extension, which contains two serines at residues 23 and 24.⁵³ To meet changes in circulatory demands requiring variations in contraction and relaxation, enhanced $\beta 1$ -adrenergic stimulation causes an increase in the production of cAMP-dependent protein kinase A (PKA).¹⁵⁶ PKA phosphorylates cTnI Ser-23/24, promoting Ca^{2+} release (Ca^{2+} desensitivity) and increased crossbridge cycle kinetics to facilitate muscle relaxation (lusitropy).¹⁵⁷⁻¹⁵⁸ Ser-23/24 phosphorylation is thought to disrupt interactions between the N-terminal extension of TnI (residues 16-29) and TnC that promote Ca^{2+} binding to Site II of TnC.⁵⁶ In transgenic animals expressing non-phosphorylatable TnI (either mutant S23A/S24A or slow sTnI, which lacks the ≈ 33 amino acid N-terminal extension), a decrease in Ca^{2+} sensitivity following $\beta 1$ -stimulation is abolished, and its lusitropic effect is reduced in isolated myocytes, isolated hearts, and *in vivo*.¹⁵⁹⁻¹⁶¹ While the effects of Ser-23/24 phosphorylation on the myofilament are known, the molecular mechanism behind the decrease in Ca^{2+} sensitivity remains elusive.

Resolving the mechanisms behind Ser-23/24 phosphorylation-induced Ca^{2+}

desensitivation in Tn, and Ca^{2+} - and myosin-dependent activation of Tn, can yield valuable insight into the molecular mechanisms behind muscle regulation, facilitating the path to create targeted drug therapies for heart failure. Heart failure, or cardiomyopathy (CM), comprises changes in cardiac contractility, electrical conduction, Ca^{2+} transients, and energy metabolism, leading to a failure of the heart to meet altered circulatory demands.¹⁶²⁻¹⁶³ Sympathetic nervous system (SNS) activation is normal with heart failure, but the myocardial response to SNS signaling is blunted by down-regulation of the β -receptor-cAMP-PKA pathway.¹⁶⁴⁻¹⁶⁵ This causes reduced phosphorylation of cTnI, leading to an increase in Ca^{2+} sensitivity; in the failing heart, Ser-23/24 phosphorylation decreases by 33-80%.¹⁶⁶⁻¹⁶⁷ Restrictive cardiomyopathy (RCM) is a form of heart failure associated with altered diastolic function and impaired ventricular filling due to increased muscle stiffness, with normal systolic function and ventricular muscle wall thickness.⁹⁰ An arginine to histidine mutation at residue 192 (R192H in human, R193H in mice) in the second actin binding site (SABS) of cTnI has been implicated in RCM.⁸⁸ Though other forms of CM are associated with increases in myofilament Ca^{2+} sensitivity, mutations associated with RCM are thought to cause the most dramatic increase in Ca^{2+} sensitivity compared to other forms of CM.⁹³ Skinned fibers from failing human hearts exhibiting increased sensitivity to Ca^{2+} and impaired diastolic function can be corrected when the fibers are treated with PKA, enhancing Ca^{2+} desensitivation and promoting relaxation.¹⁶⁸⁻¹⁷⁰ Unfortunately, the pitfalls of pharmacologically augmenting cAMP-PKA signaling are illustrated by the negative survival benefit of treatment with the phosphodiesterase III inhibitor milrinone.¹⁷¹ A PKA-mediated hyperphosphorylation of the ryanodine receptor results in diastolic Ca^{2+} leak and impaired Ca^{2+} re-uptake by

SERCA2a.¹⁷² An increase in cytosolic Ca^{2+} causes arrhythmias, stimulates maladaptive Ca^{2+} -dependent signaling cascades, and stimulates altered energy metabolism.¹⁷³

Increased Ca^{2+} sensitivity due to R192H has been reversed in skinned muscle fibers by desensitizing Tn to Ca^{2+} ,¹⁷⁴ and in mice treated with EGCG,¹⁷⁵ a green tea compound targeting TnC to reduce Ca^{2+} sensitivity.¹⁷⁶ This suggests a promising approach to develop CM therapies by directly altering the Ca^{2+} sensitivity of Tn, bypassing altered Ca^{2+} handling through increased cAMP-PKA signaling. Small molecule compounds that target the thin filament (sarcomeric modulators) and mimic the effect of PKA-dependent phosphorylation of TnI Ser-23/24 may be a viable therapeutic strategy promoting myofilament relaxation in persons with RCM. Since the N-terminus of TnI is unique to the cardiac isoform, pharmacotherapies that mimic the effect of N-TnI bisphosphorylation are likely to be specific for the myocardium.

Here, the effects on Ca^{2+} - and myosin-dependent activation by small molecules and PKA treatment were investigated using a FRET-labeled Tn assay in reconstituted thin filaments. This FRET assay monitored the activating structural change in Tn, with a FRET donor in the SABS of TnI, and a FRET acceptor in the C-lobe of TnC. Ca^{2+} and S1 titrations were performed as a 2D screening method to assess the effects on cooperativity and sensitivity with bepridil and levosimendan, proposed as Ca^{2+} sensitizers targeting the thin filament,¹⁷⁷⁻¹⁷⁸ and EGCG.¹⁷⁶ These small molecules were hypothesized to mimic effects from myosin binding or TnI Ser-23/24 phosphorylation, giving insight into their molecular mechanism. Results suggest TnI Ser-23/24-dependent desensitization to myofilament force and ATPase to Ca^{2+} may be due to enhanced inhibition, where the phosphorylated N-TnI is released from TnC to prevent IR displacement from actin, even

with Ca^{2+} and myosin binding. Bepridil and S1 appear to have a similar mechanism of increasing Ca^{2+} sensitivity in the thin filament, where bepridil stabilizes the open conformation of the N-lobe, and myosin binding enhances cTnI switch region binding to stabilize the open conformation of the N-lobe. EGCG and PKA-mediated Ser-23/24 phosphorylation appear to not share a mechanism to desensitize the thin filament for Ca^{2+} , evident by monitoring the level of Tn activation under Ca^{2+} -depleted conditions. A correlation was discovered between the deactivated (Ca^{2+} -depleted) Tn state and Ca^{2+} sensitivity. The capacity of this FRET assay as a possible high-throughput screening method (HTS) was demonstrated for small molecules targeting cardiac thin filaments to treat heart failure.

5 METHODS

Native and recombinant protein purification, fluorescent dye conjugation, labeling ratio determination, epifluorescence imaging, and force-pCa experiments were described in the Methods (Section 2).

5.1 Purification of myosin from chicken pectoralis major muscle

Skeletal myosin was purified from chicken pectoralis major muscle as described,¹⁷⁹⁻¹⁸⁰ with some modifications. Breast tissue from a freshly slaughtered young chicken was sliced into strips and ground in a food processor. Ground muscle was extracted with 0.3 M KCl, 0.15 M KH₂PO₄ (pH 6.5), 20 mM EDTA, 5 mM MgCl₂, and 1 mM ATP at 3x w/v at 4°C with stirring for 10 min. Remaining tissue was sedimented with centrifugation at 8,000 rpm using a Beckman J2-Mi centrifuge with rotor JA-10 for 25 min. The supernatant was diluted slowly with stirring with 10x v/v of cold ddH₂O. The precipitate was settled for a minimum of 1 hour. The supernatant was siphoned off, and the myosin precipitate was pelleted with centrifugation at 8,000 rpm for 45 min using a Beckman centrifuge with rotor JA-10. The pellets were re-suspended in 1 M KCl, 25 mM EDTA, and 60 mM KPO₄ (pH 6.5) at 0.25 mL/g of original muscle mass and dialyzed against 0.6 M KCl, 25 mM KPO₄ (pH 6.5), 10 mM EDTA, and 1 mM DTT overnight. Ammonium sulfate (0-30%, mass calculated with <http://www.encorbio.com/protocols/AM-SO4.htm>) was added slowly to the solution with stirring for a minimum of 30 min. The precipitate was pelleted with centrifugation at 12,000 rpm for 30 min using a Beckman centrifuge with rotor JA-14. The pellet was re-suspended and dialyzed against 0.6 M NaCl, 10 mM NaPO₄ (pH 7.0), 1 mM EDTA, and 1 mM DTT overnight.

Myosin was stored in 50% glycerol in -20°C for up to six months, and purity was confirmed using SDS-PAGE.

5.2 Myosin digest into subfragment-1

Myosin subfragment-1 (S1) was prepared as described¹⁸¹ with some modifications. Myosin was dialyzed against 20 mM MOPS (pH 7.0), 50 mM KCl, 1 mM EDTA and digested with 0.64 units chymotrypsin/1 mg myosin (α -chymotrypsin, TLCK treated, Worthington Biochemical Co., Lakewood, NJ) for 10 minutes with stirring on ice. The digestion was terminated with 5 mM phenylmethylsulfonyl fluoride (PMSF). 5 mM MgATP was added, and insoluble components were pelleted by centrifugation at 180,000 xg for 15 min. Soluble S1 in the supernatant was dialyzed into working buffer (WB: 75 mM KCl, 50 mM MOPS pH 7.0, 5 mM MgCl₂, 2 mM EGTA, 5 mM BME) and stored at 4°C for up to 1 week. Catalytically inactive S1 (dead heads) were removed by ultracentrifugation in a Beckman TL-100 ultracentrifuge at 64,000 rpm for 15 minutes (TLA-100 rotor) in the presence of 5 mM ATP and F-actin at a molar ratio of 1 S1: 2 actin. ATP was removed using dialysis against WB (Spectra/Por 2 Dialysis Membrane, MWCO 12-14 kDa, Spectrum Laboratories, Irving, TX). S1 was used within 24 hours of dead head removal. Purity was confirmed using SDS-PAGE.

5.3 Phosphorylation of TnI in regulated actin

Serines 22 and 23 of TnI in rAc were phosphorylated using the protein kinase A (PKA) catalytic subunit from bovine heart (Sigma-Aldrich, St. Louis, MO). Stock solutions of PKA were prepared at 500 units/mL (50 μ g/mL) in ddH₂O with 6 mg/mL DTT, and stored at 4°C for up to 1 week. Literature provided by Sigma-Aldrich indicated

a 15% loss of activity after 8 days when stored at 4°C.¹⁸² PKA was incubated for three hours at room temperature with rAc in WB supplemented with 5 mM MgATP at a ratio of 125 units of PKA/mg of TnI.¹⁸³ To remove unreacted ATP, rAc was sedimented by ultracentrifugation at 64,000 rpm for 15 min (Beckman TLA-100 rotor). Pellets were washed twice with WB, and reconstituted by Dounce homogenization.

The extent of phosphorylation was quantified using phosphate affinity SDS-PAGE with PeppermintStick phosphoprotein molecular weight markers (Life Technologies). Markers were loaded at 1 µg. The markers contain ovalbumin, which has two phosphorylation sites, and β-casein, which runs close to TnI. Gels were stained successively with Pro-Q Diamond phosphoprotein and SYPRO Ruby total protein stains (Life Technologies), and scanned with UV excitation (Gel Logic 112, Kodak) with an exposure time of 14 sec. Images were pseudo-colored using ImageJ 1.47v (National Institutes of Health, Bethesda, MD). The amount of loaded TnI was adjusted to 1 µg by multiplying the TnI SYPRO Ruby (S_I) and TnI Pro-Q (D_I) intensities by (S_β/S_I) , where S_β is the SYPRO Ruby band intensity of β-casein. The ratio of the Pro-Q Diamond and SYPRO Ruby band intensities (abbreviated D/S ratio) of ovalbumin (D_O/S_O) was normalized to 2, and used as the maximum normalization factor. The number of sites in TnI phosphorylated (N_P) was found using

$$N_P = \frac{D_I'/S_I'}{(D_O/S_O)/2'} \quad (13)$$

where S_I' and D_I' is the corrected SYPRO Ruby and Pro-Q Diamond band intensities of TnI.

5.4 Steady state fluorescence spectroscopy

5.4.1 Calcium titrations

Steady-state measurements were performed at 22°C on a Fluorolog-3 spectrofluorometer (Horiba) equipped with a MicroLab500 syringe dispenser (Hamilton) and Versa water bath temperature control (ThermoFisher Scientific). Singly- and doubly-labeled reporter filaments, rAc-D (with Tn-D, TnI189C*AF546, TnC127C, TnT) and rAc-DA (with Tn-DA, TnI189C*AF546, TnC127C*ATTO655, TnT), respectively, were prepared in WB (250 nM in Tn). Stock solutions of (-)epigallocatechin gallate (EGCG, Sigma-Aldrich), bepridil hydrochloride (bepridil, Sigma-Aldrich), and levosimendan (Sigma-Aldrich) were prepared at 25 mM in DMSO, aliquoted, and stored at -20°C for up to six months. Stock solutions were monitored for precipitation, and vortexed for 30 sec prior to use.

Fluorescence emission from the FRET donor was monitored (530 nm excitation, 570 nm emission, monochromator slit width 4 nm, 1 sec integration time) following 25 serial injections (2 µL) of +Ca buffer into 1 mL of sample. +Ca buffer consisted of WB supplemented with 50 mM CaCl₂. A mixing time of 3 sec was applied after the addition of each aliquot. Following the titration, the sample was denatured with 3 M guanidine hydrochloride, and the donor emission was collected. This provided the relative concentration of the donor dye. All intensity data were corrected for dilution. The intensity of the rAc-DA sample was corrected for donor concentration mismatch using

$$I'(Ca)_{DA} = I(Ca)_{DA} (I_D^* / I_{DA}^*), \quad (14)$$

where I_D^* is the intensity of the denatured (+GnHCl) rAc-D sample and I_{DA}^* is the intensity of the denatured rAc-DA sample. Ca^{2+} -dependent FRET efficiency E was calculated using

$$E(Ca) = \frac{1}{f_A} \left(1 - \frac{I'(Ca)_{DA}}{I(Ca)_D} \right), \quad (15)$$

where f_A is the labeling efficiency of the acceptor dye. Data were fit to the Hill equation

$$E = E_- + \frac{E_+ - E_-}{1 + (Ca_{50}/Ca)^{n_H}}, \quad (16)$$

where n_H is the Hill coefficient and Ca_{50} is the Ca^{2+} concentration that produces half maximal activation, E_- is the FRET efficiency without added Ca^{2+} and E_+ is the FRET efficiency with saturating Ca^{2+} .

Calcium titrations were performed on rAc-D and rAc-DA, phosphorylated rAc, and rAc supplemented with 0.5% (v/v) DMSO drug vehicle solvent, 200 μM bepridil, 200 μM levosimendan, 200 μM EGCG, and 750 nM S1. Control measurements were also performed on rAc phosphorylated with PKA (125 units/mg TnI) and 5 mM ATP, with PKA only (125 units/mg TnI), and with 5 mM ATP only.

5.4.2 Concentration of free calcium

The concentration of free Ca^{2+} was obtained using the titration protocol described above with injections into 1 mL of Fluo-4FF pentapotassium salt (Life Technologies) (250 nM) in WB. Fluorescence (490 nm excitation, 520 nm emission, 4 nm slit width, 0.25 sec integration time) was corrected for dilution. The concentration of free Ca^{2+} was calculated using

$$[Ca^{2+}]_i = K_D \frac{(F_i - F_{min})}{(F_{max} - F_i)}, \quad (17)$$

where K_D (9.7 μM) is the dissociation constant of Fluo-4FF, F_{min} is the intensity under Ca^{2+} -depleted conditions, and F_{max} is the intensity under Ca^{2+} -saturating conditions.

5.4.3 Myosin S1 titrations

Steady-state measurements were performed on the instrument detailed above. rAc-D and rAc-DA (250 nM in Tn) were suspended in WB or WB supplemented with 3 mM CaCl_2 . Fluorescence emission from the FRET donor was monitored following 200 serial injections (2 μL) of 5 μM S1 in WB. A mixing time of 3 sec was applied after the addition of each aliquot. Intensity data were corrected for dilution, and intensity of the rAc-DA sample was corrected for donor concentration mismatch. E was calculated using Eq. 3, which includes the acceptor labeling efficiency correction. FRET efficiency data were fit to the Hill equation

$$E = E_- + \frac{E_+ - E_-}{1 + (\theta_{50}/\theta)^{n_H}}, \quad (18)$$

where n_H is the Hill coefficient, θ is the total $[\text{S1}]/[\text{Actin}]$, θ_{50} is the $[\text{S1}]/[\text{Actin}]$ ratio that produces half maximal activation, E_- is the FRET efficiency without S1, and E_+ is the FRET efficiency with saturating S1.

Myosin titrations were performed in triplicate on rAc, phosphorylated rAc, and rAc supplemented with 200 μM bepridil and 200 μM EGCG.

5.4.4 Determining EC_{50} of EGCG

rAc-D and rAc-DA (250 nM in Tn) were suspended in 1 mL of WB. Fluorescence emission from the FRET donor was monitored following 200 serial injections (2 μL) of

WB supplemented with 5 μM EGCG. Intensity data were corrected as indicated above, and E was calculated using Eq. 3. FRET efficiency data were fit to the Hill equation

$$E = E_- + \frac{E_+ - E_-}{1 + (EC_{50}/EGCG)^{n_H}}, \quad (19)$$

where n_H is the Hill coefficient, EC_{50} is the [EGCG] that produces half maximal activation, E_- is the FRET efficiency without EGCG and E_+ is the FRET efficiency with saturating EGCG.

5.5 Cosedimentation assays

5.5.1 Chemomechanical binding assay

Mixtures of F-actin or rAc (10 μM in actin protomer) and S1 (20 μM) were prepared in W or WB supplemented with 5 mM MgATP, then sedimented at 64,000 rpm for 15 min in a TLA-100 rotor. Reserved sample, supernatant, and pellet were examined by quantitative SDS-PAGE. Coomassie-stained gels (GelCode Blue Safe Protein Stain, ThermoFisher Scientific) were scanned (Gel Logic 112, Kodak) for 14 sec using white light epi-illumination. Intensities of S1 and actin bands were quantified using ImageJ. Band intensities I were converted to the relative C using

$$C = (I - I_B)/\alpha, \quad (20)$$

where I_B is the background intensity and α is the staining efficiency of the S1 relative to actin. α was determined from the band intensity of the reserved sample, which contains proteins of known concentration. Measurements were performed in triplicate.

5.5.2 S1 binding to regulated actin with PKA treatment and small molecules

Phosphorylated rAc, rAc (10 μ M in actin protomer), or rAc supplemented with 8 mM bepridil or 8 mM EGCG were mixed with S1 (20 μ M) in WB, sedimented, and analyzed as described above.

5.6 Statistical analysis

Unless otherwise stated, parameters such as n_H and Ca_{50} were recovered through non-linear regression using the least squares method using GraphPad Prism ver. 6g (GraphPad Prism Software, Inc., La Jolla, CA). For Ca^{2+} titrations, E is reported as the maximum likelihood estimate, and recovered parameters are shown for $n = 1$ trial. For S1 titrations, data are plotted as the mean, with errors bars as SEM. E is reported as the maximum likelihood estimate, and recovered parameters are shown for $n = 3$ trials, except in control measurements with rAc mock-treated with PKA, where $n = 1$ trial. Standard errors obtained from the fitting are shown next to each value. The significance ($P > 0.05$) between untreated rAc filaments and filaments treated with PKA or small molecule compounds was determined using the Z-test on the mean and asymptotic SE for each parameter recovered from fits of the data to the Hill equation.¹⁸⁴ In the case of high throughput drug screening trials, compounds not producing significant shifts in Ca_{50} and θ_{50} using this test would be discarded.

6 RESULTS

6.1 Two-colored FRET in regulated actin filaments

Samples containing only a FRET donor (D), and both a FRET donor and acceptor (DA) are necessary to determine energy transfer from a directly excited donor to an acceptor fluorophore. FRET efficiency E is calculated from paired D/DA samples using $E = 1 - (I_{DA}/I_D)$, where I_{DA} is the emission intensity of the donor in the presence of an acceptor, and I_D is the emission intensity of the donor in the absence of an acceptor. Due to the sixth power dependence of distance on resonant energy transfer $R = R_0([1 - E]/E)^{1/6}$, where R is the inter-dye distance, R_0 is the Förster radius of the FRET pair, and E is FRET efficiency,¹⁰⁵ an increase in E corresponds to a decrease in the inter-dye distance. FRET efficiency was used to report Tn activation in reconstituted thin filaments, corresponding to the movement of the SABS of TnI from actin towards the N-lobe of TnC. From the multi-site FRET assay described in Sections 1-3, a FRET pair that fulfilled the requirements to report the activation-dependent structural change in Tn was chosen to pursue drug screen design. The FRET pair needed to exhibit a large Ca^{2+} -induced change in E to provide maximum resolution for discovering alterations to Tn activation from phosphorylation or small molecule binding. Figure 26A shows the engineered Tn, which contains a single Cys in the C-terminal end of the second actin-binding domain of TnI (residue 189) labeled with FRET donor AF546. A single Cys in a loop in the C-lobe of rat cardiac TnC (residue 127) was labeled with the FRET acceptor ATTO655. The loop has no role in coordinating Ca^{2+} or Mg^{2+} . TCSPC measurements of rAc filaments showed a Ca^{2+} -induced change of 21% (Table A10). The assay is sensitive to structural movements of the mobile domain of TnI with respect to the C-lobe of TnC.

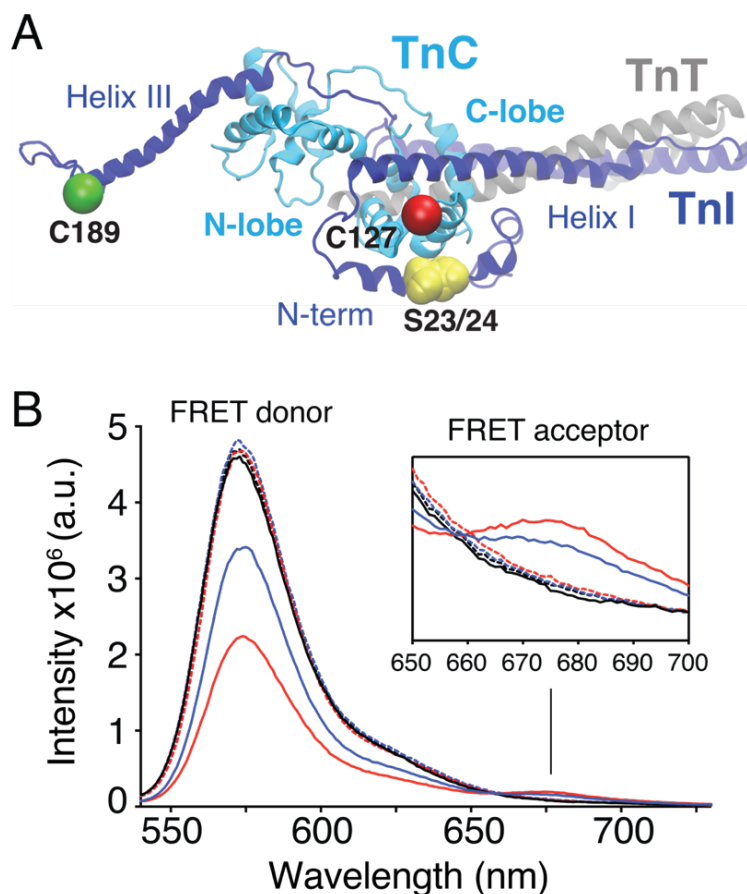


Figure 26. A steady-state FRET assay for measuring Tn activation. (A) Molecular model of the Ca²⁺-saturated 52 kDa core of Tn showing placement of FRET dyes.⁸⁴ TnC, TnI, and TnT are colored cyan, blue, and grey, respectively. The FRET donor, AF546, and FRET acceptor, ATTO655, are attached to Cys 189 of TnI (green sphere) and Cys 127 of TnC (red sphere), respectively. Ser-23/24 of TnI are represented as VDW spheres. **(B)** Fluorescence emission spectra from rAc reconstituted with the FRET donor TnI189C*AF546 (rAc-D) or both the donor and FRET acceptor TnC127C*ATTO655 (rAc-DA). rAc-D (blue dashed), rAc-D supplemented with 3 mM CaCl₂ (+Ca, red dashed), rAc-DA (blue), and rAc-DA +Ca (red). Denatured samples of rAc-D (black dashed) and rAc-DA (black) are shown. *Inset*, Sensitized emission.

Figure 26B shows the steady-state emission spectra from rAc-D and rAc-DA under Ca^{2+} -depleted (no added Ca^{2+}), Ca^{2+} -saturated (with 3 mM CaCl_2), and denatured (with 3 mM CaCl_2 and 3 M GnHCl) conditions. Denaturation with GnHCl allowed for a correction in the differences in donor concentration between rAc-D and rAc-DA samples, as donor intensity with 3 M GnHCl provided the relative concentration of the FRET donor dye in the sample.

The emission intensity of rAc-D was relatively insensitive to 3 mM CaCl_2 , while the emission intensity of rAc-DA showed a 34% decrease in the emission of the FRET donor (575 nm peak), and a corresponding 21% increase in the emission from the FRET acceptor (675 nm peak). Denaturation with 3 M GnHCl served to eliminate the emission peak from the FRET acceptor in rAc-DA samples (Figure 26B, inset). This strongly suggests the emission peak at 675 nm is fluorescence emission from the acceptor due to photons transferred from the donor to acceptor dyes through sensitized emission (FRET).

6.2 Characterizing the binding of myosin subfragment-1

Purified myosin is shown under denaturing gel conditions, where the myosin heavy chain (MHC) runs ≥ 250 kDa, and the essential light chains (ELC1/2) and the regulatory light chain (RLC) are resolved (Figure 27). Other proteins are visible in the lane with purified myosin (P2), and are most likely contaminant actin and tropomyosin. Myosin was enzymatically digested into the catalytically active myosin head, subfragment-1 (S1). Figure 28A shows how SDS-PAGE was used to monitor the progress of digestion, resolve proteins, confirm molecular weights, and determine sample purity. In the presence of EDTA, chymotryptic digestion eliminates the RLC, though ELC1/2 are still resolved.¹⁸⁵

Muscle contraction is maintained through a steady cyclic interaction between myosin motor proteins and actin filaments. Myosin binds to actin by successively forming contacts through nucleotide- and actin-dependent reorientations of different subdomains in myosin. An accurate assessment of the catalytic ability of purified S1 required the removal of all non-specific S1 binding due to catalytically inactive S1 (called deadheads), which bind irreversibly to actin in the presence of ATP. Figure 28B shows the difference between rigor and deadhead binding to actin in the presence and absence of ATP, respectively. Under rigor conditions, a 2:1 mixture of actin and S1 showed a high degree of S1 binding, evident from the pellet of the sedimented sample. An interesting note is the presence of two bands near the ELC1 isoform, where only the lower molecular weight band appears to bind to actin. The higher molecular weight band cannot be attributed to TnI or TnC, which run higher and lower, respectively. In the presence of 5 mM ATP, a small portion of S1 was bound to actin (deadheads), and a majority of S1 remained in solution (catalytically active S1).

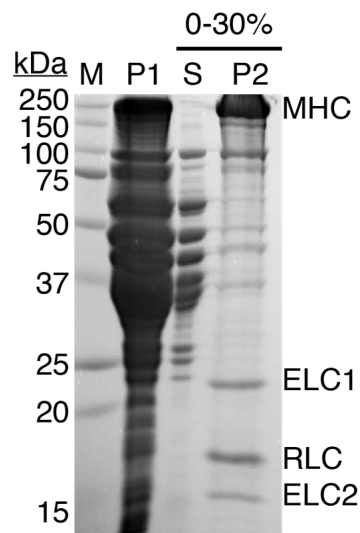


Figure 27

Figure 27. Purification of myosin from chicken pectoralis muscle. Molecular weight markers (M); the pellet containing myosin, contaminant actin (~48 kDa), and Tm (~37 kDa) from the water precipitation (P1); the supernatant (S) and pellet (P2) containing purified myosin heavy chain (MHC), essential light chains 1 (ELC1) and 2 (ELC2), and regulatory light chain (RLC) from the 0-30% $(\text{NH}_2)_4\text{SO}_4$ cut are shown.

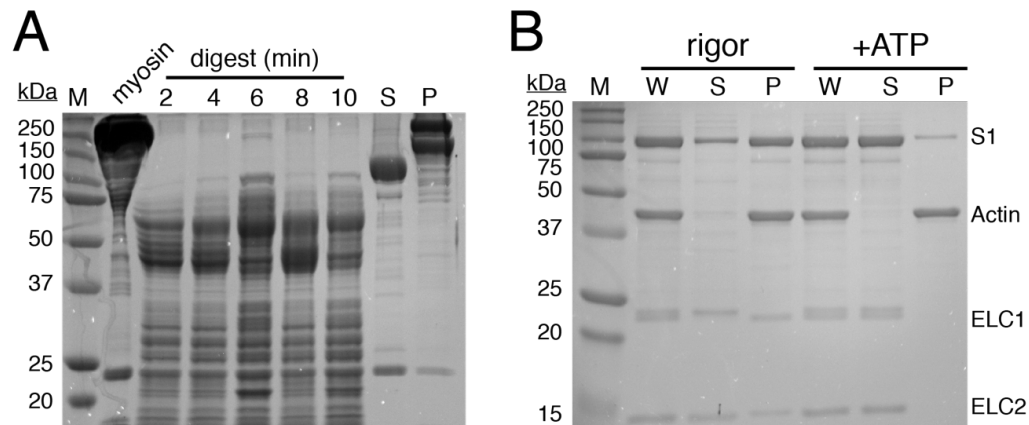


Figure 28. Chymotryptic digest of myosin into subfragment-1. **(A)** Myosin was digested with chymotrypsin (1:100, chymotrypsin:myosin) in the presence of EDTA for 10 minutes. Molecular weight markers (M), and the supernatant (S) containing S1 and pellet (P) containing undigested myosin are shown. **(B)** Removal of catalytically inactive S1. Co-sedimentation of S1 (20 μM) and actin (10 μM) in WB (rigor) and WB supplemented with 5 mM MgATP. Molecular weight markers (M), the pre-spin mixture (W), the supernatant (S), and pellet (P) for both rigor and +ATP conditions are shown. S1 in complex with either essential light chain 1 or 2 (ELC1, ELC2), and actin bands are resolved. Under rigor conditions, S1 binds actin >90%. In the presence of 5 mM MgATP, only catalytically inactive S1 bind to actin, and the supernatant contains catalytically active S1.

6.3 PKA-mediated phosphorylation of TnI Ser-23/24

PKA treatment of Tn selectively bis-phosphorylates TnI Ser-23/24.¹⁷⁰ TnI Ser-23/24 within reconstituted rAc was selectively phosphorylated with the catalytic subunit of PKA and ATP (co-factor), and these were removed by sedimentation, washing, and re-suspension of filaments. Schulenberg et al. showed the utility of characterizing protein phosphorylation using a fluorescent dual-staining approach.¹⁸⁶ SDS-PAGE with subsequent staining using Pro-Q Diamond (selectively stains phosphorylated proteins) and SYPRO Ruby (stains all proteins) was used to quantify the degree of phosphorylation in rAc. Phosphorylated ovalbumin (from the phosphoprotein standard) has two phosphorylation sites,¹⁸⁷ and was used as a control (Figure 29A). Figure 29B shows Ser-23/24 phosphorylated to $\approx 100\%$ efficiency after a 1.5 hour incubation with PKA.

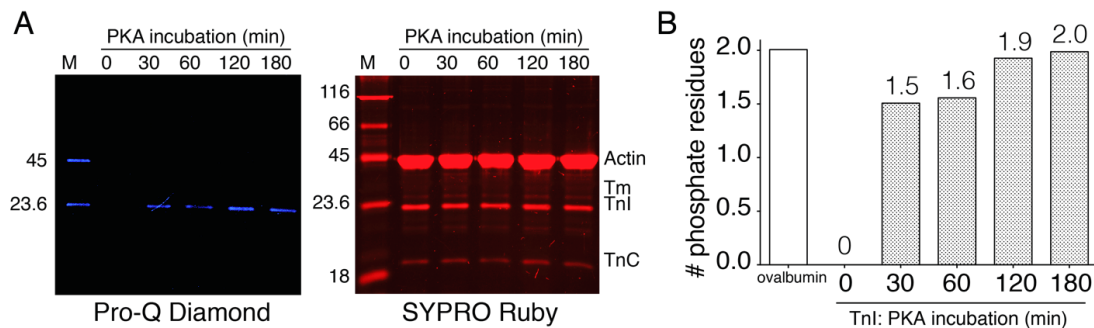


Figure 29. Quantification of PKA-dependent TnI phosphorylation. (A) Time course of PKA-treated WT rAc analyzed by 1D SDS-PAGE (12%, 29:1). Successive staining with Pro-Q Diamond (left) and SYPRO Ruby (right) provided, respectively, the level of TnI phosphorylation and total TnI. **(B)** Time-dependent efficiency of TnI phosphorylation by PKA. The number of phosphorylated residues in TnI was estimated from the intensity of TnI compared to ovalbumin (phosphorylation and molecular weight standard) in (A).

6.4 Physical characterization of regulated actin

To determine if the triple mutants required for the assay on TnI (C81I, C98S, V189C) and TnC (C35S, C84S, T127C) affected the functional properties of Tn, isometric force-pCa experiments were performed. WT (control) and mutant Tn were reconstituted with mouse cTnT with an N-terminal myc sequence attached. The efficiency of exchange of WT Tn ($80.6 \pm 1.0\%$) and mutant Tn ($69.2 \pm 3.5\%$) were estimated from Western blots of the exchanged cells (Figure 30A-B). Figure 30C shows measurements of force at different Ca^{2+} concentrations. During measurements, the sarcomere length (SL) was maintained at either 1.9 μm or 2.3 μm . At 1.9 μm and 2.3 μm SL, peak force (Figure 30D) and Ca^{2+} sensitivity (pCa_{50}) (Figure 30E) were not statistically different between fibers exchanged with WT and mutant Tn ($P > 0.05$). The mutagenesis required as part of the FRET assay design did not significantly alter the native function of Tn.

Regulated actin filaments (rAc) were reconstituted from Tn, tropomyosin (Tm), and F-actin. rAc was reconstituted with Tn containing the FRET donor (rAc-D), and with Tn containing the FRET donor and acceptor (rAc-DA). SDS-PAGE was used to assess the purity of thin filament proteins, and show rigor-S1 binding did not perturb Tn or Tm bound to actin (Figure 31). rAc was reconstituted with 5x more Tm than actin protomer to promote filament stability, but the amount of Tm bound to actin remained unchanged with excess Tm in solution, compared to rAc reconstituted with one Tm:actin protomer.

The chemical structure of the small molecule compounds bepridil, levosimendan, and EGCG used in this study are shown (Figure 32). To assess the effect on filament morphology from PKA treatment, S1 binding, DMSO, and small molecules, rAc-DA

filaments were imaged using epifluorescence (Figure 33). Filament bundling is not appreciated, and donor and acceptor dyes co-localize, suggesting Tn remains stably bound to rAc as an intact assembly.

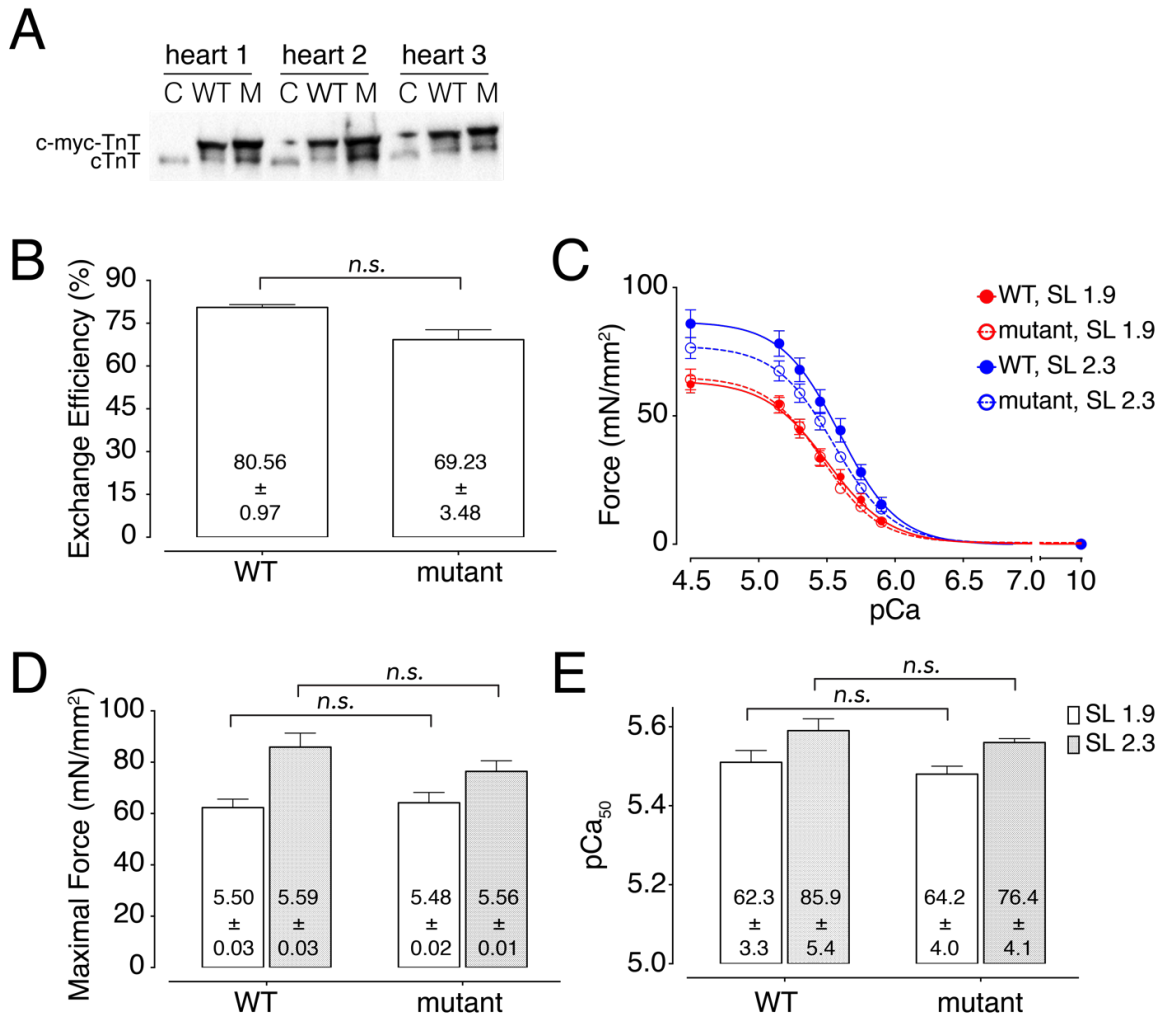


Figure 30

Figure 30. Functional characterization of mutated Tn. WT Tn consisting of myc-TnT, TnI, TnC and mutant (M) Tn consisting of myc-TnT, TnI189C, TnC127C were exchanged into skinned cardiomyocytes from rat ventricles. **(A)** Western blot analysis of reserved fibers. Exchanged myc-TnT (WT or M) was compared to native TnT to determine the Tn exchange efficiency. (WT: $n=3$; mutant: $n=3$) Also shown are lanes containing native TnT (C). **(B)** Exchange efficiency from samples in (A). Shown are the mean \pm SEM (WT: $n=3$; mutant: $n=3$). Differences were not significant ($P > 0.05$, two-way ANOVA). **(C)** Pooled data (mean \pm SEM, WT: $n=9$; mutant: $n=9$) from force-pCa measurements of fibers at short (red, 1.9 μm) and long (blue, 2.3 μm) sarcomere lengths (SL). Lines for mutant (dotted line) and WT (solid) exchanges are drawn using the mean of Ca^{2+} -sensitivity pCa_{50} and maximum force F_{max} recovered from individual fits of fibers. **(D)** Average maximum force \pm SEM from (C) for SL at 1.9 μm (white) and SL 2.3 μm (grey). **(E)** Average $\text{pCa}_{50} \pm$ SEM from (C). A consistent coloring scheme is used in (D-E).

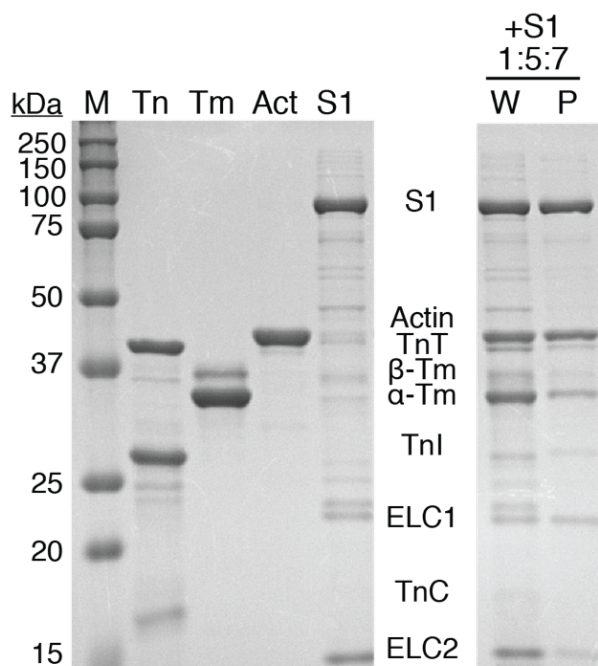


Figure 31. Assessment of sample purity of thin filaments and myosin subfragment-1.

SDS-PAGE (12%, 29:1) of reconstituted mutant Tn (TnI189C, TnC127C, TnT), Tm with α and β isoforms, actin, and S1. Molecular weight markers (M) are shown. rAc (10 μ M in actin) reconstituted with mutant Tn, Tm, and actin at a molar ratio of 1:5:7 Tn:Tm:Act was cosedimented with S1 (10 μ M). The pre-spin mixture (W) and pellet (P) are shown.



Figure 32. Chemical structures of small molecules. Shown are bepridil, levosimendan, and EGCG.

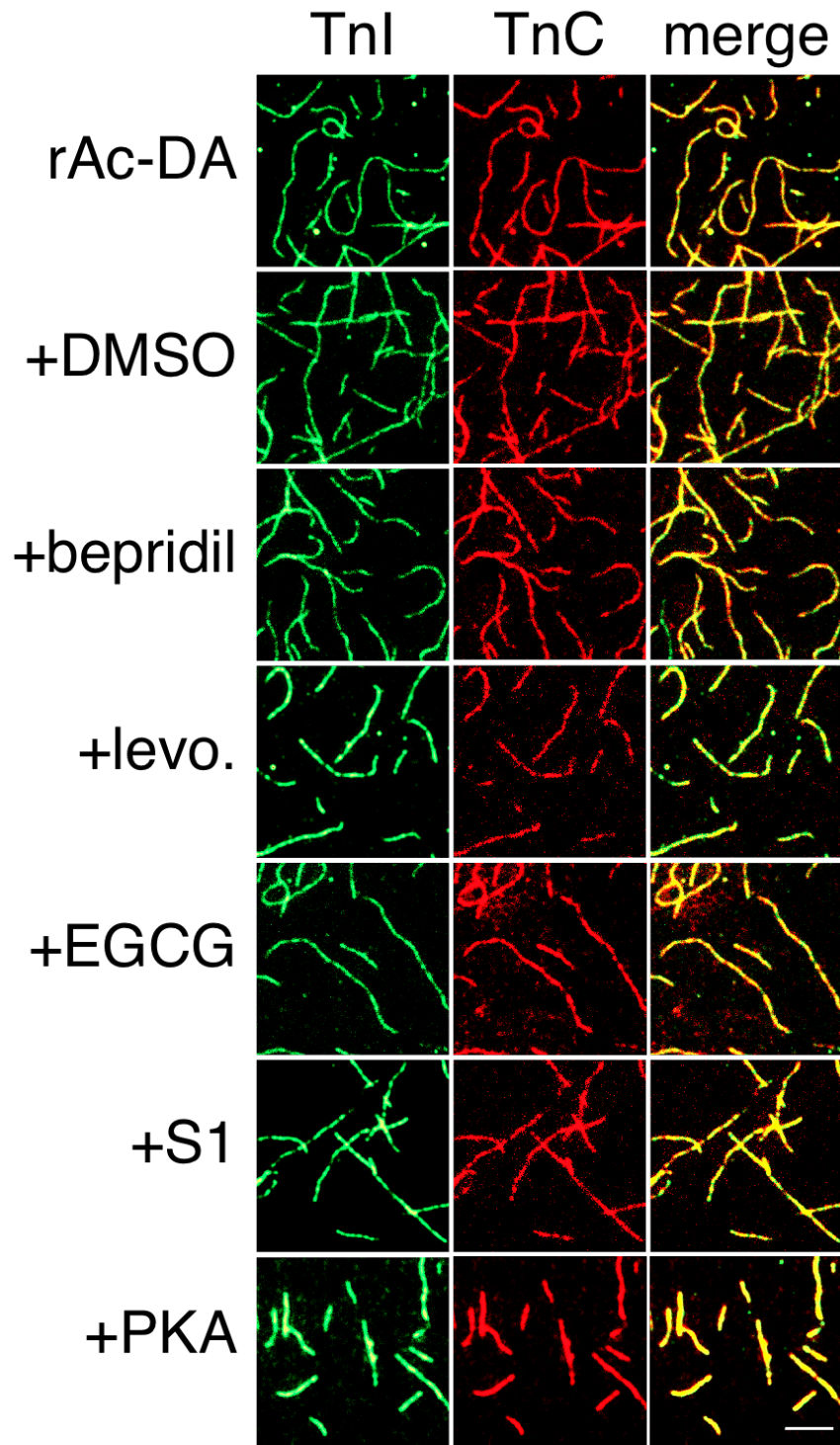


Figure 33

Figure 33. Filament morphology of rAc-DA with small molecules, myosin S1, and PKA treatment. Epifluorescence images of PKA-treated rAc-DA and rAc-DA supplemented with DMSO (0.5%, v/v), 200 μ M bepridil, 200 μ M levosimendan, 200 μ M EGCG, and 1.5 μ M S1. Filaments were diluted to 10 nM in WB and imaged on glass coverslips. Shown is the emission from directly-excited TnI189C*AF546, directly-excited TnC127C*ATTO655, and the merged images. The scale bar is 5 μ m.

6.5 Determining the concentration of free Ca^{2+}

The concentration of free Ca^{2+} in solution was determined using the Ca^{2+} sensitive dye Fluo-4FF. Figure 34A shows the emission from 500 nM Fluo-4FF in WB with serial injections of the Ca^{2+} buffer utilized in subsequent Ca^{2+} titrations of rAc: WB supplemented with 50 mM CaCl_2 . Ca^{2+} binds to Fluo-4FF in a 1:1 complex, and upon binding, the dye molecule undergoes a conformational change that allows fluorescence emission upon excitation with blue light with no spectral shift. Eq. 17 was then used to convert emission intensity to $[\text{Ca}^{2+}]_{\text{free}}$ (Figure 34B). WB alone did not have any contaminant Ca^{2+} , evident from the first point prior to injecting Ca^{2+} (injection #0). Using a fluorescent Ca^{2+} indicator provided a direct measurement of Ca^{2+} in solution with fewer variables, as opposed to Ca^{2+} calculators that give an indirect measurement of free Ca^{2+} . Ca^{2+} calculators that solve simultaneous equilibrium reactions require user-defined values prone to inaccuracies, including the absolute concentration of buffer components that compete for Ca^{2+} binding (e.g. EGTA) and instrument aliquot volume.¹⁸⁸

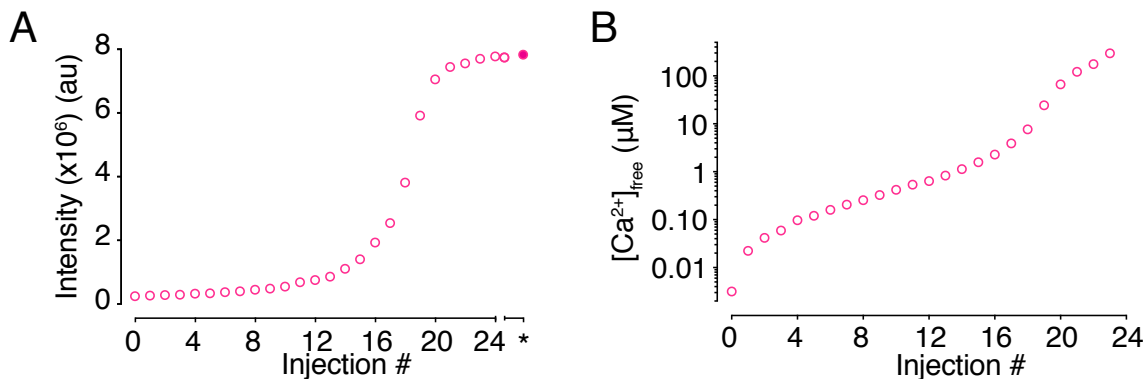


Figure 34. Calibration of the concentration of free Ca²⁺. The Ca²⁺-sensitive dye Fluo-4FF was diluted to 250 nM in WB, and serially injected with 2 μL of WB supplemented with 50 mM CaCl₂. Left, emission from Fluo-4FF (excitation, 490 nm; emission, 520 nm). The * indicates the emission from the donor after adding 100 mM CaCl₂. Right, data were corrected for dilution, and the free Ca²⁺ was calculated from the fluorescence intensities using Eq 2.5, with f_{max} equal to emission after addition of 100 mM CaCl₂ (*).

6.6 Screening for Ca²⁺-induced activation

The effect of small molecules on Ca²⁺-induced activation of Tn was assessed with Ca²⁺ titrations of rAc (250 nM in Tn) in the presence of the compound solvent (DMSO, 0.5%, v/v), bepridil (200 μM), levosimendan (200 μM), EGCG (200 μM), S1 (750 nM), and in rAc with bisphosphorylated TnI Ser-23/24 (PKA-treated). The emission from the donor in paired D/DA filaments was monitored with 2 μL serial injections of working buffer (WB: 50 mM MOPS pH 7.0, 5 mM MgCl₂, 2 mM EGTA, 5 mM BME) supplemented with 50 mM CaCl₂ (Figure 35A). Paired samples were donor concentration-matched using 3 M guanidine hydrochloride (GnHCl) using Eq. 14. Tn dissociation eliminated donor quenching through resonant energy transfer. The emission

intensity of the donor from dissociated rAc-DA was corrected to match the donor intensity from dissociated rAc-D. Intensity data from rAc-D/DA samples were also corrected for dilution, then plotted against free Ca^{2+} (Figure 35A). FRET efficiency E was then calculated from the corrected intensity data using $E = f_A^{-1}(1 - [I_{DA}/I_D])$, where f_A is the acceptor labeling efficiency, I_{DA} is the intensity of the donor from rAc-DA, and I_D is the intensity of the donor from rAc-D.

6.6.1 Bepridil and S1 both increased Tn activation and Ca^{2+} sensitivity

Figure 35C and 35D show E and normalized E , respectively, vs. free Ca^{2+} , with fits to the Hill equation. Normalized E clearly shows an increase in Ca^{2+} sensitivity with S1 and bepridil compared to untreated rAc with bepridil and S1, evident from the leftward shift of the titration curves. Bepridil increased FRET efficiency both under Ca^{2+} depleted conditions (E_{-} , apo) and Ca^{2+} -saturating conditions (E_{+} , ≈ 3 mM CaCl_2), though not as dramatically as S1 binding (Figure 35E). The recovered Ca^{2+} dissociation constant Ca_{50} and Hill coefficient n_H in Figure 35F show the similar effects induced by S1 binding and bepridil: both reduced cooperativity and significantly increased Ca^{2+} sensitivity compared to untreated filaments. Table A12 summarizes the recovered parameters from fits to the Hill equation. The Ca^{2+} sensitivity of Tn was unchanged with levosimendan. Ca_{50} and n_H with levosimendan were not significantly different from non-treated rAc.

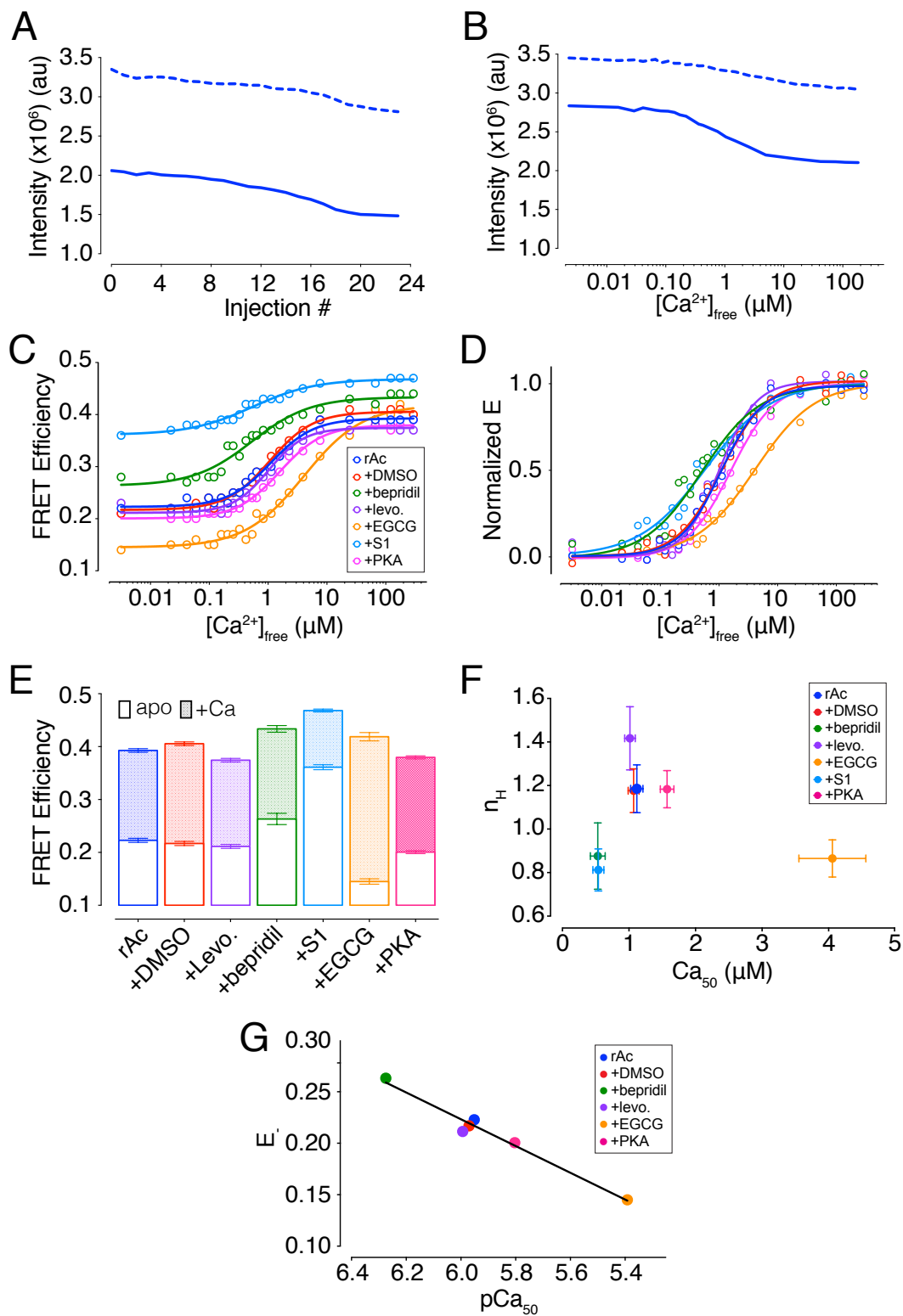


Figure 35

Figure 35. Effect of small molecules, PKA treatment, and S1 binding on the Ca^{2+} -dependent activation of regulated actin. (A) Representative traces for Ca^{2+} titrations of rAc-D (dashed) and rAc-DA (solid) at 250 nM. Fluorescence emission of the FRET donor vs. injection #. (B) Fluorescence emission from (A) corrected for dilution, and rAc-DA corrected for dilution and concentration vs. the concentration of free Ca^{2+} . (C) rAc (250 nM in Tn) (blue), PKA-treated rAc (magenta) and rAc supplemented with the drug carrier (red, 0.5% DMSO, v/v), 200 μM bepridil (green), 200 μM levosimendan (purple), 200 μM EGCG (orange), and 0.75 μM S1 (cyan) were titrated with Ca^{2+} . A consistent coloring scheme is used in (C-G). FRET efficiency was calculated from titrations of pair D/DA rAc filaments. Solid lines represent fits of the data to the Hill equation to recover the Hill coefficient (n_H) and Ca^{2+} dissociation constant (Ca_{50}) (Table A12), FRET efficiency under depleted Ca^{2+} (E_-) and the FRET efficiency under saturating Ca^{2+} (E_+). (D) Normalized data from (C). (E) Recovered E_- (open bars) and E_+ (filled bars) from fits in (C). Mean \pm asymptotic SE (error bars) are shown. (F) Recovered n_H and Ca_{50} from fits in (C). Mean \pm asymptotic SE (error bars) are shown. (G) Plot of recovered E_- vs. $\text{pCa}_{50} = -\log(Ca_{50})$ for small molecule modulators of troponin activation. Solid line is a fit of data to a first order polynomial ($R^2 = 0.97$).

6.6.2 EGCG and TnI phosphorylation reduced Ca^{2+} sensitivity

EGCG dramatically desensitized Tn to Ca^{2+} , evident from the rightward shift in the titration curve in Figure 35B, increasing the Ca_{50} from 1.12 μM for untreated rAc to 4.06 μM . PKA treatment induced a smaller, but still significant ($P < 0.05$) desensitization for Ca^{2+} . Cooperativity significantly decreased with EGCG, but was unchanged with PKA treatment. EGCG caused a ≈ 1.5 -fold decrease in E_{-} , but E_{+} recovered slightly higher compared to untreated rAc. PKA treatment caused a small ≈ 1.1 -fold decrease in E_{-} .

6.6.3 Ca^{2+} sensitivity is correlated to the Ca^{2+} -depleted FRET efficiency

Figure 35G shows the FRET efficiency under Ca^{2+} -depleted conditions E_{-} plotted against $pCa_{50} = -\log(Ca_{50})$, fit to a first order polynomial ($R^2 = 0.97$). Filaments treated with small molecules that increased Ca^{2+} sensitivity had higher E_{-} , and treated filaments with decreases in Ca^{2+} sensitivity had lower E_{-} . E_{-} , a property of Tn in the absence of Ca^{2+} , is correlated to a property of Tn under activating Ca^{2+} .

6.7 Screening for myosin-induced activation

To assess myosin-induced activation of Tn, rigor-S1 titrations were performed on PKA-treated rAc, and rAc supplemented with EGCG (200 μM) and bepridil (200 μM). The emission from the donor in paired samples (250 nM in Tn) was monitored with 2 μL serial injections of 5 μM S1 in WB (Figure 36A) under Ca^{2+} -saturating (+Ca, 3 mM CaCl_2) and Ca^{2+} -depleted conditions (apo). Donor intensity in paired rAc-D/DA samples was concentration-matched and corrected for volume as previously described (Figure 36B), and used to calculate the FRET efficiency.

6.7.1 S1-induced activation of Tn occurs independently of Ca²⁺

Figure 36C and 36D show the FRET efficiency and normalized FRET efficiency, respectively, plotted against the ratio of the total amount of S1 added to actin in the sample ($\theta_{50} = [S1]_T/[Actin]_T$) for samples under apo and +Ca conditions. Figure 36E shows the recovered FRET efficiencies with total S1 added (E_{+S1} , +1.43 μ M S1) and without S1 (E_{-S1}). E_{+S1} for apo rAc and E_{-S1} for Ca²⁺-saturated rAc were 45.9 and 43.6%, respectively, indicating activation with S1 behaved like Ca²⁺-induced activation.

Figure 36F shows the recovered Hill coefficients n_H and θ_{50} for apo and Ca²⁺ conditions, where θ_{50} is the stoichiometry that produces half maximal activation. Adding Ca²⁺ increased myosin sensitivity in rAc and with EGCG, but myosin sensitivity remained unchanged when rAc was treated with PKA. Table A13 summarizes the recovered parameters.

6.7.2 Bepridil eliminates S1-induced activation of Tn

The FRET efficiency remained unchanged for rAc supplemented with bepridil from E_{-S1} to E_{+S1} , indicating no myosin-induced Tn activation. Ca²⁺-induced activation of Tn was preserved, as seen in the Ca²⁺ titrations with bepridil.

6.7.3 EGCG and PKA treatment reduce myosin sensitivity

EGCG decreased E . as seen in the Ca²⁺ titrations; saturating S1, however, recovered E_{+S1} greater than the for rAc. The E_{+S1} for both apo and +Ca with EGCG was similar, indicating S1 activates Tn the same, regardless of the presence of Ca²⁺. So although myosin sensitivity increased with Ca²⁺, the level of S1-induced activation was unchanged with Ca²⁺. Myosin sensitivity significantly decreased under Ca²⁺ depleted

conditions for both EGCG and PKA treatment, where θ_{50} was 0.55 ± 0.05 and 0.59 ± 0.01 , respectively. When Ca^{2+} was added to rAc with EGCG, the myosin sensitivity recovered to rAc under apo Ca^{2+} conditions, whereas Ca^{2+} did not change the myosin sensitivity of PKA-treated rAc. PKA treatment induced a massive cooperativity compared to untreated filaments, with Ca^{2+} increasing cooperativity from 28.1 to 50.7.

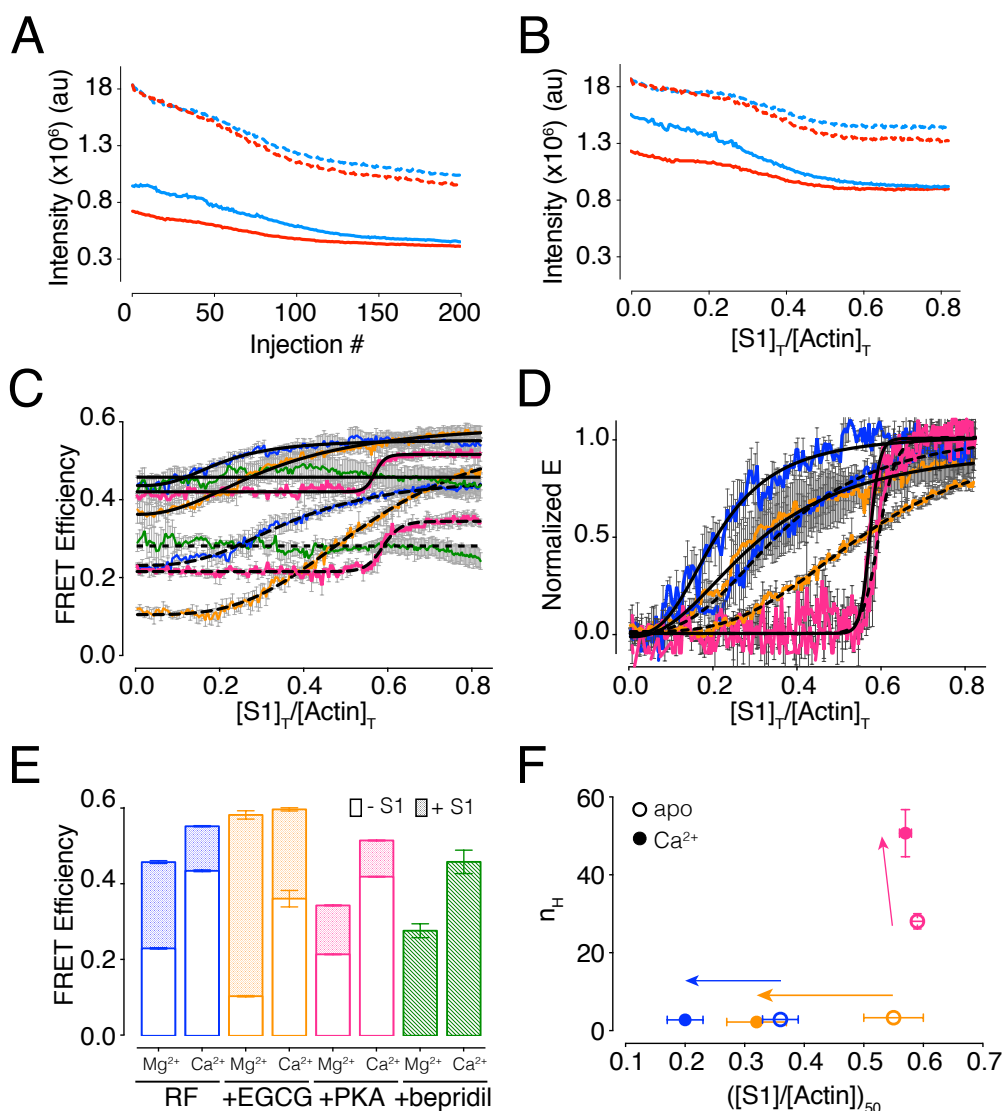


Figure 36

Figure 36. The effect of small molecules and Ca^{2+} on the activation of thin filaments by myosin. (A) Representative traces for S1-titrations of rAc-D (dashed) and rAc-DA (solid) at 250 nM in Tn under Ca^{2+} -saturated (+3 mM CaCl_2 , red) and Ca^{2+} -depleted (cyan) conditions. Fluorescence emission of the FRET donor from rAc serially injected with 2 μL of 5 μM S1 in WB. (B) Fluorescence emission from (A) from rAc-D corrected for dilution, and rAc-DA corrected for dilution and concentration relative to the total concentration of $[\text{S1}]/[\text{Actin}]$. (C) rAc (blue) and rAc supplemented with 200 μM EGCG (orange) or 200 μM bepridil (green) were titrated with S1. The calculated FRET efficiency (mean \pm SEM, $n = 3$) vs. the relative total concentration of $[\text{S1}]/[\text{Actin}]$ is shown. Measurements were performed with no Ca^{2+} (dashed lines) and with 3 mM CaCl_2 (solid lines). Smooth lines represent fits of the data to the Hill equation. The fits to PKA-treated rAc are shown (magenta). (D) Normalized FRET efficiencies from (C) for PKA-treated rAc, rAc, and rAc supplemented with 200 μM EGCG. (E) Stacked bar plot showing FRET efficiencies from the fits \pm asymptotic SE at saturating S1 (total S1 added 1.43 μM , filled), and with no S1 (open) for samples in (C). (F) Scatter plot summarizing the Hill coefficients (n_H) and relative total concentrations of $[\text{S1}]/[\text{Actin}]$ that produces half-maximal activation ($[\text{S1}]/[\text{Actin}]_{50} \pm$ asymptotic SE from the fits in (C) for PKA-treated rAc, rAc, and rAc supplemented with 200 μM EGCG with no Ca^{2+} (apo, open) and with Ca^{2+} added (3 mM CaCl_2 , filled). A consistent coloring scheme is used in (C-F).

6.8 Control measurements for PKA treatment

To determine if PKA treatment and the removal of PKA and its co-factor ATP from treated filaments influenced Tn behavior to Ca^{2+} and myosin binding, Ca^{2+} and S1 titrations were performed on paired untreated rAc filaments, PKA-treated filaments (PKA and 5 mM ATP), and filaments mock-treated with PKA and 5 mM ATP. Figure 37 shows mock-treatment did not have a significant effect ($P > 0.05$) on Ca_{50} compared to untreated filaments, where PKA treatment produced a significant increase in Ca_{50} . As expected, PKA treatment and mock treatment did not produce a significant effect on n_H . Table A14 summarizes the recovered parameters from Ca^{2+} titrations. Figure 38 shows only PKA treatment produced a significant effect on n_H and θ_{50} under both apo and +Ca conditions. Recovered parameters are listed in Table A15. PKA-mediated TnI Ser-23/24 phosphorylation is responsible for modulating Tn activation.

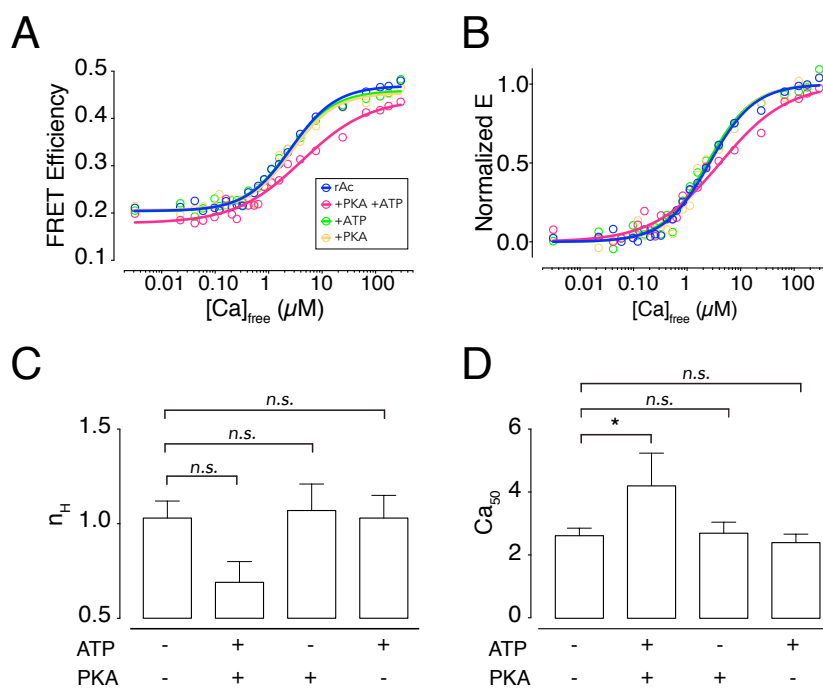


Figure 37

Figure 37. Control measurements of PKA treatment of rAc titrated with Ca^{2+} . (A)

Calculated FRET efficiency vs. free Ca^{2+} for rAc, rAc treated with PKA and ATP

(magenta), mock-treated with ATP (green), and mock-treated with PKA (tan) (250 nM in

Tn in WB). Lines represent fits to the Hill equation. (B) Normalized FRET efficiency.

(C) The recovered Hill coefficients (n_H) asymptotic SE from fits in (A). (D) The

recovered concentration of calcium to achieve half maximal activation (Ca_{50}) from fits in

(A) \pm SE. * $P < 0.05$ relative to non-treated rAc (n.s. = not significant).

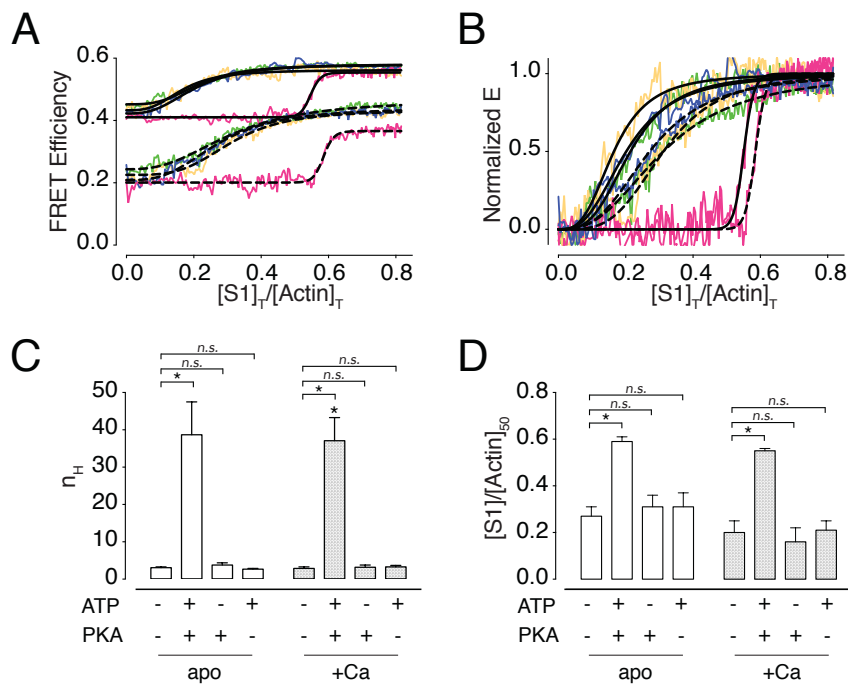


Figure 38

Figure 38. Control measurements of treatment of reporter filaments with PKA titrated with S1. (A) Calculated FRET efficiency vs. the relative total concentration of [S1]/[Actin] for rAc, rAc treated with PKA and ATP (magenta), mock-treated with ATP (green), and mock-treated with PKA (tan) in WB (apo, dashed lines) and WB supplemented with 3 mM CaCl₂ (+Ca, solid lines). Lines represent fits to the Hill equation. (B) Normalized FRET efficiency. (C) The recovered Hill coefficients (n_H) asymptotic SE from fits in (A) for apo (open) and +Ca (filled). (D) The recovered concentration of calcium to achieve half maximal activation (Ca_{50}) from fits in (A) \pm SE. * $P < 0.05$ relative to non-treated rAc for apo and +Ca (n.s. = not significant).

6.9 S1 binds to rAc with small molecules and PKA treatment

To determine if S1 was binding to rAc filaments under all conditions, SDS-PAGE was used to assess S1 binding to rAc, and rAc treated with PKA, bepridil, or EGCG. S1 (10 μ M) was cosedimented with rAc reconstituted with WT Tn (10 μ M in actin) under apo conditions and with 3 mM CaCl₂. Figure 39A shows the SDS-PAGE of the pre-spin, the supernatant, and the pellet. Densitometry analysis of the S1 and actin band intensities in the pellet gave percent S1 saturation, seen in Figure 39B. The percent saturation (>80%) shows S1 binds under all conditions.

6.10 A high throughput single point drug screen

Figure 40 shows the high throughput (HTS) strategy for screening compound libraries for potential inotropic agents, and finding the EC₅₀ for qualifying compounds. EC₅₀ is the concentration of compound that produces a half-maximal response.

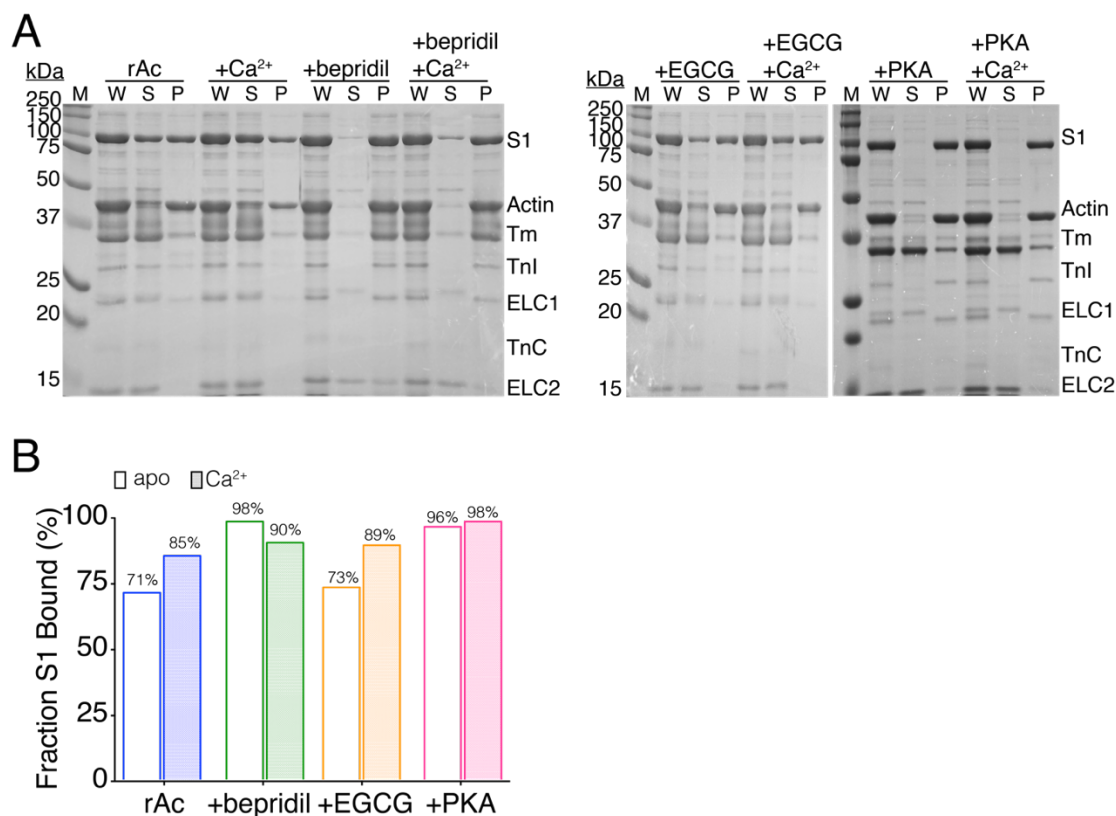


Figure 39. SDS-PAGE shows myosin binding with small molecules and PKA

treatment. (A) SDS-PAGE (12%, 29:1) showing the reserved fraction (W), supernatant (S), and pellet (P) from the cosedimentation of regulated actin (rAc) reconstituted with WT Tn (10 μ M in actin protomer) and S1 (10 μ M) in WB. The fraction of S1 bound was determined using densitometry analysis comparing the band intensities S1 and actin. rAc, PKA-treated rAc, and rAc supplemented with 200 μ M EGCG or bepridil without added Ca²⁺ and with 3 mM CaCl₂ are shown. Molecular weight markers (M), tropomyosin (Tm), TnI, TnC, and the two isoforms of the essential light chains (ELC1 and 2) are resolved. **(B)** The fraction of S1 bound is shown for rAc (blue), PKA-treated rAc (magenta), and rAc supplemented with 200 μ M EGCG (orange) and bepridil (green) without added Ca²⁺ (apo, open) and with 3 mM CaCl₂ (filled).

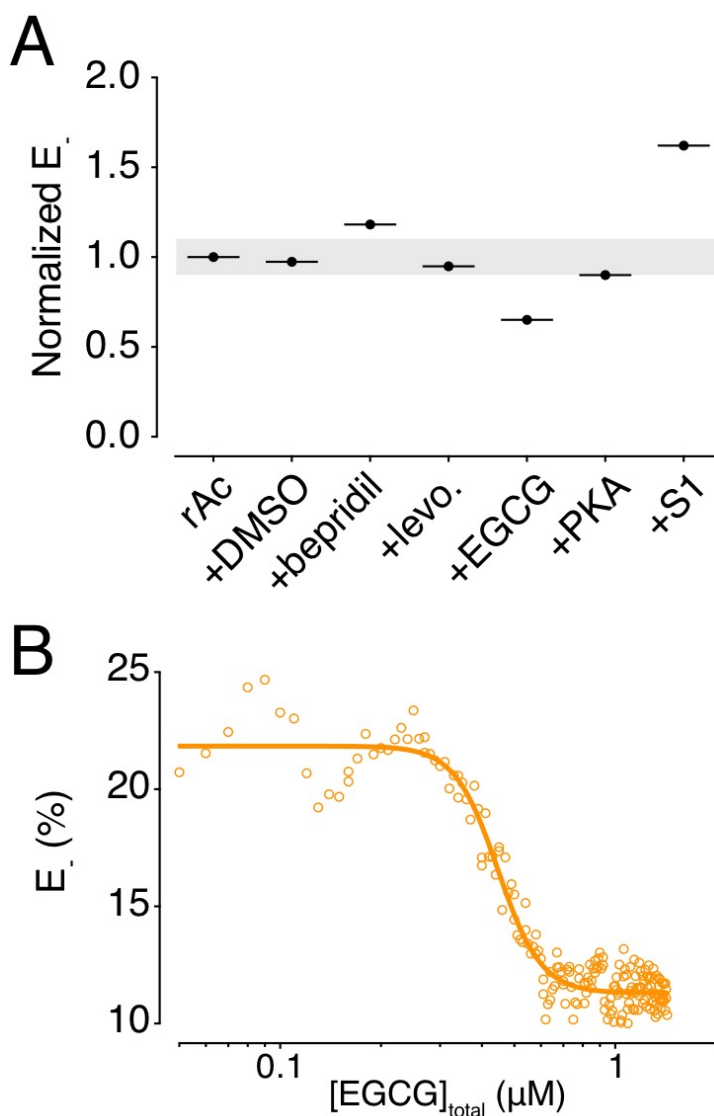


Figure 40. High throughput screening (HTS) strategy. (A) The FRET efficiency without added Ca^{2+} E_f was normalized to untreated rAc. The grey rectangle indicates a ± 0.1 threshold for E_f , where compounds above the threshold are Ca^{2+} sensitizing; compounds below the threshold are Ca^{2+} -desensitizing. **(B)** EGCG concentration-response curve illustrating HTS lead generation. (E_f) was measured for different concentrations of EGCG. Solid line is a fit to the Hill equation with $\text{EC}_{50} = 446$ nM.

7 DISCUSSION

Sarcomeric modulators are a promising therapeutic strategy in the treatment of heart failure that do not require changes in Ca^{2+} transients. Ca^{2+} inotropes increase or decrease the Ca^{2+} binding affinity of TnC without changing intracellular Ca^{2+} concentrations, shifting the population of active or inactive Tn that corresponds to a shift in contracted or relaxed sarcomeres. Insights into the mechanism of action of these molecules can facilitate informed drug design and development, which could eliminate many of the negative effects associated with compounds currently used.¹⁸⁹⁻¹⁹⁰

A compound does not need to bind directly to TnC to alter Ca^{2+} sensitivity; therefore, a drug screen developed in reconstituted thin filaments can potentially resolve effects from compounds discarded in screens with isolated TnC or Tn alone. Non-specific interactions would also be reduced. This FRET assay was designed within reconstituted thin filaments as an *in vitro* biochemical model²⁸ for muscle activation to directly monitor the activating structural change in Tn, where the SABS moves off actin and closer to TnC. A higher FRET efficiency is associated with a higher population of Tn in the active conformation. FRET provides the relative distances between the donor and acceptor dyes, positioned, respectively, on TnI189 in the SABS, and TnC127, in the C-lobe of TnC. The design of this assay was specific for drug screening, where a green-excitable FRET donor was used to reduce the possibility of photoinactivation of small molecules (drugs) by blue-shifted excitation wavelengths, e.g. blebbistatin deactivation by exposure to light below 488 nm.¹¹⁰ While other fluorescence assays in thin filaments have been developed to monitor Ca^{2+} sensitivity using changes in TnC conformation,¹⁹¹ this assay was highly sensitive to the activating structural change between TnC and TnI in reconstituted thin

filaments. The fraction of active Tn was estimated by monitoring FRET efficiency. The contributions of Ca^{2+} and rigor S1 to activate the thin filament were determined, where in native cardiomyocytes, these contributions would be difficult to resolve. This 2D screening method was applied to three previously studied compounds thought to alter the Ca^{2+} sensitivity of TnC: bepridil, levosimendan, and EGCG. The assay was validated as a drug screen to identify compounds that bind the thin filament and alter myosin sensitivity to actin and/or TnC to Ca^{2+} , while also obtaining data suggesting the molecular mechanisms behind Ca^{2+} - and myosin-dependent activation, and PKA-mediated Ca^{2+} desensitization of the thin filament.

7.1 Cooperative activation by Ca^{2+} is dependent on the presence of rigor-S1

Ca^{2+} binding to TnC is a critical step for initiating activation, but cardiac muscle activates in a highly cooperative process involving both Ca^{2+} and myosin binding. Crossbridge formation (S1 binding to actin) not only causes additional myosin binding, but also increases the Ca^{2+} sensitivity of TnC. Previous experiments have shown rigor-S1 exerts a Ca^{2+} -sensitization on thin filament activation,^{49, 136, 192} and full activation can be achieved by the S1 head alone.¹⁹³ Rigor-S1 not only sensitized regulated actin to Ca^{2+} , but also cooperatively activated Tn in a Ca^{2+} -independent manner, consistent with studies in isolated cardiomyocytes.²² The implications of Tn activating independently of Ca^{2+} hint at the possibility that Ca^{2+} -dependent Tm movement may not be required for myosin crossbridge formation. In the absence of Ca^{2+} , rigor-S1 binding could produce a conformational change in actin, forcing Tn into the active conformation. However, Ca^{2+} and S1 together maximally increased the population of active Tn, suggesting Ca^{2+} alone

does not maximally activate Tn. These results coincide with those seen by Zhou et al., who used anisotropy to show S1 changes the dynamics in the C-terminal region of TnI independently of Ca^{2+} , but both Ca^{2+} and S1 are required for maximal activation.⁸²

S1 cooperatively activated thin filaments in a Ca^{2+} -independent manner; Ca^{2+} cooperatively activated thin filaments only in the absence of S1. Ca^{2+} -induced activation of rigor-S1-bound thin filaments was negatively cooperative ($n_H = 0.8 \pm 0.1$), but S1-induced activation of thin filaments in both Ca^{2+} -depleted conditions ($n_H = 2.9 \pm 0.1$) and Ca^{2+} -saturating conditions ($n_H = 2.8 \pm 0.1$) was cooperative. The high cooperativity in S1-dependent activation suggests multiple S1 heads must cooperatively bind to the thin filament to displace a single SABS. Conversely, the cooperativity of Ca^{2+} binding was <1 in filaments with a high probability of multiple rigor-S1 heads already bound to actin (rigor-S1:actin protomer = 1:2.3). This suggests the binding of one Ca^{2+} molecule displaced one SABS from actin. Simply stated, when strong crossbridges are bound to actin, Ca^{2+} activates the thin filament non-cooperatively; rigor-S1 activates thin filaments cooperatively, whether or not Ca^{2+} is bound.

These results suggest actin conformational changes may be responsible for cooperative activation. When rigor-S1 binds to an actin protomer, conformational changes in actin may be translated from the SABS to the regulatory head of Tn, through TnT(T1) to Tm. These translated conformational changes may influence further changes in actin, allowing for S1 heads to cooperatively bind. Adding Ca^{2+} to these already semi-activated filaments still produces a conformational change in Tn regulatory head, where the SABS moves closer to TnC, having already been displaced off actin by S1 binding. This Ca^{2+} -induced conformational change is not cooperatively translated along the thin

filament. In the absence of rigor-S1 binding, Ca^{2+} -dependent conformational changes in the SABS are translated across the thin filament, allowing for cooperative activation ($n_H = 1.2 \pm 0.1$) by Ca^{2+} .

7.2 Cys84Ser substitution in TnC prevents levosimendan binding

Levosimendan is a Ca^{2+} sensitizer used in the management of acutely decompensated heart failure.¹⁹⁴⁻¹⁹⁵ Levosimendan binds weakly to the N-lobe of TnC,¹⁹⁶⁻¹⁹⁷ and exhibits Ca^{2+} -sensitizing effects in skinned muscle fibers,^{177, 196} and in isolated TnC and reconstituted Tn.¹⁷⁷ There were no effects on the level of Tn activation with levosimendan, and no changes in Ca^{2+} sensitivity using this assay. This is most likely due to the assay design. Native Cys residues in TnC and TnI were removed to covalently attach fluorescent maleimide probes to engineered Cys on residues 189 and 127 for TnI and TnC, respectively. In TnC, one of the mutations was Cys84Ser. Levijoki et al. showed levosimendan increased Ca^{2+} sensitivity in isolated WT hcTnC; when the point mutation Cys84Ser was introduced in TnC, there was no change in Ca^{2+} sensitivity with levosimendan, indicating Cys84 is necessary for levosimendan binding to the C-lobe of TnC.¹⁷⁷ Schlecht et al. also showed levosimendan did not produce a significant change in Ca^{2+} sensitivity using a FRET assay monitoring TnC conformational changes in reconstituted thin filaments, where their TnC also had the Cys84Ser mutation.¹⁹¹ This shows a potential limitation in this assay design, where engineered Tn could alter the binding of small molecules to TnC or TnI compared to native proteins.

7.3 Bepridil and rigor-S1 promote a stabilized open conformation of the N-lobe to increase Ca^{2+} sensitivity

Bepridil is a Ca^{2+} sensitizer shown to increase maximally activated force and ATPase activity in isolated myofibrils, and increase the sensitivity of the thin filament for Ca^{2+} .¹⁷⁸ X-ray crystallography studies using isolated TnC,¹⁹⁸ and NMR studies of a TnI/TnC complex¹⁹⁹ showed bepridil binds to the N-domain of TnC, stabilizing the open (active) conformation of TnC.²⁰⁰ This is consistent with the observation that bepridil increases the population of active Tn, evident by increases in E at both apo and +Ca, compared to untreated filaments (Figure 35E). This increase in E is similar to the effects of S1 binding. In the Ca^{2+} screen, S1 and bepridil equivalently increased Ca^{2+} sensitivity (Figure 35F).

The myosin screen was surprising in that there was no evident S1-induced activation of Tn in filaments treated with bepridil. From Sections 1-3, this author hypothesized actin-Tm causes a ≈ 7.4 -fold decrease in Ca^{2+} sensitivity of Tn¹³⁶ due to the displacement of the switch region away from the N-lobe of TnC as a result of SABS-actin binding. The switch region cannot, therefore, stabilize the open conformation of N-TnC, as predicted by the Herzberg model of Tn activation.⁶⁴ Bepridil is thought to increase Ca^{2+} sensitivity by stabilizing the open conformation of the N-lobe by binding to its hydrophobic pocket. If stabilizing the N-lobe were the main mechanism of action of bepridil, there should be no reason why myosin has no effect on the conformation of Tn in the presence of bepridil, particularly because bepridil does not appear to maximally activate Tn with Ca^{2+} alone (Figure 36C-D). This suggests myosin and bepridil both activate Tn using the same mechanism—that is, myosin binding to actin is enough to push the displaced switch region into the hydrophobic pocket of the N-lobe of TnC,

inducing the same effect as bepridil binding. This is evident by the S1-dependent increase in E , suggesting the SABS may be “pushed” off actin by myosin, and the switch region is “pushed” towards the N-lobe. The sedimentation experiments showed S1 was still binding to rAc in the presence of bepridil, suggesting bepridil does not act as an inhibitor of myosin. Bepridil-dependent increases in myosin ATPase activity and force generation suggest bepridil is not preventing crossbridge cycling.¹⁷⁸ Thus, it is reasonable to expect when bepridil is bound to the N-lobe of TnC and stabilizing the open conformation, myosin-induced displacement of the switch region has no further stabilizing effects on the open conformation. Indeed, the switch region may not be binding at all when bepridil is bound, as bepridil reduces the affinity of the switch region for the N-lobe ≈ 3.5 -fold.²⁰⁰ This actually supports this author’s hypothesis that the switch region may not bind to the N-lobe at all in the absence of myosin, as even in the presence of bepridil, there was no change in the level of Tn activation with Ca^{2+} . If the switch region were binding, the activation should have decreased with Ca^{2+} in the presence of bepridil. Bepridil binding to TnC and myosin binding to actin both act as Ca^{2+} sensitizers by promoting the open conformation of the N-lobe: the former does so by directly binding to the hydrophobic pocket; the latter does so indirectly, by promoting the switch region from binding to the hydrophobic pocket through some mechanism that may involve myosin-dependent actin-Tm conformational changes.

7.4 The effect of TnI Ser-23/24 phosphorylation on Tn activation

Phosphorylation of TnI Ser-23/24 increases lusitropy, enabling rapid relaxation during an increase in heart rate. To gain insights into the mechanistic action behind PKA-mediated Ca^{2+} desensitization of TnC, Ser-23/24 of TnI was phosphorylated using PKA

treatment. Ser-23/24 phosphorylation facilitates the release of the TnI N-terminal peptide from the N-lobe of TnC, promoting Ca^{2+} release from Site II.⁵⁷ Ward et al. showed the deletion of residues 1-29 of the N-terminal extension of TnI mimicked the effects of phosphorylation of Ser-23/24 to reduce Ca^{2+} sensitivity of myosin ATPase activity, suggesting phosphorylation eliminates N-TnI and N-TnC interactions.⁵⁶ PKA treatment did not dramatically alter the level Tn activation under low and high Ca^{2+} (Figure 35E) compared to non-treated filaments, but it did cause a ≈ 1.4 -fold decrease in Ca^{2+} sensitivity. This suggests conformational changes between TnC/TnI do not affect the overall architecture of Tn, meaning there are no PKA-dependent allosteric changes evident in Tn. Since the level of Tn activation remains the same, a decrease in Ca^{2+} sensitivity may be due to allosterically-induced changes focused in the Ca^{2+} coordination at Site II in the N-lobe of TnC.

An NMR study by Hwang et al. on a cTnI(1-73) fragment in complex with cTnC showed the N-TnI/N-TnC interactions fix the position of the N-lobe in space, and Ser-23/24 phosphorylation removes those restricting interactions, allowing N-TnC to move more freely.⁵⁸ They suggest when the N-lobe is rigid in space, interactions between the switch region and N-lobe could be compromised, reducing the level of Tn activation, meaning more Ca^{2+} would be required to activate Tn (reduced Ca^{2+} sensitivity). If what Hwang et al. suggest is true, the level of active Tn should decreased with Ser-23/24 phosphorylation (i.e., increase the level of SABS bound to actin, drawing the switch region away from the TnC N-lobe); instead, there was no dramatic change in Tn activation. The presence of Tm-actin could influence N-lobe dynamics in a way not evident in a fragmented TnI/TnC complex; additionally, since this dissertation predicts

Ca²⁺-dependent switch region binding is eliminated in thin filaments, no change in the level of Tn activation with PKA treatment is reasonable, as a stiffer N-lobe of TnC would not affect the switch region or SABS of TnI.

It's interesting to note Hwang et al. proposed the N-terminal extension of cTnI is a highly dynamic IDR, much like the C-terminal region of TnI (see Sections 1-3); this is in contrast to an NMR study by Howarth et al. using a cTnI(1-32) peptide, which showed a more rigid α -helical N-terminal extension that maintains the same structure independent of Ser-23/24 phosphorylation.²⁰¹ The presence of potential binding sites (actin, TnT, TnC, the remaining portion of TnI) could significantly affect the structure and dynamics of the N-terminal extension, suggesting it may be too early to designate this region as an IDR. Indeed, Howarth et al. docked their NMR structure of the N-terminal extension onto the Takeda crystal structure,²⁷ showing that when phosphorylated, residues in the N-terminal extension interact with the inhibitory region (IR) of TnI, preventing the IR from displacement from actin, subsequently increasing crossbridge inhibition.

The results from the myosin screen of PKA-treated rAc may support the Howarth hypothesis. PKA treatment caused a dramatic ≈ 1.6 - and ≈ 2.9 -fold decrease in myosin sensitivity (θ_{50} in Table A13) under apo and +Ca conditions, respectively, compared to untreated filaments. PKA treatment also significantly enhanced cooperativity for myosin binding. Previous studies using skinned cardiomyocytes showed TnI Ser-23/24 phosphorylation desensitizes force and ATPase to Ca²⁺;^{79, 202} this may be due to reduced crossbridge-mediated activation when TnI is phosphorylated. If the N-terminal extension is “blocking” the displacement of the IR when phosphorylated, it is reasonable to expect

more rigor-S/actin binding is required to induce an activating conformational change, hence why it takes so many myosin molecules to activate Tn in such an extremely cooperative manner. This also is reasonable when considering the level of active Tn in PKA-treated rAc was similar to non-treated rAc: Ser-23/24 phosphorylation does not increase the amount of IRs bound to actin; instead, it works to strengthen the inhibitory effect of IRs already bound to actin.

7.5 EGCG may destabilize Ca²⁺-dependent allosteric changes in Tn

A molecular compound specifically targeted to Tn to decrease myofilament sensitivity to Ca²⁺ is a potential therapeutic strategy for treating RCM, and other CMs that cause an increase in myofilament Ca²⁺ sensitivity. EGCG is a compound found in green tea²⁰³ that reduces myofilament Ca²⁺ sensitivity in skinned cardiac myofibrils.¹⁷⁶ In mice expressing the RCM mutation TnI(R193H), treatment with EGCG restored impaired diastolic function.¹⁷⁵ NMR studies showed EGCG binds to the hydrophobic cleft of the C-terminal domain of cTnC in the absence of TnI, and suggested EGCG may compete with TnI(34-71) binding to C-TnC, potentially weakening the anchor holding TnC onto the thin filament.²⁰⁴ This is interesting, considering the C-lobe is historically thought to play only a structural role in Tn;³¹ there are, however, known CM-causing mutations in this region,⁹⁷ suggesting a potential functional target for EGCG. Fuchs et al. showed EGCG decreases Mg²⁺ sensitivity for Sites III and IV, which may alter the conformation of the C-lobe directly and the N-lobe allosterically as the mechanism for decreased Ca²⁺ sensitivity.²⁰⁵ Is EGCG destabilizing C-TnC/N-TnI interactions, or is an allosteric change translated to Site II that facilitates Ca²⁺ release or decreases the potential for Ca²⁺ to bind?

EGCG treatment caused a ≈ 3.6 -fold decrease in Ca^{2+} sensitivity. EGCG also stabilized the inactive Tn state, evident by the sharp decrease in E under Ca^{2+} -depleted conditions (Figure 35E). This could translate into a larger number of SABS bound to actin; or into destabilized interactions between the C-TnC/N-TnI, forcing the C-lobe farther from the SABS. Destabilized interactions would hinder Ca^{2+} -dependent activating allosteric transitions from being translated to the rest of the Tn complex, effectively reducing Ca^{2+} sensitivity. The level of active Tn at saturating Ca^{2+} was not significantly different from untreated filaments, suggesting Ca^{2+} binding can still restore the active population of Tn to non-treated levels.

In the absence of Ca^{2+} , S1 increased the level of active Tn with EGCG treatment ($E_{+S1}=59.8 \pm 0.4\%$) significantly more than for untreated filaments ($E_{+S1}=45.9 \pm 0.4\%$) (Table A13). The S1-induced change in E ($\Delta E_{S1}=E_{+S1}-E_{-S1}$) for non-treated filaments is 22.8%, and for EGCG-treated filaments is a dramatic 47.9%. This suggests EGCG binding causes conformational changes that promote the inactive conformation of Tn, but does not alter (and may enhance) the ability of Tn to maximally activate with saturating S1 only. Ca^{2+} is not needed to maximally activate Tn. This would be a potential benefit for RCM treatment with EGCG: hypersensitivity to Ca^{2+} is reduced without affecting the ability of the filament to maximally activate. Li et al. showed hypersensitivity to Ca^{2+} from RCM mutations (including TnIR193H) is not due to altered Ser-23/24 TnI phosphorylation,¹⁷⁴ suggesting changes in SABS due to the R193H mutation enhance SABS displacement from actin to cause Ca^{2+} hypersensitivity. Therefore, treatment of RCM with a molecule that promotes a stabilization of the inactive state of Tn (SABS-

actin interactions), like EGCG, is a rational strategy; this was already proven viable in mice *in vivo* by Zhang et al.¹⁷⁵

The mechanism of EGCG-dependent Ca^{2+} sensitivity may simply be a numbers game—there are fewer Tn active due to either a displaced C-lobe or enhanced SABS binding— meaning more Ca^{2+} has to bind to more Tn to restore the population of active Tn. Or, destabilized interactions between TnI/TnC prevent a translation of Ca^{2+} -dependent activating conformational changes. This explains reduced myofilament Ca^{2+} sensitivity with EGCG treatment.¹⁷⁶ Therefore, EGCG may not actually prevent Ca^{2+} binding or facilitate Ca^{2+} release from Site II, therefore not altering the Ca^{2+} sensitivity of Site II at all, as Fuchs et al. predicted. Because EGCG dramatically alters the level of Tn activation and reduces cooperativity of Ca^{2+} binding, its mechanism of action to induce Ca^{2+} desensitivity differs from PKA-mediated TnI Ser-23/24 phosphorylation, which does not cause a dramatic change in the level of active Tn under Ca^{2+} -depleted conditions nor any significant changes in cooperativity.

7.6 Ca^{2+} sensitivity reflects the level of Tn activation under resting conditions

There was a strong correlation between the Ca^{2+} sensitivity ($pCa_{50} = -\log[\text{Ca}^{2+}]$) and the FRET efficiency E under Ca^{2+} -depleted conditions for compounds that target Tn (bepridil and EGCG binding to TnC) and processes directly affecting Tn subunits (PKA-mediated Ser-23/24 phosphorylation). S1 was not included, as any effects on the level of Tn activation are secondary results of S1 binding to actin. A correlation between the inactive state of Tn, and the state of Tn at non-saturating Ca^{2+} was observed. Thus, the state of Tn in the absence of Ca^{2+} influences or predisposes the behavior of Tn activation.

A lower E may be due to an increase in the fraction of Tn in the inactive state, and perturbations that increase the probability that Tn is inactive under relaxing conditions desensitize Tn to Ca^{2+} . Ca^{2+} sensitivity may reflect the fraction of active Tn under resting conditions.

This correlation could be useful for drug screening. Figure 40 shows the proof of concept for using this assay as a two-point high throughput screen. The assay requires both the donor emission for rAc-D and -DA filaments. First, the Ca^{2+} -depleted E would be determined and normalized to non-treated rAc for thin filaments in the presence of the compounds, as depicted in Figure 40A. Lead compounds exceeding the threshold (Ca^{2+} sensitizers) or falling below the threshold (Ca^{2+} desensitizers) would then undergo compound titrations to determine the EC_{50} (the [compound] that incurs a half-maximal change in E), as seen for ECGC in Figure 40B. Promising compounds could then undergo Ca^{2+} and S1 titrations to fully resolve their Ca^{2+} and myosin-sensing abilities before undergoing more expensive functional assessments in skinned fibers.

7.7 A drug screening tool— and beyond

Multiple TnI mutations have been implicated in inherited cardiomyopathies.⁸⁸ This assay would first determine changes in the fraction of active Tn, and then assess changes in Ca^{2+} and myosin sensitivity. This assay could be used to assess the effects on Ca^{2+} - and myosin-dependent activation from numerous mutations troponin, tropomyosin, actin, and S1 that have been implicated in cardiomyopathies.^{85, 206} Although altered molecular binding from the engineered Tn has proven problematic with levosimendan, a silver lining could be an assessment of altered molecular binding from disease-causing mutations, relevant in determining if a molecule is an appropriate therapeutic strategy for

a specific CM as an assessment of the binding ability of therapeutic agents to Tn with disease-causing mutations in sarcomeric proteins. Few, if any, biochemical thin filament reconstitution assays have monitored both myosin and Ca^{2+} sensitivity, in addition to revealing the fraction of active Tn. This screen could be used to expand insights into the mechanism of thin filament activation.

APPENDIX

Calculating the Förster distance (R_0). MatLab code for determining R_0 for a FRET pair.

```
%calculation of the J integral.
% units are in M^-1 cm^-1 nm^4
% donor and acceptor are peak normalized
% the x range is in common for donor and acceptor
% numerator

Error using evalin
Undefined function 'Calculating' for input arguments of type 'char'.
```

load donor emission and acceptor absorption data

```
clear all;
donorFileName = 'donor_em';
acceptorFileName = 'acceptor_abs';

%pick integer wavelengths from absorbance

Donor=load(donorFileName);
Acceptor=load(acceptorFileName);

%pick integer wavelengths from absorbance

delta = Acceptor(2,1)-Acceptor(1,1);
pick=1:int32(1/delta):length(Acceptor);
AcceptorPick=Acceptor(pick,:);

donorWavelengthMin=Donor(1,1);
donorWavelengthMax=Donor(end,1);
donorLength = length(Donor);
donorRange = [donorWavelengthMin donorWavelengthMax]

acceptorWavelengthMin=AcceptorPick(1,1);
acceptorWavelengthMax=AcceptorPick(end,1);
acceptorLength = length(AcceptorPick);
acceptorRange = [acceptorWavelengthMin acceptorWavelengthMax]

rangeMin = min([donorWavelengthMin acceptorWavelengthMin]);
rangeMax = max([donorWavelengthMax acceptorWavelengthMax]);
lambda = rangeMin:rangeMax;

%
%len = size(Donor)(1);
donorEm = 0*lambda;
acceptorEx = 0*lambda;

donorOffset=donorWavelengthMin - rangeMin % 500-250
acceptorOffset=acceptorWavelengthMin - rangeMin % 250 - 250

donorEm(donorOffset+1:donorOffset+donorLength) = Donor(1:end,2);
```

```

acceptorEx(acceptorOffset+1:acceptorOffset+acceptorLength) =
    AcceptorPick(1:end,2);

plot(lambda,donorEm);
hold on;
plot(lambda,acceptorEx);
hold off;

figure
plot(Donor(:,1),Donor(:,2));
hold on;
plot(Acceptor(:,1),Acceptor(:,2));
hold off;

```

calc RO

```

% vars
extinctionCoeff = 125000;
Qd=0.3;
kappaSquared = 2/3.;
indexOfRefraction = 1.361;

dLambda = lambda(2)-lambda(1);
% for i= 1:len
%     numerator(i)=donorEm(i)*acceptorEx(i)*lambda(i)^4*dLambda
% end

numerator =
    extinctionCoeff*dLambda*sum(donorEm.*acceptorEx.*lambda.^4);
denominator = dLambda*sum(donorEm);

J = numerator/denominator;

R0 = 0.211*(kappaSquared*Qd*J/indexOfRefraction^4)^(1/6.)

```

Published with MATLAB® R2015a

Table A1. Fitting results of rAc-TCSPC measurements of donor-only regulated actin filaments. Data represent one rAc reconstitution set. The TCSPC histogram of the FRET donor AF546 (TnI151-189) or ATTO550 (TnI196-211) was fit to a multi-exponential decay model convolved with the IRF. Conditions: rAc-D were in working buffer (apo) or WB supplemented with 3 mM CaCl₂ (+Ca).

Donor residue on TnI	Condition	Lifetime (ns) ^a			$\langle\tau_D\rangle^b$	χ^2
		τ_1	τ_2	τ_3		
151C*AF546	apo	0.32 (0.11)	1.72 (0.16)	3.82 (0.73)	3.10	1.09
	+Ca	0.33 (0.13)	1.92 (0.21)	3.76 (0.66)	2.91	0.95
160C*AF546	apo	0.15 (0.14)	1.45 (0.16)	3.75 (0.70)	2.89	1.05
	+Ca	0.17 (0.14)	1.43 (0.17)	3.70 (0.69)	2.81	0.95
167C*AF546	apo	0.25 (0.11)	1.56 (0.17)	3.79 (0.72)	3.01	1.02
	+Ca	0.31 (0.10)	1.71 (0.18)	3.79 (0.72)	3.07	1.01
174C*AF546	apo	0.20 (0.14)	1.33 (0.20)	3.69 (0.66)	2.73	1.03
	+Ca	0.15 (0.16)	1.20 (0.17)	3.72 (0.67)	2.72	1.00
177C*AF546	apo	0.14 (0.18)	1.11 (0.20)	3.61 (0.62)	2.48	1.05
	+Ca	0.24 (0.20)	1.43 (0.26)	3.66 (0.54)	2.40	1.09
182C*AF546	apo	0.11 (0.14)	1.23 (0.20)	3.69 (0.66)	2.71	1.01
	+Ca	0.13 (0.15)	1.26 (0.21)	3.67 (0.64)	2.64	0.98
189C*AF546	apo	0.08 (0.26)	0.99 (0.18)	3.50 (0.56)	2.16	1.01
	+Ca	0.12 (0.27)	1.18 (0.24)	3.52 (0.49)	2.05	1.07
196C*ATTO550	apo	0.83 (0.16)	3.64 (0.84)		3.20	1.08
	+Ca	0.92 (0.16)	3.66 (0.84)		3.22	1.12
200C*ATTO550	apo	0.66 (0.15)	3.61 (0.85)		3.16	1.12
	+Ca	0.73 (0.18)	3.72 (0.82)		3.19	1.03
204C*ATTO550	apo	0.68 (0.09)	3.69 (0.91)		3.41	1.08
	+Ca	1.64 (0.25)	3.78 (0.75)		3.24	1.34
208C*ATTO550	apo	0.13 (0.16)	1.27 (0.19)	3.54 (0.65)	2.55	1.01
	+Ca	0.12 (0.20)	1.33 (0.20)	3.56 (0.60)	2.44	0.95
211C*ATTO550	apo	0.59 (0.12)	3.69 (0.88)		3.32	1.11
	+Ca	0.75 (0.11)	3.72 (0.89)		3.40	1.06

^aLifetime (fractional amplitude).

^bAmplitude-weighted mean lifetime.

Table A2. Fitting results of rAc-TCSPC measurements of donor/acceptor regulated actin filaments with ATTO655 on TnC residue 35. Data represent one rAc

reconstitution set. The TCSPC histogram of the FRET donor AF546 (TnI151-189) or ATTO550 (TnI196-211) was fit to a multi-exponential decay model convolved with the IRF. Conditions: rAc-D were in working buffer (apo) or WB supplemented with 3 mM CaCl₂ (+Ca).

Donor residue on TnI	Condition	Lifetime (ns) ^a			$\langle\tau_{DA}\rangle^b$	χ^2	<i>E</i>
		τ_1	τ_2	τ_3			
151C*AF546	apo	0.21 (0.26)	1.17 (0.28)	3.29 (0.46)	1.91	0.99	0.38
	+Ca	0.19 (0.31)	1.16 (0.28)	3.30 (0.41)	1.74	1.03	0.40
160C*AF546	apo	0.13 (0.32)	0.99 (0.29)	3.10 (0.39)	1.55	1.05	0.46
	+Ca	0.12 (0.38)	0.86 (0.28)	3.11 (0.34)	1.35	1.13	0.52
167C*AF546	apo	0.24 (0.24)	1.24 (0.29)	3.18 (0.47)	1.92	1.02	0.36
	+Ca	0.18 (0.31)	1.11 (0.29)	3.18 (0.40)	1.66	1.06	0.46
174C*AF546	apo	0.16 (0.35)	1.00 (0.33)	3.07 (0.32)	1.36	1.18	0.50
	+Ca	0.15 (0.41)	0.94 (0.32)	3.03 (0.27)	1.17	1.24	0.57
177C*AF546	apo	0.14 (0.30)	1.04 (0.30)	3.14 (0.40)	1.62	1.04	0.35
	+Ca	0.13 (0.34)	0.95 (0.28)	3.01 (0.38)	1.46	1.01	0.39
182C*AF546	apo	0.13 (0.24)	1.08 (0.31)	3.17 (0.45)	1.79	1.10	0.34
	+Ca	0.12 (0.33)	0.98 (0.33)	3.19 (0.34)	1.45	1.19	0.45
189C*AF546	apo	0.11 (0.31)	1.00 (0.27)	3.16 (0.42)	1.63	1.05	0.25
	+Ca	0.11 (0.34)	0.95 (0.32)	3.03 (0.34)	1.37	1.10	0.33
196C*ATTO550	apo	0.17 (0.14)	1.49 (0.25)	3.42 (0.61)	2.48	1.13	0.23
	+Ca	0.23 (0.24)	1.47 (0.32)	3.39 (0.44)	2.0	1.11	0.38
200C*ATTO550	apo	0.15 (0.18)	1.59 (0.19)	3.61 (0.63)	2.6	1.05	0.18
	+Ca	0.16 (0.20)	1.32 (0.22)	3.55 (0.58)	2.37	1.10	0.26
204C*ATTO550	apo	0.12 (0.11)	1.27 (0.13)	3.50 (0.76)	2.84	1.02	0.17
	+Ca	0.11 (0.20)	1.21 (0.21)	3.42 (0.59)	2.28	1.03	0.29
208C*ATTO550	apo	0.11 (0.18)	1.13 (0.18)	3.38 (0.64)	2.37	1.15	0.07
	+Ca	0.12 (0.26)	1.08 (0.23)	3.19 (0.51)	1.90	1.05	0.22
211C*ATTO550	apo	0.12 (0.12)	1.31 (0.15)	3.54 (0.73)	2.81	1.03	0.15
	+Ca	0.13 (0.17)	1.28 (0.20)	3.46 (0.62)	2.44	1.03	0.28

^aLifetime (fractional amplitude).

^bAmplitude-weighted mean lifetime.

Table A3. Fitting results of rAc-TCSPC measurements of donor/acceptor regulated actin filaments with ATTO655 on TnC residue 89. Data represent one rAc

reconstitution set. The TCSPC histogram of the FRET donor AF546 (TnI151-189) or ATTO550 (TnI196-211) was fit to a multi-exponential decay model convolved with the IRF. Conditions: rAc-D were in working buffer (apo) or WB supplemented with 3 mM CaCl₂ (+Ca).

Donor residue on TnI	Condition	Lifetime (ns) ^a			$\langle\tau_{DA}\rangle^b$	χ^2	E
		τ_1	τ_2	τ_3			
151C*AF546	apo	0.19 (0.32)	1.06 (0.29)	3.08 (0.39)	1.57	0.96	0.49
	+Ca	0.20 (0.37)	1.04 (0.30)	3.10 (0.33)	1.41	1.07	0.52
160C*AF546	apo	0.13 (0.37)	0.94 (0.30)	2.93 (0.33)	1.29	1.13	0.55
	+Ca	0.14 (0.40)	0.93 (0.30)	3.00 (0.30)	1.22	1.06	0.56
167C*AF546	apo	0.24 (0.27)	1.18 (0.39)	3.05 (0.34)	1.56	1.04	0.48
	+Ca	0.20 (0.32)	1.09 (0.33)	2.99 (0.35)	1.46	1.08	0.52
174C*AF546	apo	0.14 (0.31)	1.03 (0.27)	3.16 (0.42)	1.64	1.02	0.4
	+Ca	0.15 (0.28)	1.01 (0.26)	3.05 (0.46)	1.70	1.08	0.38
177C*AF546	apo	0.13 (0.30)	1.00 (0.29)	3.15 (0.41)	1.61	1.06	0.35
	+Ca	0.15 (0.31)	0.93 (0.29)	3.06 (0.40)	1.53	1.05	0.36
182C*AF546	apo	0.14 (0.24)	1.11 (0.30)	3.27 (0.46)	1.87	1.03	0.31
	+Ca	0.15 (0.32)	1.07 (0.33)	3.22 (0.35)	1.52	1.15	0.42
189C*AF546	apo	0.11 (0.31)	0.98 (0.27)	3.14 (0.42)	1.61	1.08	0.26
	+Ca	0.12 (0.38)	0.95 (0.33)	2.96 (0.29)	1.23	1.19	0.4
196C*ATTO550	apo	0.14 (0.13)	1.21 (0.18)	3.37 (0.69)	2.57	1.11	0.2
	+Ca	0.18 (0.20)	1.19 (0.26)	3.22 (0.54)	2.07	1.02	0.36
200C*ATTO550	apo	0.07 (0.21)	1.23 (0.16)	3.63 (0.63)	2.50	1.05	0.21
	+Ca	0.10 (0.24)	1.21 (0.20)	3.55 (0.56)	2.26	1.01	0.29
204C*ATTO550	apo	0.12 (0.18)	1.27 (0.20)	3.48 (0.62)	2.45	0.95	0.28
	+Ca	0.13 (0.25)	1.16 (0.28)	3.30 (0.47)	1.91	1.08	0.41
208C*ATTO550	apo	0.09 (0.21)	1.01 (0.19)	3.36 (0.60)	2.22	1.02	0.13
	+Ca	0.14 (0.25)	1.22 (0.29)	3.23 (0.46)	1.88	1.06	0.23
211C*ATTO550	apo	0.15 (0.11)	1.27 (0.16)	3.49 (0.73)	2.78	0.96	0.16
	+Ca	0.14 (0.20)	1.29 (0.24)	3.38 (0.56)	2.22	1.11	0.35

^aLifetime (fractional amplitude).

^bAmplitude-weighted mean lifetime.

Table A4. Fitting results of rAc-TCSPC measurements of donor/acceptor regulated actin filaments with ATTO655 on TnC residue 127. Data represent one rAc reconstitution set. The TCSPC histogram of the FRET donor AF546 (TnI151-189) or ATTO550 (TnI196-211) was fit to a multi-exponential decay model convolved with the IRF. Conditions: rAc-D were in working buffer (apo) or WB supplemented with 3 mM CaCl₂ (+Ca).

Donor residue on TnI	Condition	Lifetime (ns) ^a			$\langle\tau_{DA}\rangle^b$	χ^2	E
		τ_1	τ_2	τ_3			
151C*AF546	apo	0.23 (0.20)	1.27 (0.30)	3.20 (0.50)	2.01	1.02	0.35
	+Ca	0.23 (0.24)	1.23 (0.34)	3.19 (0.42)	1.81	0.99	0.38
160C*AF546	apo	0.13 (0.19)	1.09 (0.26)	3.17 (0.55)	2.06	1.04	0.29
	+Ca	0.15 (0.27)	1.35 (0.35)	3.40 (0.38)	1.81	1.11	0.36
167C*AF546	apo	0.24 (0.18)	1.30 (0.27)	3.20 (0.55)	2.16	0.96	0.28
	+Ca	0.21 (0.22)	1.14 (0.31)	3.05 (0.47)	1.83	1.03	0.40
174C*AF546	apo	0.15 (0.24)	1.05 (0.30)	3.02 (0.46)	1.75	1.09	0.36
	+Ca	0.15 (0.26)	1.04 (0.33)	2.93 (0.41)	1.59	1.07	0.41
177C*AF546	apo	0.18 (0.20)	1.16 (0.29)	3.24 (0.51)	2.03	1.06	0.18
	+Ca	0.18 (0.26)	1.20 (0.28)	3.17 (0.46)	1.83	1.04	0.24
182C*AF546	apo	0.11 (0.20)	1.14 (0.25)	3.45 (0.55)	2.20	1.00	0.19
	+Ca	0.14 (0.20)	1.18 (0.26)	3.47 (0.54)	2.19	1.03	0.17
189C*AF546	apo	0.12 (0.29)	1.01 (0.30)	3.06 (0.41)	1.59	1.16	0.26
	+Ca	0.12 (0.33)	1.00 (0.32)	2.94 (0.35)	1.39	1.15	0.32
196C*ATTO550	apo	0.16 (0.17)	1.20 (0.25)	3.13 (0.58)	2.15	1.08	0.33
	+Ca	0.13 (0.24)	1.07 (0.31)	2.98 (0.44)	1.69	1.05	0.48
200C*ATTO550	apo	0.04 (0.20)	0.92 (0.11)	3.62 (0.69)	2.61	0.96	0.17
	+Ca	0.15 (0.18)	1.40 (0.22)	3.43 (0.60)	2.39	1.04	0.25
204C*ATTO550	apo	0.06 (0.18)	1.13 (0.21)	3.31 (0.61)	2.26	1.04	0.34
	+Ca	0.12 (0.20)	1.14 (0.23)	3.25 (0.57)	2.14	1.05	0.34
208C*ATTO550	apo	0.14 (0.22)	1.20 (0.24)	3.35 (0.54)	2.11	1.09	0.17
	+Ca	0.11 (0.28)	0.97 (0.30)	3.08 (0.42)	1.62	1.07	0.34
211C*ATTO550	apo	0.17 (0.14)	1.38 (0.20)	3.38 (0.66)	2.54	1.02	0.24
	+Ca	0.12 (0.20)	1.15 (0.25)	3.24 (0.55)	2.08	1.11	0.39

^aLifetime (fractional amplitude).

^bAmplitude-weighted mean lifetime.

Table A5. Correcting FRET efficiency with the acceptor labeling ratio.

Representative data from separately reconstituted rAc-D (Tn-D, TnI211C*ATTO550) and rAc-DA (Tn-DA, TnI211C*ATTO550, TnC127C*ATTO655) filaments. The lifetime of the donor in the absence and presence of an acceptor ($\langle\tau_D\rangle$ and $\langle\tau_{DA}\rangle$, respectively), FRET efficiency E , f_a -corrected FRET efficiency E_c , and the calculated inter-dye distances (R and R_c) are shown.

Trial	$\langle\tau_D\rangle$		$\langle\tau_{DA}\rangle$		f_a	E		E_c		R		R_c	
	apo	+Ca	apo	+Ca		apo	+Ca	apo	+Ca	apo	+Ca	apo	+Ca
1	3.49	3.44	3.03	2.58	0.49	0.13	0.25	0.27	0.51	8.76	7.69	7.56	6.36
2	3.32	3.4	2.54	2.08	0.85	0.23	0.39	0.28	0.46	7.79	6.90	7.51	6.59
3	3.57	3.53	3.28	2.89	0.33	0.08	0.18	0.25	0.55	9.59	8.23	7.71	6.19

Table A6. Non-corrected and f_A -corrected mean FRET efficiencies and inter-dye

distances. Representative data from separately reconstituted rAc-D (Tn-D, TnI211C*ATTO550) and rAc-DA (Tn-DA, TnI211C*ATTO550, TnC127C*ATTO655) filaments. The mean FRET efficiency E and f_A -corrected FRET efficiency E_c , and calculated inter-dye distance R and R_c are shown \pm SEM ($n = 3$).

E		E_c		R		R_c	
apo	+Ca	apo	+Ca	apo	+Ca	apo	+Ca
0.15 \pm 0.06	0.27 \pm 0.06	0.26 \pm 0.01	0.51 \pm 0.03	8.71 \pm 0.52	7.61 \pm 0.38	7.60 \pm 0.06	6.38 \pm 0.11

Table A7. FRET efficiency and inter-dye distance at acceptor position TnC35C. The average FRET efficiency calculated from the amplitude-weighted mean lifetime of the donor for rAc-D and DA in WB (apo) and WB supplemented with 3 mM CaCl₂ (+Ca), and calculated inter-dye distance (R) \pm SEM from $n = 3$ experiments are shown.

Donor residue on TnI	FRET Efficiency		R (nm)	
	apo	+Ca	apo	+Ca
151C*AF546	0.54 \pm 0.05	0.55 \pm 0.04	5.35 \pm 0.20	5.32 \pm 0.14
160C*AF546	0.68 \pm 0.03	0.77 \pm 0.06	4.85 \pm 0.10	4.48 \pm 0.25
167C*AF546	0.49 \pm 0.02	0.66 \pm 0.01	5.54 \pm 0.08	4.94 \pm 0.04
174C*AF546	0.51 \pm 0.04	0.58 \pm 0.05	5.47 \pm 0.15	5.21 \pm 0.17
177C*AF546	0.49 \pm 0.02	0.57 \pm 0.03	5.54 \pm 0.09	5.23 \pm 0.12
182C*AF546	0.38 \pm 0.06	0.53 \pm 0.08	6.45 \pm 0.26	5.40 \pm 0.30
189C*AF546	0.28 \pm 0.05	0.42 \pm 0.05	7.59 \pm 0.32	5.80 \pm 0.19
196C*ATTO550	0.27 \pm 0.04	0.41 \pm 0.09	7.59 \pm 0.26	6.85 \pm 0.46
200C*ATTO550	0.22 \pm 0.02	0.36 \pm 0.01	7.90 \pm 0.19	7.05 \pm 0.08
204C*ATTO550	0.24 \pm 0.06	0.34 \pm 0.06	7.78 \pm 0.41	7.18 \pm 0.33
208C*ATTO550	0.25 \pm 0.06	0.33 \pm 0.04	7.74 \pm 0.38	7.21 \pm 0.22
211C*ATTO550	0.20 \pm 0.01	0.34 \pm 0.04	8.06 \pm 0.10	7.14 \pm 0.20

Table A8. FRET efficiency and inter-dye distances at acceptor residue TnC89C. The average FRET efficiency calculated from the amplitude-weighted mean lifetime of the donor for rAc-D and DA in WB (apo) and WB supplemented with 3 mM CaCl₂ (+Ca), and calculated inter-dye distance (R) \pm SEM from $n = 3$ experiments is shown.

Donor residue on TnI	FRET Efficiency		R (nm)	
	apo	+Ca	apo	+Ca
151C*AF546	0.58 \pm 0.04	0.64 \pm 0.04	5.19 \pm 0.15	5.00 \pm 0.13
160C*AF546	0.71 \pm 0.02	0.77 \pm 0.04	4.74 \pm 0.09	4.50 \pm 0.09
167C*AF546	0.60 \pm 0.04	0.69 \pm 0.01	5.13 \pm 0.14	4.82 \pm 0.02
174C*AF546	0.54 \pm 0.00	0.56 \pm 0.03	5.36 \pm 0.01	5.29 \pm 0.11
177C*AF546	0.47 \pm 0.00	0.48 \pm 0.04	5.62 \pm 0.01	5.58 \pm 0.13
182C*AF546	0.36 \pm 0.03	0.49 \pm 0.06	6.06 \pm 0.15	5.54 \pm 0.22
189C*AF546	0.28 \pm 0.05	0.44 \pm 0.05	6.50 \pm 0.30	5.73 \pm 0.20
196C*ATTO550	0.31 \pm 0.03	0.46 \pm 0.04	7.30 \pm 0.16	6.58 \pm 0.19
200C*ATTO550	0.22 \pm 0.03	0.46 \pm 0.09	7.97 \pm 0.24	6.58 \pm 0.37
204C*ATTO550	0.36 \pm 0.05	0.62 \pm 0.06	7.09 \pm 0.24	5.87 \pm 0.26
208C*ATTO550	0.27 \pm 0.06	0.49 \pm 0.09	7.62 \pm 0.40	6.50 \pm 0.42
211C*ATTO550	0.24 \pm 0.01	0.45 \pm 0.01	7.76 \pm 0.10	6.61 \pm 0.06

Table A9. FRET efficiency and inter-dye distances at acceptor residue TnC127C. The average FRET efficiency calculated from the amplitude-weighted mean lifetime of the donor for rAc-D and DA in WB (apo) and WB supplemented with 3 mM CaCl₂ (+Ca), and calculated inter-dye distance (R) \pm SEM from $n = 3$ experiments is shown.

Donor residue on TnI	FRET Efficiency		R (nm)	
	apo	+Ca	apo	+Ca
151C*AF546	0.42 \pm 0.01	0.57 \pm 0.08	5.81 \pm 0.11	5.23 \pm 0.28
160C*AF546	0.37 \pm 0.04	0.46 \pm 0.04	6.04 \pm 0.17	5.64 \pm 0.13
167C*AF546	0.37 \pm 0.02	0.45 \pm 0.02	6.03 \pm 0.08	5.68 \pm 0.06
174C*AF546	0.44 \pm 0.01	0.54 \pm 0.04	5.72 \pm 0.04	5.37 \pm 0.13
177C*AF546	0.38 \pm 0.02	0.48 \pm 0.02	5.96 \pm 0.06	5.57 \pm 0.08
182C*AF546	0.21 \pm 0.01	0.29 \pm 0.06	6.89 \pm 0.05	6.44 \pm 0.30
189C*AF546	0.23 \pm 0.04	0.44 \pm 0.06	6.79 \pm 0.26	5.75 \pm 0.22
196C*ATTO550	0.25 \pm 0.07	0.46 \pm 0.08	7.81 \pm 0.53	6.62 \pm 0.36
200C*ATTO550	0.27 \pm 0.07	0.44 \pm 0.08	7.61 \pm 0.40	6.71 \pm 0.38
204C*ATTO550	0.27 \pm 0.07	0.41 \pm 0.06	7.70 \pm 0.50	6.81 \pm 0.28
208C*ATTO550	0.25 \pm 0.02	0.38 \pm 0.02	7.70 \pm 0.17	6.93 \pm 0.10
211C*ATTO550	0.26 \pm 0.01	0.51 \pm 0.03	7.60 \pm 0.06	6.38 \pm 0.11

Table A10. Calcium-induced changes in FRET efficiency and inter-dye distance in Tn within thin filaments. The mean FRET efficiency calculated from the amplitude-weighted mean lifetime of the donor in the presence or absence of an acceptor on TnC residue 35, 89, or 127 and the calculated inter-dye distance (R) in WB supplemented with 3 mM CaCl_2 (+Ca) were subtracted from the mean E or R in WB without Ca^{2+} (apo). A positive change in E or a negative change in R indicates a closer proximity of the donor residue on TnI and acceptor residue on TnC.

Donor residue	ΔE for TnC acceptor residue			ΔR for TnC acceptor residue (nm)		
	35C	89C	127C	35C	89C	127C
151	0.01	0.05	0.16	-0.03	-0.19	-0.58
160	0.09	0.06	0.10	-0.36	-0.25	-0.40
167	0.17	0.09	0.09	-0.60	-0.32	-0.35
174	0.07	0.02	0.09	-0.26	-0.07	-0.35
177	0.08	0.01	0.10	-0.30	-0.04	-0.39
182	0.15	0.13	0.07	-0.57	-0.52	-0.45
189	0.14	0.16	0.21	-0.65	-0.77	-1.05
196	0.14	0.15	0.20	-0.73	-0.72	-1.19
200	0.14	0.25	0.16	-0.85	-1.39	-0.90
204	0.10	0.27	0.15	-0.60	-1.21	-0.89
208	0.08	0.21	0.13	-0.54	-1.13	-0.77
211	0.14	0.21	0.24	-0.92	-1.15	-1.22

Table A11. FRET efficiency and inter-dye distances from steady-state FRET and theoretically-derived from the MTS molecular model. The experimentally-determined FRET efficiency calculated from peak emission intensity at 570 nm from the donor in rAc-D and rAc-DA with acceptor position TnC89C in WB supplemented with 75 mM KCl and 3 mM CaCl₂ (+Ca), and calculated inter-dye distance (R) from $n = 1$ experiment. Model-derived E were calculated from $C\alpha$ distances determined from the MTS model.

Donor residue on TnI	Experimental		Model-derived	
	E	R (nm)	E	R (nm)
151C*AF546	0.99	2.56	1.00	1.40
160C*AF546	0.99	2.56	0.97	3.00
167C*AF546	0.92	3.66	0.90	3.80
174C*AF546	0.85	4.12	0.81	4.30
177C*AF546	0.75	5.03	0.75	4.60
182C*AF546	0.74	4.62	0.58	5.20
189C*AF546	0.76	4.54	0.37	6.00

Table A12. Fitting results for Ca^{2+} titrations of PKA-treated thin filaments, and thin filaments with PKA treatment, small molecules, and S1. The FRET efficiency vs. free Ca^{2+} was fit to the Hill equation to recover estimates for FRET efficiency (%) without Ca^{2+} (apo, E_-), with 3 mM CaCl_2 (+Ca, E_+), the Ca^{2+} concentration that produces half-maximal activation Ca_{50} , and the Hill coefficient n_H . The maximum likelihood estimate \pm asymptotic SE are reported.

Sample	E_-	E_+	Ca_{50} (μM)	n_H
rAc	22.3 ± 0.4	39.3 ± 0.3	1.12 ± 0.09	1.2 ± 0.1
+DMSO	21.7 ± 0.4	40.5 ± 0.4	1.07 ± 0.08	1.2 ± 0.1
+bepidil	26.3 ± 1.1	43.4 ± 0.6	0.53 ± 0.11	0.9 ± 0.2
+levo.	21.1 ± 0.4	37.3 ± 0.4	1.05 ± 0.08	1.4 ± 0.2
+EGCG	14.5 ± 0.5	41.9 ± 0.8	4.06 ± 0.50	0.9 ± 0.1
+S1	36.1 ± 0.5	46.8 ± 0.3	0.54 ± 0.08	0.8 ± 0.1
+PKA	20.1 ± 0.3	38.0 ± 0.3	1.57 ± 0.09	1.2 ± 0.1

Table A13. Fitting results for S1 titrations of reporter filaments. The calculated FRET efficiency vs. the fractional binding of S1 to actin was fit to the Hill equation to recover the FRET efficiency (%) without S1 E_{-S1} , the FRET efficiency with saturating S1 E_{+S1} , the stoichiometry $\theta = [\text{S1}]_T/[\text{Actin}]_T$ that produces half maximal activation θ_{50} , and Hill coefficient n_H . Maximum likelihood estimate \pm asymptotic SE are reported.

Sample	E_{-S1}	E_{+S1}	θ_{50}	n_H
rAc	23.1 ± 0.2	45.9 ± 0.4	0.36 ± 0.03	2.9 ± 0.1
+ Ca^{2+}	43.6 ± 0.2	55.4 ± 0.2	0.20 ± 0.03	2.8 ± 0.2
+bepidil	27.7 ± 1.8	27.7 ± 1.8		
+bepidil + Ca^{2+}	45.9 ± 3.1	45.9 ± 3.1		
+EGCG	10.5 ± 0.2	58.4 ± 1.1	0.55 ± 0.05	3.3 ± 0.1
+EGCG + Ca^{2+}	36.2 ± 2.2	59.8 ± 0.4	0.32 ± 0.05	2.2 ± 0.1
+PKA	21.5 ± 0.1	34.5 ± 0.1	0.59 ± 0.01	28.1 ± 2.0
+PKA + Ca^{2+}	42.0 ± 0.1	51.6 ± 0.1	0.57 ± 0.01	50.7 ± 6.1

Table A14. Fitting results for Ca^{2+} titrations of phosphorylated reporter filaments, and filaments mock-treated with PKA or ATP. FRET efficiency vs. free Ca^{2+}

concentration were fit to the Hill equation, to recover estimates of FRET efficiency without Ca^{2+} (apo, E_-), FRET efficiency with 3 mM CaCl_2 (+Ca, E_+), the Ca^{2+} concentration that produces half maximal activation Ca_{50} , and the Hill coefficient n_H . Maximum likelihood estimate \pm asymptotic SE are reported.

Sample	E_-	E_+	Ca_{50} (μM)	n_H
rAc	20.4 ± 0.5	46.9 ± 0.6	2.6 ± 0.2	1.0 ± 0.1
+PKA +ATP	17.8 ± 0.5	44.2 ± 1.5	4.2 ± 1.0	0.7 ± 0.1
+PKA	20.6 ± 0.6	45.4 ± 0.8	2.7 ± 0.4	1.1 ± 0.1
+ATP	20.4 ± 0.6	45.9 ± 0.7	2.4 ± 0.3	1.0 ± 0.1

Table A15. Fitting results for S1 titrations of phosphorylated reporter filaments, and filaments mock-treated with PKA or ATP. The calculated FRET efficiency vs. the total fractional binding of S1 to actin was fit to the Hill equation to recover the FRET efficiency without S1 (apo, E_{-S1}), the FRET efficiency with saturating S1 E_{+S1} , the fractional binding of $[\text{S1}]_T/[\text{Actin}]_T$ that produces half maximal activation θ_{50} , and Hill coefficient n_H . Maximum likelihood estimate \pm asymptotic SE are reported.

Sample	E_{-S1}	E_{+S1}	θ_{50}	n_H
rAc	20.4 ± 0.3	43.6 ± 0.3	0.27 ± 0.04	3.0 ± 0.2
+ Ca^{2+}	41.8 ± 0.3	57.7 ± 0.2	0.20 ± 0.05	2.8 ± 0.4
+PKA +ATP	20.5 ± 0.1	37.5 ± 0.2	0.59 ± 0.02	38.6 ± 8.8
+PKA +ATP + Ca^{2+}	41.2 ± 0.2	55.6 ± 0.1	0.55 ± 0.01	37.0 ± 6.2
+PKA	22.1 ± 0.3	42.8 ± 1.1	0.31 ± 0.05	3.7 ± 0.6
+PKA + Ca^{2+}	42.8 ± 0.4	55.7 ± 0.2	0.16 ± 0.06	3.1 ± 0.6
+ATP	23.9 ± 0.3	46.1 ± 0.4	0.31 ± 0.06	2.6 ± 0.2
+ATP + Ca^{2+}	44.7 ± 0.2	57.4 ± 0.1	0.21 ± 0.04	3.2 ± 0.4

WORKS CITED

1. Kochanek, K. D. J., X.; Murphy, S.L.; Miniño, A.M.; Kung, H.C., Deaths: Final data for 2009. *National Vital Statistics Reports* **2011**, *60* (3).
2. Hwang, P. M.; Sykes, B. D., Targeting the sarcomere to correct muscle function. *Nat Rev Drug Discov* **2015**, *14* (5), 313-28.
3. Ebashi, S.; Endo, M.; Otsuki, I., Control of muscle contraction. *Quarterly reviews of biophysics* **1969**, *2* (4), 351-84.
4. Huxley, H.; Hanson, J., Changes in the cross-striations of muscle during contraction and stretch and their structural interpretation. *Nature* **1954**, *173* (4412), 973-6.
5. Huxley, A. F.; Niedergerke, R., Structural changes in muscle during contraction; interference microscopy of living muscle fibres. *Nature* **1954**, *173* (4412), 971-3.
6. Franzini-Armstrong, C., The sarcoplasmic reticulum and the control of muscle contraction. *FASEB journal : official publication of the Federation of American Societies for Experimental Biology* **1999**, *13 Suppl 2*, S266-70.
7. Hanson, J. L., J., The structure of F-actin and of actin filaments isolated from muscle. *Journal of molecular biology* **1963**, *6*, 46-60.
8. Holmes, K. C.; Popp, D.; Gebhard, W.; Kabsch, W., Atomic model of the actin filament. *Nature* **1990**, *347* (6288), 44-9.
9. Luther, P. K., The vertebrate muscle Z-disc: sarcomere anchor for structure and signalling. *Journal of muscle research and cell motility* **2009**, *30* (5-6), 171-85.
10. Gordon, A. M.; Homsher, E.; Regnier, M., Regulation of contraction in striated muscle. *Physiological reviews* **2000**, *80* (2), 853-924.
11. Galinska-Rakoczy, A.; Engel, P.; Xu, C.; Jung, H.; Craig, R.; Tobacman, L. S.; Lehman, W., Structural basis for the regulation of muscle contraction by troponin and tropomyosin. *Journal of molecular biology* **2008**, *379* (5), 929-35.
12. Li, X. E.; Tobacman, L. S.; Mun, J. Y.; Craig, R.; Fischer, S.; Lehman, W., Tropomyosin position on F-actin revealed by EM reconstruction and computational chemistry. *Biophysical journal* **2011**, *100* (4), 1005-13.
13. Behrmann, E.; Muller, M.; Penczek, P. A.; Mannherz, H. G.; Manstein, D. J.; Raunser, S., Structure of the rigor actin-tropomyosin-myosin complex. *Cell* **2012**, *150* (2), 327-38.
14. Rayment, I.; Holden, H. M.; Whittaker, M.; Yohn, C. B.; Lorenz, M.; Holmes, K. C.; Milligan, R. A., Structure of the actin-myosin complex and its implications for muscle contraction. *Science (New York, N.Y.)* **1993**, *261* (5117), 58-65.
15. Lynn, R. W.; Taylor, E. W., Mechanism of adenosine triphosphate hydrolysis by actomyosin. *Biochemistry* **1971**, *10* (25), 4617-24.
16. Vibert, P.; Craig, R.; Lehman, W., Steric-model for activation of muscle thin filaments. *Journal of molecular biology* **1997**, *266* (1), 8-14.
17. Kobayashi, T.; Kobayashi, M.; Gryczynski, Z.; Lakowicz, J. R.; Collins, J. H., Inhibitory region of troponin I: Ca²⁺-dependent structural and environmental changes in the troponin-tropomyosin complex and in reconstituted thin filaments. *Biochemistry* **2000**, *39* (1), 86-91.
18. Galinska, A.; Hatch, V.; Craig, R.; Murphy, A. M.; Van Eyk, J. E.; Wang, C. L.; Lehman, W.; Foster, D. B., The C terminus of cardiac troponin I stabilizes the Ca²⁺-

activated state of tropomyosin on actin filaments. *Circulation research* **2010**, *106* (4), 705-11.

19. Rosenfeld, S. S.; Taylor, E. W., The mechanism of regulation of actomyosin subfragment 1 ATPase. *The Journal of biological chemistry* **1987**, *262* (21), 9984-93.

20. Geeves, M. A.; Holmes, K. C., Structural mechanism of muscle contraction. *Annual review of biochemistry* **1999**, *68*, 687-728.

21. Bagshaw, C. R.; Eccleston, J. F.; Eckstein, F.; Goody, R. S.; Gutfreund, H.; Trentham, D. R., The magnesium ion-dependent adenosine triphosphatase of myosin. Two-step processes of adenosine triphosphate association and adenosine diphosphate dissociation. *The Biochemical journal* **1974**, *141* (2), 351-64.

22. Metzger, J. M., Myosin binding-induced cooperative activation of the thin filament in cardiac myocytes and skeletal muscle fibers. *Biophysical journal* **1995**, *68* (4), 1430-42.

23. McKillop, D. F.; Geeves, M. A., Regulation of the interaction between actin and myosin subfragment 1: evidence for three states of the thin filament. *Biophysical journal* **1993**, *65* (2), 693-701.

24. Patchell, V. B.; Gallon, C. E.; Hodgkin, M. A.; Fattoum, A.; Perry, S. V.; Levine, B. A., The inhibitory region of troponin-I alters the ability of F-actin to interact with different segments of myosin. *European journal of biochemistry / FEBS* **2002**, *269* (20), 5088-100.

25. Patchell, V. B.; Gallon, C. E.; Evans, J. S.; Gao, Y.; Perry, S. V.; Levine, B. A., The regulatory effects of tropomyosin and troponin-I on the interaction of myosin loop regions with F-actin. *The Journal of biological chemistry* **2005**, *280* (15), 14469-75.

26. Noguchi, T.; Hunlich, M.; Camp, P. C.; Begin, K. J.; El-Zaru, M.; Patten, R.; Leavitt, B. J.; Ittleman, F. P.; Alpert, N. R.; LeWinter, M. M.; VanBuren, P., Thin-filament-based modulation of contractile performance in human heart failure. *Circulation* **2004**, *110* (8), 982-7.

27. Takeda, S.; Yamashita, A.; Maeda, K.; Maeda, Y., Structure of the core domain of human cardiac troponin in the Ca(2+)-saturated form. *Nature* **2003**, *424* (6944), 35-41.

28. Bremel, R. D.; Weber, A., Cooperation within actin filament in vertebrate skeletal muscle. *Nature: New biology* **1972**, *238* (82), 97-101.

29. Sia, S. K.; Li, M. X.; Spyropoulos, L.; Gagne, S. M.; Liu, W.; Putkey, J. A.; Sykes, B. D., Structure of cardiac muscle troponin C unexpectedly reveals a closed regulatory domain. *The Journal of biological chemistry* **1997**, *272* (29), 18216-21.

30. Potter, J. D.; Gergely, J., The calcium and magnesium binding sites on troponin and their role in the regulation of myofibrillar adenosine triphosphatase. *The Journal of biological chemistry* **1975**, *250* (12), 4628-33.

31. Holroyde, M. J.; Robertson, S. P.; Johnson, J. D.; Solaro, R. J.; Potter, J. D., The calcium and magnesium binding sites on cardiac troponin and their role in the regulation of myofibrillar adenosine triphosphatase. *The Journal of biological chemistry* **1980**, *255* (24), 11688-93.

32. van Eerd, J. P.; Takahashi, K., The amino acid sequence of bovine cardiac troponin-C. Comparison with rabbit skeletal troponin-C. *Biochemical and biophysical research communications* **1975**, *64* (1), 122-7.

33. Kekenus-Huskey, P. M.; Lindert, S.; McCammon, J. A., Molecular basis of calcium-sensitizing and desensitizing mutations of the human cardiac troponin C

- regulatory domain: a multi-scale simulation study. *PLoS Comput Biol* **2012**, *8* (11), e1002777.
34. Dong, W. J.; Xing, J.; Villain, M.; Hellinger, M.; Robinson, J. M.; Chandra, M.; Solaro, R. J.; Umeda, P. K.; Cheung, H. C., Conformation of the regulatory domain of cardiac muscle troponin C in its complex with cardiac troponin I. *The Journal of biological chemistry* **1999**, *274* (44), 31382-90.
 35. Spyropoulos, L.; Li, M. X.; Sia, S. K.; Gagne, S. M.; Chandra, M.; Solaro, R. J.; Sykes, B. D., Calcium-induced structural transition in the regulatory domain of human cardiac troponin C. *Biochemistry* **1997**, *36* (40), 12138-46.
 36. Li, M. X.; Spyropoulos, L.; Sykes, B. D., Binding of cardiac troponin-I147-163 induces a structural opening in human cardiac troponin-C. *Biochemistry* **1999**, *38* (26), 8289-98.
 37. Vassylyev, D. G.; Takeda, S.; Wakatsuki, S.; Maeda, K.; Maeda, Y., Crystal structure of troponin C in complex with troponin I fragment at 2.3-Å resolution. *Proceedings of the National Academy of Sciences of the United States of America* **1998**, *95* (9), 4847-52.
 38. Tobacman, L. S.; Nihli, M.; Butters, C.; Heller, M.; Hatch, V.; Craig, R.; Lehman, W.; Homsher, E., The troponin tail domain promotes a conformational state of the thin filament that suppresses myosin activity. *The Journal of biological chemistry* **2002**, *277* (31), 27636-42.
 39. Pearlstone, J. R.; Smillie, L. B., Effects of troponin-I plus-C on the binding of troponin-T and its fragments to alpha-tropomyosin. Ca²⁺ sensitivity and cooperativity. *The Journal of biological chemistry* **1983**, *258* (4), 2534-42.
 40. White, S. P.; Cohen, C.; Phillips, G. N., Jr., Structure of co-crystals of tropomyosin and troponin. *Nature* **1987**, *325* (6107), 826-8.
 41. Leszyk, J.; Dumaswala, R.; Potter, J. D.; Gusev, N. B.; Verin, A. D.; Tobacman, L. S.; Collins, J. H., Bovine cardiac troponin T: amino acid sequences of the two isoforms. *Biochemistry* **1987**, *26* (22), 7035-42.
 42. Tobacman, L. S., Structure-function studies of the amino-terminal region of bovine cardiac troponin T. *The Journal of biological chemistry* **1988**, *263* (6), 2668-72.
 43. Chandra, M.; Montgomery, D. E.; Kim, J. J.; Solaro, R. J., The N-terminal region of troponin T is essential for the maximal activation of rat cardiac myofilaments. *Journal of molecular and cellular cardiology* **1999**, *31* (4), 867-80.
 44. Mak, A. S.; Smillie, L. B., Structural interpretation of the two-site binding of troponin on the muscle thin filament. *Journal of molecular biology* **1981**, *149* (3), 541-50.
 45. Gollapudi, S. K.; Gallon, C. E.; Chandra, M., The tropomyosin binding region of cardiac troponin T modulates crossbridge recruitment dynamics in rat cardiac muscle fibers. *Journal of molecular biology* **2013**, *425* (9), 1565-81.
 46. Tao, T.; Gong, B. J.; Grabarek, Z.; Gergely, J., Conformational changes induced in troponin I by interaction with troponin T and actin/tropomyosin. *Biochimica et biophysica acta* **1999**, *1450* (3), 423-33.
 47. Morris, E. P.; Lehrer, S. S., Troponin-tropomyosin interactions. Fluorescence studies of the binding of troponin, troponin T, and chymotryptic troponin T fragments to specifically labeled tropomyosin. *Biochemistry* **1984**, *23* (10), 2214-20.

48. Jideama, N. M.; Noland, T. A., Jr.; Raynor, R. L.; Blobe, G. C.; Fabbro, D.; Kazanietz, M. G.; Blumberg, P. M.; Hannun, Y. A.; Kuo, J. F., Phosphorylation specificities of protein kinase C isozymes for bovine cardiac troponin I and troponin T and sites within these proteins and regulation of myofilament properties. *The Journal of biological chemistry* **1996**, *271* (38), 23277-83.
49. Robinson, J. M.; Dong, W. J.; Xing, J.; Cheung, H. C., Switching of troponin I: Ca(2+) and myosin-induced activation of heart muscle. *Journal of molecular biology* **2004**, *340* (2), 295-305.
50. Syska, H.; Wilkinson, J. M.; Grand, R. J.; Perry, S. V., The relationship between biological activity and primary structure of troponin I from white skeletal muscle of the rabbit. *The Biochemical journal* **1976**, *153* (2), 375-87.
51. Potter, J. D.; Gergely, J., Troponin, tropomyosin, and actin interactions in the Ca²⁺ regulation of muscle contraction. *Biochemistry* **1974**, *13* (13), 2697-703.
52. Geeves, M. A.; Chai, M.; Lehrer, S. S., Inhibition of actin-myosin subfragment 1 ATPase activity by troponin I and IC: relationship to the thin filament states of muscle. *Biochemistry* **2000**, *39* (31), 9345-50.
53. Mittmann, K.; Jaquet, K.; Heilmeyer, L. M., Jr., A common motif of two adjacent phosphoserines in bovine, rabbit and human cardiac troponin I. *FEBS letters* **1990**, *273* (1-2), 41-5.
54. Cuello, F.; Bardswell, S. C.; Haworth, R. S.; Yin, X.; Lutz, S.; Wieland, T.; Mayr, M.; Kentish, J. C.; Avkiran, M., Protein kinase D selectively targets cardiac troponin I and regulates myofilament Ca²⁺ sensitivity in ventricular myocytes. *Circulation research* **2007**, *100* (6), 864-73.
55. Yasuda, S.; Coutu, P.; Sadayappan, S.; Robbins, J.; Metzger, J. M., Cardiac transgenic and gene transfer strategies converge to support an important role for troponin I in regulating relaxation in cardiac myocytes. *Circulation research* **2007**, *101* (4), 377-86.
56. Ward, D. G.; Cornes, M. P.; Trayer, I. P., Structural consequences of cardiac troponin I phosphorylation. *The Journal of biological chemistry* **2002**, *277* (44), 41795-801.
57. Ward, D. G.; Brewer, S. M.; Calvert, M. J.; Gallon, C. E.; Gao, Y.; Trayer, I. P., Characterization of the interaction between the N-terminal extension of human cardiac troponin I and troponin C. *Biochemistry* **2004**, *43* (13), 4020-7.
58. Hwang, P. M.; Cai, F.; Pineda-Sanabria, S. E.; Corson, D. C.; Sykes, B. D., The cardiac-specific N-terminal region of troponin I positions the regulatory domain of troponin C. *Proceedings of the National Academy of Sciences of the United States of America* **2014**, *111* (40), 14412-7.
59. Noland, T. A., Jr.; Guo, X.; Raynor, R. L.; Jideama, N. M.; Averyhart-Fullard, V.; Solaro, R. J.; Kuo, J. F., Cardiac troponin I mutants. Phosphorylation by protein kinases C and A and regulation of Ca(2+)-stimulated MgATPase of reconstituted actomyosin S-1. *The Journal of biological chemistry* **1995**, *270* (43), 25445-54.
60. Liu, B.; Lopez, J. J.; Biesiadecki, B. J.; Davis, J. P., Protein kinase C phosphomimetics alter thin filament Ca²⁺ binding properties. *PloS one* **2014**, *9* (1), e86279.

61. Kobayashi, T.; Patrick, S. E.; Kobayashi, M., Ala scanning of the inhibitory region of cardiac troponin I. *The Journal of biological chemistry* **2009**, *284* (30), 20052-60.
62. Yang, S.; Barbu-Tudoran, L.; Orzechowski, M.; Craig, R.; Trinick, J.; White, H.; Lehman, W., Three-dimensional organization of troponin on cardiac muscle thin filaments in the relaxed state. *Biophysical journal* **2014**, *106* (4), 855-64.
63. Dong, W. J.; Xing, J.; Robinson, J. M.; Cheung, H. C., Ca²⁺ induces an extended conformation of the inhibitory region of troponin I in cardiac muscle troponin. *Journal of molecular biology* **2001**, *314* (1), 51-61.
64. Herzberg, O.; Moulton, J.; James, M. N., A model for the Ca²⁺-induced conformational transition of troponin C. A trigger for muscle contraction. *The Journal of biological chemistry* **1986**, *261* (6), 2638-44.
65. Kobayashi, T.; Solaro, R. J., Calcium, thin filaments, and the integrative biology of cardiac contractility. *Annual review of physiology* **2005**, *67*, 39-67.
66. Rarick, H. M.; Tu, X. H.; Solaro, R. J.; Martin, A. F., The C terminus of cardiac troponin I is essential for full inhibitory activity and Ca²⁺ sensitivity of rat myofibrils. *The Journal of biological chemistry* **1997**, *272* (43), 26887-92.
67. Tripet, B.; Van Eyk, J. E.; Hodges, R. S., Mapping of a second actin-tropomyosin and a second troponin C binding site within the C terminus of troponin I, and their importance in the Ca²⁺-dependent regulation of muscle contraction. *Journal of molecular biology* **1997**, *271* (5), 728-50.
68. Hoffman, R. M.; Blumenschein, T. M.; Sykes, B. D., An interplay between protein disorder and structure confers the Ca²⁺ regulation of striated muscle. *Journal of molecular biology* **2006**, *361* (4), 625-33.
69. Ramos, C. H., Mapping subdomains in the C-terminal region of troponin I involved in its binding to troponin C and to thin filament. *The Journal of biological chemistry* **1999**, *274* (26), 18189-95.
70. McPherson, A., Introduction to protein crystallization. *Methods (San Diego, Calif.)* **2004**, *34* (3), 254-65.
71. Rodgers, D. W., Cryocrystallography. *Structure (London, England : 1993)* **1994**, *2* (12), 1135-40.
72. Tugarinov, V.; Hwang, P. M.; Kay, L. E., Nuclear magnetic resonance spectroscopy of high-molecular-weight proteins. *Annual review of biochemistry* **2004**, *73*, 107-46.
73. Jensen-Smith, H.; Currall, B.; Rossino, D.; Tiede, L.; Nichols, M.; Hallworth, R., Fluorescence microscopy methods in the study of protein structure and function. *Methods in molecular biology (Clifton, N.J.)* **2009**, *493*, 369-79.
74. Jin, J. P.; Zhang, Z.; Bautista, J. A., Isoform diversity, regulation, and functional adaptation of troponin and calponin. *Critical reviews in eukaryotic gene expression* **2008**, *18* (2), 93-124.
75. MacFarland, S. M.; Jin, J. P.; Brozovich, F. V., Troponin T isoforms modulate calcium dependence of the kinetics of the cross-bridge cycle: studies using a transgenic mouse line. *Archives of biochemistry and biophysics* **2002**, *405* (2), 241-6.
76. Pan, B. S.; Gordon, A. M.; Potter, J. D., Deletion of the first 45 NH₂-terminal residues of rabbit skeletal troponin T strengthens binding of troponin to immobilized tropomyosin. *The Journal of biological chemistry* **1991**, *266* (19), 12432-8.

77. Manning, E. P.; Guinto, P. J.; Tardiff, J. C., Correlation of molecular and functional effects of mutations in cardiac troponin T linked to familial hypertrophic cardiomyopathy: an integrative in silico/in vitro approach. *The Journal of biological chemistry* **2012**, *287* (18), 14515-23.
78. Konhilas, J. P.; Irving, T. C.; de Tombe, P. P., Length-dependent activation in three striated muscle types of the rat. *The Journal of physiology* **2002**, *544* (Pt 1), 225-36.
79. Solaro, R. J.; Moir, A. J.; Perry, S. V., Phosphorylation of troponin I and the inotropic effect of adrenaline in the perfused rabbit heart. *Nature* **1976**, *262* (5569), 615-7.
80. Vinogradova, M. V.; Stone, D. B.; Malanina, G. G.; Karatzaferi, C.; Cooke, R.; Mendelson, R. A.; Fletterick, R. J., Ca²⁺-regulated structural changes in troponin. *Proceedings of the National Academy of Sciences of the United States of America* **2005**, *102* (14), 5038-43.
81. Murakami, K.; Yumoto, F.; Ohki, S. Y.; Yasunaga, T.; Tanokura, M.; Wakabayashi, T., Structural basis for Ca²⁺-regulated muscle relaxation at interaction sites of troponin with actin and tropomyosin. *Journal of molecular biology* **2005**, *352* (1), 178-201.
82. Zhou, Z.; Li, K. L.; Rieck, D.; Ouyang, Y.; Chandra, M.; Dong, W. J., Structural dynamics of C-domain of cardiac troponin I protein in reconstituted thin filament. *The Journal of biological chemistry* **2012**, *287* (10), 7661-74.
83. Pirani, A.; Vinogradova, M. V.; Curmi, P. M.; King, W. A.; Fletterick, R. J.; Craig, R.; Tobacman, L. S.; Xu, C.; Hatch, V.; Lehman, W., An atomic model of the thin filament in the relaxed and Ca²⁺-activated states. *Journal of molecular biology* **2006**, *357* (3), 707-17.
84. Manning, E. P.; Tardiff, J. C.; Schwartz, S. D., A model of calcium activation of the cardiac thin filament. *Biochemistry* **2011**, *50* (34), 7405-13.
85. Chang, A. N.; Potter, J. D., Sarcomeric protein mutations in dilated cardiomyopathy. *Heart failure reviews* **2005**, *10* (3), 225-35.
86. Seidman, C. E.; Seidman, J. G., Identifying sarcomere gene mutations in hypertrophic cardiomyopathy: a personal history. *Circulation research* **2011**, *108* (6), 743-50.
87. Caleshu, C.; Sakhuja, R.; Nussbaum, R. L.; Schiller, N. B.; Ursell, P. C.; Eng, C.; De Marco, T.; McGlothlin, D.; Burchard, E. G.; Rame, J. E., Furthering the link between the sarcomere and primary cardiomyopathies: restrictive cardiomyopathy associated with multiple mutations in genes previously associated with hypertrophic or dilated cardiomyopathy. *American journal of medical genetics. Part A* **2011**, *155a* (9), 2229-35.
88. Mogensen, J.; Kubo, T.; Duque, M.; Uribe, W.; Shaw, A.; Murphy, R.; Gimeno, J. R.; Elliott, P.; McKenna, W. J., Idiopathic restrictive cardiomyopathy is part of the clinical expression of cardiac troponin I mutations. *The Journal of clinical investigation* **2003**, *111* (2), 209-16.
89. Murphy, R. T.; Mogensen, J.; Shaw, A.; Kubo, T.; Hughes, S.; McKenna, W. J., Novel mutation in cardiac troponin I in recessive idiopathic dilated cardiomyopathy. *Lancet (London, England)* **2004**, *363* (9406), 371-2.
90. Kushwaha, S. S.; Fallon, J. T.; Fuster, V., Restrictive cardiomyopathy. *The New England journal of medicine* **1997**, *336* (4), 267-76.

91. Yang, S. W.; Hitz, M. P.; Andelfinger, G., Ventricular septal defect and restrictive cardiomyopathy in a paediatric TNNI3 mutation carrier. *Cardiology in the young* **2010**, *20* (5), 574-6.
92. Gomes, A. V.; Liang, J.; Potter, J. D., Mutations in human cardiac troponin I that are associated with restrictive cardiomyopathy affect basal ATPase activity and the calcium sensitivity of force development. *The Journal of biological chemistry* **2005**, *280* (35), 30909-15.
93. Yumoto, F.; Lu, Q. W.; Morimoto, S.; Tanaka, H.; Kono, N.; Nagata, K.; Ojima, T.; Takahashi-Yanaga, F.; Miwa, Y.; Sasaguri, T.; Nishita, K.; Tanokura, M.; Ohtsuki, I., Drastic Ca²⁺ sensitization of myofilament associated with a small structural change in troponin I in inherited restrictive cardiomyopathy. *Biochemical and biophysical research communications* **2005**, *338* (3), 1519-26.
94. Marian, A. J.; Roberts, R., The molecular genetic basis for hypertrophic cardiomyopathy. *Journal of molecular and cellular cardiology* **2001**, *33* (4), 655-70.
95. Kimura, A.; Harada, H.; Park, J. E.; Nishi, H.; Satoh, M.; Takahashi, M.; Hiroi, S.; Sasaoka, T.; Ohbuchi, N.; Nakamura, T.; Koyanagi, T.; Hwang, T. H.; Choo, J. A.; Chung, K. S.; Hasegawa, A.; Nagai, R.; Okazaki, O.; Nakamura, H.; Matsuzaki, M.; Sakamoto, T.; Toshima, H.; Koga, Y.; Imaizumi, T.; Sasazuki, T., Mutations in the cardiac troponin I gene associated with hypertrophic cardiomyopathy. *Nature genetics* **1997**, *16* (4), 379-82.
96. Coppini, R.; Ho, C. Y.; Ashley, E.; Day, S.; Ferrantini, C.; Girolami, F.; Tomberli, B.; Bardi, S.; Torricelli, F.; Cecchi, F.; Mugelli, A.; Poggesi, C.; Tardiff, J.; Olivetto, I., Clinical phenotype and outcome of hypertrophic cardiomyopathy associated with thin-filament gene mutations. *Journal of the American College of Cardiology* **2014**, *64* (24), 2589-600.
97. Willott, R. H.; Gomes, A. V.; Chang, A. N.; Parvatiyar, M. S.; Pinto, J. R.; Potter, J. D., Mutations in Troponin that cause HCM, DCM AND RCM: what can we learn about thin filament function? *Journal of molecular and cellular cardiology* **2010**, *48* (5), 882-92.
98. Burton, D.; Abdulrazzak, H.; Knott, A.; Elliott, K.; Redwood, C.; Watkins, H.; Marston, S.; Ashley, C., Two mutations in troponin I that cause hypertrophic cardiomyopathy have contrasting effects on cardiac muscle contractility. *The Biochemical journal* **2002**, *362* (Pt 2), 443-51.
99. Mogensen, J.; Murphy, R. T.; Shaw, T.; Bahl, A.; Redwood, C.; Watkins, H.; Burke, M.; Elliott, P. M.; McKenna, W. J., Severe disease expression of cardiac troponin C and T mutations in patients with idiopathic dilated cardiomyopathy. *Journal of the American College of Cardiology* **2004**, *44* (10), 2033-40.
100. Pardee, J. D., Spudich, J.A., *Purification of muscle actin*. 1982; Vol. 24.
101. Smillie, L. B., Preparation and identification of alpha- and beta-tropomyosins. *Methods in enzymology* **1982**, *85 Pt B*, 234-41.
102. Xu, G. Q.; Hitchcock-DeGregori, S. E., Synthesis of a troponin C cDNA and expression of wild-type and mutant proteins in Escherichia coli. *The Journal of biological chemistry* **1988**, *263* (27), 13962-9.
103. Kruger, M.; Pfitzer, G.; Stehle, R., Expression and purification of human cardiac troponin subunits and their functional incorporation into isolated cardiac mouse

- myofibrils. *Journal of chromatography. B, Analytical technologies in the biomedical and life sciences* **2003**, 786 (1-2), 287-96.
104. Jin, J. P.; Chong, S. M.; Hossain, M. M., Microtiter plate monoclonal antibody epitope analysis of Ca²⁺- and Mg²⁺-induced conformational changes in troponin C. *Archives of biochemistry and biophysics* **2007**, 466 (1), 1-7.
105. Lakowicz, J. R., *Principles of Fluorescent Microscopy*. 3rd Edition ed.; Springer: New York, 2006.
106. Kim, S. A.; Schwille, P., Intracellular applications of fluorescence correlation spectroscopy: prospects for neuroscience. (0959-4388 (Print)).
107. Haustein, E.; Schwille, P., Fluorescence correlation spectroscopy: novel variations of an established technique. *Annu Rev Biophys Biomol Struct* **2007**, 36, 151-69.
108. Barefield, D.; Kumar, M.; de Tombe, P. P.; Sadayappan, S., Contractile dysfunction in a mouse model expressing a heterozygous MYBPC3 mutation associated with hypertrophic cardiomyopathy. *American journal of physiology. Heart and circulatory physiology* **2014**, 306 (6), H807-15.
109. Salhi, H. E.; Walton, S. D.; Hassel, N. C.; Brundage, E. A.; de Tombe, P. P.; Janssen, P. M.; Davis, J. P.; Biesiadecki, B. J., Cardiac troponin I tyrosine 26 phosphorylation decreases myofilament Ca²⁺ sensitivity and accelerates deactivation. *Journal of molecular and cellular cardiology* **2014**, 76, 257-64.
110. Sakamoto, T.; Limouze, J.; Combs, C. A.; Straight, A. F.; Sellers, J. R., Blebbistatin, a myosin II inhibitor, is photoinactivated by blue light. *Biochemistry* **2005**, 44 (2), 584-8.
111. Haas, E.; Katchalski-Katzir, E.; Steinberg, I. Z., Effect of the orientation of donor and acceptor on the probability of energy transfer involving electronic transitions of mixed polarization. *Biochemistry* **1978**, 17 (23), 5064-70.
112. Randolph, J. B.; Waggoner, A. S., Stability, specificity and fluorescence brightness of multiply-labeled fluorescent DNA probes. *Nucleic acids research* **1997**, 25 (14), 2923-9.
113. Chandra, M.; Tschirgi, M. L.; Rajapakse, I.; Campbell, K. B., Troponin T Modulates Sarcomere Length-Dependent Recruitment of Cross-Bridges in Cardiac Muscle. *Biophysical journal* **2006**, 90 (8), 2867-76.
114. Ausoni, S.; Campione, M.; Picard, A.; Moretti, P.; Vitadello, M.; De Nardi, C.; Schiaffino, S., Structure and regulation of the mouse cardiac troponin I gene. *The Journal of biological chemistry* **1994**, 269 (1), 339-46.
115. Wiederschain, G. Y., The Molecular Probes handbook. A guide to fluorescent probes and labeling technologies. *Biochemistry Moscow* **2011**, 76 (11), 1276-1276.
116. Humphrey, W.; Dalke, A.; Schulten, K., VMD: visual molecular dynamics. *Journal of molecular graphics* **1996**, 14 (1), 33-8, 27-8.
117. Leger, J.; Bouveret, P.; Schwartz, K.; Swynghedauw, B., A comparative study of skeletal and cardiac tropomyosins: subunits, thiol group content and biological activities. *Pflugers Archiv : European journal of physiology* **1976**, 362 (3), 271-7.
118. Weidtkamp-Peters, S.; Weisshart, K.; Schmiedeberg, L.; Hemmerich, P., Fluorescence correlation spectroscopy to assess the mobility of nuclear proteins. *Methods in molecular biology (Clifton, N.J.)* **2009**, 464, 321-41.

119. Schwille, P.; Haupts, U.; Maiti, S.; Webb, W. W., Molecular dynamics in living cells observed by fluorescence correlation spectroscopy with one- and two-photon excitation. *Biophysical journal* **1999**, *77* (4), 2251-65.
120. Machan, R.; Hof, M., Recent developments in fluorescence correlation spectroscopy for diffusion measurements in planar lipid membranes. *International journal of molecular sciences* **2010**, *11* (2), 427-57.
121. Eftink, M. R.; Ghiron, C. A., Fluorescence quenching studies with proteins. *Analytical biochemistry* **1981**, *114* (2), 199-227.
122. Pawley, J., Fundamental Limits in Confocal Microscopy. In *Handbook of Biological Confocal Microscopy*, Springer US: 2006.
123. Togashi, D. M.; Ryder, A. G., Assessing protein-surface interactions with a series of multi-labeled BSA using fluorescence lifetime microscopy and Forster Energy Resonance Transfer. *Biophysical chemistry* **2010**, *152* (1-3), 55-64.
124. Iqbal, A.; Arslan, S.; Okumus, B.; Wilson, T. J.; Giraud, G.; Norman, D. G.; Ha, T.; Lilley, D. M., Orientation dependence in fluorescent energy transfer between Cy3 and Cy5 terminally attached to double-stranded nucleic acids. *Proceedings of the National Academy of Sciences of the United States of America* **2008**, *105* (32), 11176-81.
125. Xing, J.; Chinnaraj, M.; Zhang, Z.; Cheung, H. C.; Dong, W. J., Structural studies of interactions between cardiac troponin I and actin in regulated thin filament using Forster resonance energy transfer. *Biochemistry* **2008**, *47* (50), 13383-93.
126. Cordina, N. M.; Liew, C. K.; Potluri, P. R.; Curmi, P. M.; Fajer, P. G.; Logan, T. M.; Mackay, J. P.; Brown, L. J., Ca²⁺-induced PRE-NMR changes in the troponin complex reveal the possessive nature of the cardiac isoform for its regulatory switch. *PloS one* **2014**, *9* (11), e112976.
127. Blumenschein, T. M. A.; Stone, D. B.; Fletterick, R. J.; Mendelson, R. A.; Sykes, B. D., Calcium-dependent changes in the flexibility of the regulatory domain of troponin C in the troponin complex. *The Journal of biological chemistry* **2005**, *280* (23), 21924--21932.
128. Jayasundar, J. J.; Xing, J.; Robinson, J. M.; Cheung, H. C.; Dong, W. J., Molecular dynamics simulations of the cardiac troponin complex performed with FRET distances as restraints. *PloS one* **2014**, *9* (2), e87135.
129. Dong, W. J.; Robinson, J. M.; Stagg, S.; Xing, J.; Cheung, H. C., Ca²⁺-induced conformational transition in the inhibitory and regulatory regions of cardiac troponin I. *The Journal of biological chemistry* **2003**, *278* (10), 8686-92.
130. Van Eyk, J. E.; Hodges, R. S., The biological importance of each amino acid residue of the troponin I inhibitory sequence 104-115 in the interaction with troponin C and tropomyosin-actin. *The Journal of biological chemistry* **1988**, *263* (4), 1726-32.
131. Narita, A.; Yasunaga, T.; Ishikawa, T.; Mayanagi, K.; Wakabayashi, T., Ca²⁺-induced switching of troponin and tropomyosin on actin filaments as revealed by electron cryo-microscopy. *Journal of molecular biology* **2001**, *308* (2), 241-61.
132. Ferguson, R. E.; Sun, Y. B.; Mercier, P.; Brack, A. S.; Sykes, B. D.; Corrie, J. E.; Trentham, D. R.; Irving, M., In situ orientations of protein domains: troponin C in skeletal muscle fibers. *Molecular cell* **2003**, *11* (4), 865-74.
133. Gao, W. D.; Atar, D.; Liu, Y.; Perez, N. G.; Murphy, A. M.; Marban, E., Role of troponin I proteolysis in the pathogenesis of stunned myocardium. *Circulation research* **1997**, *80* (3), 393-9.

134. Braunwald, E.; Kloner, R. A., The stunned myocardium: prolonged, postischemic ventricular dysfunction. *Circulation* **1982**, *66* (6), 1146-9.
135. Tachampa, K.; Kobayashi, T.; Wang, H.; Martin, A. F.; Biesiadecki, B. J.; Solaro, R. J.; de Tombe, P. P., Increased cross-bridge cycling kinetics after exchange of C-terminal truncated troponin I in skinned rat cardiac muscle. *The Journal of biological chemistry* **2008**, *283* (22), 15114-21.
136. Davis, J. P.; Norman, C.; Kobayashi, T.; Solaro, R. J.; Swartz, D. R.; Tikunova, S. B., Effects of thin and thick filament proteins on calcium binding and exchange with cardiac troponin C. *Biophysical journal* **2007**, *92* (9), 3195-206.
137. Dobesh, D. P.; Konhilas, J. P.; de Tombe, P. P., Cooperative activation in cardiac muscle: impact of sarcomere length. *American journal of physiology. Heart and circulatory physiology* **2002**, *282* (3), H1055-62.
138. Poole, K. J.; Lorenz, M.; Evans, G.; Rosenbaum, G.; Pirani, A.; Craig, R.; Tobacman, L. S.; Lehman, W.; Holmes, K. C., A comparison of muscle thin filament models obtained from electron microscopy reconstructions and low-angle X-ray fibre diagrams from non-overlap muscle. *Journal of structural biology* **2006**, *155* (2), 273-84.
139. Parry, D. A.; Squire, J. M., Structural role of tropomyosin in muscle regulation: analysis of the x-ray diffraction patterns from relaxed and contracting muscles. *Journal of molecular biology* **1973**, *75* (1), 33-55.
140. Hai, H.; Sano, K.; Maeda, K.; Maeda, Y.; Miki, M., Ca²⁺- and S1-induced conformational changes of reconstituted skeletal muscle thin filaments observed by fluorescence energy transfer spectroscopy: structural evidence for three States of thin filament. *Journal of biochemistry* **2002**, *131* (3), 407-18.
141. Wang, H.; Mao, S.; Chalovich, J. M.; Marriott, G., Tropomyosin dynamics in cardiac thin filaments: a multisite forster resonance energy transfer and anisotropy study. *Biophysical journal* **2008**, *94* (11), 4358-69.
142. Levine, B. A.; Moir, A. J.; Perry, S. V., The interaction of troponin-I with the N-terminal region of actin. *European journal of biochemistry / FEBS* **1988**, *172* (2), 389-97.
143. Kim, E.; Bobkova, E.; Hegyi, G.; Muhlrad, A.; Reisler, E., Actin cross-linking and inhibition of the actomyosin motor. *Biochemistry* **2002**, *41* (1), 86-93.
144. Willadsen, K. A.; Butters, C. A.; Hill, L. E.; Tobacman, L. S., Effects of the amino-terminal regions of tropomyosin and troponin T on thin filament assembly. *The Journal of biological chemistry* **1992**, *267* (33), 23746-52.
145. Li, M. X.; Wang, X.; Sykes, B. D., Structural based insights into the role of troponin in cardiac muscle pathophysiology. *Journal of muscle research and cell motility* **2004**, *25* (7), 559-79.
146. Rieck, D. C.; Li, K. L.; Ouyang, Y.; Solaro, R. J.; Dong, W. J., Structural basis for the in situ Ca²⁺ sensitization of cardiac troponin C by positive feedback from force-generating myosin cross-bridges. *Archives of biochemistry and biophysics* **2013**, *537* (2), 198-209.
147. Li, K. L.; Rieck, D.; Solaro, R. J.; Dong, W., In situ time-resolved FRET reveals effects of sarcomere length on cardiac thin-filament activation. *Biophysical journal* **2014**, *107* (3), 682-93.
148. Wang, H.; Chalovich, J. M.; Marriott, G., Structural dynamics of troponin I during Ca²⁺-activation of cardiac thin filaments: a multi-site Forster resonance energy transfer study. *PloS one* **2012**, *7* (12), e50420.

149. Julien, O.; Mercier, P.; Allen, C. N.; Fisette, O.; Ramos, C. H.; Lague, P.; Blumenschein, T. M.; Sykes, B. D., Is there nascent structure in the intrinsically disordered region of troponin I? *Proteins* **2011**, *79* (4), 1240-50.
150. Davis, J.; Yasuda, S.; Palpant, N. J.; Martindale, J.; Stevenson, T.; Converso, K.; Metzger, J. M., Diastolic dysfunction and thin filament dysregulation resulting from excitation-contraction uncoupling in a mouse model of restrictive cardiomyopathy. *Journal of molecular and cellular cardiology* **2012**, *53* (3), 446-57.
151. Ashrafian, H.; Redwood, C.; Blair, E.; Watkins, H., Hypertrophic cardiomyopathy: a paradigm for myocardial energy depletion. *Trends in genetics : TIG* **2003**, *19* (5), 263-8.
152. Huxley, H. E., Fifty years of muscle and the sliding filament hypothesis. *European journal of biochemistry / FEBS* **2004**, *271* (8), 1403-15.
153. Moss, R. L.; Razumova, M.; Fitzsimons, D. P., Myosin crossbridge activation of cardiac thin filaments: implications for myocardial function in health and disease. *Circulation research* **2004**, *94* (10), 1290-300.
154. Pan, B. S.; Solaro, R. J., Calcium-binding properties of troponin C in detergent-skinned heart muscle fibers. *The Journal of biological chemistry* **1987**, *262* (16), 7839-49.
155. Metzger, J. M.; Westfall, M. V., Covalent and noncovalent modification of thin filament action: the essential role of troponin in cardiac muscle regulation. *Circulation research* **2004**, *94* (2), 146-58.
156. Layland, J.; Solaro, R. J.; Shah, A. M., Regulation of cardiac contractile function by troponin I phosphorylation. *Cardiovascular research* **2005**, *66* (1), 12-21.
157. Bilchick, K. C.; Duncan, J. G.; Ravi, R.; Takimoto, E.; Champion, H. C.; Gao, W. D.; Stull, L. B.; Kass, D. A.; Murphy, A. M., Heart failure-associated alterations in troponin I phosphorylation impair ventricular relaxation-afterload and force-frequency responses and systolic function. *American journal of physiology. Heart and circulatory physiology* **2007**, *292* (1), H318-25.
158. Sakthivel, S.; Finley, N. L.; Rosevear, P. R.; Lorenz, J. N.; Gulick, J.; Kim, S.; VanBuren, P.; Martin, L. A.; Robbins, J., In vivo and in vitro analysis of cardiac troponin I phosphorylation. *The Journal of biological chemistry* **2005**, *280* (1), 703-14.
159. Fentzke, R. C.; Buck, S. H.; Patel, J. R.; Lin, H.; Wolska, B. M.; Stojanovic, M. O.; Martin, A. F.; Solaro, R. J.; Moss, R. L.; Leiden, J. M., Impaired cardiomyocyte relaxation and diastolic function in transgenic mice expressing slow skeletal troponin I in the heart. *The Journal of physiology* **1999**, *517* (Pt 1), 143-57.
160. Pi, Y.; Kemnitz, K. R.; Zhang, D.; Kranias, E. G.; Walker, J. W., Phosphorylation of troponin I controls cardiac twitch dynamics: evidence from phosphorylation site mutants expressed on a troponin I-null background in mice. *Circ Res* **2002**, *90* (6), 649-56.
161. Pi, Y.; Zhang, D.; Kemnitz, K. R.; Wang, H.; Walker, J. W., Protein kinase C and A sites on troponin I regulate myofilament Ca²⁺ sensitivity and ATPase activity in the mouse myocardium. *J Physiol* **2003**, *552* (Pt 3), 845-57.
162. Jessup, M.; Brozena, S., Heart failure. *N Engl J Med* **2003**, *348* (20), 2007-18.
163. Stanley, W. C.; Recchia, F. A.; Lopaschuk, G. D., Myocardial substrate metabolism in the normal and failing heart. *Physiol Rev* **2005**, *85* (3), 1093-129.

164. Harding, S. E.; Brown, L. A.; Wynne, D. G.; Davies, C. H.; Poole-Wilson, P. A., Mechanisms of beta adrenoceptor desensitisation in the failing human heart. *Cardiovasc Res* **1994**, *28* (10), 1451-60.
165. Bristow, M. R., beta-adrenergic receptor blockade in chronic heart failure. *Circulation* **2000**, *101* (5), 558-69.
166. Messer, A. E.; Jacques, A. M.; Marston, S. B., Troponin phosphorylation and regulatory function in human heart muscle: dephosphorylation of Ser23/24 on troponin I could account for the contractile defect in end-stage heart failure. *J Mol Cell Cardiol* **2007**, *42* (1), 247-59.
167. Bodor, G. S.; Oakeley, A. E.; Allen, P. D.; Crimmins, D. L.; Ladenson, J. H.; Anderson, P. A., Troponin I phosphorylation in the normal and failing adult human heart. *Circulation* **1997**, *96* (5), 1495-500.
168. van der Velden, J.; Papp, Z.; Zaremba, R.; Boontje, N. M.; de Jong, J. W.; Owen, V. J.; Burton, P. B.; Goldmann, P.; Jaquet, K.; Stienen, G. J., Increased Ca²⁺-sensitivity of the contractile apparatus in end-stage human heart failure results from altered phosphorylation of contractile proteins. *Cardiovasc Res* **2003**, *57* (1), 37-47.
169. Hamdani, N.; de Waard, M.; Messer, A.; Boontje, N.; Kooij, V.; van Dijk, S.; Versteilen, A.; Lamberts, R.; Merkus, D.; Dos Remedios, C.; Duncker, D.; Borbely, A.; Papp, Z.; Paulus, W.; Stienen, G.; Marston, S.; van der Velden, J., Myofilament dysfunction in cardiac disease from mice to men. *J Muscle Res Cell Motil* **2009**, in press.
170. Kooij, V.; Saes, M.; Jaquet, K.; Zaremba, R.; Foster, D. B.; Murphy, A. M.; Dos Remedios, C.; van der Velden, J.; Stienen, G. J., Effect of troponin I Ser23/24 phosphorylation on Ca²⁺-sensitivity in human myocardium depends on the phosphorylation background. *Journal of molecular and cellular cardiology* **2010**, *48* (5), 954-63.
171. Anderson, S.; Cody, R.; Packer, M.; Schwarz, R., Data Monitoring in the Prospective Randomized Milrinone Survival Evaluation: Dealing With an Agonizing Trend. In *Data Monitoring in Clinical Trials*, DeMets, D.; Furberg, C.; Friedman, L., Eds. Springer US: 2006; pp 209-219.
172. Wehrens, X. H.; Lehnart, S. E.; Marks, A. R., Intracellular calcium release and cardiac disease. *Annu Rev Physiol* **2005**, *67*, 69-98.
173. Kass, D. A.; Solaro, R. J., Mechanisms and use of calcium-sensitizing agents in the failing heart. *Circulation* **2006**, *113* (2), 305-15.
174. Li, Y.; Charles, P. Y.; Nan, C.; Pinto, J. R.; Wang, Y.; Liang, J.; Wu, G.; Tian, J.; Feng, H. Z.; Potter, J. D.; Jin, J. P.; Huang, X., Correcting diastolic dysfunction by Ca²⁺ desensitizing troponin in a transgenic mouse model of restrictive cardiomyopathy. *Journal of molecular and cellular cardiology* **2010**, *49* (3), 402-11.
175. Zhang, L.; Nan, C.; Chen, Y.; Tian, J.; Jean-Charles, P. Y.; Getfield, C.; Wang, X.; Huang, X., Calcium desensitizer catechin reverses diastolic dysfunction in mice with restrictive cardiomyopathy. *Archives of biochemistry and biophysics* **2015**, *573*, 69-76.
176. Tadano, N.; Du, C. K.; Yumoto, F.; Morimoto, S.; Ohta, M.; Xie, M. F.; Nagata, K.; Zhan, D. Y.; Lu, Q. W.; Miwa, Y.; Takahashi-Yanaga, F.; Tanokura, M.; Ohtsuki, I.; Sasaguri, T., Biological actions of green tea catechins on cardiac troponin C. *British journal of pharmacology* **2010**, *161* (5), 1034-43.
177. Levijoki, J.; Pollesello, P.; Kaivola, J.; Tilgmann, C.; Sorsa, T.; Annala, A.; Kilpelainen, I.; Haikala, H., Further evidence for the cardiac troponin C mediated

- calcium sensitization by levosimendan: structure-response and binding analysis with analogs of levosimendan. *Journal of molecular and cellular cardiology* **2000**, 32 (3), 479-91.
178. Solaro, R. J.; Bousquet, P.; Johnson, J. D., Stimulation of cardiac myofilament force, ATPase activity and troponin C Ca⁺⁺ binding by bepridil. *The Journal of pharmacology and experimental therapeutics* **1986**, 238 (2), 502-7.
179. Barylko, B.; Wagner, M. C.; Reizes, O.; Albanesi, J. P., Purification and characterization of a mammalian myosin I. *Proceedings of the National Academy of Sciences of the United States of America* **1992**, 89 (2), 490-4.
180. Margossian, S. S.; Lowey, S., Preparation of myosin and its subfragments from rabbit skeletal muscle. *Methods in enzymology* **1982**, 85 Pt B, 55-71.
181. Zheng, L.; Yu, K.; Yuan, C.; Wang, X.; Chen, S.; Kimura, I.; Konno, K., Characterization of myosin subfragment-1 of summer and winter silver carp (*Hypophthalmichthys molitrix*) muscle. *Journal of food science* **2012**, 77 (9), C914-20.
182. Product Information Protein Kinase A Catalytic Subunit from bovine heart. <https://www.sigmaaldrich.com/content/dam/sigma-aldrich/docs/Sigma/Datasheet/5/p2645dat.pdf> (accessed 09/23/15).
183. Finley, N.; Abbott, M. B.; Abusamhadneh, E.; Gaponenko, V.; Dong, W.; Gasmi-Seabrook, G.; Howarth, J. W.; Rance, M.; Solaro, R. J.; Cheung, H. C.; Rosevear, P. R., NMR analysis of cardiac troponin C-troponin I complexes: effects of phosphorylation. *FEBS letters* **1999**, 453 (1-2), 107-12.
184. Lan, K. K.; Soo, Y.; Siu, C.; Wang, M., The use of weighted Z-tests in medical research. *Journal of biopharmaceutical statistics* **2005**, 15 (4), 625-39.
185. Konno, K.; Watanabe, S., Two different preparations of subfragment-1 from scallop adductor myosin. *Journal of biochemistry* **1985**, 98 (1), 141-8.
186. Schulenberg, B.; Goodman, T. N.; Aggeler, R.; Capaldi, R. A.; Patton, W. F., Characterization of dynamic and steady-state protein phosphorylation using a fluorescent phosphoprotein gel stain and mass spectrometry. *Electrophoresis* **2004**, 25 (15), 2526-32.
187. Kinoshita-Kikuta, E.; Kinoshita, E.; Koike, T., Separation and identification of four distinct serine-phosphorylation states of ovalbumin by Phos-tag affinity electrophoresis. *Electrophoresis* **2012**, 33 (5), 849-55.
188. Dweck, D.; Reyes-Alfonso, A., Jr.; Potter, J. D., Expanding the range of free calcium regulation in biological solutions. *Analytical biochemistry* **2005**, 347 (2), 303-15.
189. Packer, M.; Carver, J. R.; Rodeheffer, R. J.; Ivanhoe, R. J.; DiBianco, R.; Zeldis, S. M.; Hendrix, G. H.; Bommer, W. J.; Elkayam, U.; Kukin, M. L.; et al., Effect of oral milrinone on mortality in severe chronic heart failure. The PROMISE Study Research Group. *The New England journal of medicine* **1991**, 325 (21), 1468-75.
190. Amsallem, E.; Kasparian, C.; Haddour, G.; Boissel, J. P.; Nony, P., Phosphodiesterase III inhibitors for heart failure. *The Cochrane database of systematic reviews* **2005**, (1), Cd002230.
191. Schlecht, W.; Li, K. L.; Hu, D.; Dong, W., Fluorescence Based Characterization of Calcium Sensitizer Action on the Troponin Complex. *Chemical biology & drug design* **2015**.
192. Martyn, D. A.; Gordon, A. M., Influence of length on force and activation-dependent changes in troponin c structure in skinned cardiac and fast skeletal muscle. *Biophysical journal* **2001**, 80 (6), 2798-808.

193. Toyoshima, Y. Y.; Kron, S. J.; McNally, E. M.; Niebling, K. R.; Toyoshima, C.; Spudich, J. A., Myosin subfragment-1 is sufficient to move actin filaments in vitro. *Nature* **1987**, 328 (6130), 536-9.
194. Bergh, C. H.; Andersson, B.; Dahlstrom, U.; Forfang, K.; Kivikko, M.; Sarapohja, T.; Ullman, B.; Wikstrom, G., Intravenous levosimendan vs. dobutamine in acute decompensated heart failure patients on beta-blockers. *European journal of heart failure* **2010**, 12 (4), 404-10.
195. Innes, C. A.; Wagstaff, A. J., Levosimendan: a review of its use in the management of acute decompensated heart failure. *Drugs* **2003**, 63 (23), 2651-71.
196. Sorsa, T.; Heikkinen, S.; Abbott, M. B.; Abusamhadneh, E.; Laakso, T.; Tilgmann, C.; Serimaa, R.; Annala, A.; Rosevear, P. R.; Drakenberg, T.; Pollesello, P.; Kilpelainen, I., Binding of levosimendan, a calcium sensitizer, to cardiac troponin C. *The Journal of biological chemistry* **2001**, 276 (12), 9337-43.
197. Robertson, I. M.; Baryshnikova, O. K.; Li, M. X.; Sykes, B. D., Defining the binding site of levosimendan and its analogues in a regulatory cardiac troponin C-troponin I complex. *Biochemistry* **2008**, 47 (28), 7485-95.
198. Li, Y.; Love, M. L.; Putkey, J. A.; Cohen, C., Bepridil opens the regulatory N-terminal lobe of cardiac troponin C. *Proceedings of the National Academy of Sciences of the United States of America* **2000**, 97 (10), 5140-5.
199. Abusamhadneh, E.; Abbott, M. B.; Dvoretzky, A.; Finley, N.; Sasi, S.; Rosevear, P. R., Interaction of bepridil with the cardiac troponin C/troponin I complex. *FEBS letters* **2001**, 506 (1), 51-4.
200. Wang, X.; Li, M. X.; Sykes, B. D., Structure of the regulatory N-domain of human cardiac troponin C in complex with human cardiac troponin I147-163 and bepridil. *The Journal of biological chemistry* **2002**, 277 (34), 31124-33.
201. Howarth, J. W.; Meller, J.; Solaro, R. J.; Trewhella, J.; Rosevear, P. R., Phosphorylation-dependent conformational transition of the cardiac specific N-extension of troponin I in cardiac troponin. *Journal of molecular biology* **2007**, 373 (3), 706-22.
202. Zhang, R.; Zhao, J.; Mandveno, A.; Potter, J. D., Cardiac troponin I phosphorylation increases the rate of cardiac muscle relaxation. *Circulation research* **1995**, 76 (6), 1028-35.
203. Nagle, D. G.; Ferreira, D.; Zhou, Y. D., Epigallocatechin-3-gallate (EGCG): chemical and biomedical perspectives. *Phytochemistry* **2006**, 67 (17), 1849-55.
204. Robertson, I. M.; Li, M. X.; Sykes, B. D., Solution structure of human cardiac troponin C in complex with the green tea polyphenol, (-)-epigallocatechin 3-gallate. *The Journal of biological chemistry* **2009**, 284 (34), 23012-23.
205. Fuchs, F.; Grabarek, Z., The green tea polyphenol (-)-epigallocatechin-3-gallate inhibits magnesium binding to the C-domain of cardiac troponin C. *Journal of muscle research and cell motility* **2013**, 34 (2), 107-13.
206. Maron, B. J.; Maron, M. S.; Semsarian, C., Genetics of hypertrophic cardiomyopathy after 20 years: clinical perspectives. *Journal of the American College of Cardiology* **2012**, 60 (8), 705-15.

CURRICULUM VITAE

Maria E. Moutsoglou

South Dakota State University
Department of Chemistry and Biochemistry
Avera Health and Science Center
Rm 037 Box 2202
Brookings, SD 57007

E-mail: maria.moutsoglou@gmail.com

PERSONAL INFORMATION

Nationality	United States and Greek dual citizenship
Place and date of birth	South Dakota (U.S.), November 12, 1987

EDUCATION

South Dakota State University, Department of Chemistry and Biochemistry, 2010-2016

Doctor of Philosophy in Biochemistry

Dissertation title: "A FRET investigation into molecular mechanisms of cardiac troponin activation in reconstituted thin filaments."

South Dakota State University, Department of Biology and Microbiology, Department of Chemistry and Biochemistry, 2006-2010

Bachelor of Science in Chemistry, Microbiology, and Biology

RESEARCH EXPERIENCE

2016-	Fermentation Scientist , Sierra Nevada Brewing Co., Chico, CA
2010-2015	Graduate Research Assistant , South Dakota State University, Brookings, SD Primary Investigator: John M. Robinson, M.D./Ph.D. Project: Development of a 2D spectroscopic drug-screening assay for monitoring the actions of inotropic agents on the thin filament. Development of a multi-site FRET assay to reveal the dynamics and structure of the C-terminal region of TnI during calcium activation. Design of a FRET assay on Tn that enables time-resolved FRET and FLIM analysis with single molecule resolution.

TEACHING EXPERIENCE

2014	Teaching Assistant , CHEM776: Laboratory Development, South Dakota State University
2010-2011	Teaching Assistant , CHEM466: Biochemistry; CHEM112-CHEM114: General Chemistry, South Dakota State University

TECHNICAL EXPERTISE

Software: Microsoft Suite, Adobe Photoshop and Illustrator, GraphPad Prism, VMD, Mac and Windows OS, ImageJ

Lab: Recombinant and native protein expression and purification using fast protein liquid chromatography (FPLC). Aseptic technique. Mutagenesis and DNA purification. Protein characterization using denaturing and native gel electrophoresis. Sedimentation assays using ultracentrifugation. Maintaining equipment and reagent stock. Managing student projects.

Spectroscopy: Fluorescent dye conjugation. Steady-state fluorescence spectroscopy. Epifluorescence imaging.

ACADEMIC COMMUNITY/MENTORSHIP EXPERIENCE

2014-2015 *Undergraduate mentor*
Project: Development of a pulldown assay to quantify myosin binding to the thin filament.

2014-2015 *Undergraduate mentor*
Project: Performing myosin S1 titrations on fluorescently-labeled actin to recover binding constants.

2013-2014 *High school student mentor (INTEL ISEF participant)*
Project: Development of a preliminary method for performing steady-state calcium titrations.

2014 *Volunteer supervisor*
Boy Scouts of America Troop 4 in Brookings, SD. Chemistry Merit Badge.

2012 *Undergraduate mentor*
Project: Development of an environmentally sensitive fluorescence assay on actin.

MEMBERSHIPS

2010-2015 Biophysical Society

AWARDS

April 2015 SDSU Sigma Xi PhD Paper Competition, First Place
Title: "A spectroscopic assay for screening calcium-sensitive drugs on cardiac thin filaments."

ABSTRACTS

M.E. Moutsoglou, John M. Robinson. (11/2015) *Mechanism of cardiotonic agents on the cardiac thin filament*. 3rd Annual Sanford Health-SDSU Biomedical Research Symposium, Sioux Falls, SD.

M.E. Moutsoglou, G.H. Kim, C. Solis-Ocampo, M. Kumar, P. de Tombe, J.M. Robinson. (11/2015) *Treating heart failure with preserved ejection fraction through troponin I phosphomimicry*. American Heart Association Scientific Sessions, Orlando, FL.

M.E. Moutsoglou, G.H. Kim, C. Solis-Ocampo, J.M. Robinson. (02/2015) *A FRET-based assay for monitoring actions of calcium sensitizers on the thin filament*. Biophysical Society 59th Annual Meeting, Baltimore, MD.

G.H. Kim, **M.E. Moutsoglou**, C. Solis-Ocampo, J.M. Robinson. (02/2015) *spFRET reveals the mechanism of myosin-dependent activation of troponin within regulated actin filaments*. Biophysical Society 59th Annual Meeting, Baltimore, MD.

C. Solis-Ocampo, **M.E. Moutsoglou**, G.H. Kim, J.M. Robinson. (02/2015) *Studying troponin within regulated actin at single molecule resolution*. Biophysical Society 59th Annual Meeting, Baltimore, MD.

M.E. Moutsoglou, G.H. Kim, C. Solis-Ocampo, S.C. Wu, J.M. Robinson. *Ca²⁺-induced structural changes in Tn: a multi-site FRET study combining TCSPC with single filament imaging*. Biophysical Society 58th Annual Meeting, San Francisco, CA.

B. Sun, **M.E. Moutsoglou**, J.M. Robinson. (02/2014) *Functional differences of unbound and weakly bound Xb states in the cardiac myofilament*. Biophysical Society 58th Annual Meeting, San Francisco, CA.

J.M. Robinson, **M.E. Moutsoglou**, C. Solis-Ocampo, G.H. Kim. (02/2014) *Fluorescence comes of age: measuring angstrom-level distance changes within single filaments of regulated actin*. Biophysical Society 58th Annual Meeting, San Francisco, CA.

S.C. Wu, **M.E. Moutsoglou**, J.M. Robinson. (02/2014) *Effects of nitrosylation on cardiac myofilament proteins*. Biophysical Society 58th Annual Meeting, San Francisco, CA. (panel presentation)

M.E. Moutsoglou, G.H. Kim, J.M. Robinson. (02/2013) *FRET assay for single molecule measurements of troponin activation*. Biophysical Society 57th Annual Meeting, Philadelphia, PA.

B. Sun, **M.E. Moutsoglou**, J.M. Robinson (02/2013) *Cardiac F-actin has two functional states*. Biophysical Society 57th Annual Meeting, Philadelphia, PA.

T.A. Baldwin, G. H. Kim, C. Solis-Ocampo, **M.E. Moutsoglou**, J.M. Robinson. (02/2013) *Experimental determination of the Forster critical distance*. Biophysical Society 57th Annual Meeting, Philadelphia, PA.

M.E. Moutsoglou, G.H. Kim, C. Solis-Ocampo, T.A. Baldwin, T.R. Deutscher, John M. Robinson. (06/2012) *Single molecule FRET measurements of cardiac troponin in surface immobilized and freely diffusing assemblies*. Myofilament Conference, Madison, WI.

M.E. Moutsoglou, G.H. Kim, T.R. Deutscher, T.A. Baldwin, J.M. Robinson. (02/2012) *Single molecule FRET measurements of cardiac troponin in freely diffusing assemblies*. Biophysical Society 56th Annual Meeting, San Diego, CA.

T.R. Deutscher, **M.E. Moutsoglou**, T.A. Baldwin, A.L. McEldowny, J.M. Robinson. (02/2012) *A novel method for introducing fluorescently labeled troponin into live cardiac myocytes*. Biophysical Society 56th Annual Meeting, San Diego, CA.

T.A. Baldwin, G.H. Kim, T.R. Deutscher, **M.E. Moutsoglou**, J.M. Robinson. (02/2012) *A comparison of donor-acceptor distance distributions derived from ensemble and single-pair FRET measurements*. Biophysical Society 56th Annual Meeting, San Diego, CA.

B. Sun, G.H. Kim, **M.E. Moutsoglou**, T.R. Deutscher, T.A. Baldwin, J.M. Robinson. (02/2012) *Conformational changes in troponin within the cardiac myofilament*. Biophysical Society 56th Annual Meeting, San Diego, CA.

J.M. Robinson, **M.E. Moutsoglou**, T. Lackey, W. Dong, M. Chinnaraj, H.C. Cheung. (02/2011). *Single molecule FRET measurements reveal incomplete activation of the cardiac myofilament by Ca²⁺*. Biophysical Society 55th Annual Meeting, Baltimore, MD